Exploring Strategies for Obtaining Cesium Lead Halide Perovskite Nanocrystals with High Photoluminescence Efficiency and Stability

A Thesis Submitted for the Degree of Doctor of Philosophy

by **Rajesh Kumar Gautam**



School of Chemistry
University of Hyderabad
Hyderabad- 500046
Telangana, India
June 2023

Dedicated to My Parents, Rakesh Kumar & Family

"Life should be great rather than long".

Dr. B. R. Ambedkar (1891-1956)

Contents

Declaration	
Certificate	
Acknowledgement	
List of Publications	
List of Conference Presentations	
Chapter-wise Thesis Organization	
Chapter 1: Introduction	
1.1. Motivation	3
1.2. Semiconductor: Bulk to NCs	3
1.3. Perovskites	6
1.3.1. Background	6
1.3.2. Crystal Structure	7
1.3.3. Surface Properties of Perovskite Nanocrystals	8
1.3.4. Optical Properties of CsPbX ₃ Perovskite Nanocrystals	1
1.3.5. Trap States in Perovskite Nanocrystals	1
1.3.6. Motivation of the Thesis Work	1:
References	1
Chapter 2: Materials, Methods and Instrumentation	
2.1. Materials	2
2.2. Methods of Synthesis	2
2.2.1. Synthesis of CsPbX ₃ (X = Cl, Br and I) Perovskites NCs	2
2.3. Post-synthetic Treatment of CsPbX ₃ (X = Cl, Br and I) NCs	2
2.3.1. Post-synthetic Treatment with Sodium Thiosulfate	2
2.3.2. Post-synthetic Treatment with Thioacetamide	2:
2.4. Optical Measurements and Instrumentation	2:
2.4.1. UV-Vis Spectrophotometer	2
2.4.2. Spectrofluorometer	2
2.4.3. Photoluminescence Quantum Yield (PLQY) Measurement	2:
2.4.4. Time-correlated Single Photon Counting (TCSPC)	2
2.4.5. Femtosecond Transient Absorption (fs-TA) Spectroscopy	2
2.5. Other Instrumental Measurements	2
References	2
Reservation	_
Chapter 3: Can Sulfur-Containing Small Systems Enhance the Photoluminesco	
Stability of the Blue-, Green- and Yellow-Emitting Perovskite Nanocrystals? A with Sodium Thiosulfate	. Case Study

33

3.1. Introduction

3.2. Results and Discussion	34
3.2.1. Synthesis and Characterization of the NCs	34
3.2.2. Optical Properties	36
3.2.3. Time Resolved Measurements	37
3.3. Summary	49
References	49
Chapter 4: Room-Temperature Treatment with Thioacetamide Yiel	ding Blue- and Green-
Emitting CsPbX ₃ Perovskite Nanocrystals with Enhanced Photolum	inescence Efficiency
and Stability	
4.1. Introduction	60
4.2. Results and Discussion	61
4.2.1 Synthesis and Characterization of the NCs	61
4.2.2. Optical Properties	63
4.2.3. Time Resolved Measurements	64
4.3. Summary	77
References	77
Chapter 5: Bidentate Ligand-Induced Enhanced PLQY and Stabilit	y of Blue-, Green- and
Red-Emitting CsPbX ₃ (X = Cl, Br, I) Perovskite NCs	
5.1. Introduction	84
5.2. Results and Discussion	85
5.2.1 Synthesis and Characterization of the NCs	85
5.2.2. Optical Properties	88
5.2.3. Time Resolved Measurements	91
5.3. Summary	99
References	99
Chapter 6: Concluding Remarks	
6.1. Overview	106
6.2. Future Scope and Challenges	107
Appendices	109

Declaration

I hereby declare that the matter embodied in the thesis entitled "Exploring Strategies for Obtaining Cesium Lead Halide Perovskite Nanocrystals with High Photoluminescence Efficiency and Stability" is the result of investigations carried out by me in the School of Chemistry, University of Hyderabad, India, under the supervision of Prof. Anunay Samanta.

In keeping with the general practice of reporting scientific investigations, acknowledgements have been made wherever the work described is based on the findings of other investigators. Any omission or error that might have crept is regretted.

University of Hyderabad, India

June, 2023

Rajesh Kumar Gautam

Professor Anunay Samanta School of Chemistry University of Hyderabad Hyderabad-500046, India



Phone: +91-40-2313 4813

Fax: +91-40-2301 1594

Email: anunay@uohyd.ac.in

Certificate

This is to certify that the thesis entitled "Exploring Strategies for Obtaining Cesium Lead Halide Perovskite Nanocrystals with High Photoluminescence Efficiency and Stability" submitted by Rajesh Kumar Gautam bearing the registration number 17CHPH30 in partial fulfilment of the requirements for the award of Doctor of Philosophy (Ph.D.) in the School of Chemistry, University of Hyderabad, India under my supervision and guidance. This thesis is free from plagiarism and has not been submitted previously in part or full to this or other University/Institution for any degree or diploma. Further, the student has following publications before submission of the thesis for adjudication and has produced evidences for the same in the form of reprints.

Parts of the thesis have been published in the following publications:

- Rajesh Kumar Gautam, Somnath Das and Anunay Samanta, Can Sulfur-Containing Small Systems Enhance the Photoluminescence and Stability of the Blue-, Green-and Yellow-Emitting Perovskite Nanocrystals? A Case Study with Sodium Thiosulfate. J. Phys. Chem. C 2021, 125, 24170-24179. (Chapter 1)
- 2. Rajesh Kumar Gautam, Somnath Das and Anunay Samanta, Room-Temperature Treatment with Thioacetamide Yielding Blue-and Green-Emitting CsPbX₃ Perovskite Nanocrystals with Enhanced Photoluminescence Efficiency and Stability. ChemNanoMat. 2022, 8, e202200029. (Chapter 2)
- 3. Rajesh Kumar Gautam, Sumanta Paul and Anunay Samanta, Bidentate Ligand-Enhanced PLQY and Stability of Blue-, Green- and Red-Emitting CsPbX₃ (X = Cl, Br, I) Perovskite NCs. (Chapter 3) (To be communicated)

The student has made presentation in the following conferences:

- "Room-Temperature Treatment with Thioacetamide Yielding Blue- and Green-Emitting CsPbX₃ Perovskite Nanocrystals with Enhanced Photoluminescence Efficiency and Stability", 19th Annual In-House Symposium of the School of Chemistry (Chemfest-2022), University of Hyderabad, Hyderabad, India, April 22-23, 2022. (Oral Presentation)
- 2. "Room-Temperature Treatment with Thioacetamide Yielding Blue- and Green-Emitting CsPbX₃ Perovskite Nanocrystals with Enhanced Photoluminescence Efficiency and Stability", 19th Annual In-House Symposium of the School of Chemistry (Chemfest-2022), University of Hyderabad, Hyderabad, India, April 22-23, 2022. (Poster Presentation)
- 3. "Mechanistic Exploration of Enhanced Photoluminescence Efficiency of Blue-, Green- and Yellow-Emitting Stable Perovskite Nanocrystals on Thiosulfate Treatment", 14th National Symposium on Radiation & Photochemistry (NSRP-2021), Indian Institute of Technology Gandhinagar, Gandhinagar, India, June 25-26, 2021. (Oral Presentation)
- 4. "Synthesis of Blue- and Green-Emitting Perovskite Nanocrystals with Near Unity Photoluminescence Efficiency through Post-synthetic Treatment with Thiosulfate salts", 17th Annual In-House Symposium of the School of Chemistry (Chemfest-2020), University of Hyderabad, Hyderabad, India, February 27-28, 2020. (Poster Presentation)

The student has passed the following courses towards the fulfilment of the coursework requirement for Ph.D. degree:

Sl. No.	Course No.	Title of the course	No. of Credits	Grade
1.	CY801	Research Proposal	4	C
2.	CY805	Instrumental Methods-A	4	В
3.	CY806	Instrumental Methods-B	4	В

Anunay Samanta

Thesis Supervisor
PROF. ANUNAY SAMANTA
SCHOOL OF CHEMISTRY
UNIVERSITY OF HYDERABAD

HYDERABAD - 500 046

Achri Mengce

School of Chemistry

University of Hyderabad

Dean SCHOOL OF CHEMISTRY

University of Hyderabad Hyderabad-500 046.

Acknowledgements

I enjoyed and learned a lot of things in the last five and half years of my PhD journey. During this period, I understood the big mantra that research needed patience and time from failure to successful work. Also, I faced several difficulties, but always took them as an opportunity and moved ahead.

I would like to thank my supervisor, Prof. Anunay Samanta, for being part of his group and he is given me a better environment to do research work. I am thankful to him for his continuous support at every stage.

I would like to thank also the former and present Dean(s) of the School of Chemistry for providing better facilities for the smooth run the research work. I thank all faculty members, non-teaching staff and especially my doctoral committee members, Prof. Samar Kumar Das and Prof. M. Durga Prasad, for their proper encouragement in several stages.

Acknowledge, I also thank AREM and Nanotechnology departments for the instrument facility at the University of Hyderabad. Thanks to Durga Prasad, Sunil, Rajesh and Vinay anna for their help during TEM, FESEM and PXRD measurements. I am also grateful to Surya and Chetan anna (from Prof. Ashwini Nangia sir's lab) for their help in many ways.

Financial assistance from the Professional development fund (PDF) is greatly acknowledged. Special thanks to the University of Hyderabad for the fellowship during my PhD period. Thanks, J. C. Bose fellowship, to my supervisor for the research lab facility.

I thank my whole family members, especially my mom and elder brother Rakesh Kumar for their continuous mental support and encouragement during this time because PhD takes a little longer time and needs a cool mindset.

I want to discuss how my interest is generated in chemistry and meted people on this long academic journey. Initially, in my 10th and 12th classes, my interest was in physics because of my elder brother Rakesh Kumar. After that, when I take admission in B.Sc. at the University of Allahabad, my interest was continuous in physics. But when I spent a little more time in my B. Sc. (II) years,

then I feel a much better response in chemistry. I continued my interest in chemistry M.Sc. from the same place, but in my M.Sc. final year again I remind physics and correlated it with physical chemistry and found some similarities, I chose physical chemistry. Then, I moved to the University of Hyderabad for PhD admission and got the opportunity to work in spectroscopy under the supervision of Prof. Anunay Samanta. I really enjoyed this PhD journey, and I learnt a lot of things, especially from every week's lab group meeting with lab-mates and sir. Initially, for one and half years I read and understood basic photochemistry and discussed the doubts with my most senior lab-mate Navendu bhaiya. He helped me too much in the initial stage and guided me also on what I should and not do. Sudipta and Saddam bhaiya also helped me regarding the lab instruction and others. Sneha didi had an excellent experience about the Hyderabad restaurant and food ordering for the lab party. Apurba bhaiya was a very helpful and motivated person. He was always asking, Rajesh what are you reading and asking questions then said you are going on a good track then my confidence little started from there. I am very thankful to him because he started to learn me about the basic reaction method of perovskite NCs and instruments operating knowledge step-wise. Then, slowly I started my research work, and whenever I feel doubt, then always discussed with him. Tasnim didi was also a very helpful guy. She was shown me the firsttime real experience of hot-injection synthesis of green-emitting CsPbBr₃ perovskite NCs. Then slowly, my interest started in perovskites NCs and also, I discussed with her my minor or major research problems and she helped me a lot. I am very thankful to Somnath, he was a very helpful person and discussed with him very frankly whether research works or other things. Sumanta was my PhD batch mate, helped me in various ways, and I learnt better experience with him in this long journey from start to end. Alila also was my batch mate and I felt a better experience with her whether any research topic or personal discussion. Ramavath Babu, he had joined as a postdoc in our lab, and I also learned a better experience from him. I enjoyed a lot with all my lab mates, whether inside the campus or outside campus tour trip or party.

I also enjoyed with my PhD batch mate friends whether friends' birthday celebrations or birthday parties. I must thank Noorul for being part of roommate with me in room number 45, ground floor annex hostel for almost 2 years. Then I shifted to single room wing B-207 NRS hostel first floor. I also enjoyed with Isha, she was the leader of our friend's group and always plans to go outside from the campus with friends Alila, Noorul, and Mujahid at the weekend time. Mostly all the

beautiful places we visited in Hyderabad and enjoyed a lot. In 2019, my own younger brother Rahul Kumar Gautam had taken PhD admission in the computer science department then we both started our first-time cooking in the NRS hostel and enjoyed a lot so far. I also enjoyed the time with my other PhD batch mates friends; Suraj, Shabbir, Asif, Kirti, Intzar, Isfaq, Naresh, Smruti, Arun, Shrinivas, Rina Rajesh, Manas, Vinay, Dinesh, Archana, Hafijur and Daradi. I also meted with other friends on campus and got a good experience. I love too much the University of Hyderabad campus and never felt alone at any time because of the better diversified-environment which cannot explain.

At the end, I would say that I have enjoyed very much with my work, lab mates, and friends. I want to thank everyone for your kind love and support in this PhD journey.

Rajesh Kumar Gautam

June, 2023

List of Publications

Thesis Chapters Publications

- 1. Rajesh Kumar Gautam, Somnath Das and Anunay Samanta, Can Sulfur-Containing Small Systems Enhance the Photoluminescence and Stability of the Blue-, Green-and Yellow-Emitting Perovskite Nanocrystals? A Case Study with Sodium Thiosulfate. *J. Phys. Chem. C* **2021**, 125, 24170-24179. (Chapter 1)
- 2. <u>Rajesh Kumar Gautam</u>, Somnath Das and Anunay Samanta, Room-Temperature Treatment with Thioacetamide Yielding Blue-and Green-Emitting CsPbX₃ Perovskite Nanocrystals with Enhanced Photoluminescence Efficiency and Stability. *ChemNanoMat.* **2022**, 8, e202200029. (**Chapter 2**)
- 3. <u>Rajesh Kumar Gautam</u>, Sumanta Paul and Anunay Samanta, Bidentate Ligand-Enhanced PLQY and Stability of Blue-, Green- and Red-Emitting CsPbX₃ (X = Cl, Br, I) Perovskite NCs. (Chapter 3) (To be communicated)

Others Publications

4. Navendu Mondal, Apurba De, Sudipta Seth, Tasnim Ahmed, Somnath Das, Sumanta Paul, Rajesh Kumar Gautam and Anunay Samanta, Dark Excitons of the Perovskites and Sensitization of Molecular Triplets. *ACS Energy Lett.* **2021**, 6, 588-597. (*Perspective*)

List of Conference Presentations

Poster Presentation

- 1. "Room-Temperature Treatment with Thioacetamide Yielding Blue- and Green-Emitting CsPbX₃ Perovskite Nanocrystals with Enhanced Photoluminescence Efficiency and Stability", **19**th **Annual In-House Symposium of the School of Chemistry (Chemfest-2022)**, University of Hyderabad, Hyderabad, India, April 22-23, 2022.
- "Synthesis of Blue- and Green-Emitting Perovskite Nanocrystals with Near Unity Photoluminescence Efficiency through Post-synthetic Treatment with Thiosulfate salts", 17th Annual In-House Symposium of the School of Chemistry (Chemfest-2020), University of Hyderabad, Hyderabad, India, February 27-28, 2020.

Oral Presentation

- 1. "Room-Temperature Treatment with Thioacetamide Yielding Blue- and Green-Emitting CsPbX₃ Perovskite Nanocrystals with Enhanced Photoluminescence Efficiency and Stability", **19**th **Annual In-House Symposium of the School of Chemistry (Chemfest-2022),** University of Hyderabad, Hyderabad, India, April 22-23, 2022.
- "Mechanistic Exploration of Enhanced Photoluminescence Efficiency of Blue-, Green- and Yellow-Emitting Stable Perovskite Nanocrystals on Thiosulfate Treatment", 14th National Symposium on Radiation & Photochemistry (NSRP-2021), Indian Institute of Technology Gandhinagar, Gandhinagar, India, June 25-26, 2021.

Chapter-wise Organization of the Thesis

This thesis is organized into six chapters. Chapter 1 provides a brief introduction on semiconductor materials and the effect of quantum confinement on their band structures. The discussion is then focused on a promising class of semiconductors, namely the perovskites, and their various characteristics such as crystal structure and defects, formability criteria, surface and optical properties and stability. In chapter 2, details of preparation and characterization of various perovskite NCs using different techniques (such as TEM, EDX, FT-IR, XPS, and PXRD) are discussed. Various instruments and methods were used in this study and basic principles of the UV-Vis absorption, emission and time-correlated single photon counting (TCSPC) measurements have been discussed. An outline of the setup used for femtosecond transient absorption is provided. The working chapters start with **chapter 3**, in which the effect of post-synthetic treatment of the CsPbX₃ (X = Cl, Br, I) perovskite NCs, which emit in the blue-, green-, and yellow region, with sodium thiosulfate on their photoluminescence (PL) characteristics is reported. Chapter 4 explores the influence of room temperature post-synthetic treatment of the blue-, and greenemitting perovskites NCs with thioacetamide on their PL efficiency and stability. In **chapter 5**, we have investigated whether and to what extent bidentate capping ligand can improve the photoluminescence and stability of the CsPbX₃ NCs. Chapter 6 presents a summary of the findings of this thesis work and highlights future scope and challenges.

CHAPTER 1

Introduction

Overview

In this chapter, a brief introduction on semiconductor materials, highlighting the effect of quantum confinement on their band structures is provided. Then discussion is focused on a particular type of semiconductors NCs, perovskite NCs with general formula, APbX₃ ($A = Cs^+$, MA⁺, FA⁺, and $X = Cl^-$, Br⁻, I⁻), which are the main theme of this study. Characteristics properties such as crystal structure, their formability criteria, surface and optical properties, stability, electronic structure of defect-intolerant and defect-tolerant, and types of defects are discussed.

1.1. Motivation

Current world has been observing lots of challenges, and continuously growing energy demand is one such big problem which will be even more serious in the coming days. Rapid downturn of conventional energy sources is a big problem in this regard. Therefore, unconventional (renewable) energy sources, which are easily available, are of great significance in current energy demand. Solar energy is the most abundant renewable energy source that can be used with full potential worldwide. The lead-halide perovskite solar cells, which came much late (in 2009), attracted worldwide attention owing to their easy and inexpensive fabrication with fascinating efficiencies (>25%). Not only in photovoltaics, but also these lead halide based perovskites have shown potential application in LEDs, lasers and other optoelectronic devices. However, these materials are also not free from limitations hindering their utility in photovoltaics and optoelectronic that will be discussed thoroughly in this thesis. The primary focus of this thesis is probing the optical properties of the perovskite nanocrystals employing a number of spectroscopic and microscopic tools and designing new strategies for better utilization of these materials in optoelectronic and photovoltaic applications.

1.2. Semiconductor: Bulk to NCs

The electrical conductivity of a semiconductor material is in between a metal and an insulator.² The conductivity of semiconductors depend on their bandgap energies and band structures. The transition of an electron from the valence band (VB) to the conduction band (CB) requires a particular amount of photon energy equal to or greater than the band gap. By providing ionizing radiation, electron can be excited from VB to CB leaving behind a hole at VB. When these electron and hole recombine radiatively through Coulombic interaction then materials emit photon. In case of semiconductor materials ionization is achieved through photo excitation. These charged electron and hole can act as free-charge carrier and they may be mobilized in presence of an external electric field. The conductivity of semiconductor materials depends on the mass of the photogenerated charge carriers, and their rest masses are replaced with their effective masses as latter determines mobility of the carriers inside the crystals.³ The minimum energy needed to

generate electron-hole pair is given below. ^{3,4}

$$E = E_g + E_{e, kin} + E_{h, kin}$$

Where E_g is the bandgap of the material, $E_{h, kin}$ and $E_{e, kin}$ represent the kinetic energy of the photogenerated hole and electron, respectively.

Due to the coulombic interaction, the photogenerated electron and hole form an electrically neutral quasi-particle, called 'exciton', whose energy is expressed as ^{3,4}

$$E_{exciton} = E_g - \frac{R_y}{n^2} + \frac{\hbar^2 k^2}{2(m_e^* + m_h^*)}$$

Where n is an integer number, R_y is exciton Rydberg energy, \hbar denotes the reduced Planck's constant and m_e^* and m_h^* indicate the effective masses of electron and hole, respectively, and k is the exciton wave vector.

Another important parameter to consider in this context is exciton Bohr radius (a₀). Exciton Bohr radius is the most probable distance between electron and hole in an exciton. Exciton Bohr radius is a function of the dielectric constant of the material (ε) and effective masses of electrons and holes and it is expressed as ⁴

$$a_0 = \frac{\hbar^2 \varepsilon}{e^2} \left(\frac{1}{m_e^*} + \frac{1}{m_h^*} \right)$$

The nanocrystalline forms of the semiconductor materials are quite attractive due to their unique properties compared to its bulk form. These unique properties originate from the 'quantum confined' nature of the excitons.⁵ Although the meaning of confinement means the confinement of excitonic wavefunction. However, a system is quantum confined or not is determined by considering the exciton Bohr radius and the size of the NCs.⁶ The change in NCs diameter leads to a change in optoelectronic properties. The dimensionality and size of the materials have direct influence on their band structures. For example, if the size of nanocrystals increases, then bandgap energy decreases. Figure 1.1a provides a schematic description of a three-dimensional (3D bulk), two-dimensional (2D, confined in one direction), one-dimensional (1D, confined in one direction),

and zero-dimensional (0D, confined in three directions) nanostructures.⁷ The bandgap of the system increases with increase of confinement. The general expression, which describes the bandgap energy of such a quantum-confined system, is shown below.^{5,6}

$$E_{g}(QD) = E_{g}(bulk) + \frac{\hbar^{2}\pi^{2}}{2m_{e}^{*}R^{2}} + \frac{\hbar^{2}\pi^{2}}{2m_{h}^{*}R^{2}} - \frac{1.786e^{2}}{\varepsilon R} - 0.248E_{Ry}^{*}$$

$$where, E_{Ry}^{*} = 13605.8 \frac{1}{\varepsilon} \left(\frac{m_{0}}{m_{e}^{*}} + \frac{m_{0}}{m_{h}^{*}}\right)^{-1}$$

Where, E_g (bulk) and E_g (QD) represent the bandgap of the bulk and confined system, respectively. The second and third terms arise due to the electron and hole confinement energy, respectively. The fourth term describes the Coulombic attraction energy between the electron and hole. The final term corresponds to exciton Rydberg energy, which arises due to spatial correction between electron and hole. The final term is generally considered negligible and becomes essential for very low dielectric constant materials. All these equations are based considering the spherical effective mass approximation of both electron and hole and the spherically symmetric confining potentials for spherical quantum dots.^{5,6} Besides spherically symmetric confining potentials, attractive Coulomb interaction is also present in these systems. Therefore, there can be two limiting possibilities depending on the ratio between the radius of the quantum dot (R) and the effective Bohr radius (a₀) of the bulk exciton. For R/a₀ greater than 1, the exciton is considered a bound quasi-particle with very low confinement energy, and such systems are called weakly confined.⁶ However, for R/a₀ less than 1, the confinement increases and the electron-hole are considered individual particles with very little spatial correction between them, and such systems are designated to be strongly quantum confined. It has been observed that the boundary of the strongconfinement regime is valid for up to about $R = 2a_0$.

An example of quantum confinement effect is shown in figure 1.1b, highlighting the tunability of bandgap of CdSe NCs with size. As NCs size decreases quantum confinement of the system increases which results blue shift in PL peak position.⁸

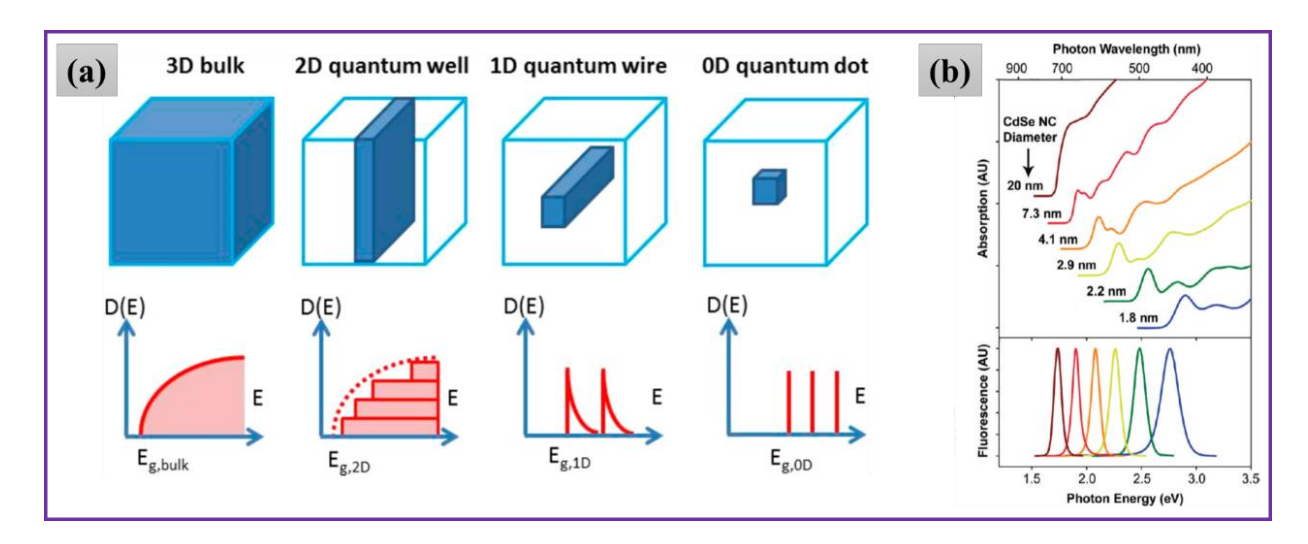


Figure 1.1. (a) Effect of quantum confinement on the bandgap and density of states of 3D, 2D, 1D and 0D systems. Adapted from ref. 7. (b) Size dependent tunable bandgap and PL intensity of CdSe QDs of different diameters. Adapted from ref. 8.

1.3. Perovskites

1.3.1. Background

Perovskite is a naturally occurring mineral of calcium titanate (CaTiO₃), discovered by German mineralogist *Gustav Rose* in 1839, and it was named after the Russian mineralogist *Lev Perovski*. Later, materials having a similar crystal structure to CaTiO₃ with general formula ABX₃ are referred to as perovskite materials. In the last few years, cesium lead halide perovskite nanocrystals (NCs) have been considered as promising materials in optoelectronic and photovoltaic applications due to their excellent optical and electronic properties.⁹ Metal halide perovskites such as CsPbX₃, Cs₄PbX₆, CsPb₂X₅ etc. (X = halides) were reported first in 1893.¹⁰ Since these perovskites are ionic crystals, studies of their photoconductivity were one of the significant focuses.^{11,12} After that, in 2009, following the landmark work by Miyasaka and co-workers, application of the lead halide perovskites as solar energy harvesters gained significant interest.¹³ So far, a power conversion efficiency (PCE) of greater than 25%¹ is reported for perovskite system. The synthesis of CsPbX₃ NCs was first reported by Kovalenko and co-workers in 2015 and they achieved high photoluminescence quantum yield (PLOY) ~50-90% for these NCs.⁹ The high PL of these

perovskite NCs make them potential candidates in application of display devices and light emitting diodes (LEDs).¹⁴ Ease of synthesis of these colloidal NCs generated considerable interest among the material scientists and till date a huge number of papers published on various aspects of synthesis.¹⁵ Perovskite NCs exhibit excellent optical properties, such as large absorption coefficient, long carrier mobility, bandgap tunability, and high defect tolerance, which make them potential candidate for several optoelectronic applications.^{14–17}

1.3.2. Crystal Structure

In ABX₃, A cation size is bigger than the B cation, and X is the halide anion. In general, the B cation is octahedrally coordinated in the BX_6^{4-} unit, and at the void of the cubic unit, the A cation sits (Figure 1.2a). Our focus is on APbX₃ types of perovskites NCs (with A = Cs⁺, MA⁺ (CH₃NH₃⁺), FA⁺ (CH (NH₂) + etc., B = Pb²⁺ etc., and X = Cl⁻, Br⁻, Γ) and we have discussed all these systems in this thesis work. The crystal structure of the NCs depends on the size of the constituting ions; for example, if we vary the size of the X anions, the crystal structure also changes, and some distortion is introduced in the structure.

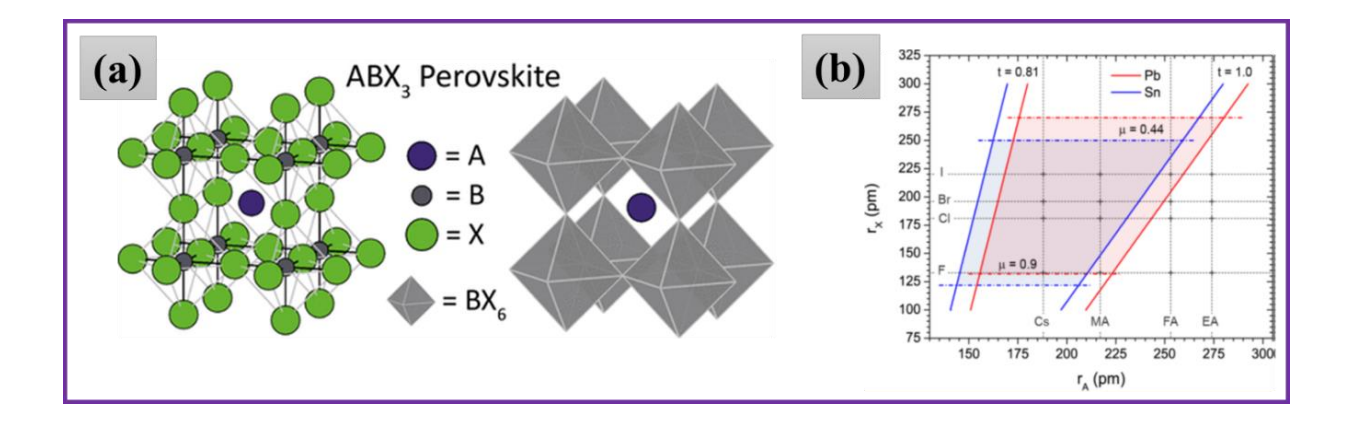


Figure 1.2. (a) Schematic representation of the cubic structure of the perovskite NCs. Adapted from ref. 18. (b) Formability of 3D lead and tin halide perovskites as a function of the radii of Asite cation and halide anion. The dashed and solid lines show the bounds of the octahedral and tolerance factors, respectively. Adapted from ref. 16.

The A cation also plays a crucial role in perovskite formability. A larger long chain organic cation can interfere in the 3D network of the perovskite structure and leads to the formation of layered perovskites. ²⁰ The Goldschmidt tolerance factor (t) and octahedral factor (μ) define the formability of the 3D perovskite structure which are expressed as

$$t = \frac{r_A + r_X}{\sqrt{2}(r_B + r_X)}; \qquad \mu = \frac{r_B}{r_{AX}}$$

Where r_A , r_B and r_X denote the ionic radii of the A, B cations and X anion, respectively. For the favourable perovskite structure, the values of the tolerance factor and octahedral factor should be in the range of $0.81 \le t \le 1.0$ and $0.44 \le \mu \le 0.9$, respectively. The formability of halide perovskite can be predicted using the chart (Figure 1.2b). The shaded region corresponds to the favoured perovskite structure.

1.3.3. Surface Properties of Perovskite Nanocrystals

In nano-dimension, the optical properties of the perovskite NCs are very sensitive to the surface. The NCs are generally passivated by long chain alkyl ligands, which play important role in maintaining their crystal integrity. ^{15,21} These materials are susceptible to the surface defects due to the high surface-to-volume ratio indicating more numbers of atoms present on the NCs surface. In case of perovskite NCs long-chain ligands such as oleylamine (OLA) and oleic acid (OA) play important role in stabilizing the NCs and formation of homogeneous colloidal dispersion thus aggregation is avoided. These ligands also passivate the surface traps, which arise from the dangling orbitals in the NCs. ²¹ Theoretical and experimental studies show insight into their binding nature. ²² The OLA⁺ cation substitutes the Cs⁺ cation and stabilizes the NCs because of the interaction of -NH₃⁺ group with Br⁻ through H-bonding at the NCs surface. ²² However, binding of these ligands is highly dynamic in nature and this is detrimental to the NCs stability (Figure 1.4a). ^{21,23,24} The facile protonation and deprotonation of these ligands lead to dynamic equilibrium, which facilitates the desorption of surface-bound capping ligands, thus creating under-coordinated lead ion on the surface and forming inter-bandgap trap states. ^{24,25} Since, the exciton binding energy of these NCs is low and the exciton readily form free carriers at room temperature (RT), which

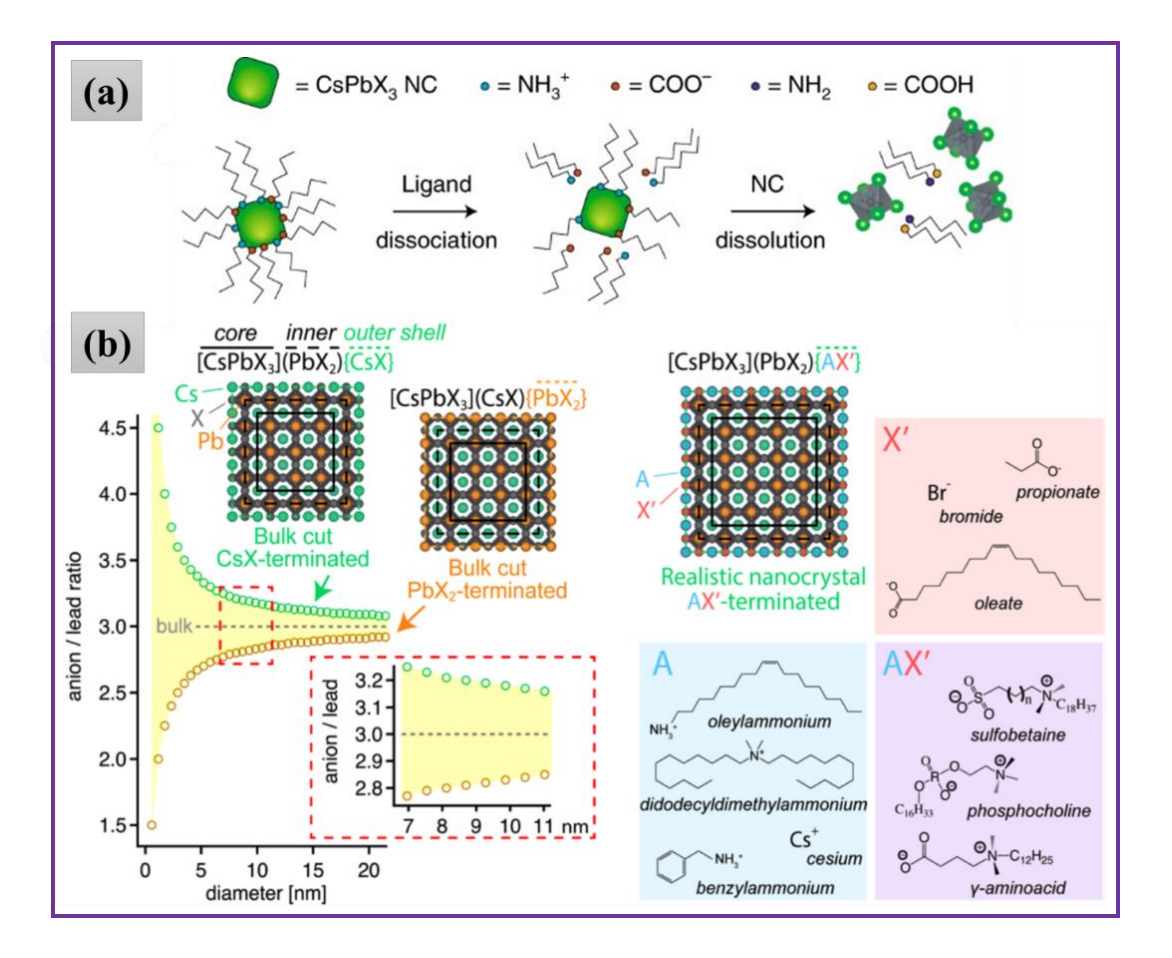


Figure 1.4. (a) Schematic representation showing the lead halide perovskite NCs lose their colloidal stability and structural integrity due to desorption of weakly bound surface ligands. Adapted from ref. 23. (b) Models showing the surface stoichiometry of CsPbX₃ NCs. Adapted from ref. 28.

undergo rapid nonradiative recombination through inter-bandgap surface trap states and decrease the photoluminescence quantum yield (PLQY).^{9,24} The PL properties are also very sensitive to the external factors. When exposing them to moisture, water and heat, the materials' PLQY and stability decrease. Recent studies suggest that some alternative capping ligands have much better binding interaction with these NCs surface and improve the optoelectronic properties of the NCs. In this regard, researchers have found that the zwitterionic capping ligands are very useful.^{26,27}

The binding of surface capping ligand depends on the stoichiometry of the NCs.²⁸ There can be two possibilities of the surface termination, [CsX] or [PbX₂]. However, the former is thermodynamically more favourable than later. As ligands bind to the surface of the CsPbX₃ NCs realistically [PbX₂] termination can be represented as [CsPbX₃] (PbX₂) (AX'), where AX' is the capping ligand and 'A' is the monovalent alkylammonium and/or Cs⁺ cation, whereas X' is monovalent halide and/or oleate anion (Figure 1.4b).²⁸

1.3.4. Optical Properties of CsPbX₃ Perovskite Nanocrystals

Optical absorption and emission spectra of colloidal CsPbX₃ NCs can be tuned over the entire visible spectral region by adjusting their composition (ratio of halides in mixed halide NCs) and particle size (quantum-size effects) (Figure 1.5).⁹ The exchange of halides can also be possible post-synthetically at room temperature. The PLQY of these NCs ranges from 1-100%. Among them, red-emitting CsPbI₃ was reported having near-unity absolute quantum yield, green-emitting

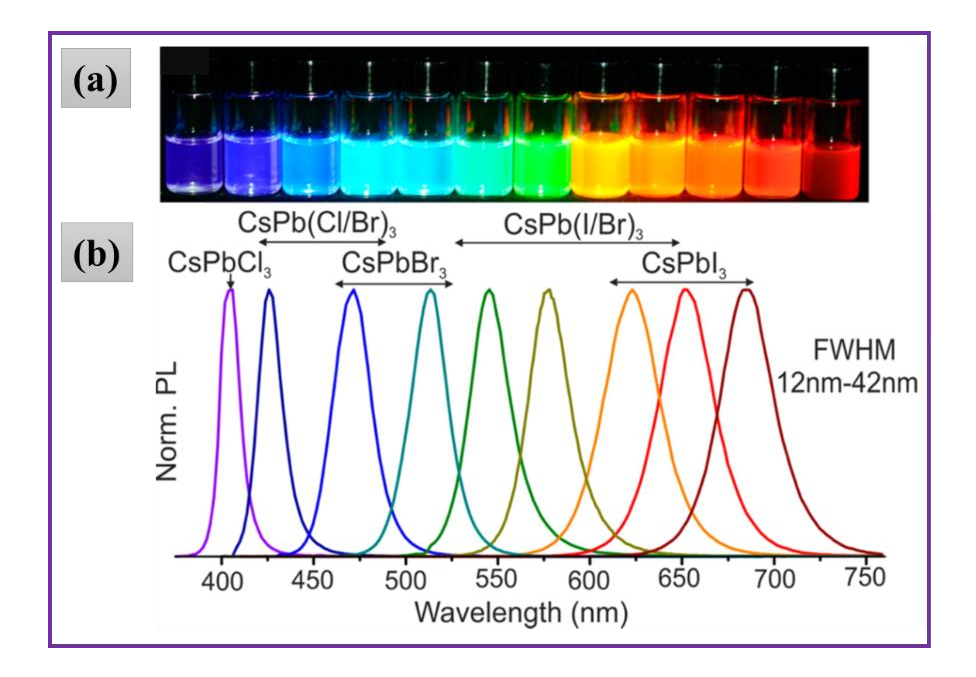


Figure 1.5. (a) Colloidal solution of CsPbX₃ NCs in toluene under 365 nm UV lamp (b) PL spectra of size- and halides composition-tunable bandgap of perovskite NCs. Adapted from ref. 9.

CsPbBr₃ typically showed PLQY in the range 60–80%, and for the high-energy blue emitting CsPbCl₃ NCs, the PLQY is mostly remained in the low range (1-10%).¹⁵ The variation in the number/density of trap is responsible for such large variation in the PLQY. However, several Insitu and post-synthetic strategies are available for improving the PLQY of blue-, green- and redemitting perovskites upto near unity.^{27,29,30}

1.3.5. Trap States in Perovskites Nanocrystals

In lead-halide perovskite (CsPbX₃), the valence band (VB) is formed by the Pb-6s and X-np orbitals and the conduction band (CB) is formed by the Pb-6p orbitals, giving an s-like and p-like symmetry, respectively.³¹ Perovskite materials contain anti-bonding and non-boding orbitals in the VB and CB (Figure 1.6a).³² This particular property of band structure makes them defect-tolerant. However, perovskite NCs are not completely free from surface defects.²³ Even though oleic acid and oleylamine are widely used as capping ligands for protecting and passivating the surface of the NCs, the environment of the capping ligands around the surface of the NCs is highly dynamic in nature.^{21,24} Due to weak binding of these ligands the surface of the NCs frequently gets uncapped

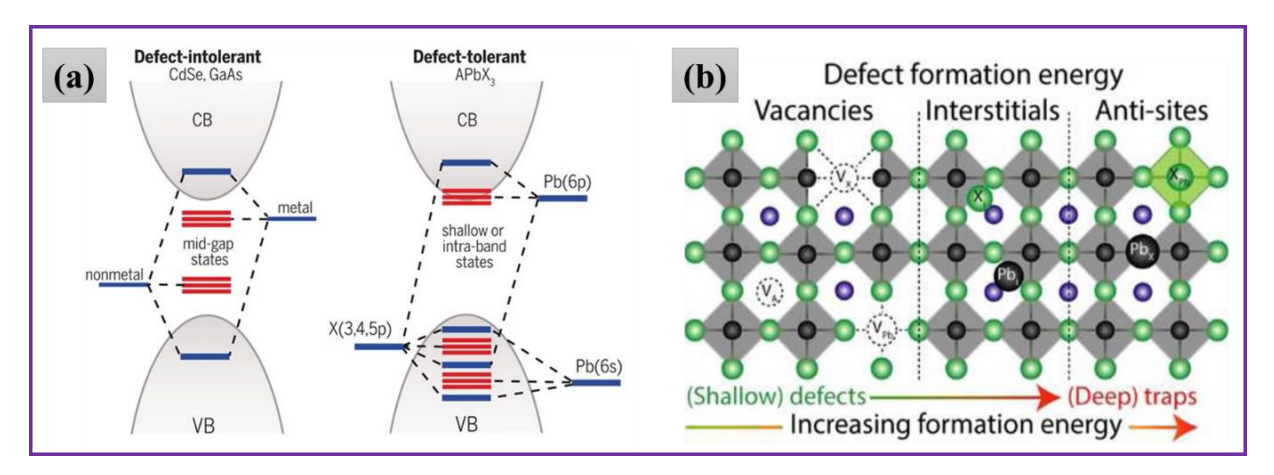


Figure 1.6. Schematics comparison of the electronic structures for defect-intolerant conventional semiconductor and defect-tolerant perovskites. Adapted from ref. 32. (b) Types of defects in perovskite NCs with increasing their formation energy and depths in the bandgap. Adapted from ref. 23.

and introduces defect states.^{24,25,33} Low defect formation energy of these materials also facilitates formation of defects in their crystal structure. Specifically, halide vacancies play a significant role in forming trap states, and thus have detrimental effect on PL properties.²³ While the trap states formed by these defects are energetically shallow for the green/red-emitting CsPbBr₃/CsPbI₃ NCs, but deep in nature for the blue-emitting CsPb(Cl/Br)₃ NCs. The latter exhibits poor optical properties with PLQY in a range of ~1–15%.³⁴ The trap states also can be formed when the ion occupies an interstitial or anti-site position of perovskites (Figure 1.6b).²³

As perovskite NCs are ionic crystals, the dynamic lattice disorder also creates defects. The size of each constituent of the perovskite NCs plays an important role on stability of these NCs. For example, the CsPbI₃ NCs always face structure instability because big-size iodide ions form tilted PbI₆⁴⁻ octahedral unit,¹⁹ which is responsible for phase change from red-emitting perovskite phase to non-emitting non-perovskite. Such kinds of distortion also leads to formation of the shallow trap states within the bandgap. The organic perovskites NCs (MAPbBr₃ and FAPbBr₃) show high PLQY, but the FA-based system is more stable than MA because of low formation energy.

1.3.6. Motivation of the Thesis Work

In nano-dimension, the PL properties of the CsPbX₃ (Cl, Br, I) perovskites are very sensitive to the nature of the surface due to high surface-to-volume ratio. In fact, sub-unity PLQY and instability of the colloidal solutions of these NCs demonstrate the surface defects in these systems. Maintaining the fragile organic-inorganic interfaces of the NCs continues to remain as a difficult exercise. Although oleic acid (OA) and oleylamine (OLA) are commonly used as capping ligands for protecting and passivating the surface of the NCs, but these are highly dynamic in nature. Facile protonation and deprotonation of these ligands lead to a dynamic equilibrium, which assists desorption of surface-bound capping ligand shell during isolation and purification of the colloidal NCs (creating uncoordinated Pb²⁺ on the NCs surface), resulting in a loss of colloidal stability and decrease in PLQY. This eventually also contributes to the loss of structural integrity of the NCs often resulting in bulk polycrystalline materials. Excess lead from lead-rich (or halide-deficient) surface creates deep or shallow inter-bandgap energy levels, which trap the charge carriers and

decrease the PLQY of the NCs. The inefficient surface passivation leads to the formation defect states, which facilitate nonradiative relaxation of the photoexcited NCs. Hence, a judicious choice of the capping ligands is one of the most effective approaches for surface passivation of the NCs. Towards this goal, herein, we explore how sulfur-containing small inorganic molecules (sodium thiosulfate and thioacetamide) influences the stability and PL efficiency of the blue-emitting CsPb(Cl/Br)₃, green-emitting CsPbBr₃, and yellow-emitting CsPbBr_{1.5}I_{1.5} perovskite NCs. Having found that these post-synthetic treatments are not quite effective for violet-emitting CsPbCl₃ and red-emitting CsPbI₃ NCs, we have introduced a bidentate ligand, ethylenediammonium dihalide (EDAX₂) for preparation of phase-pure, monodispersed, stable and highly luminescent CsPbCl₃ and CsPbI₃ NCs. The results indeed show that this ligand is very effective for the preparation of high quality CsPbBr₃, CsPb(Br/Cl)₃ and CsPb(Br/I)₃ NCs.

References

- (1) Alta, F. Best Research-Cell Efficiencies. *Nrel* **2023**, 1.
- (2) Peter Y. Yu, M. cardona. Fundamental of Semiconductors: Physics and Materials Properties.; *Springer*, **2010**.
- (3) Brian Henderson, G. F. I. Optical Spectroscopy of Inorganic Solids.; *Clarendon Press, Oxford*, **1989**.
- (4) Gaponenko, S. V. Introduction to Nanophotonics.; Cambridge University Press, 2010.
- (5) Kayanuma, Y. Quantum-Size Effects of Interacting Electrons and Holes in Semiconductor Microcrystals with Spherical Shape. *Phys. Rev. B* **1988**, *38*, 9797–9805.
- (6) G. T. Einevoll. Confinement of Excitons in Quantum Dots. *Phys. Rev. B* **1992**, *45*, 3410–3417.
- (7) Katan, C.; Mercier, N.; Even, J. Quantum and Dielectric Confinement Effects in Lower-

- Dimensional Hybrid Perovskite Semiconductors. *Chem. Rev.* **2019**, *119*, 3140–3192.
- (8) Smith, A. M.; Nie, S. Semiconductor Nanocrystals: Structure, Properties, and Band Gap Engineering. *Acc. Chem. Res.* **2010**, *43*, 190–200.
- (9) Protesescu, L.; Yakunin, S.; Bodnarchuk, M. I.; Krieg, F.; Caputo, R.; Hendon, C. H.; Yang, R. X.; Walsh, A.; Kovalenko, M. V. Nanocrystals of Cesium Lead Halide Perovskites (CsPbX₃, X = Cl, Br, and I): Novel Optoelectronic Materials Showing Bright Emission with Wide Color Gamut. *Nano Lett.* 2015, 15, 3692–3696.
- (10) H. L. Wells. Über Die Cäsium- Und Kalium-Bleihalogenide. *Zeitschrift für Anorg. Chemie* **1893**, *3*, 195–210.
- (11) Møller, C. K. A Phase Transition in Cæsium Plumbochloride. *Nature* **1957**, *180*, 981–982.
- (12) MØLLER, C. K. Crystal Structure and Photoconductivity of Cæsium Plumbohalides. *Nature* **1958**, *182*, 131.
- (13) Kojima, A.; Teshima, K.; Shirai, Y.; Miyasaka, T. Organometal Halide Perovskites as Visible-Light Sensitizers for Photovoltaic Cells. *J. Am. Chem. Soc.* **2009**, *131*, 6050–6051.
- (14) Van Le, Q.; Jang, H. W.; Kim, S. Y. Recent Advances toward High-Efficiency Halide Perovskite Light-Emitting Diodes: Review and Perspective. *Small Methods*. **2018**, 2, 1700419.
- (15) Shamsi, J.; Urban, A. S.; Imran, M.; De Trizio, L.; Manna, L. Metal Halide Perovskite Nanocrystals: Synthesis, Post-Synthesis Modifications, and Their Optical Properties. *Chem. Rev.* 2019, 119, 3296–3348.
- (16) Manser, J. S.; Christians, J. A.; Kamat, P. V. Intriguing Optoelectronic Properties of Metal Halide Perovskites. *Chem. Rev.* **2016**, *116*, 12956–13008.
- (17) Zhou, Y.; Chen, J.; Bakr, O. M.; Sun, H. T. Metal-Doped Lead Halide Perovskites: Synthesis, Properties, and Optoelectronic Applications. *Chem. Mater.* **2018**, *30*, 6589–6613.

(18) Akkerman, Q. A.; Manna, L. What Defines a Halide Perovskite? *ACS Energy Lett.* **2020**, 5, 604–610.

- (19) Abhishek Swarnkar, Wasim J. Mir, A. N. Can B- Site Doping or Alloying Improve Thermal- and Phase-Stability of All-Inorganic CsPbX₃ (X = Cl, Br, I) Perovskites? *ACS Energy Lett.* **2018**, 3, 286–289.
- (20) Mitzi, D. B. Templating and Structural Engineering in Organic-Inorganic Perovskites. *J. Chem. Soc. Dalt. Trans.* **2001**, 1–12.
- (21) Seth, S.; Ahmed, T.; De, A.; Samanta, A. Tackling the Defects, Stability, and Photoluminescence of CsPbX₃ Perovskite Nanocrystals. *ACS Energy Lett.* **2019**, *4*, 1610–1618.
- (22) Ravi, V. K.; Santra, P. K.; Joshi, N.; Chugh, J.; Singh, S. K.; Ghosh, P.; Nag, A. Origin of the Substitution Mechanism for the Binding of Organic Ligands on the Surface of CsPbBr₃ Perovskite Nanocubes. *J. Phys. Chem. Lett.* **2017**, *8*, 4988–4994.
- (23) Akkerman, Q. A.; Rainò, G.; Kovalenko, M. V.; Manna, L. Genesis, Challenges and Opportunities for Colloidal Lead Halide Perovskite Nanocrystals. *Nat. Mater.* **2018**, *17*, 394–405.
- (24) De Roo, J.; Ibáñez, M.; Geiregat, P.; Nedelcu, G.; Walravens, W.; Maes, J.; Martins, J. C.; Van Driessche, I.; Kovalenko, M. V.; Hens, Z. Highly Dynamic Ligand Binding and Light Absorption Coefficient of Cesium Lead Bromide Perovskite Nanocrystals. *ACS Nano* **2016**, *10*, 2071–2081.
- (25) Syed Akhil, V. G. Vasavi Dutt, N. M. Completely Amine-Free Open-Atmospheric Synthesis of High-Quality Cesium Lead Bromide (CsPbBr₃) Perovskite Nanocrystals. *Chem. Eur. J.* **2020**, 26, 17195–17202.
- (26) Krieg, F.; Ochsenbein, S. T.; Yakunin, S.; Ten Brinck, S.; Aellen, P.; Süess, A.; Clerc, B.; Guggisberg, D.; Nazarenko, O.; Shynkarenko, Y.; Kumar, S.; Shih, C. J.; Infante, I.;

- Kovalenko, M. V. Colloidal CsPbX₃ (X = Cl, Br, I) Nanocrystals 2.0: Zwitterionic Capping Ligands for Improved Durability and Stability. *ACS Energy Lett.* **2018**, *3*, 641–646.
- (27) Pan, J.; Shang, Y.; Yin, J.; De Bastiani, M.; Peng, W.; Dursun, I.; Sinatra, L.; El-Zohry, A. M.; Hedhili, M. N.; Emwas, A. H.; Mohammed, O. F.; Ning, Z.; Bakr, O. M. Bidentate Ligand-Passivated CsPbI₃ Perovskite Nanocrystals for Stable Near-Unity Photoluminescence Quantum Yield and Efficient Red Light-Emitting Diodes. *J. Am. Chem. Soc.* **2018**, *140*, 562–565.
- (28) Bodnarchuk, M. I.; Boehme, S. C.; Ten Brinck, S.; Bernasconi, C.; Shynkarenko, Y.; Krieg, F.; Widmer, R.; Aeschlimann, B.; Günther, D.; Kovalenko, M. V.; Infante, I. Rationalizing and Controlling the Surface Structure and Electronic Passivation of Cesium Lead Halide Nanocrystals. *ACS Energy Lett.* **2019**, *4*, 63–74.
- (29) Mondal, N.; De, A.; Samanta, A. Achieving Near-Unity Photoluminescence Efficiency for Blue-Violet-Emitting Perovskite Nanocrystals. *ACS Energy Lett.* **2019**, *4*, 32–39.
- (30) Gautam, R. K.; Das, S.; Samanta, A. Can Sulfur-Containing Small Systems Enhance the Photoluminescence and Stability of the Blue-, Green- And Yellow-Emitting Perovskite Nanocrystals? A Case Study with Sodium Thiosulfate. *J. Phys. Chem. C* **2021**, *125*, 24170–24179.
- (31) Becker, M. A.; Vaxenburg, R.; Nedelcu, G.; Sercel, P. C.; Shabaev, A.; Mehl, M. J.; Michopoulos, J. G.; Lambrakos, S. G.; Bernstein, N.; Lyons, J. L.; Stöferle, T.; Mahrt, R. F.; Kovalenko, M. V.; Norris, D. J.; Rainò, G.; Efros, A. L. Bright Triplet Excitons in Caesium Lead Halide Perovskites. *Nature* 2018, 553, 189–193.
- (32) Kovalenko, M. V.; Protesescu, L.; Bodnarchuk, M. I. Properties and Potential Optoelectronic Applications of Lead Halide Perovskite Nanocrystals. *Science* **2017**, *358*, 745–750.
- (33) Yassitepe, Emre; Yang, Zhenyu; Voznyy, Oleksandr; Kim, Younghoon; Walters, Grant;

Castañeda, Juan Andres; Kanjanaboos, Pongsakorn; Yuan, Mingjian; Gong, Xiwen; Fan, Fengjia; Pan, Jun; Hoogland, Sjoerd; Comin, Riccardo; Bakr, Osman M.; Padilha, Lazaro A.;, A. F. . S. H. Amine-Free Synthesis of Cesium Lead Halide Perovskite Quantum Dots for Efficient Light-Emitting Diodes. *Adv. Funct. Mater.* **2016**, 26, 8757–8763.

(34) Nenon, D. P.; Pressler, K.; Kang, J.; Koscher, B. A.; Olshansky, J. H.; Osowiecki, W. T.; Koc, M. A.; Wang, L. W.; Alivisatos, A. P. Design Principles for Trap-Free CsPbX₃ Nanocrystals: Enumerating and Eliminating Surface Halide Vacancies with Softer Lewis Bases. *J. Am. Chem. Soc.* **2018**, *140*, 17760–17772.

CHAPTER 2

Materials, Methods and Instrumentation

Overview

In this chapter, details of synthesis of different materials, their characterization, instrumental techniques used for various studies are presented. Sources of chemicals used post-synthetic methodologies and purification of the perovskite NCs used for our studies are detailed. The instrumental details and basic principles of time-correlated single photon counting technique, spectrofluorimeter and UV-Vis spectrophotometer are discussed. The basic principles of femtosecond transient absorption measurements are outlined. Finally, we provided details of various instruments (XPS, EDX, PXRD, TEM, FT-IR etc.) used for characterization of these materials and PLQY measurements.

2.1. Materials

Cesium carbonate (Cs₂CO₃, 99.99%), 1-octadecene (ODE, 90%), oleic acid (OA, 90%), oleylamine (OLA, technical grade 70%), tri-octyl phosphine (TOP, 97%), PbCl₂ (99.99%), PbBr₂ (99.99%), PbI₂ (99%), and methyl acetate (MeOAc, anhydrous, 99.5%), sodium thiosulfate pentahydrate (Na₂S₂O₃.5H₂O, >99%), thioacetamide (TAA, ACS reagent, >99%), ethylenediammonium dichloride (EDACl₂, \geq 99%), ethane-1,2-diammonium bromide (EDABr₂, \geq 98%) and ethylenediammonium diiodide (EDAI₂, 99%) were purchased from Sigma-Aldrich. Toluene and hexane were purchased from Finar Chemicals. Toluene was distilled following standard procedure, and the remaining chemicals were used without further purification.

2.2. Methods of Synthesis

2.2.1. Synthesis of $CsPbX_3$ (X = Cl, Br and I) Perovskites NCs

The synthesis of the NCs consisted of two steps: the first step was preparation of cesium-oleate (Cs-oleate) and the second one was the synthesis of the NC.

Step 1. Preparation of Cs-oleate: The stock solution of Cs-oleate was prepared by following a reported method with minor modifications.¹ 0.102 g of Cs₂CO₃, 0.5 mL of OA and 5 mL of ODE were loaded into a 50 mL double-necked round bottle (RB) flask. This solution was dried for 1 h at 120°C under vacuum and then heated to 140 °C until completely dissolved Cs₂CO₃. The Cs-oleate solution was pre-heated at 120°C before every use to avoid precipitation at RT.

Step 2. Preparation of CsPbX3 NCs: All CsPbX3 NCs were prepared by following conventional hot-injection method.¹ In another 50 mL RB, PbX₂ (0.188 mmol) such as PbCl₂ (0.052 g, for CsPbCl₃ NCs), PbBr₂ (0.069 g for CsPbBr₃ NCs), PbI₂ (0.087 g for CsPbI₃ NCs) (or their mixtures used for mixed halides synthesis), 5 mL of ODE, 0.5 mL of OLA and 0.5 mL OA were mixed and heated under vacuum at 120°C for 1 h. After complete solubilization of PbX₂ salts, the temperature of the solution subsequently increased to 160°C under N₂ conditions. Once the reaction attained the 160°C temperature, pre-heated 0.5 mL Cs-oleate solution was quickly injected; 5s later, the reaction mixture was cooled by the ice-water bath (Figure 2.1). For CsPbCl₃ NCs, 1 mL of TOP was injected at 150°C for complete solubilization

of the PbCl₂ salt, then injected Cs-oleate at 170°C and cooled after 1 min. Then, the synthesized NCs were separated from the crude reaction mixture through centrifugation at 7600 rpm for 8 min. The supernatant containing solvent (ODE), unreacted salts, and excess ligands was discarded. The precipitate was dispersed in 2-3 mL of a non-polar solvent such as toluene or hexane for further studies.

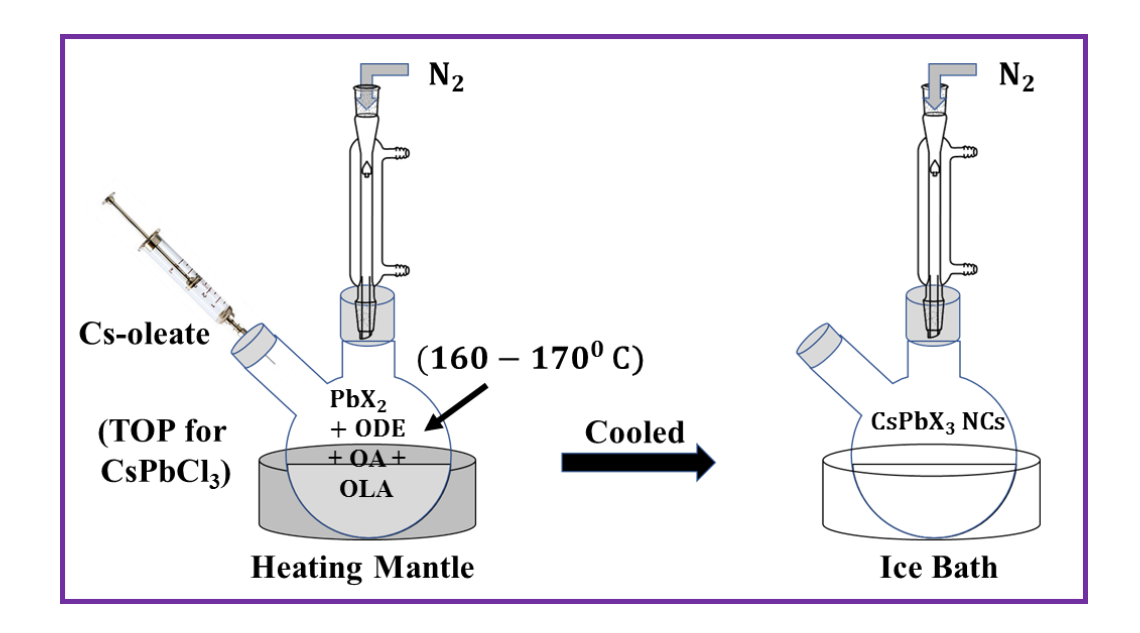


Figure 2.1. Schematic showing the hot-injection method of synthesis of colloidal CsPbX₃ perovskite NCs.

2.3. Post-synthetic Treatment of $CsPbX_3$ (X = Cl, Br and I) NCs

2.3.1. Post-synthetic Treatment with Sodium Thiosulfate: The post-synthetic treatment of the blue-, green-, and yellow-emitting CsPbX₃ NCs with sodium thiosulfate (Na₂S₂O₃·5H₂O) was performed under ambient conditions at RT.² Took \sim 2 mL of colloidal dispersion (\sim nM concentration) in toluene of the NCs in a 25 mL RB flask and magnetically stirred with sodium thiosulfate for 1 h, which was found to be the optimum time for completion of the treatment. As sodium thiosulfate has very limited solubility in nonpolar toluene, it was separated easily from the NCs dispersion through centrifugation at 3000 rpm for 3 min. The supernatant containing the NCs in toluene is called treated NCs and was used for future experiments.

2.3.2. Post-synthetic Treatment with Thioacetamide: The post-synthetic treatment of the blueand green-emitting CsPbX₃ NCs with thioacetamide (TAA) was carried out at RT under ambient conditions.³ For this purpose, ~1 mL diluted solution of the NCs (of μM concentration) in toluene was taken and stirred with solid TAA for 1 h, which was found to be the optimum time for the treatment of the NCs after which no change in the optical properties was noted. Due to the limited solubility of TAA in toluene, it was removed easily from the solution through centrifugation at 7600 rpm for 10 min. For purification purposes, the supernatant containing NCs was then mixed with methyl acetate (1:1 volume ratio) and then again centrifuged at 7000 rpm for 5 min to confirm the elimination of excess unreacted salt. The supernatant was discarded, and the precipitate of the treated NCs was dispersed in toluene for further studies.

2.4. Optical Measurements and Instrumentation

2.4.1. UV-Vis Spectrophotometer

Steady-state UV-Vis absorption spectra were measured using Cary100 (Varian) spectrophotometer, which comprises; tungsten and deuterium lamps for measurements in the visible (380-700 nm) and UV-light (180-370 nm) regions, respectively. A photomultiplier tube (PMT) served as a detector. Before actual measurements on sample, baseline correction was done to remove any contribution from the cuvette or solvent so that it cannot affect the absorption spectra of sample.

2.4.2. Spectrofluorometer

Steady-state emission spectra were measured using a spectrofluorometer (FluoroLog-3, Horiba Jobin Yvon). In this setup, a high-pressure xenon arc lamp was used as the excitation source which covered a wide illumination range (250 nm to infrared). The sample fluorescence was recorded at the right-angled position with respect to the incident light.

2.4.3. Photoluminescence Quantum Yield (PLQY) Measurement

The PLQY of the perovskite NCs was calculated by using the following equation with appropriate dye molecule as reference.

$$QY_S = QY_R \times (I_S/I_R) \times (OD_R/OD_S) \times n_S^2/n_R^2$$

Where, *OD* and *n* represent the optical density at the excitation wavelength and refractive index of the solvent, respectively. *I* represents the integrated area under the PL spectrum. *S* and *R* denote the sample (i.e., NCs) and reference compound (i.e., dye), respectively.

For the violet- and blue-emitting CsPbCl₃ and CsPb(Cl/Br)₃ NCs, 9,10-diphenylanthracene dye in toluene/hexane solution (QY = 0.93) was used.⁴ For green-emitting CsPbBr₃ NCs, coumarin 153 dye in ethanol solution (QY = 0.546) was used. For yellow- and red-emitting CsPbBr_{1.5}I_{1.5} and CsPbI₃ NCs, rhodamine 6G dye in an aqueous medium (QY = 0.95) was used.^{5,6}

2.4.4. Time-correlated Single Photon Counting (TCSPC)

TCSPC fluorescence technique (5000, Horiba Jobin Yvon IBH) was used to measure the PL decay profile of a photoexcited sample.⁷ The sample was excited with a short laser pulse (δ -pulse), and then recorded the fluorescence response as a function of time. The basic principle of a TCSPC technique is like a stop-watch; the *START* signal begins either by the photons from the excitation pulse, called forward mode or by the photons coming from the sample's fluorescence, called reverse mode. Our measurements were carried out in reverse mode. In this mode, when electrical pulse associated with the optical signal passes through the constant

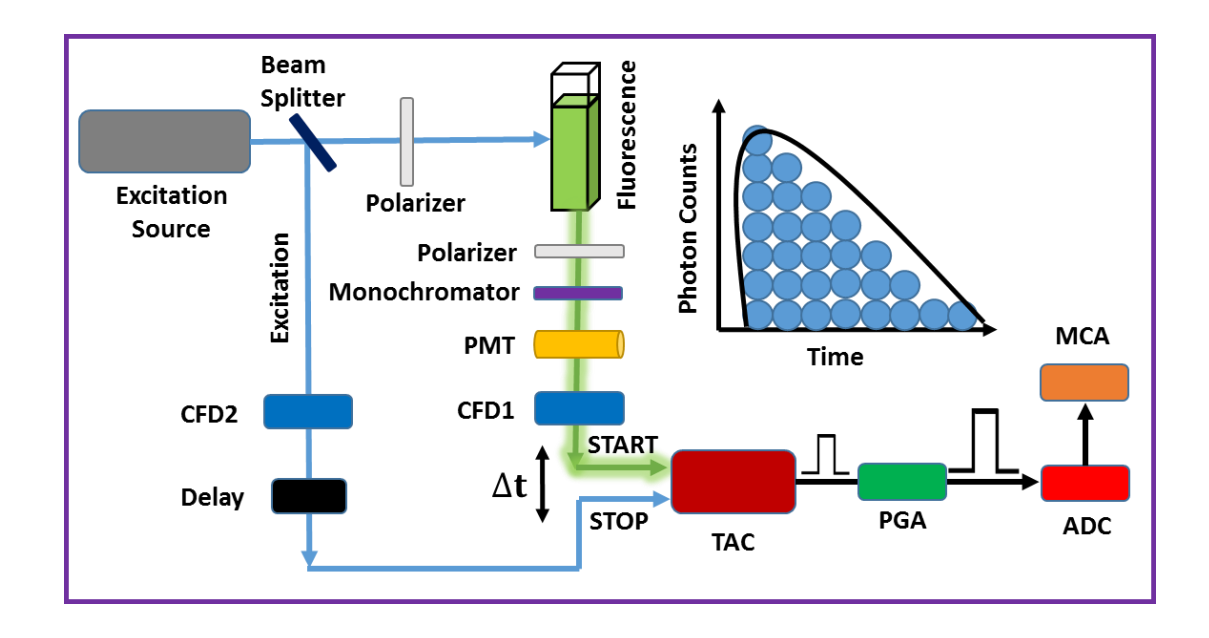


Figure 2.2. Schematic explanation of working principle of a TCSPC set-up (in reverse mode).

fraction discriminator (CFD2) to the time-to-amplitude convertor (TAC) (Figure 2.2) and photons associated with the fluorescence signal passes through a monochromator and reaches CFD1. The *START* pulse starts the charging of the capacitor in the TAC, and it continues charging until the *STOP* pulse comes. The excitation pulse passes through CFD2 and after a certain delay, reaches the TAC, then the capacitor discharges, worked as *STOP* pulse. The output of TAC is analogous to the time delay between the *STOP* and *START* pulses. The final output is amplified through a programmable gain amplifier (PGA) and converted to a digital signal by analog-to-digital convertor (ADC). The height analysis of this output is performed by MCA. Similarly, repeating this process generates a histogram of PL intensity changes over time.

Here, we used the PicoBrite laser diodes as excitation sources (375, 405 and 481 nm) with a 1MHz repetition rate. The pulse width of the laser output was measured by recording the pulse response of a dilute aqueous solution of Ludox scatter. The FWHM varied between 60-100 ps depending on the laser diode used. A micro-channel plate (MCP) photomultiplier (Hamamatsu R3809U-50) was used as a detector. The data were fitted to a non-linear least-squares iterative method using IBH DAS6 (Version 2.2) software. For a typical nth order multiexponential decay, the δ-pulse response is given as

$$I\left(t\right) = \sum_{t=1}^{n} \alpha_{i} \; exp\left(-t/\tau_{i}\right)$$

Where τ_i and α_i represent the lifetime and amplitude of the i^{th} component, respectively.

2.4.5. Femtosecond Transient Absorption (fs-TA) Spectroscopy

Principle

TA spectroscopy is a pump-probe spectroscopy, which is one of the useful techniques for ultrafast time-resolved studies.^{8,9} In this technique, the sample is photo-excited with a pump laser pulse to generate the transient species, which is monitored by a broad-band white probe pulse, that comes after a certain delay time (Figure 2.3).¹⁰ By varying the pump-probe delay we can measure the transient spectra and temporal evolution of the transient species.¹⁰

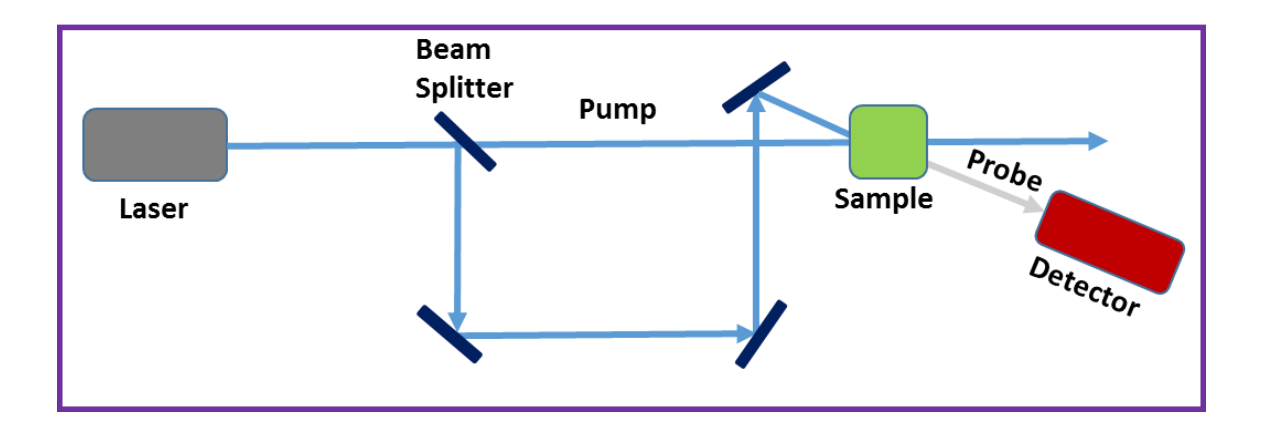


Figure 2.3. Basic working principle of TA measurement technique.

When pump is in play then the probe records the absorbance of the photo-excited species and to record the absorbance of unexcited species, pump beam is blocked by an external chopper. The transmitted intensity of the probe beam is used to calculate the differential absorbance (ΔA) i.e., absorbance during pump-on minus pump-off of the sample. Mathematically, ΔA is expressed as 10

$$\Delta A (\lambda, t) = A_{pump-on} - A_{pump-off} = A_{ex}(\lambda, t) - A_{gs}(\lambda)$$

$$\Delta A(\lambda,t) = log \frac{I_{0,ex}(\lambda)}{I_{ex}(\lambda,t)} - log \frac{I_{0,gs}(\lambda)}{I_{gs}(\lambda)} = log \frac{I_{gs}(\lambda)}{I_{ex}(\lambda,t)}$$

Where, A_{gs} and A_{ex} are the absorbance of the ground state and excited state species, respectively. I_0 and I are the intensity of the incident and transmitted light, respectively.

TA spectrum can consist of several features as shown in Figure 2.4. But the general characteristic signals are associated with ground state bleach, excited state absorption and stimulated emission.¹⁰ Which are explain as,

(i) Ground state bleach (GSB): when the system has ground state absorption then GSB signal appears as a negative signal in TA spectra region. Here, the pump pulse boosts a fraction of the

population of the sample to an excited state and the probe pulse experiences a lower population in the ground state. Hence, more light is transmitted for the excited sample compared to the unexcited one explaining a negative ΔA value in the spectral region of the ground-state absorption (Figure 2.4).

- (ii) Excited state absorption (ESA): When a system is populated in excited state, the broadband probe pulse can promote some of them to higher allowed states. In such case, the transmitted intensity associated with that wavelength of the probe pulse will be decreased for the excited species as compared to the unexcited species. Hence, absorbance is increased therefore, ΔA appears as a positive signal (Figure 2.4). Although the generation of new transient species by photoexcitation and if it has any characteristic absorption feature then ΔA will also appear as a positive signal in the TA measurement.¹⁰
- (iii) Stimulated emission (SE): Through photoexcitation by a pump-pulse, when the probe pulse passes through the excited state species, it can depopulate some of the excited species to

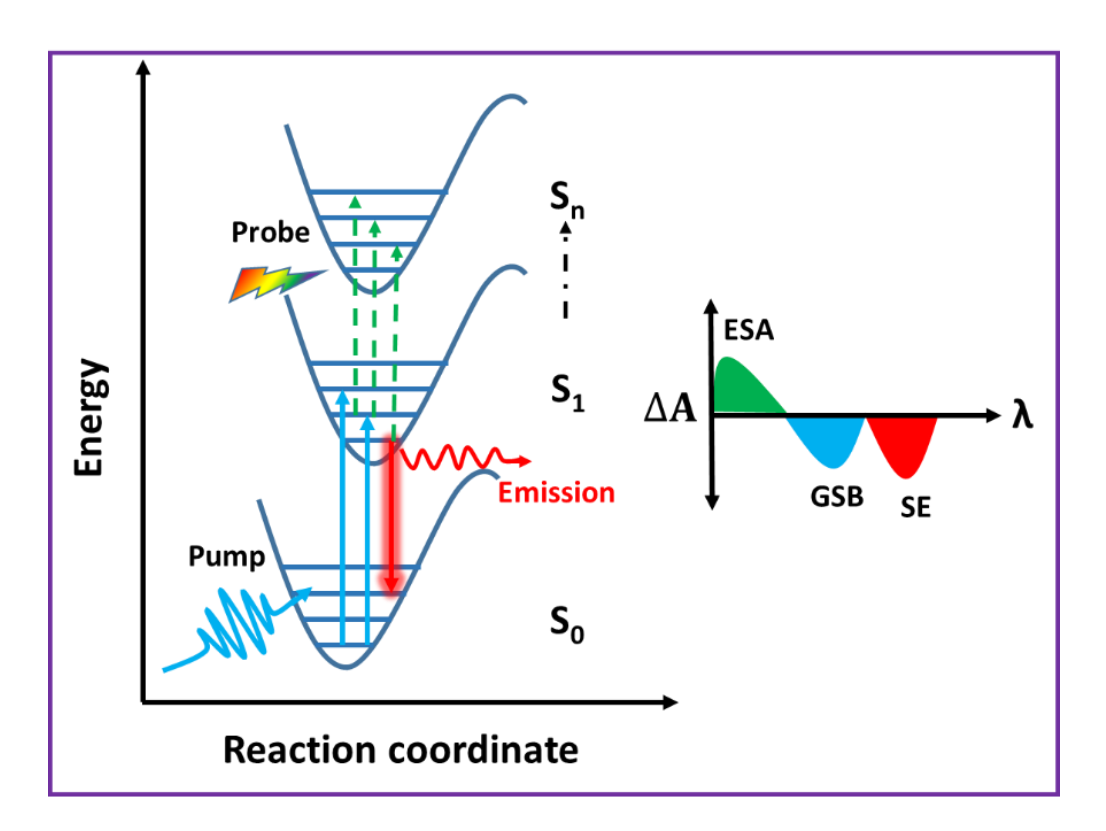


Figure 2.4. A Sketch of the various processes measured by the pump-probe technique. In right side, the ΔA vs wavelength plot shows the different signal features.

the ground state and emit photons. The detector then detects more transmitted light compared to the unexcited molecule. Hence, ΔA appears as a negative signal (Figure 2.4). In such cases where the Stokes shift is very small, spectral difference between GSB signal and SE emission can be difficult to determine and the overall feature appears as a broad negative signal.

TA Measurement

The setup consisted of a mode-locked Ti:sapphire seed laser (Mai Tai, Spectra Physics) operating at 80 MHz repetition rate with an output centering at 800 nm, which was directed to a Ti:sapphire regenerative amplifier (Spitfire Ace, Spectra Physics). A high power Q-switched laser (Empower, Spectra Physics) was used for pumping the amplifier. The amplified output of 800 nm (4.2 W) operating at 1 KHz repetition rate was divided into two parts: The major part of the beam (3 W) was directed toward the optical parametric amplifier (Topas-Prime, Spectra Physics) to generate the excitation wavelength used here. The remaining part of the amplified beam was passed through an optical delay line of ~4 ns followed by a rotating CaF₂

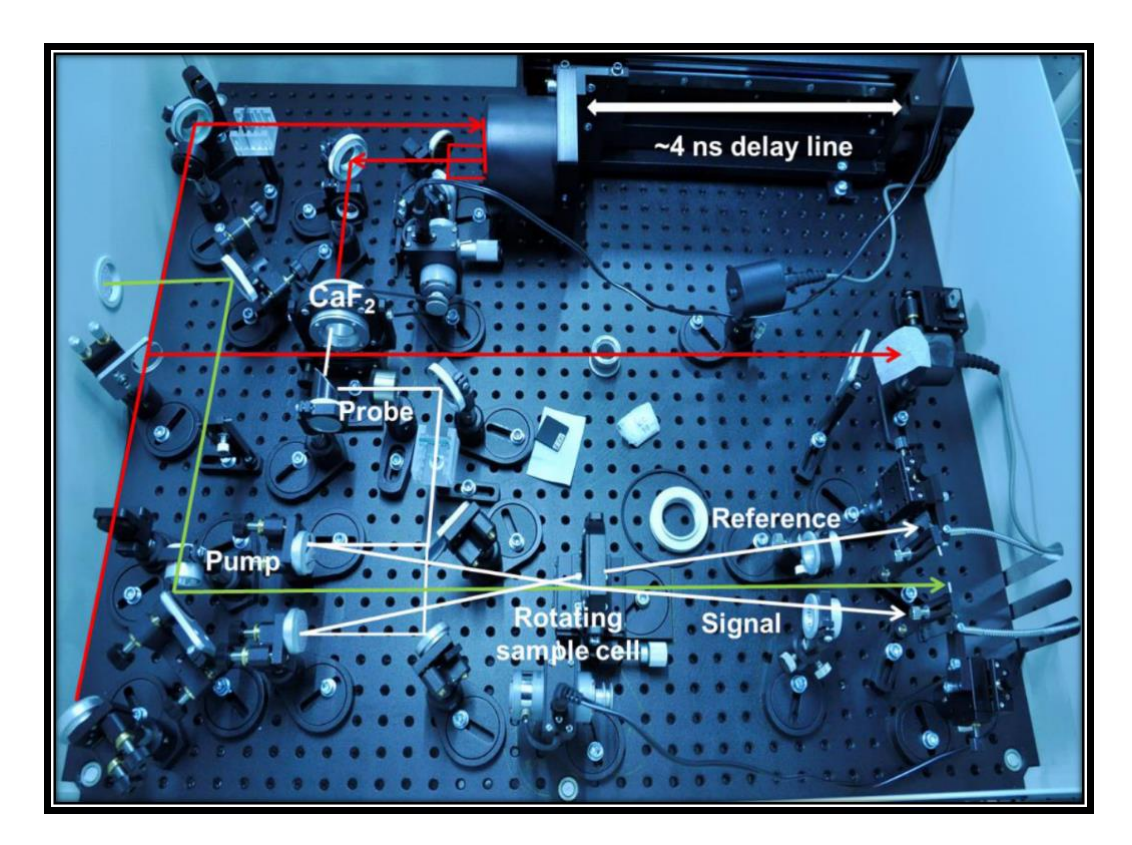


Figure 2.5. Different components and optical layout of the spectrometer of the pump-probe setup used in our study. Adapted from ref. 9.

crystal to generate white light (350-850 nm) continuum (Figure 2.5). The white light was passed through a beam splitter to generate a signal and reference beam and was directed to the detector (photodiode array) through a fiber coupling unit to record the pump induced changes at different delay times of the probe beam. All measurements were performed under very low excitation densities (4–5 μ J/cm²) to avoid any nonlinear interaction. All spectra presented here were chirp-corrected, and the instrumental resolution was ~120 fs.

2.5. Other Instrumental Measurements

Powder X-ray diffraction (PXRD): PXRD patterns of the thin-films of the sample were measured by a Bruker D8 Advance Diffractometer (Bruker-AXS, Karlsruhe, Germany) using Cu-K α X-radiation (λ = 1.5406 Å) at 40 kV and 30 mA power. The samples were prepared by drop-casting colloidal dispersion of NCs onto thin glass plate.

Transmission electron microscopy (TEM): The TEM images of the NCs were measured using JEM-F200 transmission electron microscope (JEOL) at an accelerating voltage of 200 kV. The samples for TEM measurements were prepared by drop-casting a dilute solution of NCs on a carbon-coated Cu-grid and all samples were kept in high vacuum for 24 h before measurement.

Fourier transformed infrared spectroscopy (FTIR): FTIR measurements were performed using a Bruker Tensor II spectrometer. A drop-casted colloidal solution of NCs was used for the measurement.

Field-emission scanning electron microscopy (**FESEM**): FESEM images were recorded using a Carl Zeiss Ultra 55 microscope. Energy dispersive X-ray (EDX) spectra and elemental mapping measurements were recorded using Oxford Instruments X-Max^N SDD (50 mm²) system and INCA analysis software. Samples for the FESEM measurement were prepared by drop-casting of colloidal solutions on thin glass plate, followed by drying under vacuum for 12 h before measurement.

X-ray photoelectron spectroscopy (XPS): XPS measurements were performed using Thermo Scientific K-Alpha+ spectrometer. Micro-focused monochromatic X-ray source was generated at 70 W with a spot size of 400 μ m. The energy resolution of the spectrometer was set at 0.5 eV at a pass energy of 50 eV. The base pressure of the chamber was maintained at 5×10^{-10} Torr during the analysis. Low energy electrons from the flood gun were used for charge

compensation. The XPS samples were also prepared by drop-casting an optimum concentration of the NCs solution onto a thin glass plate.

References

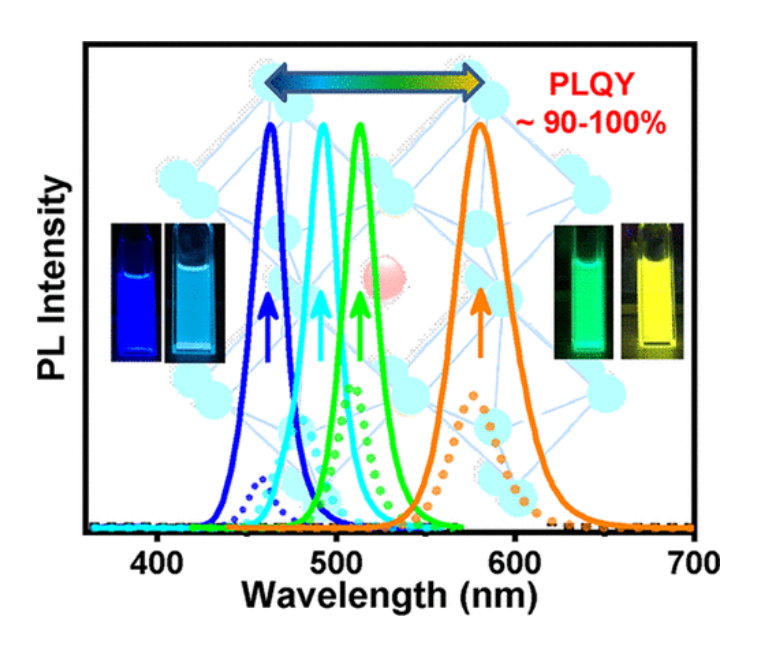
- (1) Protesescu, L.; Yakunin, S.; Bodnarchuk, M. I.; Krieg, F.; Caputo, R.; Hendon, C. H.; Yang, R. X.; Walsh, A.; Kovalenko, M. V. Nanocrystals of Cesium Lead Halide Perovskites (CsPbX₃, X = Cl, Br, and I): Novel Optoelectronic Materials Showing Bright Emission with Wide Color Gamut. *Nano Lett.* **2015**, *15*, 3692–3696.
- (2) Gautam, R. K.; Das, S.; Samanta, A. Can Sulfur-Containing Small Systems Enhance the Photoluminescence and Stability of the Blue-, Green- And Yellow-Emitting Perovskite Nanocrystals? A Case Study with Sodium Thiosulfate. *J. Phys. Chem. C* **2021**, *125*, 24170–24179.
- (3) Gautam, R. K.; Das, S.; Samanta, A. Room-Temperature Treatment with Thioacetamide Yielding Blue- and Green- Emitting CsPbX₃ Perovskite Nanocrystals with Enhanced Photoluminescence Efficiency and Stability. *ChemNanoMat.* **2022**, 8, e202200029.
- (4) Maciejewski, A.; Steer, R. P. Spectral and Photophysical Properties of 9,10-Diphenylanthracene in Perfluoro-n-Hexane: The Influence of Solute-Solvent Interactions. *J. Photochem.* **1986**, *35*, 59–69.
- (5) Rurack, K.; Spieles, M. Fluorescence Quantum Yields of a Series of Red and Near-Infrared Dyes Emitting at 600-1000 Nm. *Anal. Chem.* **2011**, *83*, 1232–1242.
- (6) Kubin, R. F.; Fletcher, A. N. Fluorescence Quantum Yields of Some Rhodamine Dyes. *J. Lumin.* **1982**, *27*, 455–462.
- (7) Valeur, B.; Berberan-Santos, M. N. Molecular Fluorescence: Principles and Applications, 2nd edn.; *Wiley-VCH Verlag GmbH*, *Weinheim*, **2001**.
- (8) Berera, R.; van Grondelle, R.; Kennis, J. T. M. Ultrafast Transient Absorption Spectroscopy: Principles and Application to Photosynthetic Systems. *Photosynth. Res.*

2009, *101*, 105–118.

- (9) De, A. Ultrafast Carrier Dynamics and Charge Transfer Processes in Photoexcited Perovskite Nanocrystals, *University of Hyderabad, India*, **2020**.
- (10) Ruckebusch, C.; Sliwa, M.; Pernot, P.; de Juan, A.; Tauler, R. Comprehensive Data Analysis of Femtosecond Transient Absorption Spectra: A Review. *J. Photochem. Photobiol. C Photochem. Rev.* **2012**, *13*, 1–27.

CHAPTER 3

Can Sulfur-Containing Small Systems Enhance the Photoluminescence and Stability of the Blue-, Green- and Yellow-Emitting Perovskite Nanocrystals? A Case Study with Sodium Thiosulfate



J. Phys. Chem. C 2021, 125, 24170-24179

Overview

Cesium lead halide perovskite nanocrystals (NCs) are the most promising materials for photovoltaic and optoelectronic applications in recent years. However, lack of long-term stability and consequent deterioration of optical properties with time have been major challenges for commercialization of the perovskite-based devices. In this context, we report that even room-temperature treatment of blue-emitting CsPbCl_{1.5}Br_{1.5} and CsPbClBr₂ NCs, green-emitting CsPbBr₃ NCs, and yellow-emitting CsPbBr_{1.5}I_{1.5} NCs with sodium thiosulfate (Na₂S₂O₃·5H₂O) can not only lead to huge enhancement of the photoluminescence quantum yield (PLQY, to ~100% for the blue/green-emitting NCs and ~90% for the yellow-emitting NCs) but also add superior stability to these NCs under different environmental stresses. While the time-resolved PL and ultrafast transient absorption studies show suppression of the nonradiative recombination channels, other measurements reveal that the improved optical characteristics and stability of these substances are by the formation of Pb–S bonds between undercoordinated surface Pb and thiosulfate. The outstanding PLQY and much improved long-term stability of the treated NCs make them attractive components for perovskite-based optoelectronic applications.

3.1. Introduction

In recent years, cesium lead halide (CsPb X_3 , X = Cl, Br, and I) perovskite NCs have been receiving great attention because of their potential in photovoltaic and optoelectronic applications such as solar cells, 1,2 photodetectors, lasers, 4,5 and light-emitting diodes (LEDs) due to their excellent optical properties such as defect-tolerant nature, ⁷ large absorption coefficient, ⁸ tunable photoluminescence (PL) throughout the entire visible region, 8-10 high PLOY, 11-14 and narrow emission bandwidth (full width at half-maximum, FWHM).⁸ However, in their nanodimension, the PL properties are very sensitive to the surface of the NCs and the observed PLQY values are often far from satisfactory. 14-17 Stabilizing the fragile organic-inorganic interfaces of the CsPbX3 NCs continues to remain as a challenging exercise even today. Even though oleic acid (OA) and oleylamine (OLA) are widely used as capping ligands for protecting and passivating the surface of the NCs,8 the environment of the capping ligands around the surface of the NCs is highly dynamic in nature. 18 Facile protonation and deprotonation of OLA and OA lead to a dynamic equilibrium, which facilitates desorption of surface-bound capping ligands, thus exposing the surface of the NCs (and creating uncoordinated lead ions on the surface), forming inter-bandgap trap (defect) states. 18-20 Due to low exciton binding energy in these systems, free carriers are readily formed at room temperature (RT), which undergo rapid nonradiative recombination through the inter-bandgap surface trap states, thereby decreasing the PLOY. 8,18 This inefficient surface passivation also contributes to the deterioration of the colloidal stability of the NCs under ambient conditions. 18,21 While the trap states are energetically shallow for the green/red-emitting CsPbBr₃/CsPbI₃ NCs, but deep in nature for the blue-emitting CsPb(Cl/Br)₃ NCs, the latter exhibits poor optical properties with PLOY in a range of $\sim 1-15\%$. This impedes the utility of the blueemitting NCs in optoelectronic applications as compared to the other perovskites.²³

Several in situ and post-synthetic strategies for suppression of the halide vacancy-related surface defects, ^{24–29} removal of the lead nanoparticles from the surface, ^{11,30–33} curing octahedral distortion by doping the B-site with smaller metal ions, ^{34–43} and capping the surface by ligands that bind stronger than the native ligands, OA and OLA, ^{4,12,44–48} have been reported to obtain stable and

highly luminescent all-inorganic perovskite NCs. A judicious choice of the capping ligands is one of the most effective approaches for surface passivation of the NCs. Thiol-based systems are known to improve the optoelectronic and photovoltaic performance of lead-based metal chalcogenide quantum dots (QDs) because of the strong soft-soft interaction between Pb²⁺ (soft acid) and S²⁻ (soft base) at the surface.⁴⁹ Pan et al. first applied this strategy to the perovskites and showed that post-synthetic treatment of CsPbBr₃ NCs with didodecyldimethylammonium sulfide increases their air-stability and enhances the PLQY from 49 to 70% through the formation of a sulfide-enriched protective surface layer.⁴ Zheng and co-workers then fabricated a solar cell by using thiol-modified CH₃NH₃PbI₃ as an energy harvester with improved stability and performance.⁵⁰ Relying on the strong affinity of sulfur with undercoordinated lead, the long-chain organic thiols have often been used for increasing the PLQY and stability of green-emitting CsPbBr₃ NCs by suppressing the surface trap states.^{44,51} Very recently, Bakr and co-workers succeeded in enhancing the PLQY of blue-emitting CsPb(Br_xCl_{1-x})₃ NCs close to near-unity by using long-chain organic thiocyanate.⁴⁵ The effect of small sulfur-containing inorganic salts on the optical properties of perovskite NCs has remained unexplored till date.

Herein, we explore how sulfur-containing small inorganic salt influences the stability and PL efficiency of the blue-emitting CsPb(Cl/Br)₃, green-emitting CsPbBr₃, and yellow-emitting CsPbBr_{1.5}I_{1.5} perovskite NCs. We demonstrate that RT treatment of these systems with sodium thiosulfate results in an extraordinary improvement of PLQY to near-unity (~100%) for blue/green-emitting NCs and ~90% for the yellow-emitting NCs, thus covering a wide region of the visible spectrum. Effective elimination of the halide vacancy-related inter-bandgap defect states through the formation of strong Pb–S bonds at the surface is shown to be the key factor contributing toward the exceptional optical properties and improved stability of the NCs.

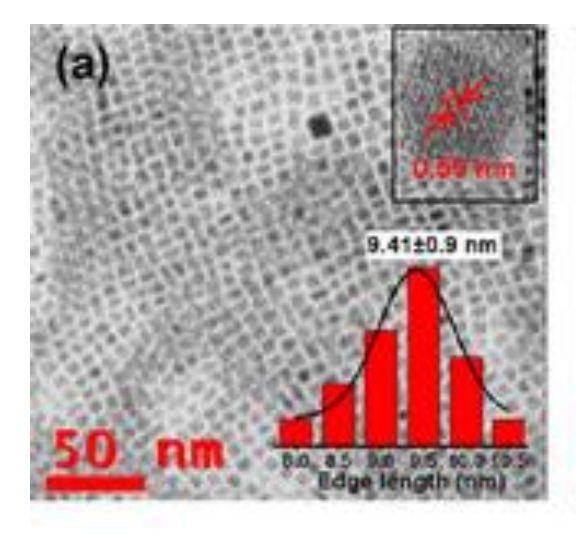
3.2. Results and Discussion

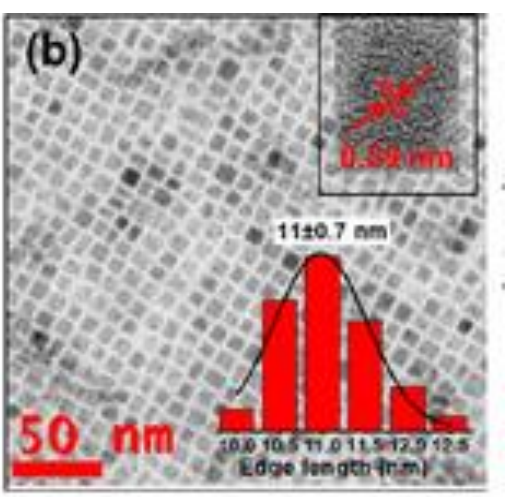
3.2.1. Synthesis and Characterization of the NCs

The colloidal CsPbBr3 and mixed-halide NCs were synthesized following a known procedure with

some minor modifications (details in the Chapter 2).⁸ The colloidal dispersion of purified NCs in dry toluene was used for further investigations. The post-synthetic treatment was carried out at RT under ambient conditions, the details of which are provided in the chapter 2.

The transmission electron microscope (TEM) images of the as-synthesized CsPbBr₃ NCs show cubic morphology with an average edge length of \sim 9.4 \pm 0.9 nm (Figure 3.1a). Interestingly, the treated CsPbBr₃ NCs, though they retain the cubic morphology, exhibit a slightly longer edge length of \sim 11.0 \pm 0.7 nm (Figure 3.1b). A small increase in particle size after post-synthetic treatment is not uncommon. This can happen due to self-repair or ripening of the NCs during ligand exchange and during the passivation of undercoordinated Pb²⁺ by thiosulfate ions at the surface (discussed later). A similar trend is observed for the mixed-halide NCs as well upon thiosulfate treatment (Figure A1.1). Both pristine and treated CsPbBr₃ NCs possess an identical interplanar spacing (d) of 0.59 nm corresponding to the (100) planes of the cubic NCs (insets of Figure 3.1a, b), indicating that the thiosulfate treatment does not affect the crystal structure of the NCs. The unchanged powder X-ray diffraction (PXRD) patterns (Figure 3.1c) also indicate that the pristine and treated CsPbBr₃ NCs possess a cubic phase and no additional peak for the treated samples implies that the post-synthetic treatment predominately takes place at the surface of the NCs. A similar unchanged PXRD pattern has also been observed for the pristine and treated mixed-halide systems (Figure A1.2).





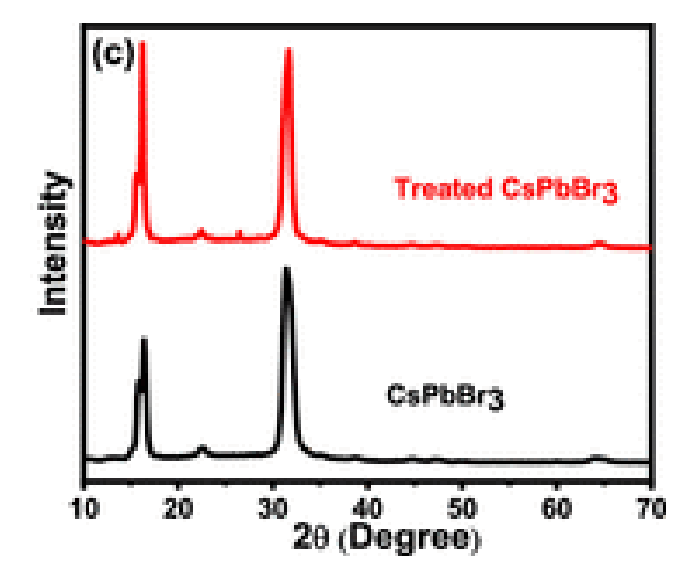


Figure 3.1. TEM images of the (a) as-synthesized CsPbBr₃ and (b) treated CsPbBr₃ NCs. The insets show high-resolution TEM images of the NCs with similar interplanar distance for (100) planes. (c) PXRD patterns of CsPbBr₃ NCs before and after the treatment.

3.2.2. Optical Properties

The UV-Vis absorption and emission spectra of the pristine and treated NCs are similar in nature except that these are slightly red-shifted for the treated NCs (Figure 3.2). The small red-shifts of the absorption and PL spectra are due to the small increase in the size of the NCs after treatment. A5,51 While the spectral features of the pristine and treated samples are not very different, the PL of the samples enhances dramatically after the treatment (Figure 3.2) without any change in the FWHM of the PL spectra. The PLQY values of the treated samples of green-emitting CsPbBr₃ ($\lambda_{em} = 512$ nm) and blue-emitting CsPbCl_{1.5}Br_{1.5} NCs ($\lambda_{em} = 463$ nm) are found to be near-unity ($\sim 100\%$) from initial values of ~ 35 and $\sim 11\%$, respectively, with $\sim 3-5$ nm red-shift of the PL maxima (Figure 3.2a,b). The other mixed-halide systems also exhibit an excellent PL enhancement after treatment. For example, the PLQY values of the as-synthesized CsPbClBr₂ and CsPbBr_{1.5}I_{1.5} NCs increase from ~ 48 to $\sim 100\%$ in the cyan region and from ~ 30 to $\sim 90\%$ in the yellow region, respectively (Figure 3.2c, d). Thus, we have been able to successfully enhance the PLQY of samples emitting in the range of ~ 463 to ~ 581 nm, demonstrating the effectiveness

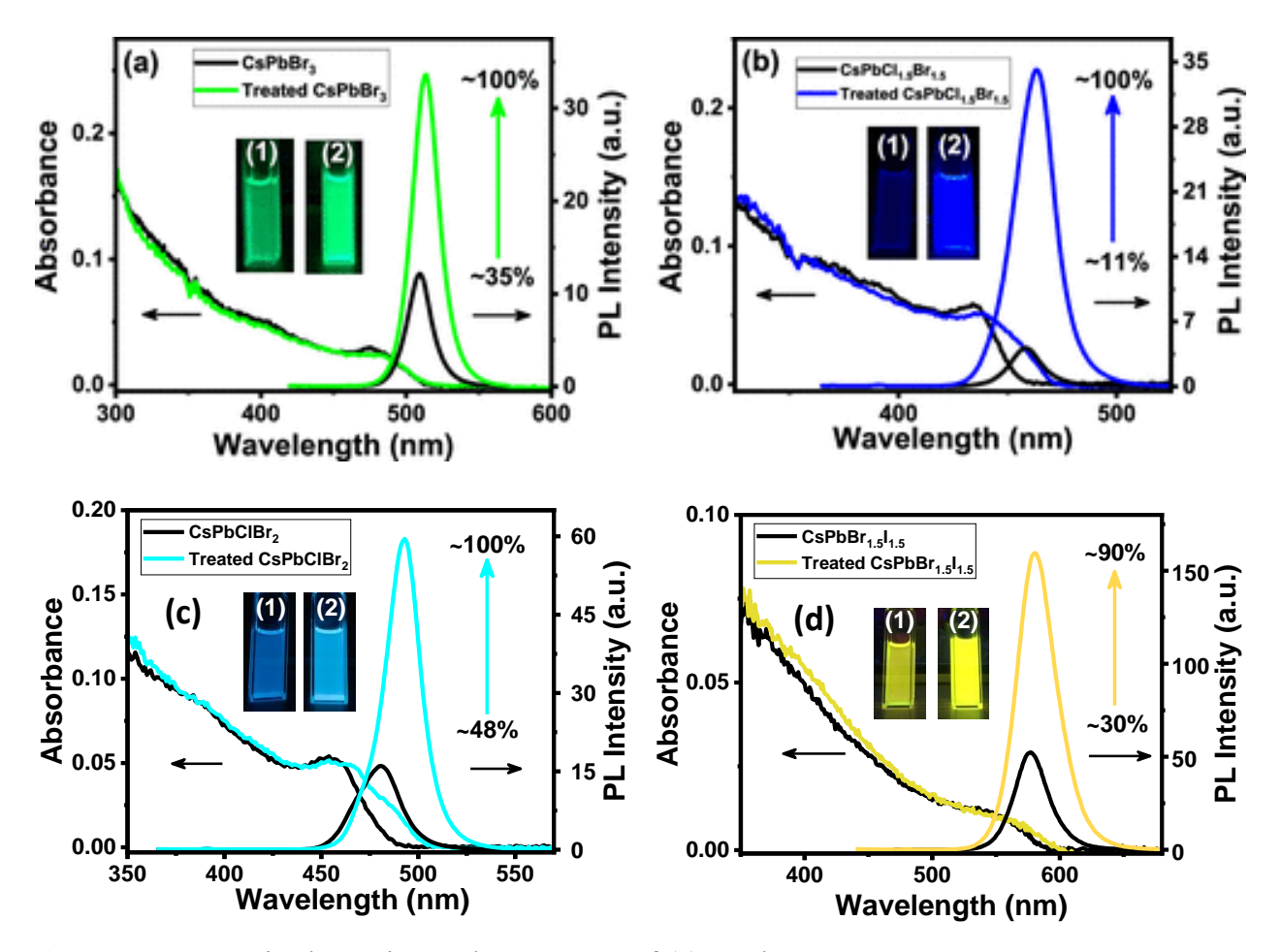


Figure 3.2. UV–Vis absorption and PL spectra of (a) CsPbBr₃ (b) CsPbCl_{1.5}Br_{1.5} (c) CsPbClBr₂ and (d) CsPbBr_{1.5}I_{1.5} NCs before and after the thiosulfate treatment. Insets show the digital images of both the NCs before (1) and after (2) the treatment under 365 nm UV light (8 W). A much brighter emission from the treated samples is clearly visible from the digital images.

of our post-synthetic approach over a wide range of the visible spectrum covering from the blue-green-yellow-emitting region (Figure A1.3).

3.2.3. Time Resolved Measurements

In order to understand the exceptional optical properties of the treated NCs, we have studied the time-resolved PL behavior of the systems using a time-correlated single photon counting (TCSPC) fluorescence technique. A substantially improved PL lifetime is observed for all the treated NCs

(Figure 3.3). The PL decay profiles of the as-synthesized and treated CsPbBr₃, CsPbCl_{1.5}Br_{1.5}, CsPbClBr₂ and CsPbBr_{1.5}I_{1.5} NCs are shown in Figure 3.3, and the analyzed decay components are presented in Table 3.1. As can be seen, the as-synthesized CsPbBr₃ NCs exhibit a triexponential decay behavior comprising a 2.97 ns component due to band-edge excitonic recombination,³⁰ whose amplitude is significantly higher for the treated CsPbBr₃ NCs (24% vs

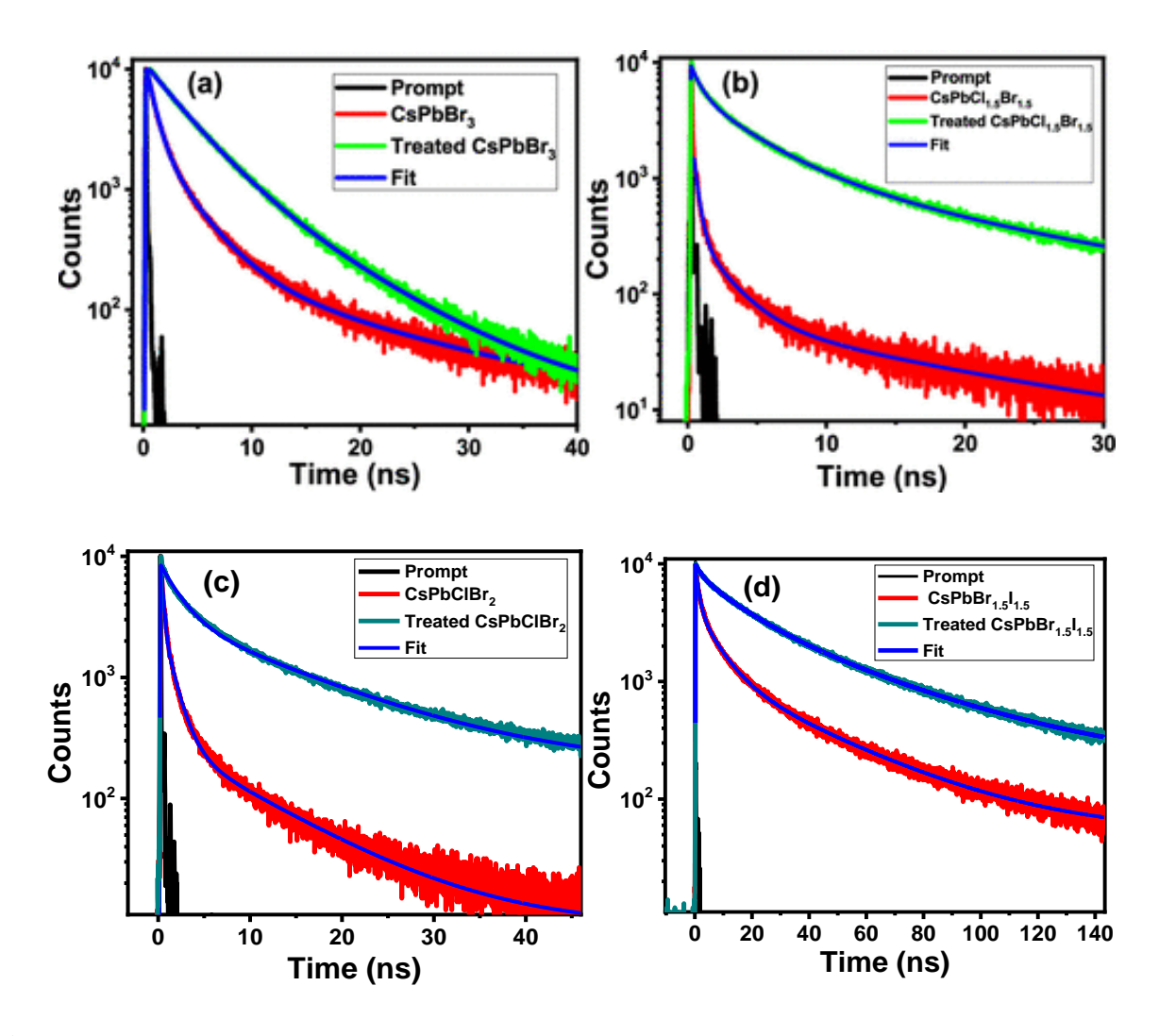


Figure 3.3. PL decay behavior of as-synthesized and treated (a) CsPbBr₃ (b) CsPbCl_{1.5}Br_{1.5} (c) CsPbClBr₂ and (d) CsPbBr_{1.5}I_{1.5} NCs. Diode laser sources of $\lambda_{ex} = 404$ and 376 nm were used as the excitation source of the NCs. The decay profiles were monitored at their respective PL maxima.

Table 3.1. Fluorescence Decay Parameters of the As-synthesized and Treated CsPbBr₃ and CsPbCl_{1.5}Br_{1.5}, CsPbClBr₂ and CsPbBr_{1.5}I_{1.5} NCs and Calculated Radiative (k_r) and Nonradiative (k_{nr}) Rate Constants.

Samples	$\tau_1(\alpha_1)^a/ns$	τ2(α2)/ns	τ ₃ (α ₃)/ns	PLQY	<τ _{amp} >b/	k _r /ns ⁻¹	k _{nr} /ns ⁻¹
				(%)	ns		
CsPbBr ₃	2.97(0.24)	14.5(0.02)	0.78(0.74)	~35	1.58	0.22	0.41
Treated CsPbBr ₃	3.43(0.8)	8.17(0.20)		~100	4.34	0.23	0.0023
CsPbCl _{1.5} Br _{1.5}	2.12(0.15)	15.8(0.03)	0.34(0.82)	~11	1.07	0.10	0.83
Treated CsPbCl _{1.5} Br _{1.5}	3.94(0.46)	15.5(0.14)	0.73(0.40)	~100	4.27	0.23	0.0023
CsPbClBr ₂	1.2(0.18)	9.64(0.02)	0.19(0.80)	~48	0.56	0.85	0.92
Treated CsPbClBr ₂	4.12(0.42)	16.8(0.21)	0.77(0.37)	~100	5.54	0.18	0.002
CsPbBr _{1.5} I _{1.5}	7.27(0.32)	34.4(0.12)	1.25(0.56)	~30	7.15	0.04	0.09
Treated CsPbBr _{1.5} I _{1.5}	14.8(0.46)	45.3(0.38)	2.46(0.16)	~90	24.41	0.03	0.004

 $[^]a\alpha_i$ is the fractional contribution associated with i-th life-time component. $^b<\tau_{amp}>=\Sigma\tau_i\alpha_i/\Sigma\alpha_i,\ k_r=PLQY/<\tau_{amp}>$ and $k_{nr}=(1-PLQY)/<\tau_{amp}>$.

80%). The longest component (14.5 ns) with a very small contribution (2%) is attributed to shallow trap-mediated excitonic recombination,⁵⁶ whose contribution also increases significantly for the treated NCs. Most interestingly, the shortest component (0.78 ns), which was the major radiative recombination process in pristine CsPbBr₃ NCs, completely vanishes after the treatment. Complete

elimination of this shortest sub-nanosecond component, which arises due to the surface trap states, indicates that the treated CsPbBr₃ NCs are largely free from surface defects. 30,42 In the case of CsPbCl_{1.5}Br_{1.5} NCs, the contribution of the band-edge radiative recombination increases from 15 to 46% and that of the trapping component decreases by nearly 50% (Figure 3.3b). A prominent influence of the post-synthetic treatment on the PL decay behavior of the other mixed-halide systems is also observed (Figure 3.3c, d). The radiative and nonradiative rate constants (k_r and k_{nr} , respectively), estimated from the measured PLQY and $\langle \tau_{amp} \rangle$ values, show that the k_{nr} value decreases by factors of ~178 for CsPbBr₃ and ~360 for the CsPbCl_{1.5}Br_{1.5} NCs upon treatment (Table 3.1), indicating a significantly suppressed nonradiative recombination and high PLQY of the systems. The PL decay parameters of the other mixed-halide CsPbClBr₂ and CsPbBr_{1.5}I_{1.5} systems are listed in Table 3.1. and show the k_{nr} value decreases by factors of ~450 and 25 respectively.

We also investigated the spectral and temporal characteristics of the transients produced upon the photoexcitation of the as-synthesized and treated CsPbBr₃ NCs by transient absorption (TA) measurements with femtosecond time resolution. As can be seen, the TA spectral features of both the as-synthesized and treated samples are characterized by a sharp negative excitonic bleach signal ($\Delta A = -Ve$) and photoinduced absorption ($\Delta A = +Ve$) at the higher energy side of it (Figure 3.4a, b).^{42,57} A slight red-shift of the bleach signal (from ~506 to 509 nm) on the surface treatment of the CsPbBr₃ NCs is consistent with the shift of the excitonic peak in the steady-state absorption spectra mentioned above. Although the TA spectral features of both the samples are very similar, bleach recovery is much faster for the as-synthesized NCs (Figure 3.4a) compared to the treated sample (Figure 3.4b), which is clearly reflected in the bleach recovery dynamics of the samples. The bleach recovery dynamics (Figure 3.4c) of the as-synthesized CsPbBr₃ NCs is bi-exponential with one ultrafast component of ~54.5 \pm 4.7 ps (23%) arising from carrier trapping and a long recombination component of >850 ps (77%).⁴² However, this dynamic is single exponential and much slower for the treated CsPbBr₃ NCs. The presence of only long (>850 ps) recombination component in the treated NCs indicates effective elimination of the pre-existing nonradiative trap

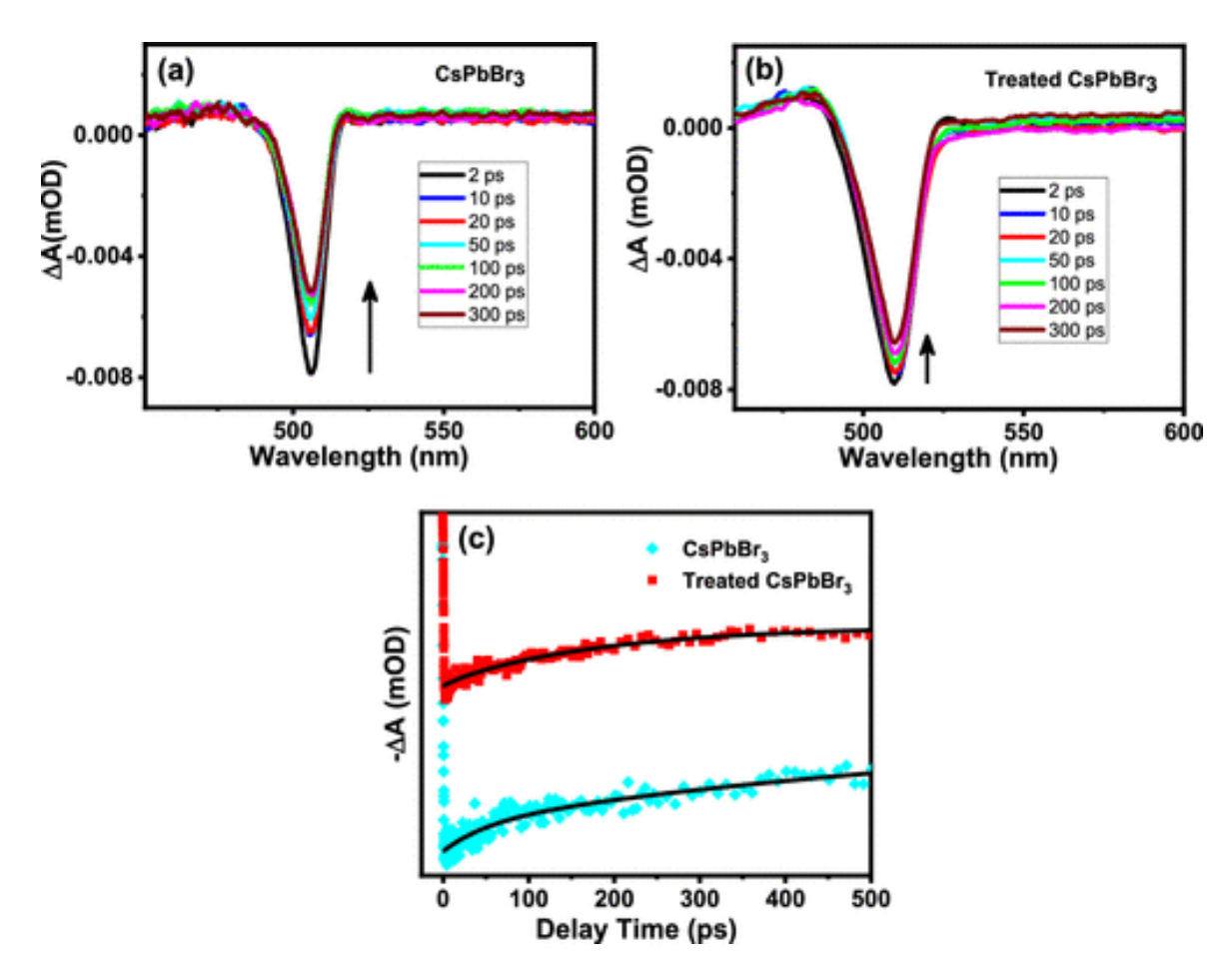


Figure 3.4. TA spectra ($\lambda_{ex} = 350$ nm) of the (a) as-synthesized and (b) treated CsPbBr₃ NCs. (c) Comparison of the bleach recovery dynamics of the two samples. The kinetic parameters obtained upon bi-exponential fitting to the data are 54.5 ± 4.70 ps (0.23) and >850 ps (0.77) for the assynthesized CsPbBr₃ NCs, while in the case of the treated sample, the recovery dynamics is single exponential with a time constant of >850 ps.

centers in the treated CsPbBr₃ NCs, and therefore, electron-hole radiative recombination is the major process.

Let us now analyze various factors to determine what contribute(s) to the exceptional optical properties of the treated NCs. A similar lattice spacing and unchanged PXRD patterns of the NCs

before and after the treatment suggest that the crystal structure of the NCs is not affected by the treatment, and the thiosulfate salt merely modifies the surface of the NCs. The elemental analysis of a large area of field emission scanning electron microscopy (FESEM) images of the assynthesized and treated CsPbBr₃ NCs by energy dispersive X-ray (EDX) measurements (Figure 3.5a) shows that the Br:Pb ratio in as-synthesized CsPbBr₃ NCs is (\sim 2.76) significantly lower than the expected ratio (3.0), indicating bromide deficiency (or undercoordinated Pb²⁺) in the sample. This is a common reason for the poor PLQY of the NCs as it enables rapid nonradiative recombination of the photogenerated charge carriers. 14,22 Very interestingly, in the treated CsPbBr₃ NCs, this ratio is even lower (Br:Pb \approx 2.69). It is important to note that due to proximity of the S K and Pb M multiplets, the signal at ~2.4 keV appears as an overlapping signal of both the elements, and therefore, it is difficult to resolve the lines in our setup, which has a resolution of ~130 eV. 58,59 This is why the EDX signals of the as-synthesized (Figure A1.4) and treated (Figure 3.5a) CsPbBr₃ NCs are quite similar in the stated region. For this reason, even though the elemental analysis of the treated CsPbBr₃ NCs (Figure 3.5a) constantly exhibits a low (~0.61%) "S" content in the EDX spectra, it should not be used as convincing evidence of the presence of sulfur in the sample. However, elemental mapping of the treated CsPbBr₃ NCs washed with MeOAc, which shows a homogeneous distribution of "S" (in addition to the constituent elements Cs, Pb, and Br) throughout the scanned area of the sample, suggests the presence of S in the treated NCs (Figure A1.5). In order to obtain better insights into the chemical environment of the elements in the treated NCs, we have performed X-ray photoelectron spectroscopy (XPS) measurements of the as-synthesized and treated CsPbBr₃ NCs, which show characteristic peaks of the constituent elements Cs, Pb, and Br at their expected regions (Figure A1.6). The appearance of an additional peak at ~159 eV only for the treated CsPbBr₃ NCs establishes the presence of thiosulfate at the surface of the treated NCs as this peak corresponds to the Pb-S bond (Figure 3.5b). 51 The presence of the "S 2p" peak even for the washed sample suggests the bound nature of thiosulfate to the NCs (Figure A1.7). As sulfide forms strong Pb-S bonds owing to a strong soft-acid and soft-base interaction, both Pb 4f peaks ($4f_{5/2}$ and $4f_{7/2}$) of the treated CsPbBr₃ NCs are shifted to a higher binding energy by $\sim 0.18 \text{ eV}$ (Figure 3.5d).⁶⁰

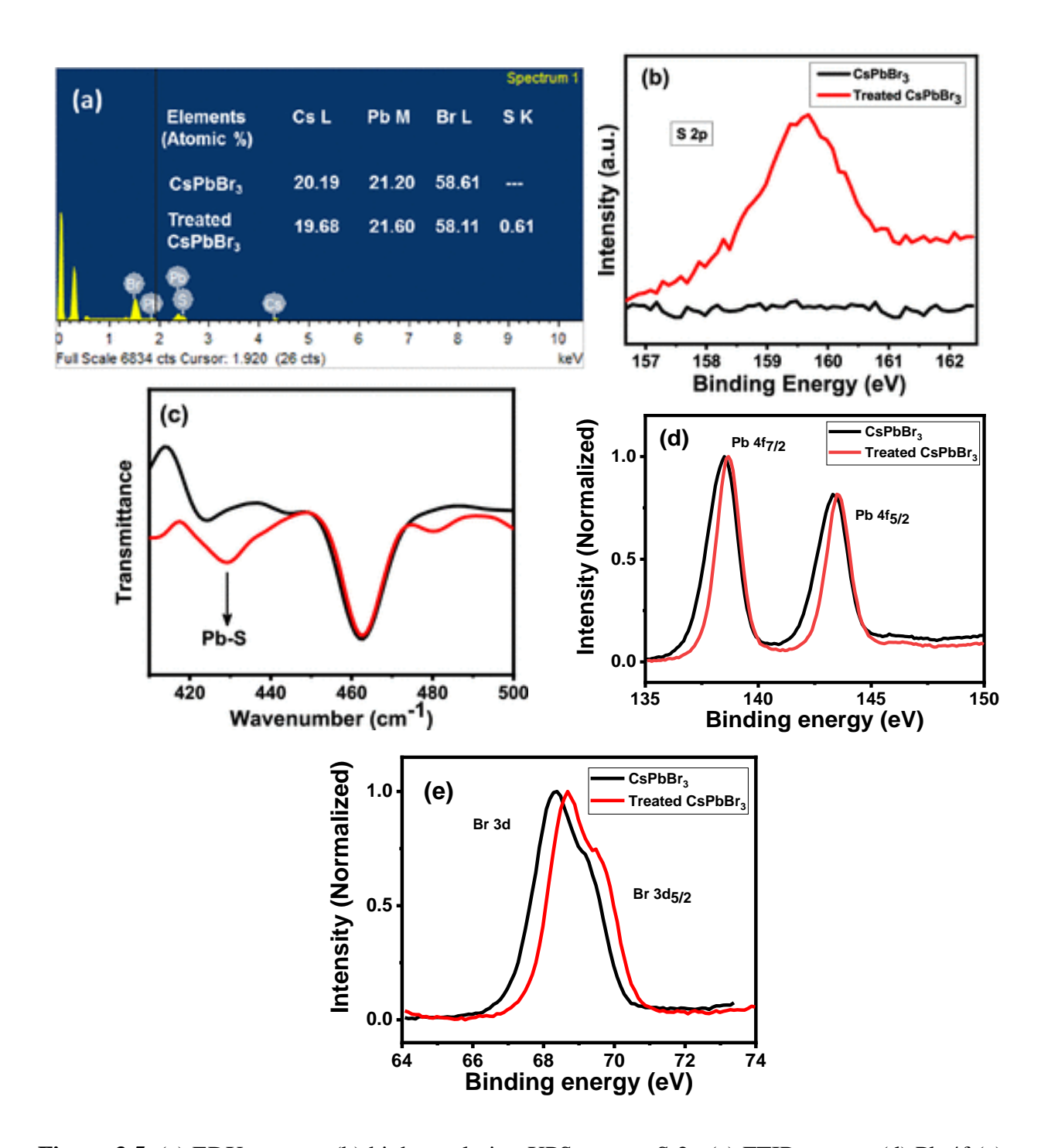


Figure 3.5. (a) EDX spectra, (b) high-resolution XPS spectra S 2p (c) FTIR spectra (d) Pb 4f (e) Br 3d of as-synthesized and thiosulfate-treated CsPbBr₃ NCs. The XPS data was calibrated with respect to the C 1s peak at \sim 285.0 eV.

Interestingly, the binding energy of the Br $3d_{5/2}$ core level spectra is also blue-shifted by ~0.7 eV in the treated NCs (Figure 3.5e). This indicates that the electron density around the central Pb²⁺ cation is impacted by the formation of the Pb–S bonds, leading to an adjustment in chemical bonding between Pb²⁺ and Br⁻ in the lead bromide octahedral units of the treated NCs, which in turn strengthens the Pb–Br bonds, causing a shift of the Br 3d XPS peak at higher energy.^{60–62} Like in EDX measurements, here also the calculated Br/Pb ratio in treated CsPbBr₃ NCs is found to be slightly lower than that in as-synthesized CsPbBr₃ NCs (Table 3.2). The sulfur content obtained from XPS measurements is however found to be slightly higher to that obtained from

Table 3.2. Calculated ratio of the atomic % of the as-synthesized and treated CsPbBr₃ NCs as obtained from XPS measurements. The Cs:Pb:Br atomic % ratio for the samples were obtained by dividing the integrated area under the corresponding XPS peaks with atomic sensitivity factor (ASF) values for each of the elements. The ASF values for Cs 3d, Pb 4f, Br 3d and S 2p are 7.2, 6.7, 0.83 and 0.668 respectively.

Samples	Arc	Atomic % ratio (w.r.t. Pb)						
	Cs/7.2	Pb/6.7	Br/0.83	S/0.668	Cs/Pb	Pb/Pb	Br/Pb	S/Pb
CsPbBr ₃	38,480.09	38,450.21	106,120.18		1	1	2.7	
Treated CsPbBr ₃	13,403.20	15,537.89	41,128.65	637.05	0.86	1	2.6	0.041

EDX studies. The surface ligand environment of the NCs is further assessed by FTIR measurements (Figure A1.8). The emergence of a new peak at ~430 cm⁻¹ reconfirms the formation of Pb–S bonds at the surface in treated CsPbBr₃ NCs (Figure 3.5c).⁵⁰ It is interesting to note that the intensity of the peaks due to the asymmetric and symmetric stretching of the carboxylate (COO⁻) ion and N–H bending at 1541, 1400, and 1572 cm⁻¹, respectively,⁶³ is reduced for the

treated CsPbBr₃ NCs, indicating that the thiosulfate ion replaces some of the oleate and oleylammonium ligands from the surface of the CsPbBr₃ NCs (Figure 3.6a, b). The partial replacement of the native surface ligands by sulfur-containing moieties, reported previously for CsPbBr₃ NCs, is attributed to the strong binding affinity of sulfide toward uncoordinated lead, resulting in strong Pb–S bonds.^{44,60} A distinct peak at ~1128 cm⁻¹ in the FTIR spectra of treated CsPbBr₃ NCs, which is a characteristic absorption feature of the S=O bond,⁶⁴ suggests binding of

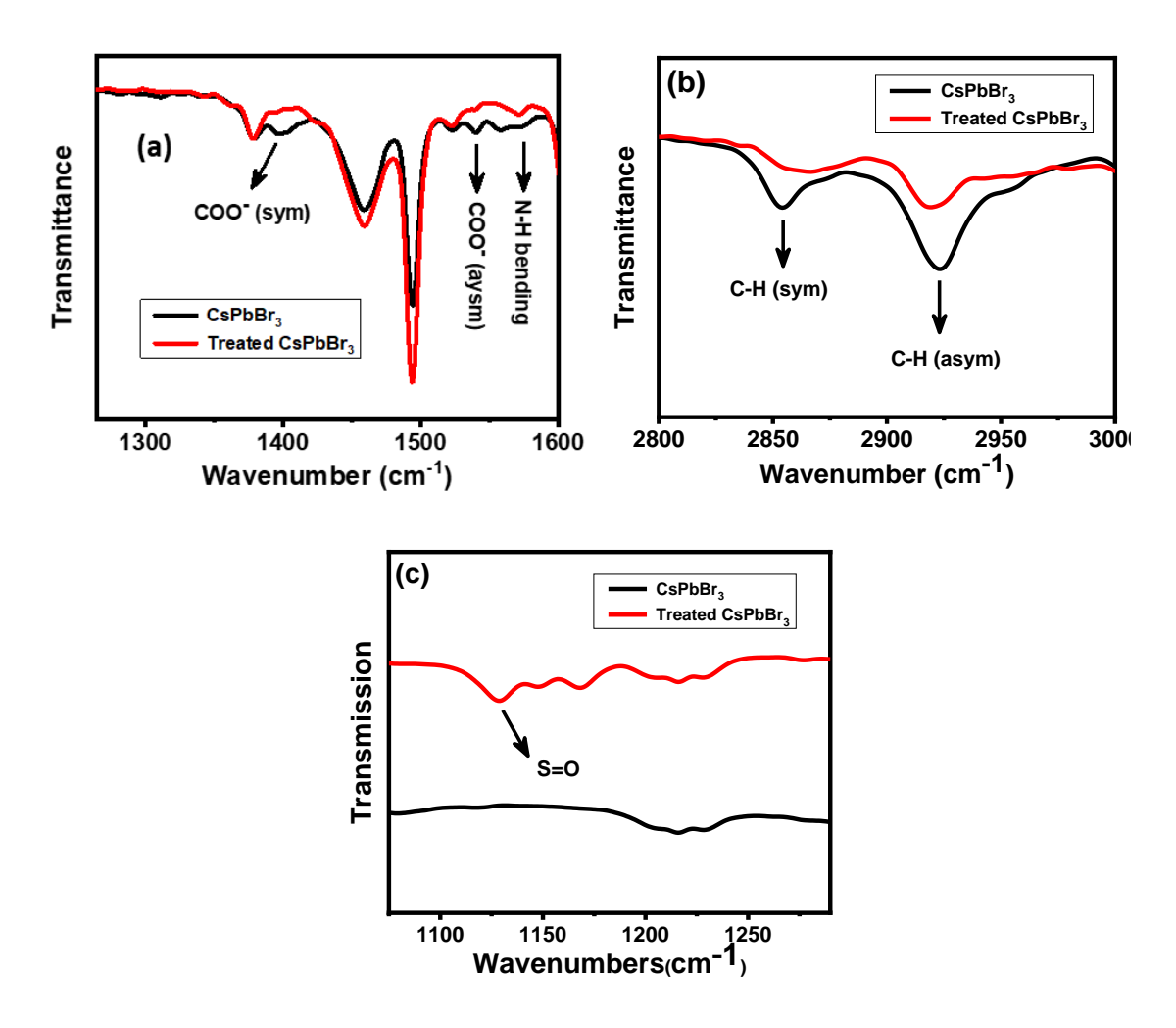


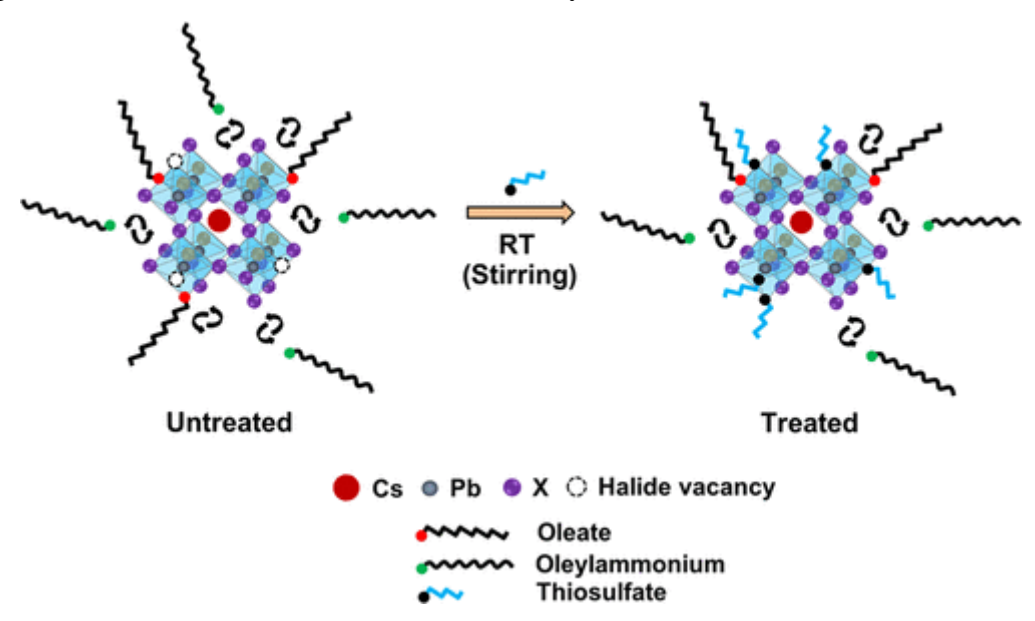
Figure 3.6. FTIR spectra of the as-synthesized and treated CsPbBr₃ NCs (a, b) the exchange of OA and OLA with thiosulfate and (c) S=O stretching band on the surface of the NCs.

thiosulfate with the surface Pb through its sulfur end (Figure 3.6c). The partial replacement of the native ligands with a concomitant decrease in their signals in FTIR spectra is a reflection of anchoring of thiosulfate at the surface of treated NCs. 44,55 Sodium thiosulfate is a stable compound; it decomposes when heated above 150 °C or in the presence of strong acids (like HCl and H₂SO₄). 65,66 As our post-synthetic treatment was carried out at RT and in the absence of any strong acid, we believe that thiosulfate remains in its native form during and after the treatment. The possibility of the NCs catalyzing its decomposition, forming PbS, was also considered, but similar TEM images and PXRD patterns of the NCs before and after the treatment and the absence of any characteristic features of decomposition products including PbS rule out this possibility.

Bromide vacancy at the surface of as-synthesized CsPbBr3 NCs results in the formation of undercoordinated Pb atoms with a net positive charge, which acts as potential electron-trapping centers.⁶⁷ The photogenerated electrons are readily trapped in these sites and subsequently recombine non-radiatively, resulting in poor PLQY.^{22,67} Thiosulfate fills the surface halide vacancies by interacting with the undercoordinated Pb atoms through the S atom, forming strong Pb-S bonds at the surface of the treated NCs. The passivation of halide vacancies through the formation of new Pb-S bonds effectively removes the pre-existing electron traps and enhances band-edge excitonic recombination, resulting in near-unity PLQY of the NCs. 45,68 A small decrease in the Br/Pb ratio, as indicated by the EDX and XPS data, is presumably a reflection of the exchange of few oleylammonium cations with thiosulfate and their subsequent removal from the surface as oleylammonium bromides of the treated CsPbBr₃ NCs. In addition, as indicated by the FTIR data, some of the oleate ions are also replaced by thiosulfate owing to the strong affinity of sulfur toward Pb. This agrees with literature information on the partial exchange of native ligands on the formation of Pb-S bonds with organic thiols and other sulfur-containing salts. 44,60 Thus, effective passivation of undercoordinated Pb through the formation of strong Pb-S bonds with thiosulfate and concomitant suppression of the nonradiative recombination centers contribute to the exceptional optical properties of the treated NCs (Scheme 3.1). It is however important to note here that apart from the undercoordinated Pb sites, thiosulfate occupies very limited places

on the NCs surface and hence do not remove all the native surface ligands as observed earlier in few instances. 11,30

Scheme 3.1. Schematic Representation of Halide Vacancy Passivation and Partial Ligand Exchange at the Surface of CsPbX₃ NCs after Post-synthetic Treatment with Sodium Thiosulfate.



The lack of long-term stability of the perovskite-based devices is probably one of the major issues for wide-scale applications of these substances. The treated NCs are found to be much more stable under different external conditions (Figure 3.7 and Figures A1.9). As can be seen from Figure 3.7a, the as-synthesized CsPbBr₃ NCs hold just ~24% of its initial PL intensity after 4 days under ambient conditions (with ~4 nm red-shift of the emission maxima, Figure A1.9a); on the other hand, the treated NCs retain 84% of the same initial PL intensity for over a week under similar conditions (Figure 3.7a) without any shift of the PL maxima (Figure A1.9b), demonstrating a much superior air-stability. The treated samples exhibit superior photostability as well. For example, under continuous illumination of UV light (365 nm, 8 W) for 7 h, the treated CsPbBr₃ NCs hold ~80% of its initial PL intensity, while the as-synthesized CsPbBr₃ NCs retains only <10% of the PL intensity under similar conditions (Figure 3.7b, A1.9c, d). A superior air- and photostability of

treated CsPbCl_{1.5}Br_{1.5} NCs is also observed (Figure 3.7c, d). We attribute this much improved air and photostability of the treated NCs to the formation of strong Pb–S bonds at the surface, which not only passivates the halide vacancies but also provides a robust and less fragile surface ligand environment than that present in as-synthesized NCs.⁴⁴

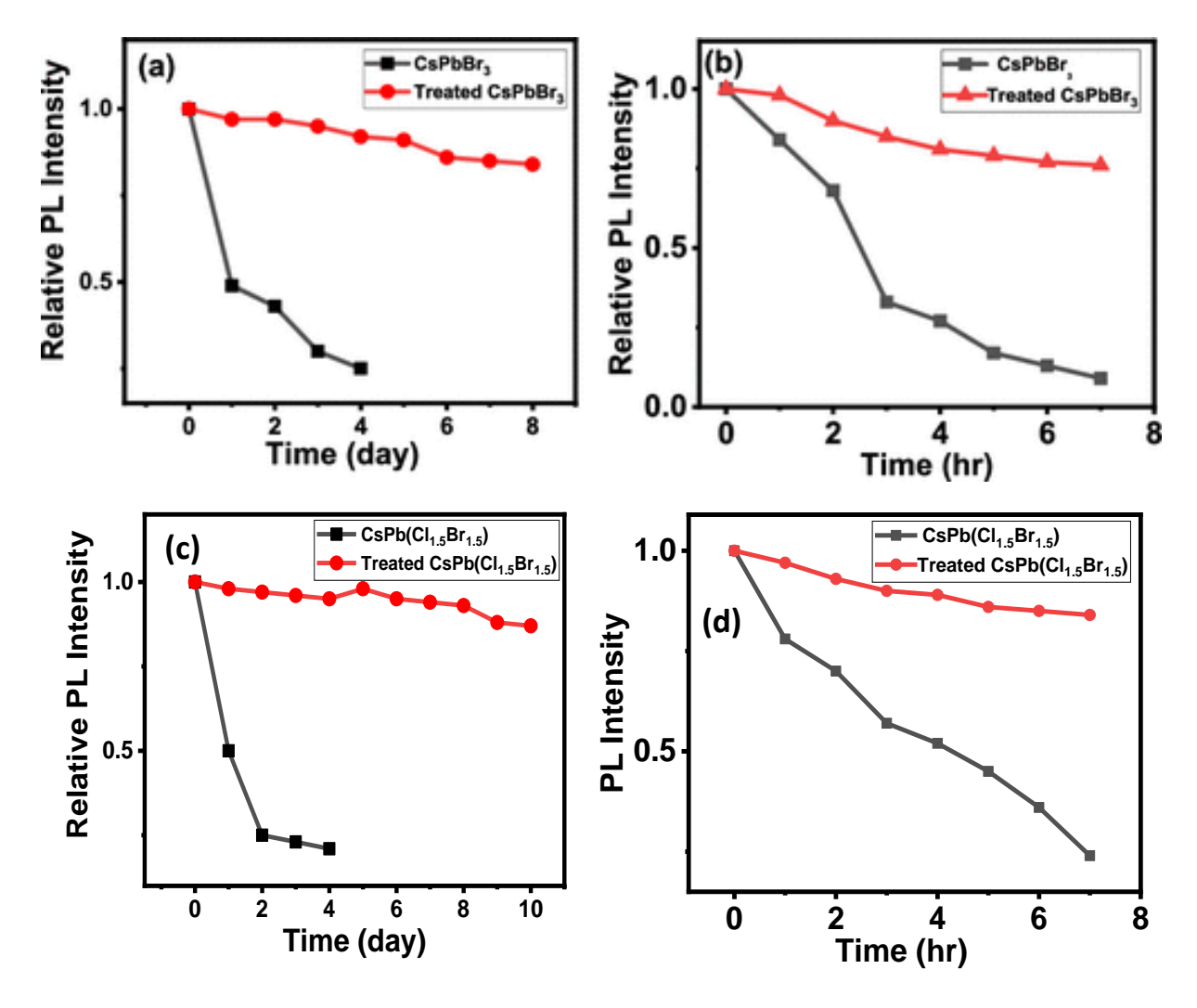


Figure 3.7. Comparison of the stability of as-synthesized and treated CsPbBr₃ and CsPbCl_{1.5}Br_{1.5} NCs under (a, c) ambient conditions and (b, d) continuous UV light (365 nm, 8 W) illumination.

3.3. Summary

A room-temperature post-synthetic treatment of the blue-emitting CsPb(Cl/Br)₃, green-emitting CsPbBr₃, and yellow-emitting CsPb(Br/I)₃ NCs with Na₂S₂O₃·5H₂O under ambient conditions is shown to dramatically improve the PLQY (~90–100%) of these systems, which cover a wide range of the visible spectrum. The treated samples also exhibit high stability under different external conditions. The results imply that the halide vacancy-related surface defects in these systems can be effectively passivated by small sulfur-containing systems through formation of strong Pb–S bonds with undercoordinated lead on the surface. The excellent photoluminescence properties and high stability of these NCs make them promising candidates for perovskite-based optoelectronic applications.

References

- (1) Kojima, A.; Teshima, K.; Shirai, Y.; Miyasaka, T., Organometal Halide Perovskites as Visible-Light Sensitizers for Photovoltaic Cells. *J. Am. Chem. Soc.* **2009**, *131*, 6050–6051.
- (2) Liang, J.; Wang, C.; Wang, Y.; Xu, Z.; Lu, Z.; Ma, Y.; Zhu, H.; Hu, Y.; Xiao, C.; Yi, X.; Zhu, G.; Lv, H.; Ma, L.; Chen, T.; Tie, Z.; Jin, Z.; Liu, J., All-Inorganic Perovskite Solar Cells. *J. Am. Chem. Soc.* **2016**, 138, 15829–15832.
- (3) Ramasamy, P.; Lim, D.-H.; Kim, B.; Lee, S.-H.; Lee, M.-S.; Lee, J.-S., All-inorganic cesium lead halide perovskite nanocrystals for photodetector applications. *Chem. Commun.* **2016**, *52*, 2067-2070
- (4) Pan, J.; Sarmah, S. P.; Murali, B.; Dursun, I.; Peng, W.; Parida, M. R.; Liu, J.; Sinatra, L.; Alyami, N.; Zhao, C.; Alarousu, E.; Ng, T. K.; Ooi, B. S.; Bakr, O. M.; Mohammed, O. F., Air Stable Surface-Passivated Perovskite Quantum Dots for Ultra-Robust, Single- and Two-Photon-Induced Amplified Spontaneous Emission. *J. Phys. Chem. Lett.* **2015**, *6*, 5027–5033.

- (5) Yakunin, S.; Protesescu, L.; Krieg, F.; Bodnarchuk, M. I.; Nedelcu, G.; Humer, M.; Luca, G. D.; Fiebig, M.; Heiss, W.; Kovalenko, M. V., Low-threshold amplified spontaneous emission and lasing from colloidal nanocrystals of caesium lead halide perovskites. *Nature Communications* **2015**, *6*, 8056.
- (6) Zhang, X.; Lin, H.; Huang, H.; Reckmeier, C.; Zhang, Y.; Choy, W. C. H.; Rogach, A. L., Enhancing the Brightness of Cesium Lead Halide Perovskite Nanocrystal Based Green Light-Emitting Devices through the Interface Engineering with Perfluorinated Ionomer. *Nano Lett.* **2016**, 16, 1415–1420.
- (7) Kovalenko, M. V.; Protesescu, L.; Bodnarchuk, M. I., Properties and potential optoelectronic applications of lead halide perovskite nanocrystals. *Science* **2017**, *358*, 745-750.
- (8) Protesescu, L.; Yakunin, S.; Bodnarchuk, M. I.; Krieg, F.; Caputo, R.; Hendon, C. H.; Yang, R. X.; Walsh, A.; Kovalenko, M. V., Nanocrystals of Cesium Lead Halide Perovskites (CsPbX₃, X = Cl, Br, and I): Novel Optoelectronic Materials Showing Bright Emission with Wide Color Gamut. *Nano Lett.* **2015**, *15*, 3692–3696.
- (9) Nedelcu, G.; Protesescu, L.; Yakunin, S.; Bodnarchuk, M. I.; Grotevent, M. J.; Kovalenko, M. V., Fast Anion-Exchange in Highly Luminescent Nanocrystals of Cesium Lead Halide Perovskites (CsPbX₃, X = Cl, Br, I). *Nano Lett.* **2015**, *15*, 5635–5640.
- (10) Dutt, V. G. V.; Akhil, S.; Mishra, N., Fast, tunable and reversible anion-exchange in CsPbBr₃ perovskite nanocrystals with hydrohalic acids. *CrystEngComm* **2020**, *22*, 5022-5030.
- (11) Koscher, B. A.; Swabeck, J. K.; Bronstein, N. D.; Alivisatos, A. P., Essentially Trap-Free CsPbBr₃ Colloidal Nanocrystals by Postsynthetic Thiocyanate Surface Treatment. *J. Am. Chem. Soc.* **2017**, *139*, 6566–6569.
- (12) Pan, J.; Shang, Y.; Yin, J.; Bastiani, M. D.; Peng, W.; Dursun, I.; Sinatra, L.; El-Zohry, A. M.; Hedhili, M. N.; Emwas, A.-H.; Mohammed, O. F.; Ning, Z.; Bakr, O. M., Bidentate Ligand-Passivated CsPbI₃ Perovskite Nanocrystals for Stable Near-Unity Photoluminescence Quantum Yield and Efficient Red Light-Emitting Diodes. *J. Am. Chem. Soc.* **2018**, *140*, 562–565.

- (13) Dutta, A.; Behera, R. K.; Pal, P.; Baitalik, P. D. S.; Pradhan, D. N., Near-Unity Photoluminescence Quantum Efficiency for All CsPbX₃ (X = Cl, Br, and I) Perovskite Nanocrystals: A Generic Synthesis Approach. *Angew. Chem. Int. Ed.* **2019**, *58*, 5552–5556.
- (14) Seth, S.; Ahmed, T.; De, A.; Samanta, A., Tackling the Defects, Stability, and Photoluminescence of CsPbX₃ Perovskite Nanocrystals. *ACS Energy Lett.* **2019**, *4*, 1610–1618.
- (15) Tachikawa, T.; Karimata, I.; Kobori, Y., Surface Charge Trapping in Organolead Halide Perovskites Explored by Single-Particle Photoluminescence Imaging. *J. Phys. Chem. Lett.* **2015**, *6*, 3195–3201.
- (16) Pradhan, N., Tips and Twists in Making High Photoluminescence Quantum Yield Perovskite Nanocrystals. *ACS Energy Lett.* **2019**, *4*, 1634–1638.
- (17) Dutt, V. G. V.; Akhil, S.; Mishra, N., Surface Passivation Strategies for Improving Photoluminescence and Stability of Cesium Lead Halide Perovskite Nanocrystals. *ChemNanoMat* **2020**, *6*, 1730-1742.
- (18) Roo, J. D.; Ibáñez, M.; Geiregat, P.; Nedelcu, G.; Walravens, W.; Maes, J.; Martins, J. C.; Driessche, I. V.; Kovalenko, M. V.; Hens, Z., Highly Dynamic Ligand Binding and Light Absorption Coefficient of Cesium Lead Bromide Perovskite Nanocrystals. *ACS Nano* **2016**, *10*, 2071–2081.
- (19) Yassitepe, E.; Yang, Z.; Voznyy, O.; Kim, Y.; Walters, G.; Castañeda, J. A.; Kanjanaboos, P.; Yuan, M.; Gong, X.; Fan, F.; Pan, J.; Hoogland, S.; Comin, R.; Bakr, O. M.; Padilha, L. A.; Nogueira, A. F.; Sargent, E. H., Amine-Free Synthesis of Cesium Lead Halide Perovskite Quantum Dots for Efficient Light-Emitting Diodes. *Adv. Funct. Mater.* **2016**, *26*, 8757 –8763.
- (20) Akhil, S.; Dutt, V. G. V.; Mishra, D. N., Completely Amine-Free Open-Atmospheric Synthesis of High-Quality Cesium Lead Bromide (CsPbBr₃) Perovskite Nanocrystals. *Chem. Eur. J.* **2020**, *26*, 1–9.
- (21) Dutta, A.; Dutta, S. K.; Adhikari, S. D.; Pradhan, D. N., Phase-Stable CsPbI₃ Nanocrystals:

The Reaction Temperature Matters. *Angew. Chem. Int. Ed.* **2018**, *57*, 9083 –9087.

- (22) Nenon, D. P.; Pressler, K.; Kang, J.; Koscher, B. A.; Olshansky, J. H.; Osowiecki, W. T.; Koc, M. A.; Wang, L.-W.; Alivisatos, A. P., Design Principles for Trap-Free CsPbX₃ Nanocrystals: Enumerating and Eliminating Surface Halide Vacancies with Softer Lewis Bases. *J. Am. Chem. Soc.* **2018**, *140*, 17760–17772.
- (23) Shamsi, J.; Urban, A. S.; Imran, M.; Trizio, L. D.; Manna, L., Metal Halide Perovskite Nanocrystals: Synthesis, Post-Synthesis Modifications, and Their Optical Properties. *Chem. Rev.* **2019**, *119*, 3296–3348.
- (24) Woo, J. Y.; Kim, Y.; Bae, J.; Kim, T. G.; Kim, J. W.; Lee, D. C.; Jeong, S., Highly Stable Cesium Lead Halide Perovskite Nanocrystals through in Situ Lead Halide Inorganic Passivation. *Chem. Mater.* **2017**, *29*, 7088–7092.
- (25) Wu, Y.; Wei, C.; Li, X.; Li, Y.; Qiu, S.; Shen, W.; Cai, B.; Sun, Z.; Yang, D.; Deng, Z.; Zeng, H., In Situ Passivation of PbBr₆⁴⁻ Octahedra toward Blue Luminescent CsPbBr₃ Nanoplatelets with Near 100% Absolute Quantum Yield. *ACS Energy Lett.* **2018**, *3*, 2030–2037.
- (26) Behera, R. K.; Adhikari, S. D.; Dutta, S. K.; Dutta, A.; Pradhan, N., Blue-Emitting CsPbCl₃ Nanocrystals: Impact of Surface Passivation for Unprecedented Enhancement and Loss of Optical Emission. *J. Phys. Chem. Lett.* **2018**, *9*, 6884–6891.
- (27) Shao, H.; Zhai, Y.; Wu, X.; Xu, W.; Xu, L.; Dong, B.; Bai, X.; Cui, H.; Song, H., High brightness blue light-emitting diodes based on CsPb(Cl/Br)₃ perovskite QDs with phenethylammonium chloride passivation. *Nanoscale* **2020**, *12*, 11728-11734.
- (28) Dutta, A.; Behera, R. K.; Dutta, S. K.; Adhikari, S. D.; Pradhan, N., Annealing CsPbX₃ (X = Cl and Br) Perovskite Nanocrystals at High Reaction Temperatures: Phase Change and Its Prevention. *J. Phys. Chem. Lett.* **2018**, *9*, 6599–6604.
- (29) Chen, Y.-C.; Chou, H.-L.; Lin, J.-C.; Lee, Y.-C.; Pao, C.-W.; Chen, J.-L.; Chang, C.-C.; Chi, R.-Y.; Kuo, T.-R.; Lu, C.-W.; Wang, D.-Y., Enhanced Luminescence and Stability of Cesium

Lead Halide Perovskite CsPbX₃ Nanocrystals by Cu²⁺-Assisted Anion Exchange Reactions. *J. Phys. Chem. C* **2019**, *123*, 2353–2360.

- (30) Ahmed, T.; Seth, S.; Samanta, A., Boosting the Photoluminescence of CsPbX₃ (X = Cl, Br, I) Perovskite Nanocrystals Covering a Wide Wavelength Range by Postsynthetic Treatment with Tetrafluoroborate Salts. *Chem. Mater.* **2018**, *30*, 3633–3637.
- (31) Wang, S.; Wang, Y.; Zhang, Y.; Zhang, X.; Shen, X.; Zhuang, X.; Lu, P.; Yu, W. W.; Kershaw, S. V.; Rogach, A. L., Cesium Lead Chloride/Bromide Perovskite Quantum Dots with Strong Blue Emission Realized via a Nitrate-Induced Selective Surface Defect Elimination Process. *J. Phys. Chem. Lett.* **2019**, *10*, 90–96.
- (32) Li, F.; Liu, Y.; Wang, H.; Zhan, Q.; Liu, Q.; Xia, Z., Postsynthetic Surface Trap Removal of CsPbX₃ (X = Cl, Br, or I) Quantum Dots via a ZnX₂/Hexane Solution toward an Enhanced Luminescence Quantum Yield. *Chem. Mater.* **2018**, *30*, 8546–8554.
- (33) Shen, X.; Wang, S.; Zhang, X.; Wang, H.; Zhang, X.; Wang, C.; Gao, Y.; Shi, Z.; Yu, W. W.; Zhang, Y., Enhancing the efficiency of CsPbX₃ (X = Cl, Br, I) nanocrystals via simultaneous surface peeling and surface passivation. *Nanoscale* **2019**, *11*, 11464-11469.
- (34) Yong, Z.-J.; Guo, S.-Q.; Ma, J.-P.; Zhang, J.-Y.; Li, Z.-Y.; Chen, Y.-M.; Zhang, B.-B.; Zhou, Y.; Shu, J.; Gu, J.-L.; Zheng, L.-R.; Bakr, O. M.; Sun, H.-T., Doping-Enhanced Short-Range Order of Perovskite Nanocrystals for Near-Unity Violet Luminescence Quantum Yield. *J. Am. Chem. Soc.* **2018**, *140*, 9942–9951.
- (35) Yao, J.-S.; Ge, J.; Han, B.-N.; Wang, K.-H.; Yao, H.-B.; Yu, H.-L.; Li, J.-H.; Zhu, B.-S.; Song, J.-Z.; Chen, C.; Zhang, Q.; Zeng, H.-B.; Luo, Y.; Yu, S.-H., Ce³⁺-Doping to Modulate Photoluminescence Kinetics for Efficient CsPbBr₃ Nanocrystals Based Light-Emitting Diodes. *J. Am. Chem. Soc.* **2018**, *140*, 3626–3634.
- (36) De, A.; Das, S.; Mondal, N.; Samanta, A., Highly Luminescent Violet- and Blue-Emitting Stable Perovskite Nanocrystals. *ACS Materials Lett.* **2019**, *1*, 116–122.

- (37) Vitoreti, A. B. F.; Agouram, S.; Fuente, M. S. d. I.; Muñoz-Sanjosé, V.; Schiavon, M. A.; Mora-Seró, I., Study of the Partial Substitution of Pb by Sn in Cs–Pb–Sn–Br Nanocrystals Owing to Obtaining Stable Nanoparticles with Excellent Optical Properties. *J. Phys. Chem. C* **2018**, *122*, 14222–14231.
- (38) Li, S.; Shi, Z.; Zhang, F.; Wang, L.; Ma, Z.; Yang, D.; Yao, Z.; Wu, D.; Xu, T.-T.; Tian, Y.; Zhang, Y.; Shan, C.; Li, X. J., Sodium Doping-Enhanced Emission Efficiency and Stability of CsPbBr₃ Nanocrystals for White Light-Emitting Devices. *Chem. Mater.* **2019**, *31*, 3917–3928.
- (39) Stam, W. v. d.; Geuchies, J. J.; Altantzis, T.; Bos, K. H. W. v. d.; Meeldijk, J. D.; Aert, S. V.; Bals, S.; Vanmaekelbergh, D.; Donega, C. d. M., Highly Emissive Divalent-Ion-Doped Colloidal CsPb_{1-x}MxBr₃ Perovskite Nanocrystals through Cation Exchange. *J. Am. Chem. Soc.* **2017**, *139*, 4087–4097.
- (40) Bi, C.; Wang, S.; Li, Q.; Kershaw, S. V.; Tian, J.; Rogach, A. L., Thermally Stable Copper(II)-Doped Cesium Lead Halide Perovskite Quantum Dots with Strong Blue Emission. *J. Phys. Chem. Lett.* **2019**, *10*, 943–952.
- (41) Mondal, N.; De, A.; Samanta, A., Achieving Near-Unity Photoluminescence Efficiency for Blue-Violet-Emitting Perovskite Nanocrystals. *ACS Energy Lett.* **2019**, *4*, 32–39.
- (42) Das, S.; De, A.; Samanta, A., Ambient Condition Mg²⁺ Doping Producing Highly Luminescent Green- and Violet-Emitting Perovskite Nanocrystals with Reduced Toxicity and Enhanced Stability. *J. Phys. Chem. Lett.* **2020**, *11*, 1178–1188.
- (43) Zhang, X.; Wang, H.; Hu, Y.; Pei, Y.; Wang, S.; Shi, Z.; Colvin, V. L.; Wang, S.; Zhang, Y.; Yu, W. W., Strong Blue Emission from Sb³⁺-Doped Super Small CsPbBr₃ Nanocrystals. *J. Phys. Chem. Lett.* **2019**, *10*, 1750–1756.
- (44) Uddin, M. A.; Mobley, J. K.; Masud, A. A.; Liu, T.; Calabro, R. L.; Kim, D.-Y.; Richards, C. I.; Graham, K. R., Mechanistic Exploration of Dodecanethiol-Treated Colloidal CsPbBr₃ Nanocrystals with Photoluminescence Quantum Yields Reaching Near 100%. *J. Phys. Chem. C* **2019**, *123*, 18103–18112.

- (45) Zheng, X.; Yuan, S.; Liu, J.; Yin, J.; Yuan, F.; Shen, W.-S.; Yao, K.; Wei, M.; Zhou, C.; Song, K.; Zhang, B.-B.; Lin, Y.; Hedhili, M. N.; Wehbe, N.; Han, Y.; Sun, H.-T.; Lu, Z.-H.; Anthopoulos, T. D.; Mohammed, O. F.; Sargent, E. H.; Liao, L.-S.; Bakr, O. M., Chlorine Vacancy Passivation in Mixed Halide Perovskite Quantum Dots by Organic Pseudohalides Enables Efficient Rec. 2020 Blue Light-Emitting Diodes. *ACS Energy Lett.* **2020**, *5*, 793–798.
- (46) Almeida, G.; Ashton, O. J.; Goldoni, L.; Maggioni, D.; Petralanda, U.; Mishra, N.; Akkerman, Q. A.; Infante, I.; Snaith, H. J.; Manna, L., The Phosphine Oxide Route toward Lead Halide Perovskite Nanocrystals. *J. Am. Chem. Soc.* **2018**, *140*, 14878–14886.
- (47) Pan, J.; Quan, L. N.; Zhao, Y.; Peng, W.; Murali, B.; Sarmah, S. P.; Yuan, M.; Sinatra, L.; Alyami, N. M.; Liu, J.; Yassitepe, E.; Yang, Z.; Voznyy, O.; Comin, R.; Hedhili, M. N.; Mohammed, O. F.; Lu, Z. H.; Kim, D. H.; Sargent, E. H.; Bakr, O. M., Highly Efficient Perovskite-Quantum-Dot Light-Emitting Diodes by Surface Engineering. *Adv. Mater.* **2016**, *28*, 8718-8725.
- (48) Akhil, S.; Dutt, V. G. V.; Mishra, N., Surface Modification for Improving Photoredox Activity of CsPbBr₃ Nanocrystals. *Nanoscale Adv.* **2021**, *3*, 2547-2553.
- (49) Barkhouse, D. A. R.; Pattantyus-Abraham, A. G.; Levina, L.; Sargent, E. H., Thiols Passivate Recombination Centers in Colloidal Quantum Dots Leading to Enhanced Photovoltaic Device Efficiency. *ACS Nano* **2008**, *2*, 2356–2362.
- (50) Cao, J.; Yin, J.; Yuan, S.; Zhao, Y.; Li, J.; Zheng, N., Thiols as interfacial modifiers to enhance the performance and stability of perovskite solar cells. *Nanoscale* **2015**, *7*, 9443-9447.
- (51) Ruan, L.; Shen, W.; Wang, A.; Zhou, Q.; Zhang, H.; Deng, Z., Stable and conductive lead halide perovskites facilitated by X-type ligands. *Nanoscale* **2017**, *9*, 7252-7259.
- (52) Rurack, K.; Spieles, M., Fluorescence Quantum Yields of a Series of Red and Near-Infrared Dyes Emitting at 600–1000 nm. *Anal. Chem.* **2011,** 83, 1232–1242.
- (53) Morris, J. V.; Mahaney, M. A.; Huber, J. R., Fluorescence quantum yield determinations. 9,10-Diphenylanthracene as a reference standard in different solvents. *J. Phys. Chem.* **1976**, *80*, 969–974.

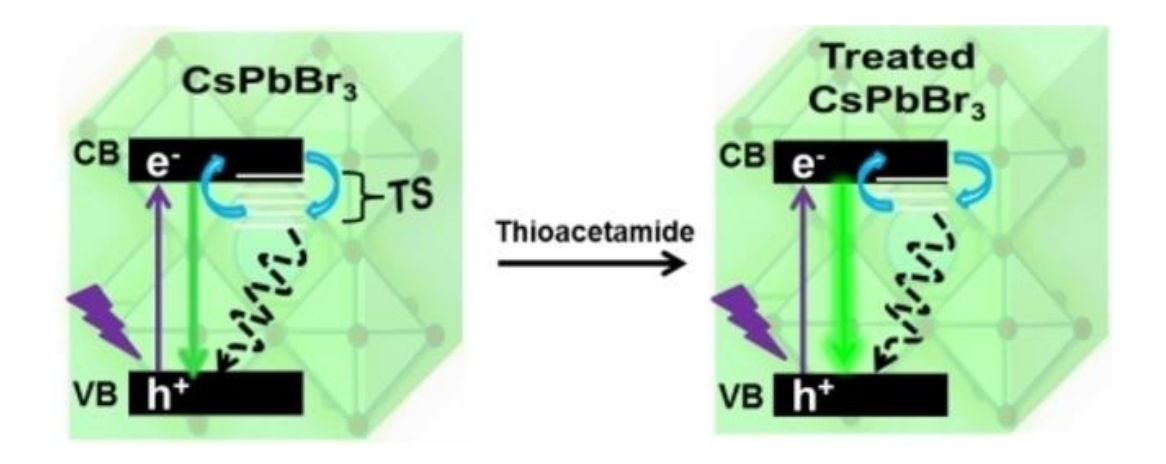
- (54) R.F.Kubin; A.N.Fletcher, Fluorescence quantum yields of some rhodamine dyes. *J. Lumin.* **1982,** 27, 455-462.
- (55) De, A.; Das, S.; Samanta, A., Hot Hole Transfer Dynamics from CsPbBr₃ Perovskite Nanocrystals. *ACS Energy Lett.* **2020**, *5*, 2246–2252.
- (56) Chirvony, V. S.; González-Carrero, S.; Suárez, I.; Galian, R. E.; Sessolo, M.; Bolink, H. J.; Martínez-Pastor, J. P.; Pérez-Prieto, J., Delayed Luminescence in Lead Halide Perovskite Nanocrystals. *J. Phys. Chem. C* **2017**, *121*, 13381–13390.
- (57) Mondal, N.; Samanta, A., Complete ultrafast charge carrier dynamics in photo-excited all-inorganic perovskite nanocrystals (CsPbX₃). *Nanoscale* **2017**, *9*, 1878-1885.
- (58) Newbury, D. E., Mistakes Encountered During Automatic Peak Identification of Minorand Trace Constituents in Electron-Excited Energy Dispersive X-Ray Microanalysis. *Scanning* **2009**, *31*, 91-101.
- (59) Thompson, K., The Role of Energy Resolution in Collecting World-Class Data for EDS. *Thermo Fisher Scientific Technical Notes* 52537 **2013**.
- (60) Baek, S.; Kim, Y.; Kim, S.-W., Highly photo-stable CsPbI₃ perovskite quantum dots via thiol ligand exchange and their polymer film application. *J. Ind. Eng. Chem.* **2019**, *83*, 279-284.
- (61) Chen, J.-K.; Ma, J.-P.; Guo, S.-Q.; Chen, Y.-M.; Zhao, Q.; Zhang, B.-B.; Li, Z.-Y.; Zhou, Y.; Hou, J.; Kuroiwa, Y.; Moriyoshi, C.; Bakr, O. M.; Zhang, J.; Sun, H.-T., High-Efficiency Violet Emitting All-Inorganic Perovskite Nanocrystals Enabled by Alkaline-Earth Metal Passivation. *Chem. Mater.* **2019**, *31*, 3974–3983.
- (62) Huynh, K. A.; Bae, S.-R.; Nguyen, T. V.; Do, H. H.; Heo, D. Y.; Park, J.; Lee, T.-W.; Le, Q. V.; Ahn, S. H.; Kim, S. Y., Ligand-Assisted Sulfide Surface Treatment of CsPbI₃ Perovskite Quantum Dots to Increase Photoluminescence and Recovery. *ACS Photonics* **2021**, *8*, 1979–1987.
- (63) Berti, I. O. P. D.; Cagnoli, M. V.; Pecchi, G.; Alessandrini, J. L.; Stewart, S. J.; Bengoa, J. F.; Marchetti, S. G., Alternative low-cost approach to the synthesis of magnetic iron oxide

nanoparticles by thermal decomposition of organic precursors. *Nanotechnology* **2013**, *24*, 175601-175612.

- (64) Yang, D.; Li, X.; Zhou, W.; Zhang, S.; Meng, C.; Wu, Y.; Wang, Y.; Zeng, H., CsPbBr₃ Quantum Dots 2.0: Benzenesulfonic Acid Equivalent Ligand Awakens Complete Purification. *Adv. Mater.* **2019**, *31*, 1900767-1900774.
- (65) Dinegar, R. H.; Smellie, R. H.; Mer, V. K. L., Kinetics of the Acid Decomposition of Sodium Thiosulfate in Dilute Solutions. *J. Am. Chem. Soc.* **1951,** *73*, 2050–2054.
- (66) Mizoguchi, T.; Takei, Y.; Okabe, T., The Chemical Behaviour of Low Valence Sulfur Compounds. X.¹⁾ Disproportionation of Thiosulfate, Trithionate, Tetrathionate and Sulfite under Acidic Conditions. *Bulletin of The Chemical Society of Japan* **1976**, *49*, 70-75.
- (67) Noel, N. K.; Abate, A.; Stranks, S. D.; Parrott, E. S.; Burlakov, V. M.; Goriely, A.; Snaith, H. J., Enhanced Photoluminescence and Solar Cell Performance via Lewis Base Passivation of Organic–Inorganic Lead Halide Perovskites. *ACS Nano* **2014**, *8*, 9815–9821.
- (68) Cai, T.; Li, F.; Jiang, Y.; Liu, X.; Xia, X.; Wang, X.; Peng, J.; Wanga, L.; Daoud, W. A., In situ inclusion of thiocyanate for highly luminescent and stable CH₃NH₃PbBr₃ perovskite nanocrystals. *Nanoscale* **2019**, *11*, 1319-1325.

CHAPTER 4

Room-Temperature Treatment with Thioacetamide Yielding Blue-and Green-Emitting CsPbX₃ Perovskite Nanocrystals with Enhanced Photoluminescence Efficiency and Stability



ChemNanoMat. 2022, 8, e202200029

Overview

While multiple protocols are currently available for obtaining green- and red-emitting lead halide perovskite nanocrystals (NCs) with near-unity photoluminescence quantum yield (PLQY), achieving this target for the blue-emitting NCs is still quite challenging. This is an impediment to the development of perovskite-based highly efficient white LEDs of which blue is an essential component. Herein, we show that room-temperature treatment of the blue-emitting CsPbCl_{1.5}Br_{1.5}, cyan-emitting CsPbClBr₂ and green-emitting CsPbBr₃ NCs with thioacetamide not only enhances the PLQY to near-unity (~ 97-99%) without affecting the PL maximum and bandwidth, but also improves the stability of the systems significantly. The investigation reveals that effective passivation of under-coordinated surface Pb²⁺ through formation of Pb-S and Pb-NH₂ bonds and removal of excess lead atoms suppress the nonradiative recombination channels and enhances the PLQY and stability of the NCs. Outstanding PL efficiency and superior long-term stability make these systems potential ingredients for various lighting and display applications.

4.1. Introduction

Cesium lead halide (CsPbX₃ X = Cl, Br or I) perovskite NCs have attracted considerable attention in recent years as promising materials for optoelectronic applications as photodetectors,¹ light-emitting diodes (LEDs),² TV displays and laser $^{[3,4]}$ due to their excellent optical properties, such as high PLQY $^{5-8}$ with narrow emission bandwidth, 9 composition- and size-dependent tunability of the band gap over the entire visible region of the electromagnetic spectrum. $^{9-12}$

However, the PL properties of these NCs are very sensitive to the surface due to high surface-tovolume ratio. 7,13,14 Indeed, sub-unity PLQY and instability of the colloidal solution are reflection of the surface defects in these systems that need to be eliminated for obtaining NCs with high PLOY and greater colloidal stability. The literature suggests that excess lead from lead-rich (or halide-deficient) surface creates deep or shallow inter-bandgap energy levels, which trap the charge carriers and decrease the PLQY of the perovskite NCs.⁵ An important point to note here is that as these trap states are shallow in nature in green- emitting CsPbBr₃ NCs, these systems possess fairly high PLQY (typically, ~ 50-80%). In contrast, the trap states are deep in nature in violet-emitting CsPbCl₃ and blue-emitting CsPb(Cl/Br)₃ NCs and the PLQY of these systems are typically <5% and <40%, respectively. 15-17 It is quite challenging to produce brightly luminescent blue-emitting NCs with near-unity PLQY. The literature suggests that post-synthetic surface modification is an effective way of eliminating excess lead from the surface 5,18-20 and suppressing halide deficiency related defects. ^{21–25} However, a common post-synthetic method for enhancing the PLOY of both green and blue-emitting NCs to near-unity is rather limited. 18,26 Taking advantage of strong interaction between sulfur and lead sulfur-containing systems are often used for the suppression of defects arising from under-coordinated Pb2+ of the halide deficient surface. 27,28 It should be noted in this context that most of the surface passivation studies on greenemitting CsPbBr₃ NCs have been carried out using long chain thiols except in two cases. ^{26,29} Bakr and co-workers recently used a thiocyanate salt to enhance the PLQY of the CsPb(Br_xCl_{1-x})₃ NCs in a post-synthetic treatment.²⁹ Relying on the formation of strong Pb-S bonds with undercoordinated lead atoms, we recently showed that PLQY of the green-emitting CsPbBr3, blueemitting CsPb(Cl/Br)₃ and yellow-emitting CsPb(Br/I)₃ NCs can be boosted to near-unity upon treatment with sodium thiosulfate.²⁶ Zhang and co-workers showed that an aqueous solution of thiourea post-synthetically changes CsPbBr₃ NCs to stable nanowires with enhanced PLQY of ~ 60%.³⁰ However, this is again limited only to the green- emitting CsPbBr₃ NCs.

In this work, we examine how a small sulfur-containing system, thioacetamide (TAA), which is structurally similar to thiourea, can influence the optical properties and stability of the perovskite NCs. The results show that room temperature (RT) post-synthetic treatment of blue-emitting CsPbCl_{1.5}Br_{1.5}, cyan-emitting CsPbClBr₂ and green-emitting CsPbBr₃ NCs with TAA enhances the PLQY from an initial value of ~ 12–25% to near-unity (~ 97–99%). The experimental data suggests that effective passivation of under-coordinated Pb²⁺ of the surface and removal of excess Pb by TAA impart exceptional PLQY to the NCs through suppression of nonradiative recombination channels. Furthermore, formation of strong Pb-S bonds provides robust ligand environment around the NCs that improves their colloidal stability under various external conditions.

4.2. Results and Discussion

4.2.1. Synthesis and Characterization of the NCs

The colloidal CsPbBr₃ and mixed halide CsPb(Cl/Br)₃ NCs were synthesized by minor modification of a known method (details in chapter 2).⁹ The purified NCs were dispersed in toluene for further studies. A diluted version (μM concentration) of the above colloidal solution was used for the post-synthetic treatment with TAA under ambient condition. The transmission electron microscope (TEM) images show cubic morphology of the as-synthesized and treated CsPbBr₃ NCs with average edge length of ~ 9.7 nm, which remains unchanged after the post-synthesis treatment (Figure 4.1a, b). A similar observation is made for the CsPbCl₃, CsPbCl_{1.5}Br_{1.5}, CsPbClBr₂ and CsPbCl₂Br NCs with average edge lengths between ~ 9.5 to 11.3 nm (Figure A2.1). The high resolution TEM images of the as-synthesized and treated CsPbBr₃ NCs show identical inter-planar distance (d) of ~ 0.58 nm corresponding to the (100) lattice plane (insets figure 4.1a, b).⁹ The

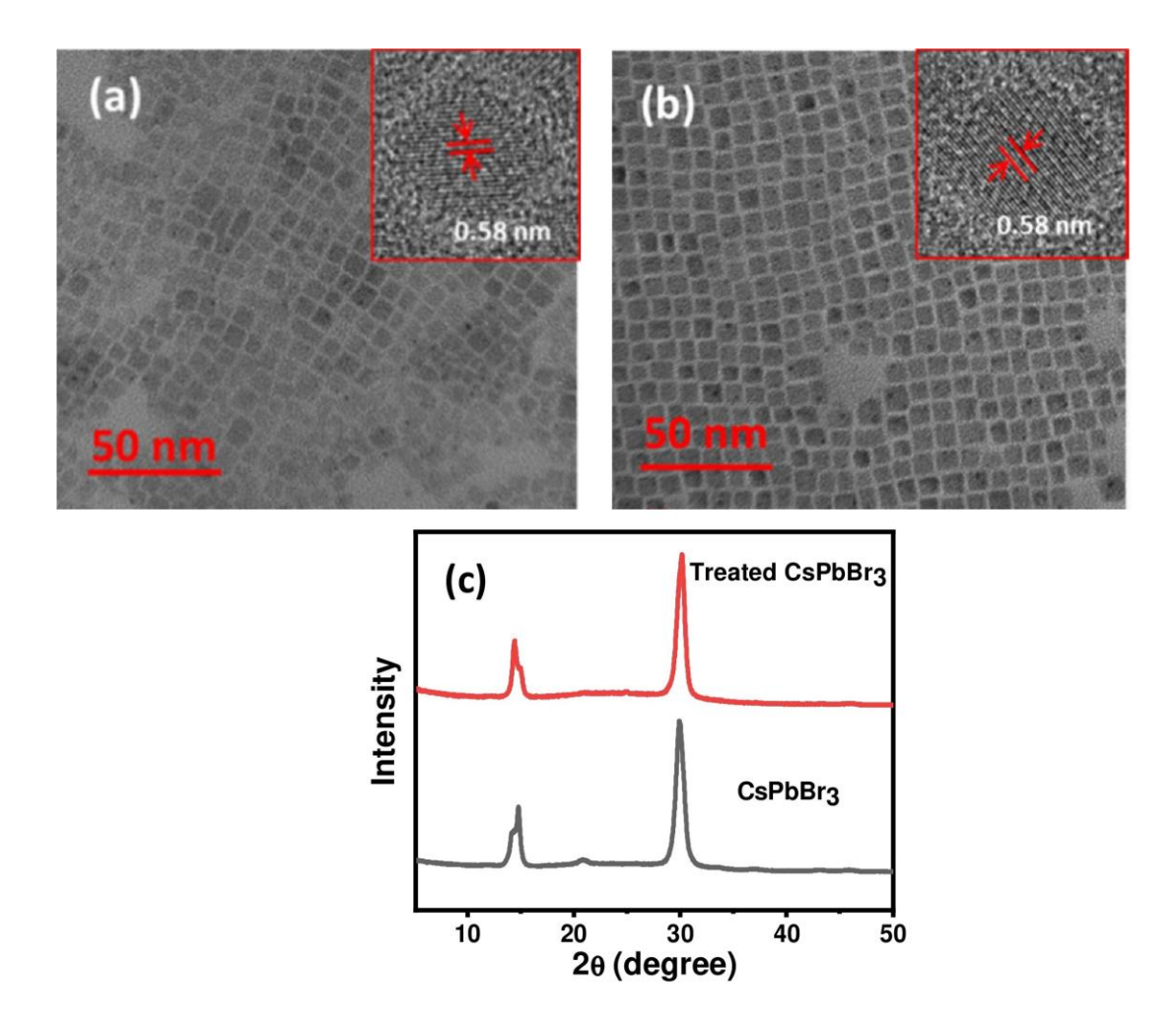


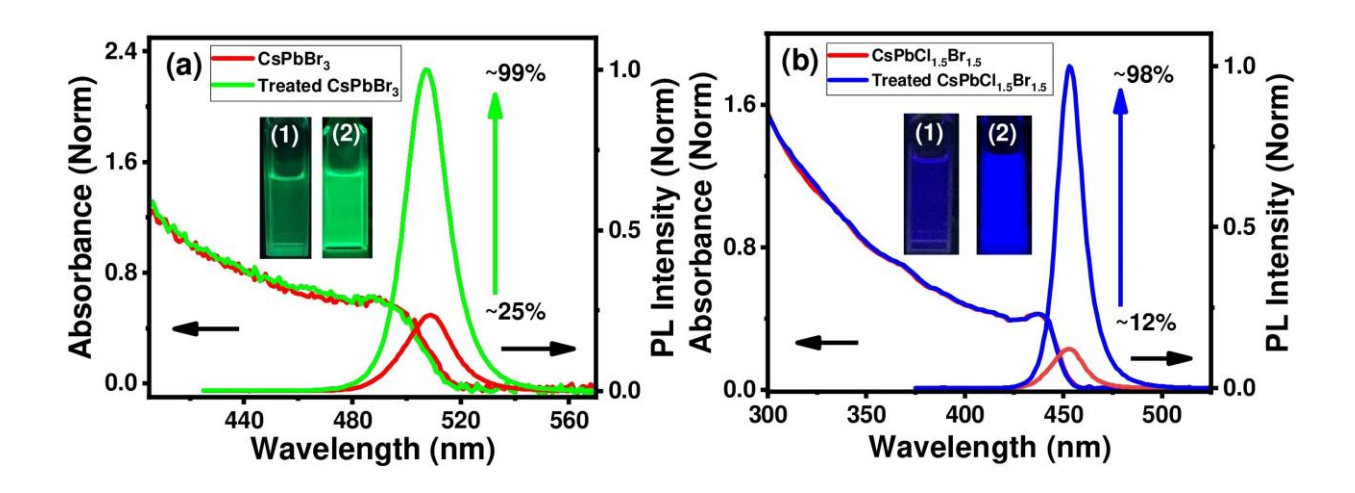
Figure 4.1. TEM images of the (a) as-synthesized and (b) treated CsPbBr₃ NCs. The insets show corresponding HR-TEM images indicating same interplanar distance. (c) XRD patterns of assynthesized and treated CsPbBr₃ NCs.

unchanged powder X-ray diffraction (PXRD) patterns of the CsPbBr₃ NCs and absence of any additional peak after the post-synthetic treatment indicate no change in crystal structure of the NCs (Figure 4.1c) implying that it is only the surface that gets modified after the TAA treatment. The splitting of the (100) diffraction peak is perhaps an indication of the presence of orthorhombic phase, whose proportion increases slightly after treatment, as evident from switching of the peak intensities around ~14 degrees. ³¹ The blue-emitting CsPbCl_{1.5}Br_{1.5}, cyan-emitting CsPbClBr₂, and

violet-emitting CsPbCl₂Br and CsPbCl₃ NCs also preserve their cubic crystal structure after the treatment (Figure A2.2).

4.2.2. Optical Properties

Although the absorption and emission spectral features of the systems before and after the treatment are very similar, a substantial enhancement of the PL intensity for all the systems is observed following the treatment. For example, the PLQY of green-emitting CsPbBr₃, blue-emitting CsPbCl_{1.5}Br_{1.5} and cyan- emitting CsPbClBr₂ NCs is increased to near-unity (~ 97–99%) from the initial values of 25%, 12%, and 15%, respectively (Figure 4.2a, b, c). Even for the violet-emitting CsPbCl₃ and CsPbCl₂Br NCs, a substantial improvement of the PLQY to ~ 23% and ~ 62% from the initial values of < 1% and 14%, respectively is noticed (Figure 4.2d, e). Thus, our post-synthetic method is quite effective for a variety of systems emitting in the 400-510 nm region of the visible spectrum. The bright digital images of the treated NCs highlight the enhanced PL of the NCs (inset of Figure 4.2). A point to note here is that a small (~ 2 nm) blue- shift of the PL maxima is observed after the treatment only in the case of CsPbBr₃ NCs, though no such shift of the absorption spectrum observed. This blue-shift is presumably due to the removal of shallow trap states of the as-synthesized CsPbBr₃ NCs. The observation of near-unity PLQY of the treated mixed-halide NCs is quite remarkable considering that these are blue- emitting NCs and very few post-synthetic strategies can achieve this feat.



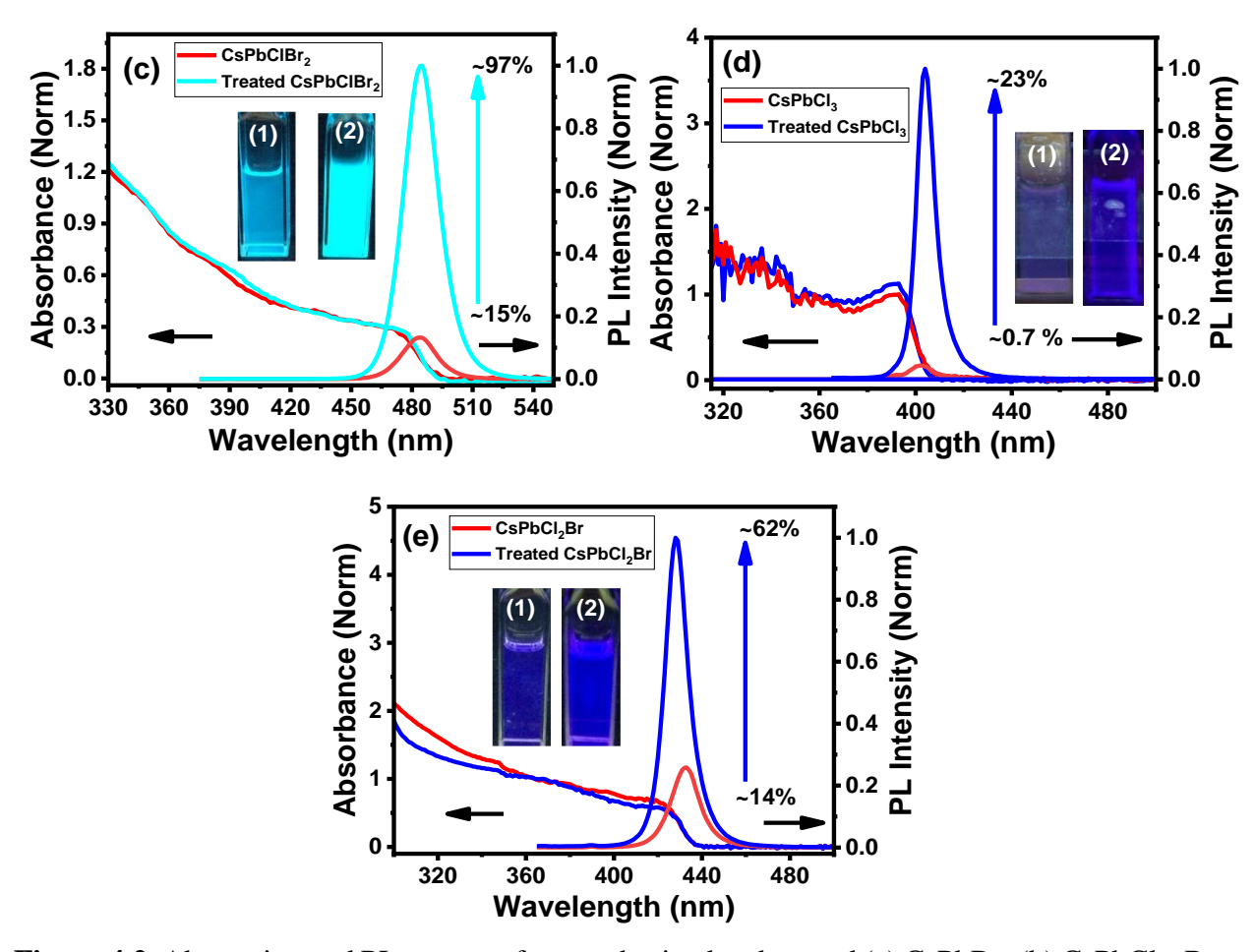
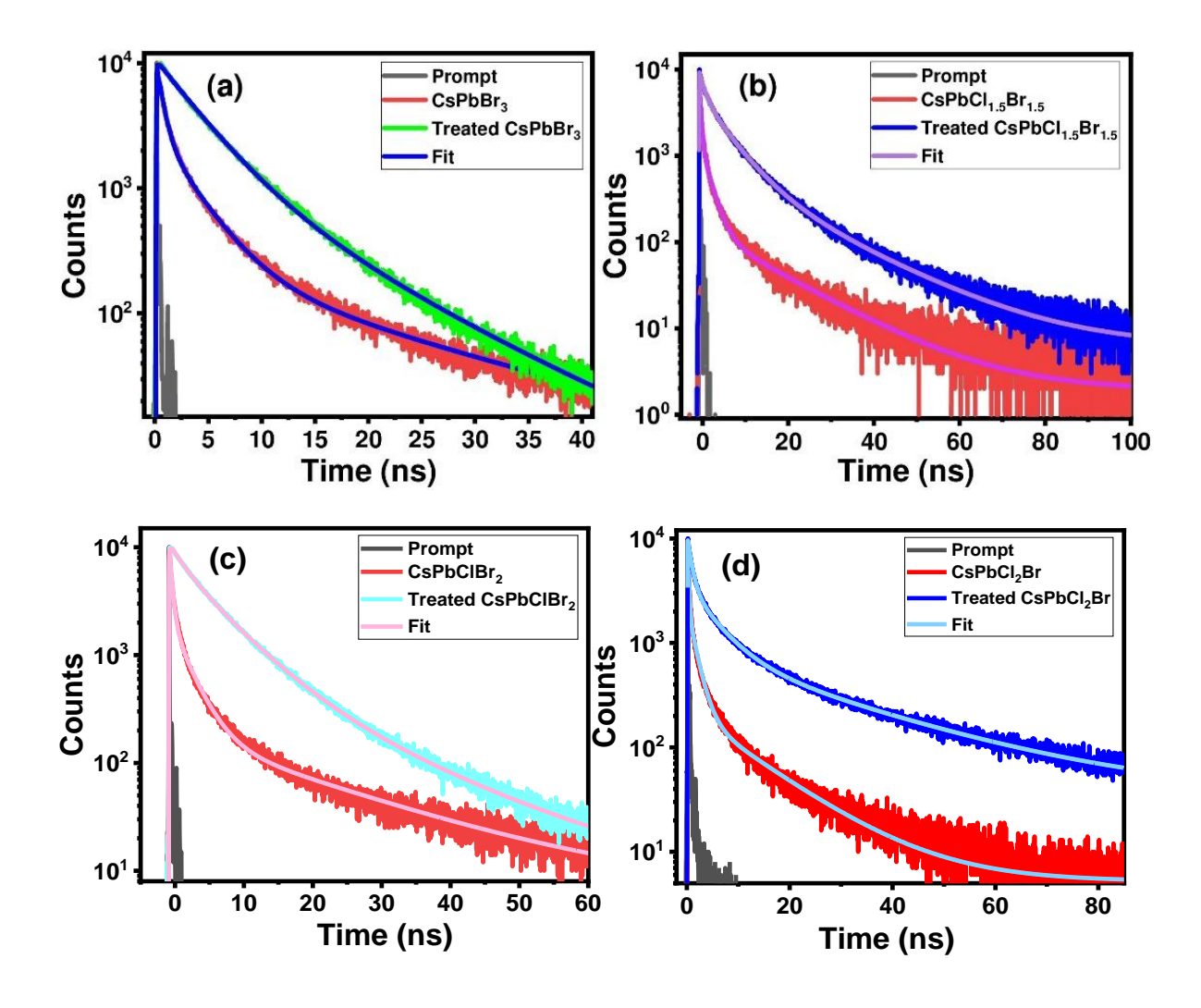


Figure 4.2. Absorption and PL spectra of as-synthesized and treated (a) CsPbBr₃ (b) CsPbCl_{1.5}Br_{1.5} and (c) CsPbClBr₂ (d) CsPbCl₃ (e) CsPbCl₂Br NCs. Insets show the photographs of as-synthesized (1) and treated (2) NCs under 365 nm UV light.

4.2.3. Time Resolved Measurements

In order to understand the associated photophysical processes in the NCs before and after the treatment, PL decay behavior of the systems is studied using a time-correlated single photon counting (TCSPC) fluorescence setup. The PL decay profile of the as-synthesized CsPbBr₃ NCs changes from tri-exponential to a bi-exponential one after the treatment (Figure 4.3a). The contribution of the 3.02 ns component (Table 4.1), which arises from band-edge excitonic recombination, increases from 25% to 85% on treatment indicating more efficient radiative

recombination process in the treated system. Similarly, the long-component (16.60 ns), which arises from shallow trap-mediated band-edge radiative recombination ³² increases from just 2% to 15%. Interestingly, the shortest sub- nanosecond component (0.56 ns), which was the major radiative recombination process in as-synthesized CsPbBr₃ NCs, vanishes after the treatment. This component, which can be attributed to surface defect related nonradiative recombination process in as-synthesized CsPbBr₃ NCs, is completely eliminated in the treated system. ^{18,31} In the case of CsPbCl_{1.5}Br_{1.5}, CsPbClBr₂, and CsPbCl₂Br NCs (Figure 4.3b,c,d), though the PL decay profile remains tri-exponential even after the treatment, a much higher contribution of the band-edge



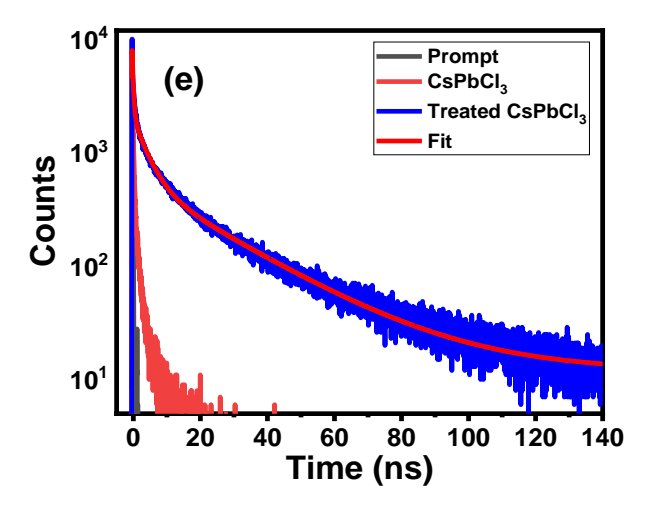


Figure 4.3. PL decay profiles of the as-synthesized and treated (a) CsPbBr₃ (b) CsPbCl_{1.5}Br_{1.5} (c) CsPbClBr₂ (d) CsPbCl₂Br and (e) CsPbCl₃ NCs. The decay profiles were obtained by exciting the spectrum at 375 and 405 nm using a diode laser and by monitoring the PL at their respective PL maxima.

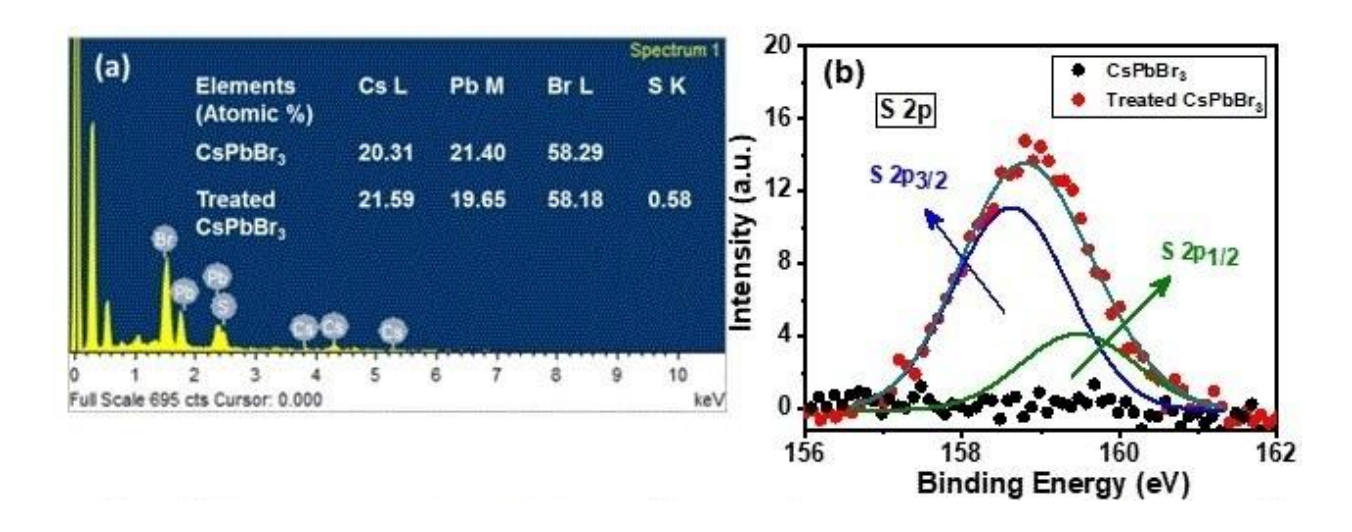
excitonic recombination (16% vs 50%), (16% vs 66%) and (11% vs 64%), with substantial decrease of the trapping component (82% vs 43%), (82% vs 25%) and (87% vs 28%) corroborates significant suppression of nonradiative recombination and much improved PLQY of the treated NCs (Table 4.1). In all cases, the shortest component is attributed to surface trap related nonradiative recombination, the intermediate one to direct band-edge radiative recombination and the long component to shallow trap related band-edge radiative recombination process. $^{18,31-33}$ A quantitative estimate of the radiative and nonradiative rate constants (k_r and k_{nr} , respectively) in as- synthesized and treated NCs is made from the measured PLQY and lifetime data. A decrease in the k_{nr} value by a factor of ~ 30-230 in treated CsPbBr₃, CsPbCl_{1.5}Br_{1.5} CsPbClBr₂ and CsPbCl₂Br NCs, demonstrates significant suppression of the nonradiative recombination processes. The much improved decay profile, associated decay parameters, and the k_r , k_{nr} values of the violet-emitting CsPbCl₃ NCs (Figure 4.3e and Table 4.1).

Table 4.1. PL lifetime (τ_i) components, average lifetime $<\tau_{amp}>$, PLQY, radiative (k_r) and nonradiative (k_{nr}) rate constants in as-synthesized and treated CsPbBr₃, CsPbCl_{1.5}Br_{1.5}, CsPbClBr₂, CsPbCl₂Br and CsPbCl₃ NCs.

Samples	$\tau_1(\alpha_1)^{\#}/ns$	$\tau_2(\alpha_2)/ns$	τ ₃ (α ₃)/ns	PLQY	<τ _{amp} >§	k _r /ns ⁻¹	k _{nr} /n
				(%)	/ns		s ⁻¹
CsPbBr ₃	3.02(0.25)	16.6(0.02)	0.56(0.72)	~25	1.55	0.16	0.48
Treated	3.63(0.85)	9.66(0.15)		~99	4.33	0.22	0.00
CsPbBr ₃							22
CsPbCl _{1.5} Br _{1.5}	2.04(0.16)	15.61(0.01)	0.34(0.82)	~12	0.83	0.14	1
Treated	5.55(0.50)	17.14(0.07)	1.29(0.43)	~98	4.53	0.21	0.00
CsPbCl _{1.5} Br _{1.5}							44
CsPbClBr ₂	2.56(0.16)	19.63(0.01)	0.36(0.82)	~15	1.0	0.15	0.85
Treated	5.91(0.66)	15.89(0.08)	2.01(0.25)	~97	5.76	0.17	0.00
CsPbClBr ₂	3.91(0.00)	13.69(0.06)	2.01(0.23)	~91	5.70	0.17	52
CsPbCl ₂ Br	1.53(0.11)	12.29(0.01)	0.13(0.87)	~14	0.41	0.34	2.1
	,	,	` ,				
Treated	5.07(0.64)	25.79(0.07)	0.84(0.28)	~62	5.33	0.11	0.07
CsPbCl ₂ Br							1
CsPbCl ₃				~0.7			
Treated	1.0(0.77)	6.27(0.02)	0.09(0.20)	~23	0.91	0.25	0.84
CsPbCl ₃							

 $^{\#}\alpha_{i}$ represents the amplitude of the i-th lifetime component. $^{\$}$ $<\tau_{amp}>=\Sigma\tau_{i}\alpha_{i}/\Sigma\alpha_{i},\ k_{r}=PLQY/<\tau_{amp}>$ > and $k_{nr}=(1-PLQY)/<\tau_{amp}>$.

As mentioned already, TAA-treatment modifies the surface of the NCs without affecting the crystal structure of the system. We now attempt to determine the nature of change of the surface environment. Elemental analysis of the as-synthesized and treated NCs, made by scanning a large area of field emission scanning electron microscopy (FESEM) images (EDX measurement), shows a Br: Pb ratio of ~ 2.72 in CsPbBr₃, indicating a bromide deficient or lead-rich surface of the assynthesized NCs (Figure 4.4a). The increase of this ratio to ~ 2.96 after treatment indicates removal of excess lead from the surface of NCs. 5,18,19 It is important to note that although the EDX spectra and elemental analysis of the treated CsPbBr₃ NCs show a small but reproducible value of S, close proximity and multiplet nature of Pb M and S L lines make it difficult to comment on the presence of 'S' in treated NCs from this data. 34,35 However, evenly distributed S in the elemental mapping of the treated CsPbBr₃ NCs confirms the presence of sulfur containing species at the surface of the treated NCs (Figure A2.4). Further insight on the environment of the surface elements is accessed through XPS measurements. The XPS survey spectra of the as-synthesized and treated CsPbBr₃ NCs show very similar energy bands of Cs, Pb and Br, indicating similar elemental composition for both the NCs (Figure A2.5). Interestingly, a clear peak at ~ 159.11 eV corresponding to 'S 2p' is observed in the high-resolution XPS spectra of only the treated CsPbBr₃ NCs (Figure 4.4b),



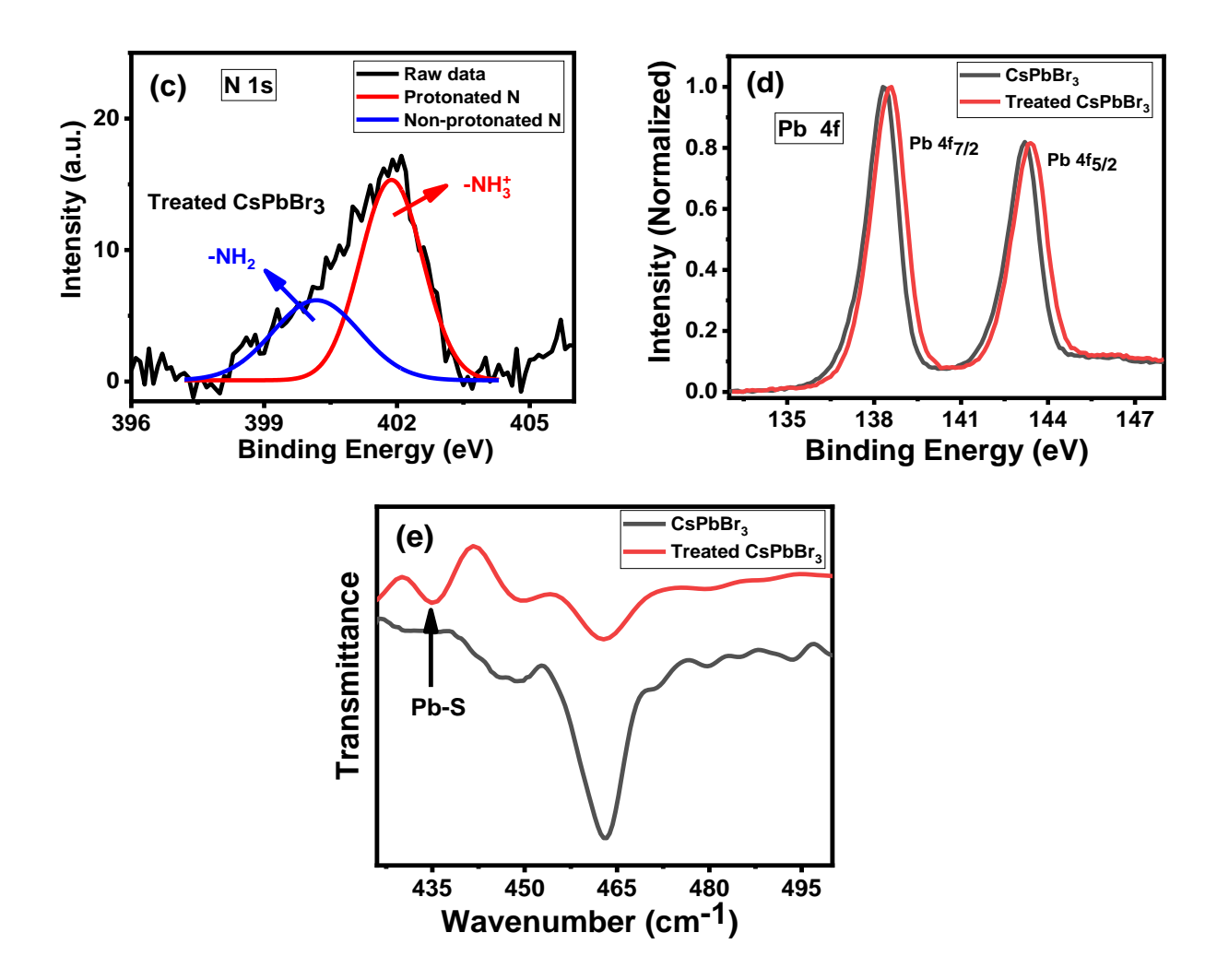


Figure 4.4. (a) EDX spectra of treated CsPbBr₃ NCs. The inset shows atomic % of the constituting elements. High resolution XPS spectra of (b) S 2p (c) N 1s (d) Pb 4f of as-synthesized and treated CsPbBr₃ NCs. The S 2p and N 1s peak are deconvoluted into two peaks. (e) FTIR spectra of assynthesized and treated NCs. The XPS data was calibrated with respect to C 1s peak at \sim 285 eV.

reconfirming the presence of TAA at the surface of the NCs. The 'S 2p' peak can be easily deconvoluted into two peaks at 159.5 and 158.5 eV corresponding to $2p_{1/2}$ and $2p_{3/2}$, respectively (Figure 4.4b).²⁷ The S $2p_{3/2}$ signal in treated sample suggests that TAA binds to under-coordinated

Pb²⁺ of the surface through S.^{28,30} Interestingly, the high-resolution 'N 1s' XPS spectra of the CsPbBr₃ NCs also show a noticeable change after the treatment (Figure 4.4c, A2.6). In case of treated CsPbBr₃ NCs, this signal can easily be deconvoluted into two signals with peaks at 400.1 and 401.8 eV, corresponding to unprotonated amine (-NH₂) and protonated amine (-NH₃+), respectively (Figure 4.4c).³⁶ The low-energy peak suggests formation of Pb-NH₂ bond as well in treated NCs through coordination of the -NH₂ moiety of TAA with under-coordinated Pb²⁺.^{36,37} In the high resolution spectra, both the Pb 4f peaks (4f_{7/2} and 4f_{5/2}) are shifted to higher binding energy by ~ 0.27 eV for the treated NCs (Figure 4.4d), which can be explained by the formation of strong Pb-S and Pb-NH₂ bonds at the surface.^{26,28,38} The calculated Br/Pb ratio of 2.7 and 2.94 in assynthesized and treated CsPbBr₃ NCs, respectively (Table 4.2) indicates removal of excess lead atoms from the surface of the NCs. This observation is in agreement with the EDX data

Table 4.2. Atomic % ratio in as-synthesized and treated CsPbBr₃ NCs obtained from XPS measurements. The Br/Pb atomic % ratios were obtained by dividing the integrated area under the corresponding XPS peaks by the atomic sensitivity factor (ASF) values for each of the elements. The ASF values for Pb 4f, Br 3d and S 2p are 6.7, 0.83 and 0.668, respectively.

Samples	Area under the curve of elements/ASF			Atomic % ratio (w.r.t. Pb)		
	Pb/6.7	Br/0.83	S/0.668	Br/Pb	S/Pb	
CsPbBr ₃	346627	937415		2.70		
Treated CsPbBr ₃	312553	918950	38076	2.94	0.12	

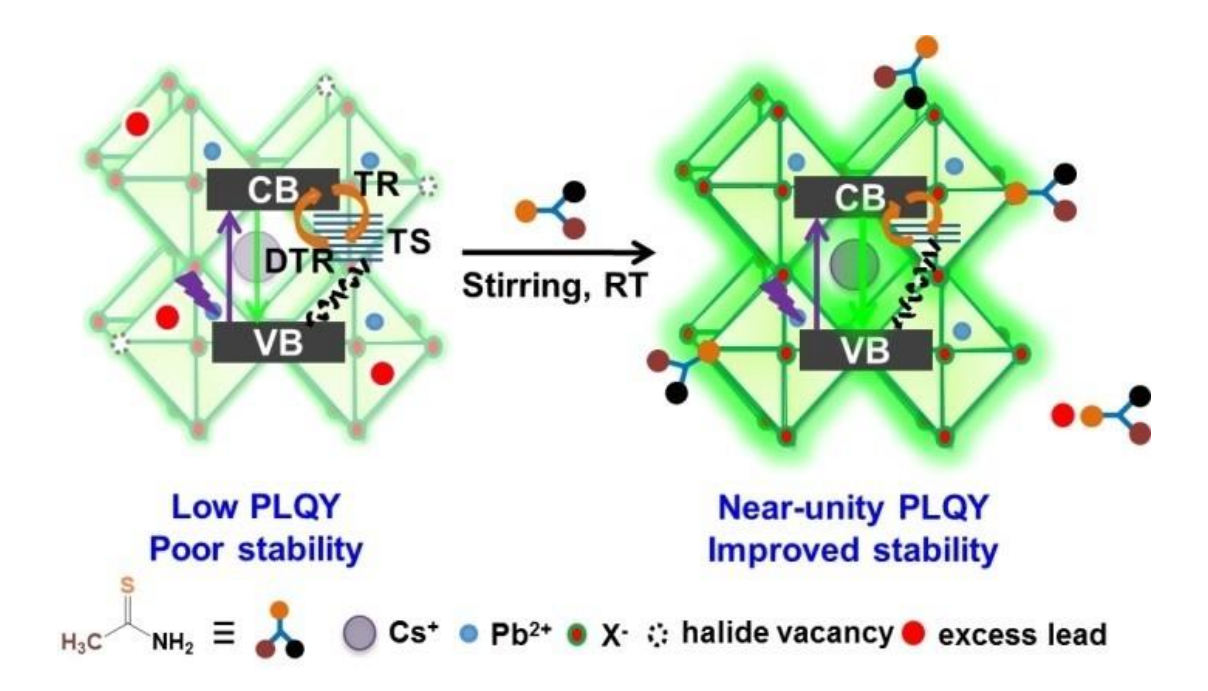
discussed above. It is important to note that in this particular case, the amount of surface lead atoms is probably very less (typically < 15%), and is beyond the detection limit of XPS.⁵ This is why no spectral feature for the Pb⁰ species could be observed at the lower energy side of $4f_{7/2}$ and $4f_{5/2}$ peaks in the high resolution Pb 4f XPS spectra. A similar observation was made in the case of

post-synthesis surface treatment of CsPbBr₃ NCs with thiocyanate salts.⁵ The attachment of TAA through formation of Pb-S bond is also confirmed by observation of distinct Pb-S stretching band at ~ 435 cm⁻¹ in the FTIR spectra of the treated CsPbBr₃ NCs (Figure 4.4e).³⁹ The adsorption of TAA also contributes to higher intensity of the C-H stretching and N-H bending (scissoring) bands of the treated NCs (Figure A2.8).⁴⁰ Thus it is evident that TAA passivates the surface of the NCs by attaching it with the under-coordinated surface Pb²⁺ through both 'S' and 'N' ends of the amino moiety. Thiophene and pyridine having donor sites similar to that in TAA are also known to form coordinate or dative covalent bond with under-coordinated Pb²⁺ leading to effective suppression of surface defects.⁴¹

Lead rich surface of the perovskite NCs is known to have deleterious effect on the optical properties of the NCs providing inter band-gap (shallow or deep) trap states at the surface of the NCs, which facilitate nonradiative recombination of the photo-generated charge carriers and decrease the PLQY of the systems.^{5,18} It is evident from the above discussion that removal of excess lead atoms from the lead-rich surface of the as-synthesized NCs by post-synthetic treatment with TAA effectively suppresses the shallow-electron trap states in treated NCs and enhances the PLQY of the system. Our post-synthetic treatment not only removes excess lead atom from surface, but also passivates the surface trap-states arising from halide vacancies, which form undercoordinated Pb²⁺, a positive charge center.⁴¹ The photogenerated electrons are dragged into these trap sites and later recombine with holes nonradiatively. TAA can interact with these centers and neutralize the excess positive charge forming strong Pb-S and Pb-NH₂ bonds that suppresses the nonradiative recombination process.^{29,41} Therefore, as pictorially shown in Scheme 4.1, effective suppression of the surface defects through elimination of excess lead atoms and passivation of under-coordinated Pb²⁺ enhances the radiative recombination greatly leading to dramatically improved PLQY of the NCs.

Long chain commonly used surface capping agent like oleylammonium cation (OAm⁺), which is for protecting the surface of the perovskite NCs, acts as insulating layer that obstructs the charge transport process and deteriorates the device performance.⁴² Additionally, the binding of OAm⁺

with the surface is dynamic in nature due to its deprotonation by oleate or halides. This exposes the surface of the NCs to the external environment and destabilizes the particles. 43,44 Post-synthetic



Scheme 4.1. Schematic representation of the associated photophysical processes in the untreated and treated CsPbX₃ NCs. The VB, CB, TR, DTR and TS denote valence band, conduction band, trapping recombination, de-trapping recombination and trap states, respectively.

surface treatment with quaternary ammonium salt like didodecyldimethylammonium bromide (DDAB) though improves the optical properties and stability of the perovskite NCs, ^{45,46} in some cases, it produces morphological species with reduced PLQY. Surface passivation by small ligands is an attractive approach of protecting a surface without obstructing the charge transport process in real applications. Relying on the strong binding affinity of sulfur towards lead, small sulfur-containing species are expected to be effective alternatives to the long chain insulating ligands (including thiols). However, Bakr and co-workers although succeeded in enhancing the PLQY of the CsPb(Br_xCl_{1-x})₃ NCs to near-unity using thiocyanate, the method works only for one

blue-emitting ($\lambda_{em} = 468$ nm) NCs.²⁹ Li et al. found that post-synthetic treatment of the CsPbBr3 NCs with thiourea leads to morphological transformation of these NCs into 1D nanowires.³⁰ Though these two reports on post-synthetic surface treatment with small sulfur-containing ligands are not very encouraging, our recent study involving thiosulfate shows effective passivation of the under-coordinated Pb²⁺ through formation of strong Pb-S bond and near-unity PLQY of a range of systems emitting in the 460-580 nm region without affecting the morphology and crystal structure of the NCs.²⁶ In the present work, however, we demonstrate that RT treatment not only passivates the trap states related to the under-coordinated Pb²⁺ ions by forming strong bonds with TAA, but unlike other sulfur-containing systems, it also effectively removes excess lead atom from the surface enabling near-unity PLQY and much improved stability of the NCs emitting in a wide blue-green region. Table 4.3 collects the data on post-synthetic treatment of the perovskite NCs with small sulfur-containing ligands.

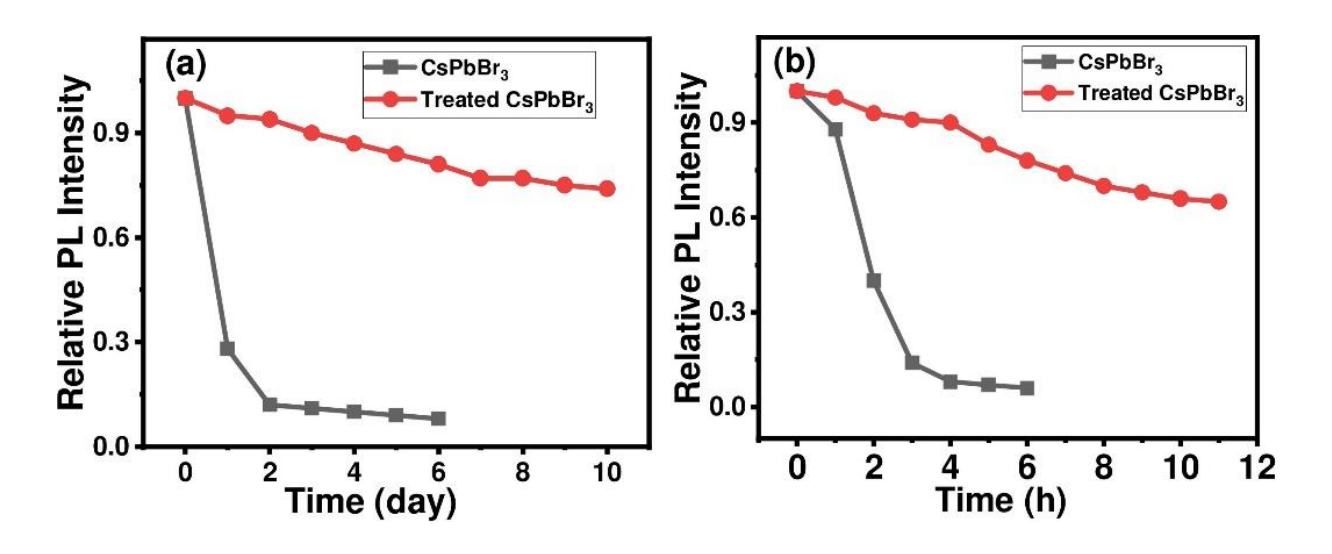
Table 4.3. A comparison of the different post-synthetic treatment using small sulfur containing ligands on the optical properties and stability of the NCs.

Systems	Morpho- logical changes	Sulfur- containing ligands used for post-synthetic treatment	PLQY (%)	λ _{em} (nm)	Stability	Ref.
CsPbBr ₃	NA	Sodium and ammonium thiocyanate	~100	509	Retains ~88% of initial PL after >85 h of UV illumination	5
CsPbBr ₃ CsPbCl ₃	NCs to NWs	aqueous solution of thiourea	>60	447	CsPbBr ₃ NWs: stable for >2 months under ambient condition and ~95% of	30
CsPbCl _{1.5} Br _{1.5} CsPbBr _{1.5} I _{1.5}				345 to 552	initial PL is retained after 2h in presence of water	

ROOM-TEMPER	ATURE TRE	ATMENT			СНАР	TER 4
$CsPb(Br_xCl_{1-x})_3$	NA	Thiocyanate	~100	~468		29
CsPbCl _{1.5} Br _{1.5}	NA	Sodium	~100	463	CsPbBr ₃ NCs:	
CsPbClBr ₂		thiosulfate	"	493	retains ~84% and ~80% of initial PL after 8 days under	
CsPbBr ₃			"	512	ambient condition and 7h of	
CsPbBr _{1.5} I _{1.5}			~90	581	continuous UV light illumination, respectively.	
					respectively.	26
					CsPbCl _{1.5} Br _{1.5} NCs:	
					retains >80% of	
					initial PL intensity after 10 days	
					under ambient condition and 7h	
					of continuous UV	
					light illumination.	
CsPbBr ₃	NA	Thioacetamide	~99	508	CsPbBr ₃ NCs:	
CsPbClBr ₂			~97	485	maintains ~76% and ~65% of	
CsPbCl _{1.5} Br _{1.5}			~98	453	initial PL intensity after 10 days and 11h under ambient	
CsPbCl ₂ Br			~62	428	condition and UV light illumination,	
CsPbCl ₃			~23	404	respectively.	This
					CsPbCl _{1.5} Br _{1.5} NCs: maintains ~80% of initial PL intensity after 11	wor- k
					days under ambient condition and 10h of UV light illumination.	

ROOM-TEMPERATURE TREATMENT			CHAP'	TER 4
			CsPbCl ₃ NCs: ~90% and 75% of initial PL intensity is retained after 6 days and 7 h under ambient condition and UV light illumination, respectively.	

Lack of long-term stability of the perovskite NCs is a major limiting factor for their wide scale applications. Interestingly, we found that the treated perovskite NCs exhibit significantly improved stability compared to the as-synthesized NCs under various conditions (Figure 4.5). For example, while the as-synthesized NCs hold just ~ 8% of its initial PL after 6 days under ambient condition with ~ 3 nm red-shift of emission maximum, the treated CsPbBr₃ NCs maintains ~ 76% of its initial PL intensity even after 10 days under similar condition without any shift of the PL spectrum (Figure 4.5a, A2.9a, b). The treated CsPbBr₃ NCs also exhibit much improved photo-stability. Almost ~ 65% of its initial PL intensity is retained after 11 h continuous illumination of UV light (365 nm, 8 W), whereas the as- synthesized NCs can hold just ~ 6% of the same under similar condition for the 6 h (Figure 4.5b, A2.9c, d). The treated blue emitting CsPbCl_{1.5}Br_{1.5} NCs are also found to be much more stable compared to the untreated sample. For example, the treated



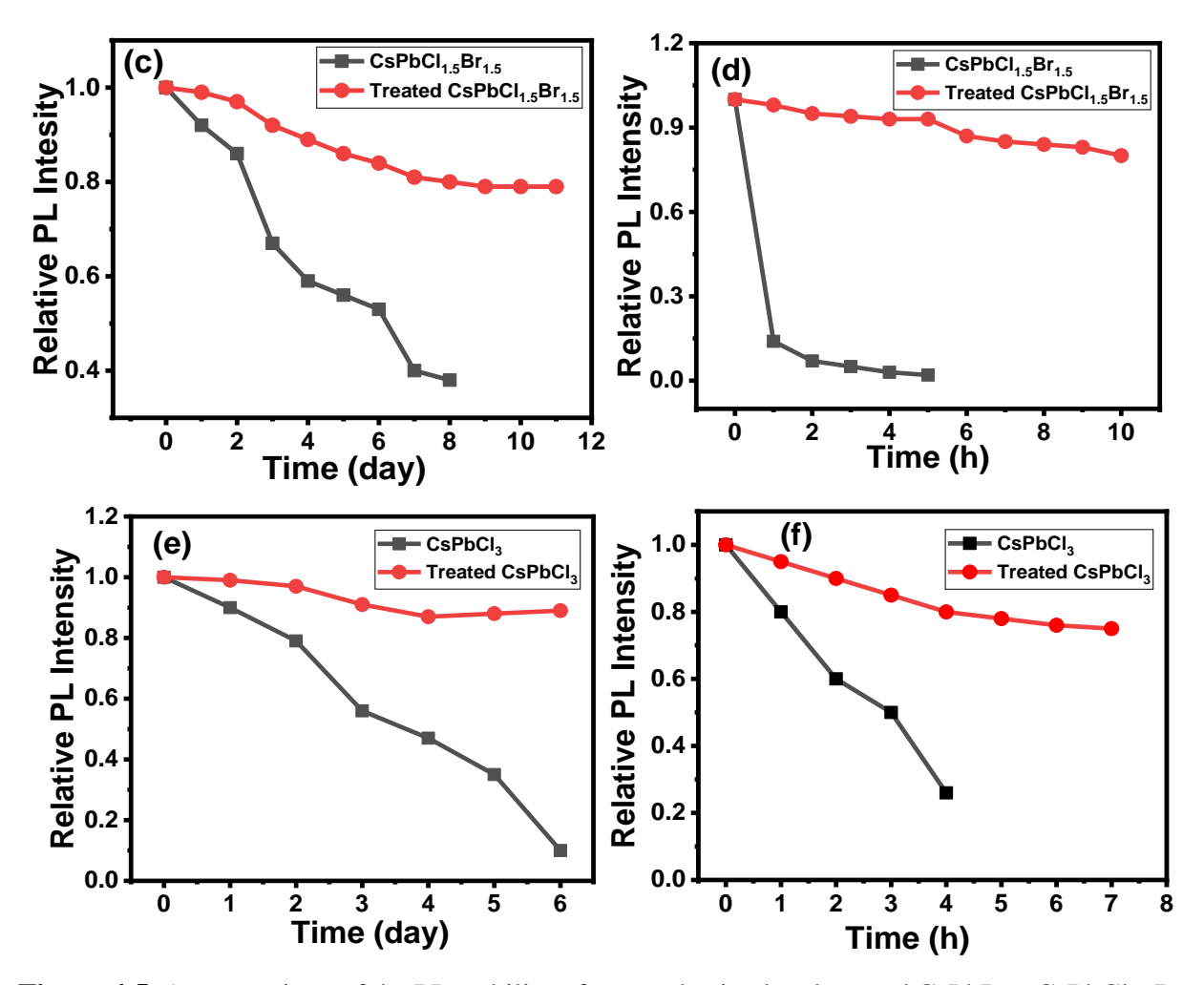


Figure 4.5. A comparison of the PL stability of as-synthesized and treated CsPbBr₃, CsPbCl_{1.5}Br_{1.5} and CsPbCl₃ NCs under (a, c, e) ambient condition and (b, d, f) continuous UV light (365 nm, 8 W) illumination.

CsPbCl_{1.5}Br_{1.5} NCs maintain \sim 80% of initial PL intensity after \sim 11 days under ambient conditions (Figure 4.5c), whereas untreated sample retains just \sim 5% of the initial PL intensity after 8 days of storage under similar condition. The treated CsPbCl_{1.5}Br_{1.5} NCs are more resistant to UV light as well (Figure 4.5d). Similarly the treated CsPbCl₃ NCs are found to be more stable retaining \sim 90% and \sim 75% of initial PL (as against \sim 10% and \sim 25% of the untreated sample) after 6 days and 7 h under ambient condition and continuous irradiation of UV light, respectively (Figure 4.5e, f). It is thus evident that the treated NCs not only exhibit exceptional optical properties, but also show

much improved air- and photo-stability in colloidal dispersion. Formation of strong Pb-S bond with higher bond dissociation energy compared to the Pb-Br or Pb-Cl bonds ⁴⁸ provides a robust and less fragile ligand environment at the surface of the NCs and superior colloidal air stability of the treated NCs.

4.3. Summary

In conclusion, we have shown that a facile RT post-synthetic surface modification of the blue-emitting CsPbCl_{1.5}Br_{1.5}, cyan- emitting CsPbClBr₂ and green-emitting CsPbBr₃ NCs with TAA dramatically enhances their PLQY up to near-unity (~ 97–99%) with moderate improvement up to ~ 62% and ~ 23% even for the violet-emitting CsPbCl₂Br and CsPbCl₃ NCs, covering a wide 400-510 nm region of the visible spectrum. Removal of excess lead atoms and passivation of under-coordinated Pb²⁺ effectively suppress the surface trap states, leading to enhanced radiative recombination, enabling dramatically improved PLQY of the NCs. Formation of strong Pb-S bonds at the surface contributes toward the superior stability of the treated NCs under various external stresses making them potentially attractive systems for optoelectronic applications.

References

- (1) P. Ramasamy, D.-H. Lim, B. Kim, S.-H. Lee, M.-S. Lee, J.-S. Lee, Chem. Commun. 2016, 52, 2067.
- (2) X. Zhang, H. Lin, H. Huang, C. Reckmeier, Y. Zhang, W. C. H. Choy, A. L. Rogach, *Nano Lett.* **2016**, *16*, 1415.
- (3) J. Pan, S. P. Sarmah, B. Murali, I. Dursun, W. Peng, M. R. Parida, J. Liu, L. Sinatra, N. Alyami, C. Zhao, E. Alarousu, T. K. Ng, B. S. Ooi, O. M. Bakr, O. F. Mohammed, *J. Phys. Chem. Lett.* **2015**, *6*, 5027–5033.
- (4) S. Yakunin, L. Protesescu, F. Krieg, M. I. Bodnarchuk, G. Nedelcu, M. Humer, G. D. Luca, M. Fiebig, W. Heiss, M. V. Kovalenko, *Nat. Commun.* **2015**, *6*, 8056.
- (5) B. A. Koscher, J. K. Swabeck, N. D. Bronstein, A. P. Alivisatos, J. Am. Chem. Soc. 2017, 139, 6566–6569.

- (6) J. Pan, Y. Shang, J. Yin, M. D. Bastiani, W. Peng, I. Dursun, L. Sinatra, A. M. El-Zohry, M. N. Hedhili, A. H. Emwas, O. F. Mohammed, Z. Ning, O. M. Bakr, *J. Am. Chem. Soc.* 2018, 140, 562–565.
- (7) S. Seth, T. Ahmed, A. De, A. Samanta, ACS Energy Lett. 2019, 4, 1610–1618.
- (8) S. Das, A. Samanta, ACS Energy Lett. 2021, 6, 3780.
- (9) L. Protesescu, S. Yakunin, M. I. Bodnarchuk, F. Krieg, R. Caputo, C. H. Hendon, R. X. Yang, A. Walsh, M. V. Kovalenko, *Nano Lett.* **2015**, *15*, 3692–3696.
- (10) G. Nedelcu, L. Protesescu, S. Yakunin, M. I. Bodnarchuk, M. J. Grotevent, M. V. Kovalenko, *Nano Lett.* **2015**, *15*, 5635–5640.
- (11) V. G. V. Dutt, S. Akhil, N. Mishra, CrystEngComm. 2020, 22, 5022.
- (12) A. Dey, J. Ye, A. De, E. Debroye, S. K. Ha, E. Bladt, A. S. Kshirsagar, Z.Wang, J. Yin, Y. Wang, L. N. Quan, F. Yan, M. Gao, X. Li, J. Shamsi, T. Debnath, M. Cao, M. A. Scheel, S. Kumar, J. A. Steele, M. Gerhard, L. Chouhan, K. Xu, X.-g. Wu, Y. Li, Y. Zhang, A. Dutta, C. Han, I. Vincon, A. L. Rogach, A. Nag, A. Samanta, B. A. Korgel, C.-J. Shih, D. R. Gamelin, D. H. Son, H. Zeng, H. Zhong, H. Sun, H. V. Demir, I. G. Scheblykin, I. Mora- Seró, J. K. Stolarczyk, J. Z. Zhang, J. Feldmann, J. Hofkens, J. M. Luther,

 J. Pérez-Prieto, L. Li, L. Manna, M. I. Bodnarchuk, M. V. Kovalenko, M. B. J. Roeffaers, N. Pradhan, O. F. Mohammed, O. M. Bakr, P. Yang, P. Müller- Buschbaum, P. V. Kamat, Q. Bao, Q. Zhang, R. Krahne, R. E. Galian, S. D. Stranks, S. Bals, V. Biju, W. A. Tisdale, Y. Yan, R. L. Z. Hoye, L. Polavarapu, ACS Nano 2021, 15, 10775–10981.
- (13) N. Pradhan, ACS Energy Lett. **2019**, 4, 1634–1638.
- (14) V. G. V. Dutt, S. Akhil, D. N. Mishra, ChemNanoMat. 2020, 6, 1730.
- (15) D. P. Nenon, K. Pressler, J. Kang, B. A. Koscher, J. H. Olshansky, W. T. Osowiecki, M. A. Koc, L.-W. Wang, A. P. Alivisatos, *J. Am. Chem. Soc.* **2018**, *140*, 17760–17772.
- (16) S. Paul, T. Ahmed, S. Das, A. Samanta, J. Phys. Chem. C 2021, 125, 23539–23547.
- (17) A. De, S. Das, N. Mondal, A. Samanta, ACS Materials Lett. 2019, 1, 116.

- (18) T. Ahmed, S. Seth, A. Samanta, *Chem. Mater.* **2018**, *30*, 3633–3637.
- (19) S. Wang, Y. Wang, Y. Zhang, X. Zhang, X. Shen, X. Zhuang, P. Lu, W. W. Yu, S. V. Kershaw, A. L. Rogach, *J. Phys. Chem. Lett.* **2019**, *10*, 90–96.
- (20) F. Li, Y. Liu, H. Wang, Q. Zhan, Q. Liu, Z. Xia, Chem. Mater. 2018, 30,8546–8554.
- (21) X. Shen, S. Wang, X. Zhang, H. Wang, X. Zhang, C. Wang, Y. Gao, Z. Shi,
- W. W. Yu, Y. Zhang, *Nanoscale* **2019**, *11*, 11464.
- (22) J. Y. Woo, Y. Kim, J. Bae, T. G. Kim, J. W. Kim, D. C. Lee, S. Jeong, *Chem. Mater.* **2017**, 29, 7088–7092.
- (23) Y. Wu, C. Wei, X. Li, Y. Li, S. Qiu, W. Shen, B. Cai, Z. Sun, D. Yang, Z.Deng, H. Zeng, *ACS Energy Lett.* **2018**, *3*, 2030–2037.
- (24) R. K. Behera, S. D. Adhikari, S. K. Dutta, A. Dutta, N. Pradhan, J. Phys. Chem. Lett. 2018, 9, 6884–6891.
- (25) H. Shao, Y. Zhai, X. Wu, W. Xu, L. Xu, B. Dong, X. Bai, H. Cui, H. Song,

Nanoscale **2020**, 12, 11728.

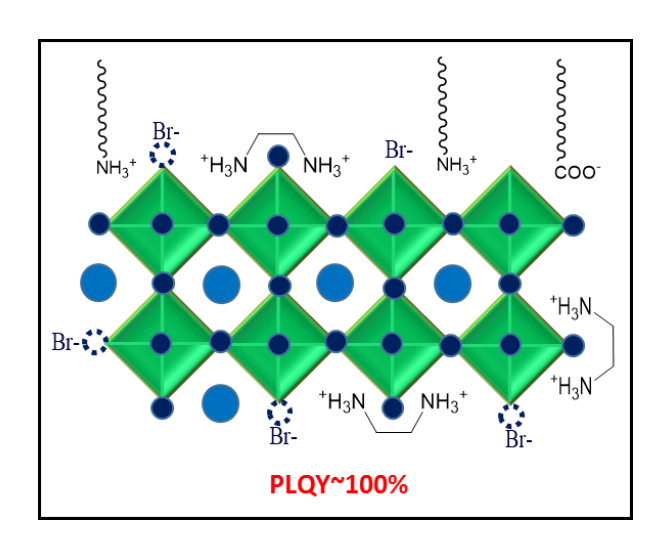
- (26) R. K. Gautam, S. Das, A. Samanta, J. Phys. Chem. C 2021, 125, 24170–24179.
- (27) M. A. Uddin, J. K. Mobley, A. A. Masud, T. Liu, R. L. Calabro, D.-Y. Kim, C. I. Richards, K. R. Graham, *J. Phys. Chem. C* **2019**, *123*, 18103–18112.
- (28) L. Ruan, W. Shen, A. Wang, Q. Zhou, H. Zhang, Z. Deng, Nanoscale 2017, 9, 7252.
- (29) X. Zheng, S. Yuan, J. Liu, J. Yin, F. Yuan, W.-S. Shen, K. Yao, M. Wei, C. Zhou, K. Song, B.-B. Zhang, Y. Lin, M. N. Hedhili, N. Wehbe, Y. Han, H.-T. Sun, Z.-H. Lu, T. D. Anthopoulos, O. F. Mohammed, E. H. Sargent, L.-S. Liao, O. M. Bakr, *ACS Energy Lett.* **2020**, *5*, 793–798.
- (30) P. Li, D. Yang, Y. Tan, M. Cao, Q. Zhong, M. Chen, H. Hu, B. Sun, Y. Xu, Q. Zhang, *ACS Appl. Mater. Interfaces* **2019**, 11, 3351-3359.
- (31) S. Das, A. De, A. Samanta, J. Phys. Chem. Lett. **2020**, 11, 1178–1188.

- (32) V. S. Chirvony, S. Gonzalez-Carrero, I. Suarez, R. E. Galian, M. Sessolo, H. J. Bolink, J. P. Martínez-Pastor, J. Perez-Prieto, *J. Phys. Chem. C* **2017**,121, 13381–133.
- (33) V. G. V. Dutt, S. Akhil, N. Mishra, *Nanoscale* **2021**, *13*, 14442.
- (34) D. E. Newbury, *Scanning* **2009**, *31*, 91.
- (35) K. Thompson, Thermo Fisher Scientific Technical Note 52537, 2013.
- (36) C. Zhang, Q. Wan, L. K. Ono, Y. Liu, W. Zheng, Q. Zhang, M. Liu, L. Kong, L. Li, Y. Qi, *ACS Energy Lett.* **2021**, *6*, 3545–3554.
- (37) Q. Zhong, M. Cao, Y. Xu, P. Li, Y. Zhang, H. Hu, D. Yang, Y. Xu, L. Wang, Y. Li, X. Zhang, Q. Zhang, *Nano Lett.* **2019**, *19*, 4151.
- (38) S. Baek, Y. Kim, S.-W. Kim, J. Ind. Eng. Chem. 2020, 83, 279.
- (39) J. Cao, J. Yin, S. Yuan, Y. Zhao, J. Lib, N. Zheng, *Nanoscale* **2015**, *7*, 9443.
- (40) C. Lu, H. Li, K. Kolodziejski, C. Dun, W. Huang, D. Carroll, S. M. Geyer, Nano Res. 2018, 11, 762.
- (41) N. K. Noel, A. Abate, S. D. Stranks, E. S. Parrott, V. M. Burlakov, A. Goriely, H. J. Snaith, *ACS Nano* **2014**, *8*, 9815.
- (42) J. Tang, K. W. Kemp, S. Hoogland, K. S. Jeong, H. Liu, L. Levina, M. Furukawa, X. Wang, R. Debnath, D. Cha, K. W. Chou, A. Fischer, A. Amassian, J. B. Asbury, E. H. Sargent, *Nat. Mater.* **2011**, *10*, 765.
- (43) F. Krieg, S. T. Ochsenbein, S. Yakunin, S. t. Brinck, P. Aellen, A. Süess, B. Clerc, D. Guggisberg, O. Nazarenko, Y. Shynkarenko, S. Kumar, C.-J. Shih, I. Infante, M. V. Kovalenko, *ACS Energy Lett.* **2018**, *3*, 641.
- (44) S. Akhil, V. G. V. Dutt, N. Mishra, Chem. Eur. J. 2020, 26, 17195.
- (45) C. Lee, Y. Shin, A. Villanueva-Antolí, S. D. Adhikari, J. Rodriguez-Pereira, J. M. Macak, C. A. Mesa, S. Giménez, S. J. Yoon, A. F. Gualdrón-Reyes, I. Mora-Seró, *Chem. Mater.* **2021**, *33*, 8745–8757.
- (46) J. Pan, L. N. Quan, Y. Zhao, W. Peng, B. Murali, S. P. Sarmah, M. Yuan, L. Sinatra, N. M. Alyami, J.

- Liu, E. Yassitepe, Z. Yang, O. Voznyy, R. Comin, M. N. Hedhili, O. F. Mohammed, Z. H. Lu, D. H. Kim, E. H. Sargent, O. M.Bakr, *Adv. Mater.* **2016**, *28*, 8718.
- (47) S. K. Balakrishnan, P. V. Kamat, Chem. Mater. 2018, 30, 74.
- (48) D. R. Lide, CRC Handbook of Chemistry and Physics, 87 ed., CRC Press: Boca Raton, FL, 2007.
- (49) J. V. Morris, M. A. Mahaney, J. R. Huber, J. Phys. Chem. 1976, 80, 969.
- (50) K. Rurack, M. Spieles, Anal. Chem. 2011, 83, 1232.
- (51) A. De, S. Das, A. Samanta, ACS Energy Lett. 2020, 5, 2246–2252.

CHAPTER 5

Bidentate Ligand-Induced Enhanced PLQY and Stability of Blue-, Green- and Red-Emitting CsPbX₃ (X = Cl, Br, I) Perovskite NCs



(To be communicated)

Overview

Colloidal cesium lead halide (CsPbX₃, X = Cl, Br, I) perovskite NCs have recently emerged as potential photovoltaic and optoelectronic material. However, their processing and applications are hindered by loss of colloidal stability and consequent degradation of optical properties under storage in ambient condition. Herein we show that phase-pure, monodispersed, stable and highly luminescent CsPbX₃ NCs can be obtained by tweaking the conventional hot-injection method employing ethylenediammonium dihalide (EDAX₂), which serves as an additional bidentate ligand as well as a halide source. In particular, CsPbI₃ NCs, which are known to be unstable, exhibit a stability of two months in ambient condition upon use of EDAI₂. It is shown that binding of EDA²⁺ significantly removes the trap states originated from surface defects. The outstanding PLQY and much improved long-term stability of the NCs synthesized using small chain coordinating ligand make them attractive for optoelectronic applications.

5.1. Introduction

All-inorganic cesium lead halide (CsPb X_3 , X = Cl, Br and I) perovskite nanocrystals (NCs) have recently emerged as ideal candidate for optoelectronic applications¹⁻⁶ because of their excellent optical properties such as narrow emission, which can be easily tuned through the whole visible range via simple compositional variation.^{7–9} The as-synthesized red-emitting CsPbI₃ and greenemitting CsPbBr₃ NCs show moderate to high PLQY (60-90%),^{7,10} whereas violet-emitting CsPbCl₃ and blue-emitting CsPb(Br/Cl)₃ NCs often exhibit very low PLQY (1-40%). ¹⁰⁻¹² This impedes the utility of these NCs in optoelectronic applications. ¹⁰ These NCs also exhibit low colloidal stability in presence of polar solvents, in humid condition and towards photoirradiation. These two issues significantly limit their employment in actual devices. The nature of the surface of the semiconductor NCs has been a dominant factor in determining the optical properties and stability of the NCs. A highly pressing challenge related to the organic–inorganic interfaces of the CsPbX3 NCs is highly dynamic nature of binding of the surface capping ligands (oleylammonium halide and oleylammonium oleate)^{7,13} and oppositely charged atoms in the surface of the NCs. This leads to desorption of the protective ligand shell during isolation and purification of colloidal NCs (creating uncoordinated Pb²⁺ on the NCs surface), ^{13–15} resulting in a loss of colloidal stability and decrease in PLQY. This eventually also leads to the loss of structural integrity of the NCs often resulting in bulk polycrystalline materials. This inefficient surface passivation leads to the formation defect states, which facilitate nonradiative relaxation of the photoexcited NCs. 16,17 The trap states formed by these defects are energetically shallow for the green/red-emitting CsPbBr₃/CsPbI₃ NCs, but deep in nature for the violet-emitting CsPbCl₃ and blue-emitting CsPb(Cl/Br)₃ NCs, which explains observed low PLQY of the violet-, and blue-emitting perovskite NCs.¹⁰

Plenty of in-situ and post-synthetic methods for suppression of the halide vacancy-related surface defects, ^{18–23} removal of the lead nanoparticles from the surface ^{18,24–27} and curing octahedral distortion by B-site doping with smaller metal ions ^{11,28–31} have been reported to obtain stable and highly luminescent all-inorganic perovskite NCs. Recently, remarkable progress in obtaining

stable and highly luminescent CsPbX₃ NCs has been achieved by strengthening the binding of the capping ligands to the NCs surface with bidentate ligands, which serve as robust passivating agents. Bidentate ligands having two functional groups that can bind to NCs are of special interest because of their stronger binding ability compared to oleic acid and oleylamine through chelate effect. Bakr et al. showed that highly stable CsPbI₃ NCs with near unity PLQY can be obtained by using 2, 2'-iminodibenzoic acid (IDA) as bidentate ligand. Krieg et al. used long-chain zwitterionic molecules (sulfobetaines, phosphocholines, γ amino acids, etc.) as capping ligands for CsPbX₃ NCs, and found that these ligands remarkably increase the durability and stability due to chelation. In subsequent studies, they have shown the effectiveness of this class of ligand by employing soy lecithin, a phospholipid, as a capping agent that confers high stability for CsPbBr₃ NCs because it maximizes the repulsion between the NCs and prevents aggregation due to its brush like structure.

An important point to note here is that except for 2, 2'-iminodibenzoic acid (IDA), 32 most of the bidentate ligands used so far for improving the stability and PLQY of the NCs possess long insulating carbon chain, which hinders charge carrier transport across the interface making these systems not suitable for optoelectronic applications like LED. 33,35 In order to overcome this problem, in this work, we have prepared high quality CsPbX₃ NCs using short chain bidentate ligand, ethylenediammonium dihalide (EDAX₂, X = Cl, Br and I). The CsPbX₃ NCs obtained by using EDAX₂ ligands are denoted as EDA-CsPbX₃ throughout the manuscript.

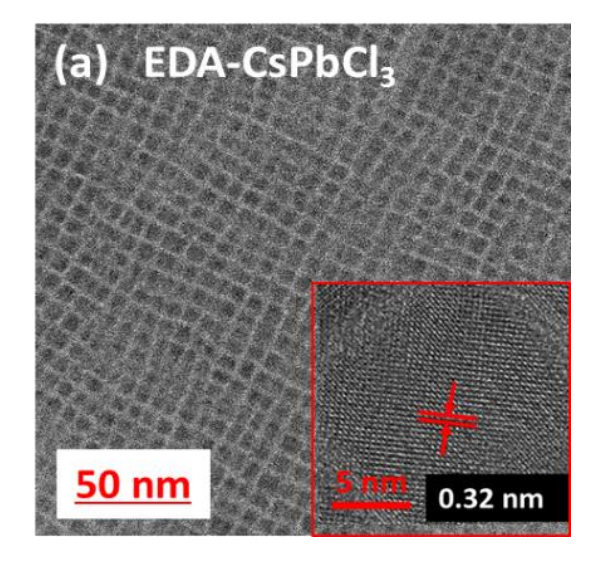
5.2. Results and Discussion

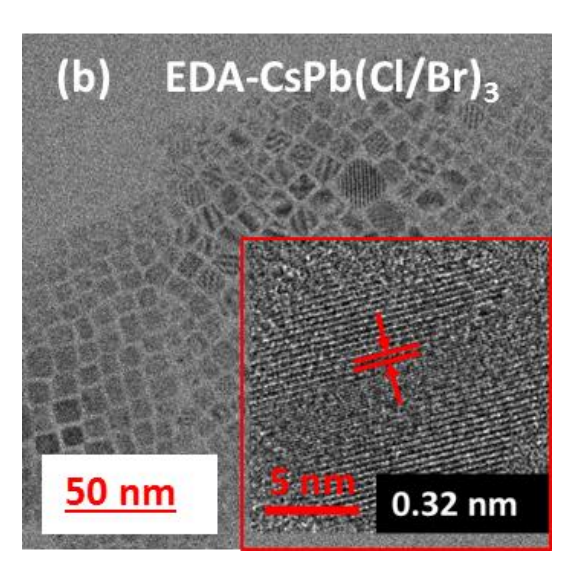
5.2.1. Synthesis and Characterization of the NCs

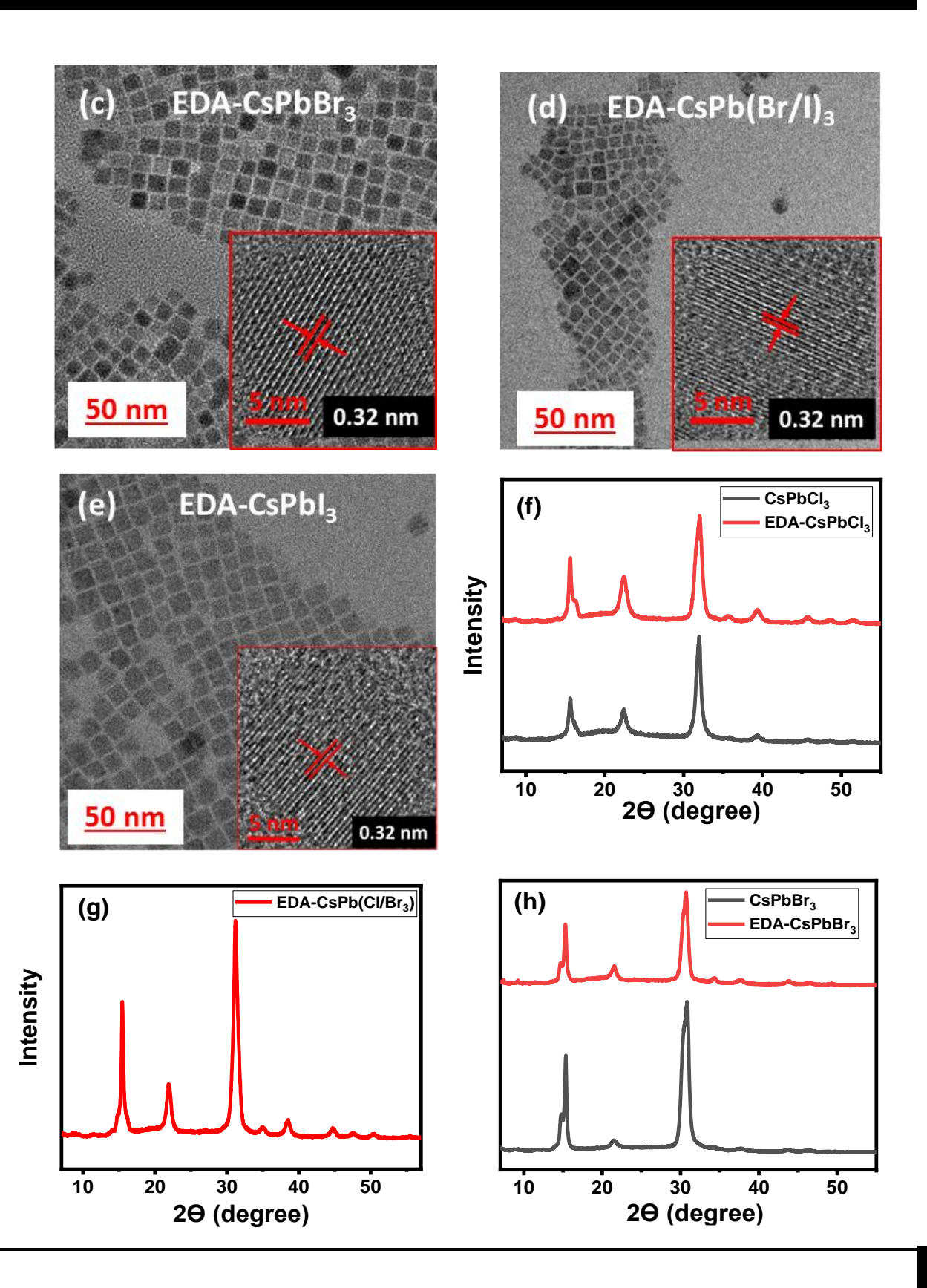
The colloidal CsPbX₃ and mixed-halide NCs were prepared by tweaking the conventional synthesis method using bidentate EDAX₂ ligands.⁷ The hot-injection synthesis of CsPbX₃ NCs with ethylenediammonium dihalide (EDAX₂, X = Cl, Br and I) ligands was carried out by following a reported procedure with minor modification,⁷ ODE (5 mL), PbX₂ (0.188 mmol), EDAX₂ (0.10 mmol), OA (0.5 mL) and OLA (0.5 mL) were loaded into a 50 mL double-necked

RB flask and heated at 120 °C under vacuum for 1 h until the complete solubilization of the PbX₂ and EDAX₂ salts. The temperature of the solution was increased to 160°C under the N₂ environment, and thereafter, 0.5 mL of pre-heated Cs-oleate solution was rapidly injected into the mixture solution. The reaction mixture was cooled in an ice bath after 5 sec of injection. For CsPbCl₃ NCs, 1 mL TOP at 150°C was added for complete solubilization of PbCl₂ salts. The crude solution was centrifuged at 7600 rpm for 10 min to separate unreacted species from the NCs and discarded it. Then, the precipitate was collected and dispersed in 4 mL hexane for further studies.

Bright field transmission electron microscopy (TEM) images indicate cubic morphology and narrow size distribution of the EDA-CsPbX₃ NCs with average edge-length of ~8.90, 12.00, ~12.30, 12.70 and ~13.00 nm of the EDA-CsPbCl₃, EDA-CsPb(Cl/Br)₃, EDA-CsPbBr₃, EDA-CsPb(Br/I)₃ and EDA-CsPbI₃ NCs, respectively (Figure 5.1a-e). The CsPbX₃ NCs obtained by conventional synthesis also exhibit similar edge length (Figure A3.1a-c). The high-resolution TEM images of the EDA-CsPbCl₃, EDA-CsPb(Cl/Br)₃, EDA-CsPbBr₃, EDA-CsPb(Br/I)₃ and EDA-CsPbI₃ NCs show a similar inter-planar distance (d) of ~0.32 nm corresponding to







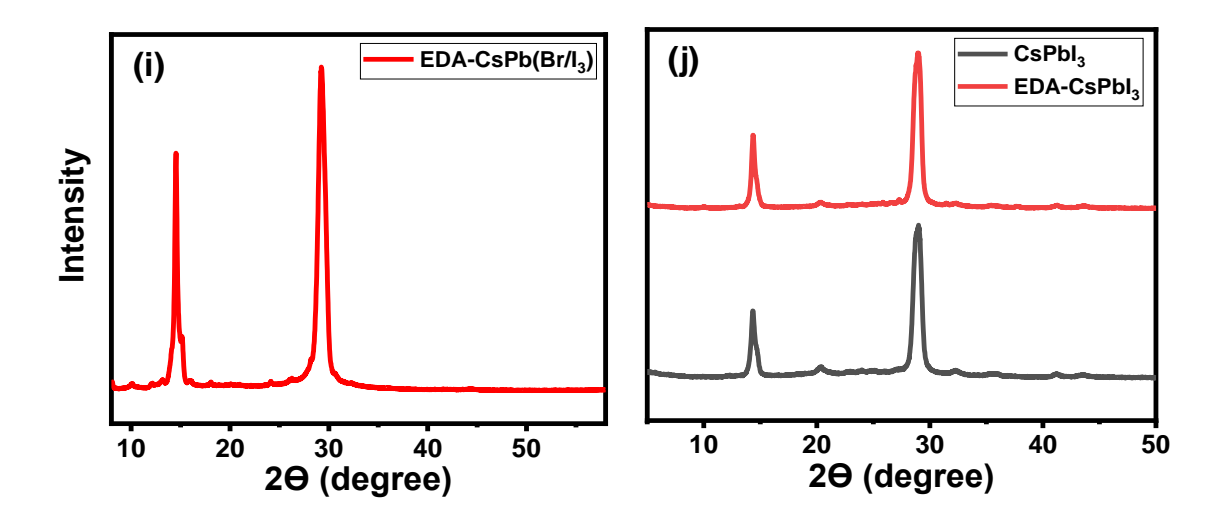


Figure 5.1. TEM images of the (a) EDA-CsPbCl₃ (b) EDA-CsPb(Cl/Br)₃ (c) EDA-CsPbBr₃ (d) EDA-CsPb(Br/I)₃ and (e) EDA-CsPbI₃ NCs. Insets depict high-resolution TEM images showing lattice spacing corresponding to the (200) planes. PXRD patterns of (f) CsPbCl₃ and EDA-CsPbCl₃, (g) EDA-CsPb(Cl/Br)₃ (h) CsPbBr₃ and EDA-CsPbBr₃ (i) EDA-CsPb(Br/I)₃ (j) CsPbI₃ and EDA-CsPbI₃ NCs.

the (200) lattice planes (Figure 5.1a-e). The observation of no noticeable change of inter-planar distance in EDA-CsPbX₃ and CsPbX₃ NCs indicates that EDAX₂ does not lead to any structural changes. This is further confirmed by comparing the PXRD patterns of the EDA-CsPbX₃ NCs and CsPbX₃ NCs (Figure 5.1f-j). We found that both CsPbX₃ and EDA-CsPbX₃ NCs exhibit exactly same PXRD patterns.

5.2.2. Optical Properties

The excellent optical properties of the EDA-CsPbX₃ NCs is evident from their high PLQY and narrow FWHM of the PL emission covering the entire visible region (400-700 nm) (Figure 5.2). The PL maxima for EDA-CsPbCl₃, EDA-CsPb(Cl/Br)₃, EDA-CsPbBr₃, EDA-CsPb(Br/I)₃ and EDA-CsPbI₃ appear at 403, 454, 509, 592 and 683 nm, respectively. The PLQY observed for EDA-CsPbCl₃, EDA-CsPb(Cl/Br)₃, EDA-CsPbBr₃, EDA-CsPb(Br/I)₃ and EDA-CsPbI₃ NCs are ~53%, 100%, 100%, 93% and 95%, respectively (Figure 5.2a-e). The high PLQY of these NCs

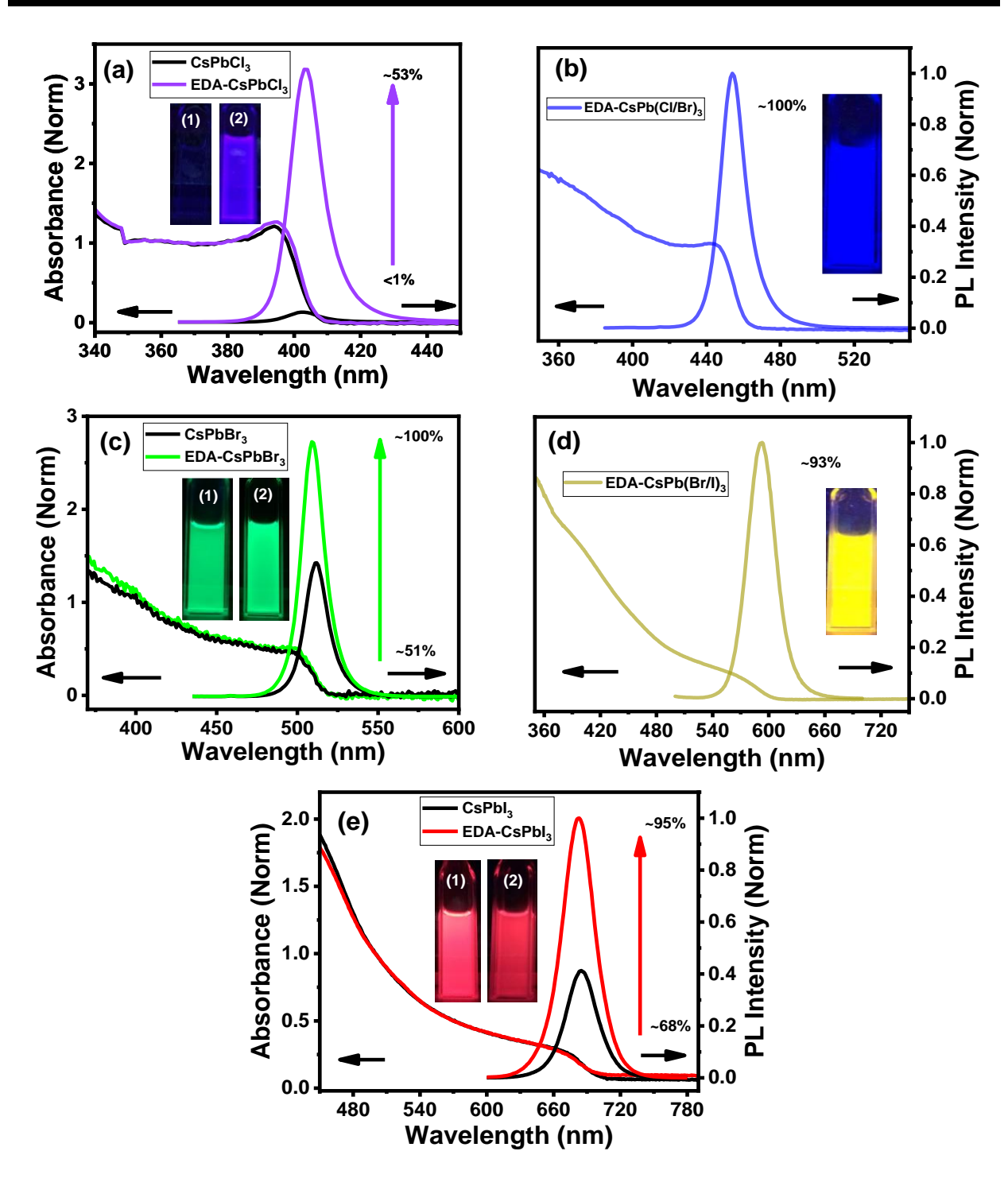


Figure 5.2. (a-e) panels show the UV-vis absorption and emission spectra of the CsPbX₃ and EDA-CsPbX₃ samples. Insets show digital images of the systems under exposure to 365 nm UV-light.

Table 5.1. A comparison of PLQY and stability of different bidentate ligand based CsPbX3 NCs.

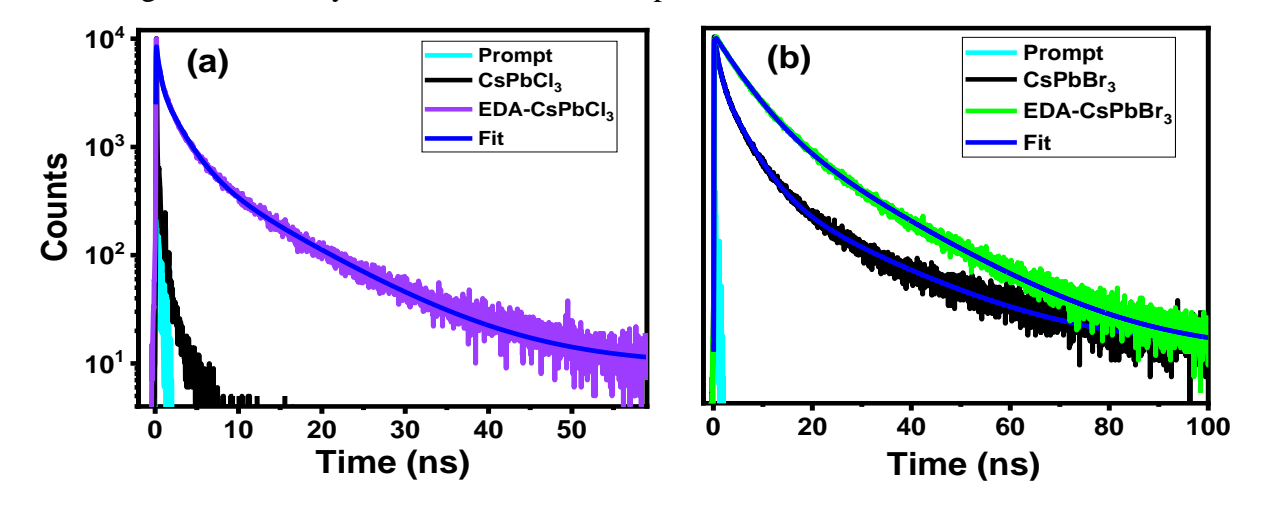
Systems	Bidentate ligands used for NCs synthesis	PLQY (%)	Stability	Ref.
CsPbI ₃	2,2'-iminodibenzoic acid	95	PL intensity 90% over 15 days	32
CsPbBr ₃	3-(N,N- dimethyloctadecylammonio)- propanesulfonate	90	70-90% for 28-50 days	33
CsPbBr ₃	soy lecithin			34
CsPbBr ₃	DTDB	92.3	76% after 17 h in water medium	35
CsPbCl ₃	EDAX ₂ (Cl, Br, I)	53	CsPbCl3: 93% after 50 days	
CsPbBr ₃		100	under ambient. CsPbBr3:	
CsPbI ₃		95	94% after 50 days under ambient, 86%	
CsPb(Cl/Br) ₃		100	after 12 h continuous illumination UV,	This work
CsPb(Br/I) ₃		93	76% after 48 h water resistance under ambient.	WOZI
			CsPbI3: 87% after 50 days under ambient, 80% after 12 h continuous illumination of UV, 70% after 48 h water resistance under ambient.	

indicates elimination of the surface traps on binding of EDA^{2+} . However, the $CsPbCl_3$, $CsPbBr_3$ and $CsPbI_3$ NCs obtained by conventional method exhibit PLQY of <1%, 51% and 68%

respectively. It can be seen from Table 5.1, the PLQY values of the CsPbX₃ NCs obtained by this method are comparable to or better than other recently developed synthesis methods for these NCs.

5.2.3. Time Resolved Measurements

To understand the photophysical processes of the CsPbX₃ NCs prepared by two different methods we have recorded their PL decay profiles (Figure 5.3). EDA-CsPbCl₃ NCs exhibit a triexponential decay profile, consisting of a very short (0.39 ns), a long (9.64 ns) and an intermediate (2.26 ns) component (Table 5.2). The 2.26 ns component, which has the major contribution, is attributed to the band-edge excitonic recombination whereas, the short and long components are assigned to PL originating from deep and shallow trap mediated recombination processes, frespectively. The CsPbCl₃ NCs obtained from conventional method exhibit ultrafast PL decay that could not be time-resolved in our TCSPC setup (Figure 5.3a). The CsPbBr₃ NCs show a tri-exponential PL decay profile, which is dominated by the fast-trapping component (75%), whereas EDA-CsPbBr₃ NCs exhibit bi-exponential PL decay profile with major contribution from the excitonic recombination (79%) (Figure 5.3b). Complete removal of the sub-nanosecond trapping component in the case of EDA-CsPbBr₃ NCs clearly indicates that the EDABr₂ ligand effectively removes the surface trap states. ^{16,17} Both CsPbI₃ and EDA-CsPbI₃



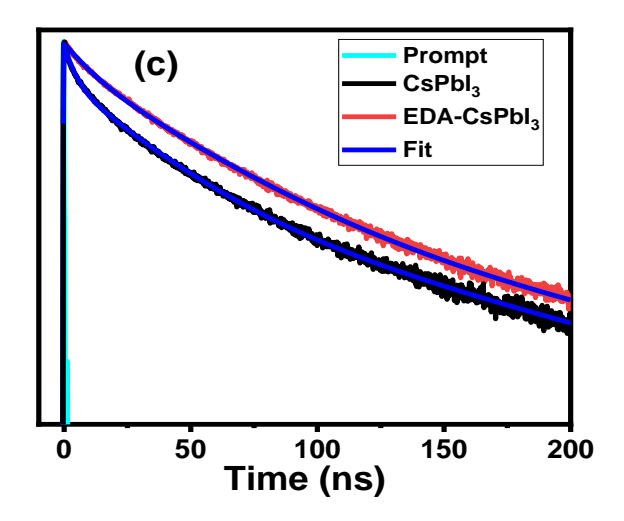


Figure 5.3. PL decay profiles of (a) CsPbCl₃ and EDA-CsPbCl₃, (b) CsPbBr₃ and EDA-CsPbBr₃ and (c) CsPbI₃ and EDA-CsPbI₃ NCs recorded by exciting the samples at 376, 405 and 481 nm, respectively. The PL decay profiles were monitored at the respective PL maxima of the samples.

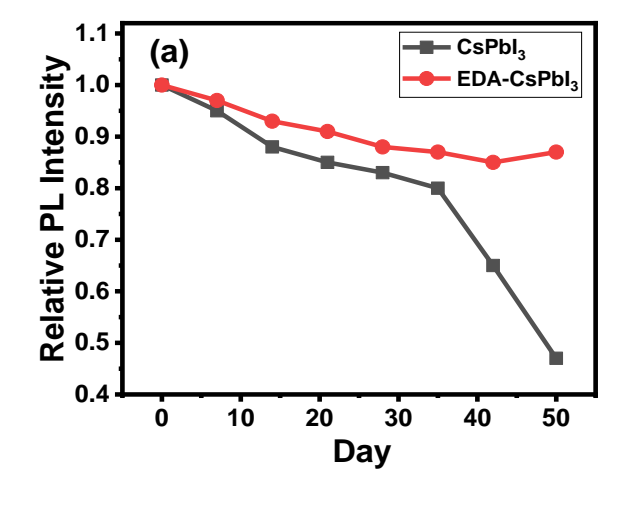
Table 5.2. Fluorescence decay parameters of the CsPbX₃ and EDA-CsPbX₃ NCs and their average lifetime ($\langle \tau_{amp} \rangle$), radiative (k_r) and nonradiative (k_{nr}) rate constants.

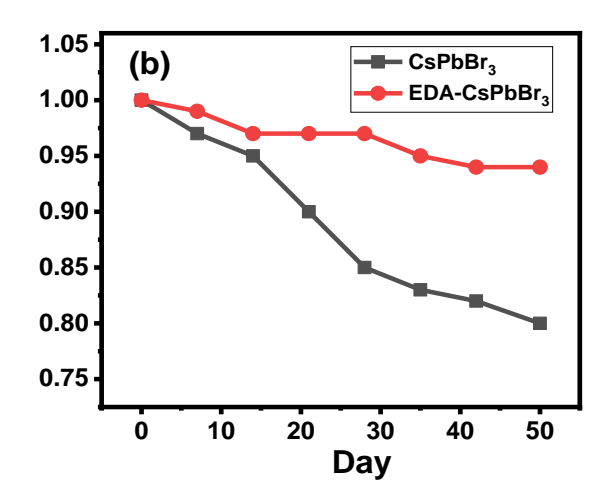
Samples	$\tau_1(\alpha_1)/ns$	$\tau_2(\alpha_2)/ns$	τ ₃ (α ₃)/ns	PLQY	<τ _{amp} >/	k _r /ns ⁻¹	k _{nr} /ns ⁻¹
				(%)	ns		
CsPbCl ₃				~<1			
EDA-CsPbCl ₃	2.26(0.55)	9.64(0.08)	0.39(0.36)	~53	2.25	0.23	0.20
CsPbBr ₃	4.15(0.34)	18.24(0.04)	0.75(0.61)	~51	2.68	0.19	0.18
EDA-CsPbBr ₃	5.21(0.79)	16.03(0.20)		~100	7.52	0.13	0.0013
CsPbI ₃	8.72(0.40)	41.72(0.59)		~68	28.52	0.023	0.01
EDA-CsPbI ₃	12.32(0.66)	49.48(0.33)		~95	37.33	0.025	0.0013

NCs show bi-exponential PL decay profile (Figure 5.3c). While the EDA-CsPbI₃ NCs exhibit

major contribution (66%) of the band-edge recombination (12 ns component), the CsPbI₃ NCs obtained by conventional method exhibit of a long component (41.72 ns) as major component (59%) that originates from shallow trap mediated recombination. The nonradiative rate constant (k_{nr}), estimated from the measured PLQY and average PL lifetime, is found to decrease from 0.18 ns⁻¹ in CsPbBr₃ NCs to 0.0013 ns⁻¹ in EDA-CsPbBr₃ NCs. The k_{nr} value for CsPbI₃ NCs decreases by a factor of 10 upon use of EDAI₂ as a capping ligand. Much improved average lifetimes and lower k_{nr} values for EDA-CsPbX₃ NCs reconfirm that EDAX₂ effectively eliminates the surface trap states in these NCs.

The lack of stability of the perovskite NCs is an important issue for their device applications. Among these NCs, red-emitting CsPbI₃ NCs, because of their low band gap, are most promising for solar photovoltaic applications. However, these NCs exhibit lowest phase stability among the CsPbX₃ NCs. The CsPbI₃ NCs prepared by this method are found to exhibit exceptional stability under atmospheric condition and in polar solvents. For example, the PL intensity of EDA-CsPbI₃ NCs decreases only $\sim 13\%$ (with no change in PL peak positions) after 50 days of storage in ambient condition (Figure 5.4a, A3.3a, b). However, for the CsPbI₃ NCs, 53% of initial PL is lost under similar condition. The powder X-ray diffraction (PXRD) patterns of these samples (monitored for 35 days) show that the CsPbI₃ film starts degrading to the δ -CsPbI₃ phase within 2 days, and a complete transition is observed within 3 days (Figure 5.5a). However, no





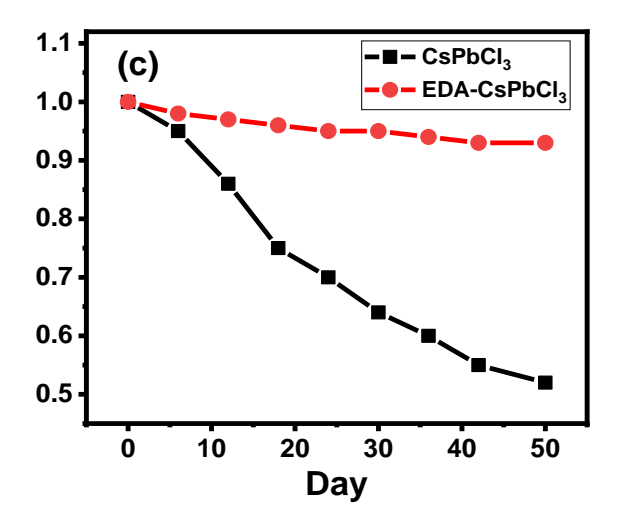


Figure 5.4. Air-stability of (a) CsPbI₃ and EDA-CsPbI₃,(b) CsPbBr₃ and EDA-CsPbBr₃ and (c) CsPbCl₃ and EDA-CsPbCl₃ NCs under ambient condition.

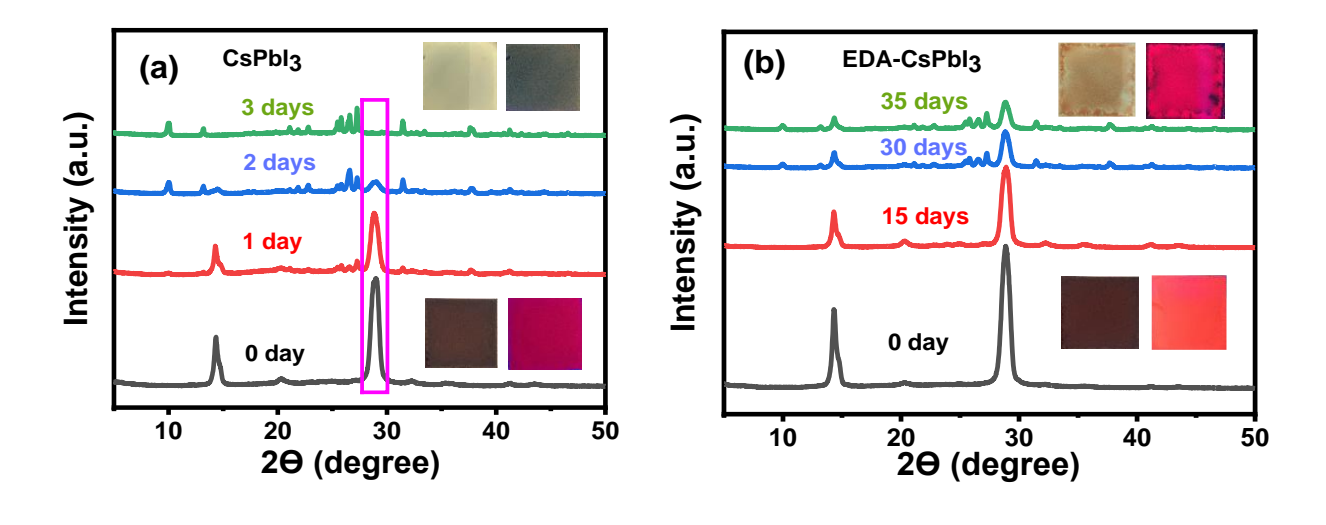


Figure 5.5. Comparison of the PXRD patterns of (a) CsPbI₃ and (b) EDA-CsPbI₃ NCs at different time periods under ambient condition. Insets show digital images of films of the NCs under day-light (left) and UV-light (right) stored under ambient conditions.

noticeable phase change of the EDA-CsPbI₃ film was observed during this period. The sample

remains in its α-phase even after 15 days under ambient conditions (Figure 5.5b). The excellent photostability of the EDA-CsPbI₃ NCs is evident from the fact that only a 20% reduction of PL intensity is observed after ~12 h of continuous UV illumination (365 nm, 8W), whereas, for CsPbI₃ NCs, PL decreases to 50% under similar condition with no shift in PL peak (Figure 5.6a, A3.4a, b). We have also checked stability of these NCs in presence of water. The EDA-CsPbI₃ NCs display significant resistance to water retaining ~70% PLQY in the presence of water even after 2 days of storage under ambient condition, whereas, for CsPbI₃ NCs, the PL decreases to

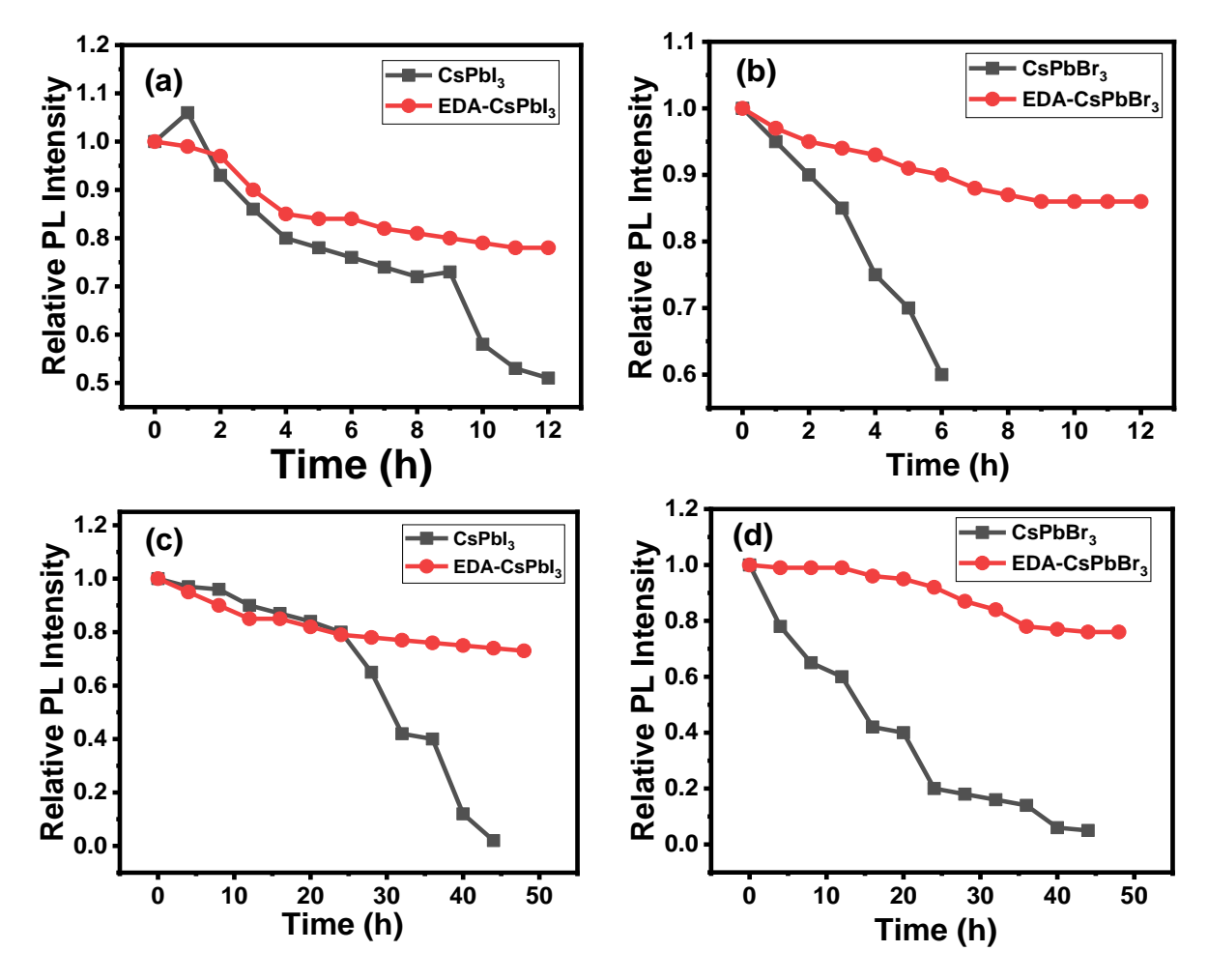


Figure 5.6. (a, b) Photostability and (c, d) water stability of CsPbI₃ and EDA-CsPbI₃, CsPbBr₃ and EDA-CsPbBr₃ NCs stored under continuous UV illumination (365 nm, 8 W) and under ambient conditions respectively.

1% under similar condition (Figure 5.6c, A3.5a, b). The stability of the green-emitting CsPbBr₃ and violet emitting CsPbCl₃ NCs obtained by our method are also quite impressive (Figure 5.4b, c). A PLQY of 94% and 86% is maintained for EDA-CsPbBr₃ after 50 days of storage under ambient condition (Figure 5.4b, A3.3c, d) and after 12 h of continuous illumination by UV lamp (Figure 5.6b, A3.4c, d), respectively. However, the CsPbBr₃ NCs retain a PLQY of 80% and 60% under similar condition, respectively. The EDA-CsPbBr₃ NCs also show very good water resistance. This is evident from the retention of ~76% PL after 48 h storage in water under ambient condition, whereas, the CsPbBr₃ holds ~5% under similar condition (Figure 5.6d, A3.5c, d). The impressive air-stability of the EDA-CsPbCl₃ NCs is evident from retention of 93% of initial PLQY after 50 days of storage under ambient condition (Figure 5.4c, A3.3e, f).

The factors responsible for exceptional characteristics of the EDA-CsPbX₃ NCs are determined using EDA-CsPbBr₃ and CsPbBr₃ NCs as model systems. The energy dispersive X-ray (EDX) measurement shows Cs:Pb:Br:N ratio of 0.79:1:3.68:1.95 and 0.88:1:3.09:1.60 for EDA-CsPbBr₃ and CsPbBr₃ NCs, respectively (Figure 5.7a), indicating that former has a bromide rich surface compared to the later. The Cs:N ratio obtained from EDX studies indicate an increase in N content and decrease in Cs content for the EDA-CsPbBr₃ NCs.³⁵ The Cs deficient and N efficient surface indicates that some surface Cs⁺ are replaced by -NH₃⁺ of the EDA²⁺ ligand. The X-ray photoelectron spectroscopy (XPS) measurements provide additional insight into the chemical environment of the elements. The XPS survey spectra confirm the presence of all constituent elements of these NCs (Figure A3.6). The Br 3d peaks can be resolved into Br 3d_{5/2}, Br 3d_{3/2} peaks for CsPbBr₃ NCs.³⁵ A slight blue shift of the 3d_{5/2} (by 0.22 eV) and 3d_{3/2} peaks (by 0.07 eV) for EDA-CsPbBr₃ NCs (Figure 5.7b) indicates stronger Pb-Br interaction on the surface of the EDA-CsPbBr₃ NCs compared to CsPbBr₃ NCs. Similarly, a blue shift of the Pb 4f_{5/2} and Pb 4f_{7/2} peaks is also observed in the case of EDA-CsPbBr₃ NCs suggesting that excess Br⁻ ions are strongly bonded to the uncoordinated Pb²⁺ surface of these NCs. ^{17,35} The binding of the EDABr₂ ligand on NCs' surface is further proved by FTIR measurement. The EDA-CsPbBr₃ NCs exhibit much higher peak intensity at ~965 cm⁻¹ arising from stretching vibration of the C-N⁺ bond (Figure 5.7c) and at 1641cm⁻¹ due to asymmetric vibration of the N-H bond of -NH₃⁺

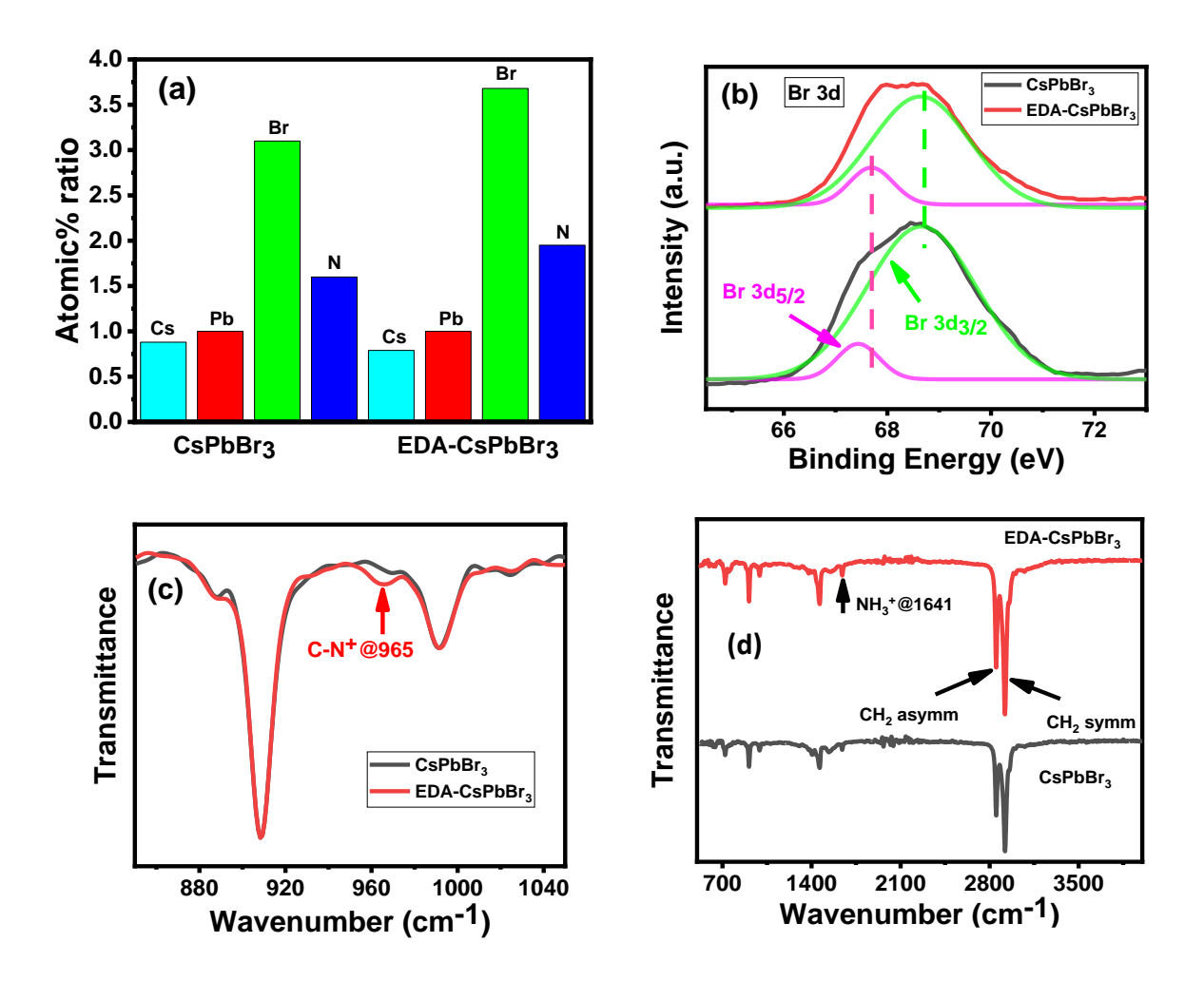


Figure 5.7. (a) Atomic % ratio (with respect to Pb) of the constituting elements of the CsPbBr₃ and EDA-CsPbBr₃ NCs calculated from the EDX measurements. High-resolution XPS spectra of the (b) Br 3d peak of CsPbBr₃ and EDA-CsPbBr₃ NCs de-convoluted into two peaks. (c, d) FTIR spectra of the CsPbBr₃ and EDA-CsPbBr₃ NCs.

compared to pure $CsPbBr_3$ NCs (Figure 5.7d).³⁵ This reconfirms the binding of EDA^{2+} in addition to OLA^+ on the surface of $EDA-CsPbX_3$ NCs.

The ionic surface of the perovskite NCs passivated by OAmH⁺ is highly dynamic in nature due to its loose association with the surface. Deprotonation of OAmH⁺, bound to the surface halides through weak H bond, by processes like OAmH⁺ + OA⁻ = OAm + OAH or OAmH⁺ + X^- =

OAm + HX leads to its desorption and sometimes results in concomitant removal of X^- from the surface, and introduction of X^- -vacancy-related surface defects. However, in the present case,

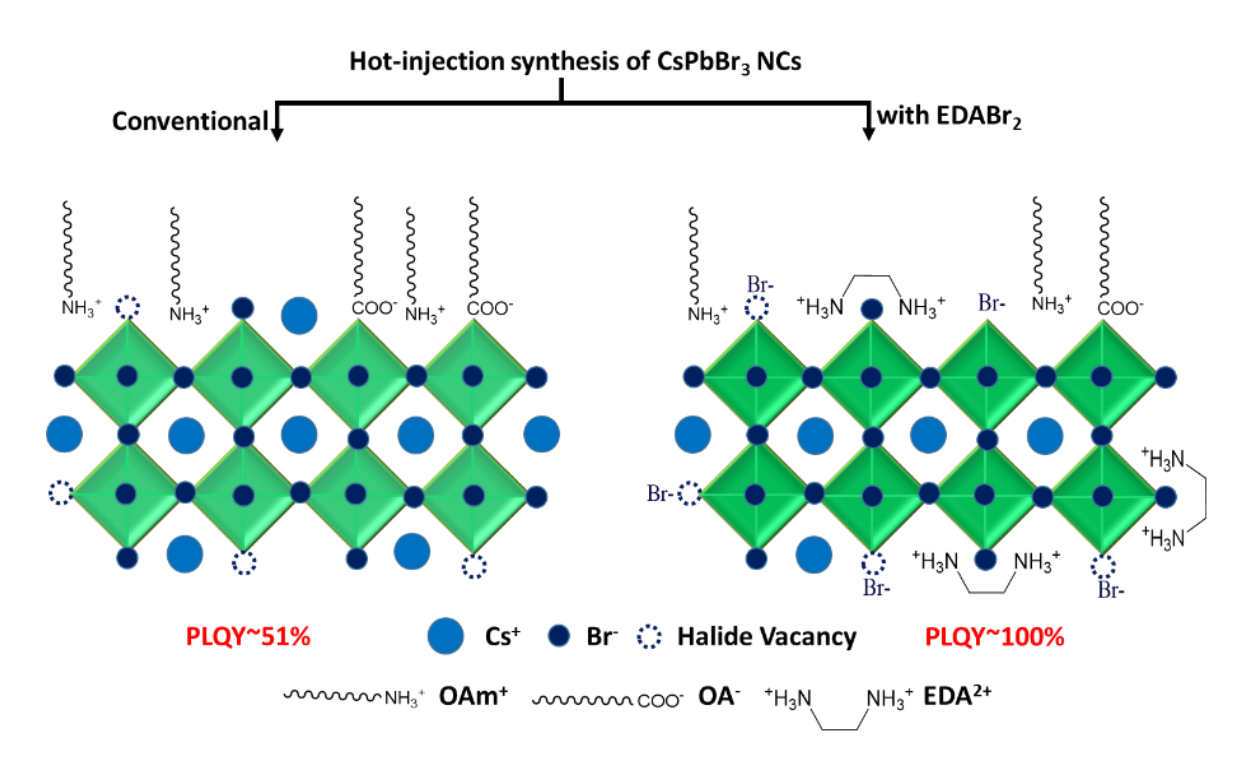


Figure 5.8. Schematic representation of the surface passivation of the CsPbBr₃ NCs by EDABr₂.

much stronger binding of the bidentate EDA²⁺ ligand to the halide rich surface compared to the traditional weak binding of OAmH⁺ provides greater stability to the NCs. Undercoordinated Pb²⁺ ions arising from the halide vacancies at the surface of the CsPbX₃ NCs form inter-band-gap deep defect states, which facilitate nonradiative recombination of the photogenerated charge carriers, and decreases the PLQY of the NCs. In the present case, strong binding of EDA²⁺ with surface Pb²⁺ effectively eliminates the surface defects arising from undercoordinated Pb²⁺, and enhances the PLQY of these NCs. This point is illustrated in Figure 5.8.

5.3. Summary

It is shown that high quality all-inorganic lead halide perovskite NCs emitting in the 400-700 nm region can be obtained employing short chain bidentate ligands, EDAX₂. The high phase purity, narrow size distribution, high PLQY and excellent stability of these NCs obtained by a common method are attributed to the efficacy of this class of short chain ligands in passivating the defect states and providing necessary protection to the NCs. The excellent photoluminescence properties and high stability of these NCs make them promising candidates for perovskite-based optoelectronic applications. The present work not only provides a method for the direct synthesis of good quality CsPbX₃ NCs, but also provides useful insight for the design and development of even better ligands for surface passivation of these NCs.

References

- (1) Liang, J.; Wang, C.; Wang, Y.; Xu, Z.; Lu, Z.; Ma, Y.; Zhu, H.; Hu, Y.; Xiao, C.; Yi, X.; Zhu, G.; Lv, H.; Ma, L.; Chen, T.; Tie, Z.; Jin, Z.; Liu, J. All-Inorganic Perovskite Solar Cells. J. Am. Chem. Soc. 2016, 138, 15829–15832.
- (2) Kojima, A.; Teshima, K.; Shirai, Y.; Miyasaka, T. Organometal Halide Perovskites as Visible-Light Sensitizers for Photovoltaic Cells. *J. Am. Chem. Soc.* **2009**, *131*, 6050–6051.
- (3) Zhang, X.; Lin, H.; Huang, H.; Reckmeier, C.; Zhang, Y.; Choy, W. C. H.; Rogach, A. L. Enhancing the Brightness of Cesium Lead Halide Perovskite Nanocrystal Based Green Light-Emitting Devices through the Interface Engineering with Perfluorinated Ionomer. Nano Lett. 2016, 16, 1415–1420.
- (4) Yakunin, S.; Protesescu, L.; Krieg, F.; Bodnarchuk, M. I.; Nedelcu, G.; Humer, M.; De Luca, G.; Fiebig, M.; Heiss, W.; Kovalenko, M. V. Low-Threshold Amplified Spontaneous Emission and Lasing from Colloidal Nanocrystals of Caesium Lead Halide

- Perovskites. Nat. Commun. 2015, 6, 8056.
- (5) Pan, J.; Sarmah, S. P.; Murali, B.; Dursun, I.; Peng, W.; Parida, M. R.; Liu, J.; Sinatra, L.; Alyami, N.; Zhao, C.; Alarousu, E.; Ng, T. K.; Ooi, B. S.; Bakr, O. M.; Mohammed, O. F. Air-Stable Surface-Passivated Perovskite Quantum Dots for Ultra-Robust, Single- and Two-Photon-Induced Amplified Spontaneous Emission. *J. Phys. Chem. Lett.* 2015, 6, 5027–5033.
- (6) Ramasamy, P.; Lim, D. H.; Kim, B.; Lee, S. H.; Lee, M. S.; Lee, J. S. All-Inorganic Cesium Lead Halide Perovskite Nanocrystals for Photodetector Applications. *Chem. Commun.* **2016**, *52*, 2067–2070.
- (7) Protesescu, L.; Yakunin, S.; Bodnarchuk, M. I.; Krieg, F.; Caputo, R.; Hendon, C. H.; Yang, R. X.; Walsh, A.; Kovalenko, M. V. Nanocrystals of Cesium Lead Halide Perovskites (CsPbX₃, X = Cl, Br, and I): Novel Optoelectronic Materials Showing Bright Emission with Wide Color Gamut. *Nano Lett.* 2015, 15, 3692–3696.
- (8) Dutt, V. G. V.; Akhil, S.; Mishra, N. Fast, Tunable and Reversible Anion-Exchange in CsPbBr₃ perovskite Nanocrystals with Hydrohalic Acids. *CrystEngComm.* **2020**, 22, 5022–5030.
- (9) Nedelcu, G.; Protesescu, L.; Yakunin, S.; Bodnarchuk, M. I.; Grotevent, M. J.; Kovalenko, M. V. Fast Anion-Exchange in Highly Luminescent Nanocrystals of Cesium Lead Halide Perovskites (CsPbX₃, X = Cl, Br, I). *Nano Lett.* **2015**, *15*, 5635–5640.
- (10) Nenon, D. P.; Pressler, K.; Kang, J.; Koscher, B. A.; Olshansky, J. H.; Osowiecki, W. T.; Koc, M. A.; Wang, L. W.; Alivisatos, A. P. Design Principles for Trap-Free CsPbX₃ Nanocrystals: Enumerating and Eliminating Surface Halide Vacancies with Softer Lewis Bases. J. Am. Chem. Soc. 2018, 140, 17760–17772.
- (11) De, A.; Das, S.; Mondal, N.; Samanta, A. Highly Luminescent Violet- And Blue-Emitting

- Stable Perovskite Nanocrystals. ACS Mater. Lett. 2019, 1, 116–122.
- (12) Paul, S.; Ahmed, T.; Das, S.; Samanta, A. Effect of Lead:Halide Precursor Ratio on the Photoluminescence and Carrier Dynamics of Violet- And Blue-Emitting Lead Halide Perovskite Nanocrystals. J. Phys. Chem. C 2021, 125, 23539–23547.
- (13) De Roo, J.; Ibáñez, M.; Geiregat, P.; Nedelcu, G.; Walravens, W.; Maes, J.; Martins, J. C.; Van Driessche, I.; Kovalenko, M. V.; Hens, Z. Highly Dynamic Ligand Binding and Light Absorption Coefficient of Cesium Lead Bromide Perovskite Nanocrystals. *ACS Nano* **2016**, *10*, 2071–2081.
- (14) Syed Akhil, V. G. Vasavi Dutt, N. M. Completely Amine-Free Open-Atmospheric Synthesis of High- Quality Cesium Lead Bromide (CsPbBr₃) Perovskite Nanocrystals. *Chem. Eur. J.* **2020**, 26, 17195–17202.
- (15) Yassitepe, Emre; Yang, Zhenyu; Voznyy, Oleksandr; Kim, Younghoon; Walters, Grant; Castañeda, Juan Andres; Kanjanaboos, Pongsakorn; Yuan, Mingjian; Gong, Xiwen; Fan, Fengjia; Pan, Jun; Hoogland, Sjoerd; Comin, Riccardo; Bakr, Osman M.; Padilha, Lazaro A.;, A. F. . S. H. Amine-Free Synthesis of Cesium Lead Halide Perovskite Quantum Dots for Efficient Light-Emitting Diodes. *Adv. Funct. Mater.* 2016, 26, 8757–8763.
- (16) Gautam, R. K.; Das, S.; Samanta, A. Can Sulfur-Containing Small Systems Enhance the Photoluminescence and Stability of the Blue-, Green- And Yellow-Emitting Perovskite Nanocrystals? A Case Study with Sodium Thiosulfate. J. Phys. Chem. C 2021, 125, 24170–24179.
- (17) Gautam, R. K.; Das, S.; Samanta, A. Room-Temperature Treatment with Thioacetamide Yielding Blue- and Green-Emitting CsPbX₃ Perovskite Nanocrystals with Enhanced Photoluminescence Efficiency and Stability. *ChemNanoMat.* **2022**, 8, e202200029.
- (18) Ahmed, T.; Seth, S.; Samanta, A. Boosting the Photoluminescence of CsPbX₃ (X = Cl, Br,I) Perovskite Nanocrystals Covering a Wide Wavelength Range by Postsynthetic

- Treatment with Tetrafluoroborate Salts. Chem. Mater. 2018, 30, 3633–3637.
- (19) Woo, J. Y.; Kim, Y.; Bae, J.; Kim, T. G.; Kim, J. W.; Lee, D. C.; Jeong, S. Highly Stable Cesium Lead Halide Perovskite Nanocrystals through in Situ Lead Halide Inorganic Passivation. *Chem. Mater.* **2017**, *29*, 7088–7092.
- (20) Behera, R. K.; Das Adhikari, S.; Dutta, S. K.; Dutta, A.; Pradhan, N. Blue-Emitting CsPbCl 3 Nanocrystals: Impact of Surface Passivation for Unprecedented Enhancement and Loss of Optical Emission. *J. Phys. Chem. Lett.* **2018**, *9*, 6884–6891.
- (21) Wu, Y.; Wei, C.; Li, X.; Li, Y.; Qiu, S.; Shen, W.; Cai, B.; Sun, Z.; Yang, D.; Deng, Z.; Zeng, H. In Situ Passivation of PbBr₆⁴ Octahedra toward Blue Luminescent CsPbBr₃ Nanoplatelets with Near 100% Absolute Quantum Yield. *ACS Energy Lett.* **2018**, *3*, 2030–2037.
- (22) Shao, H.; Zhai, Y.; Wu, X.; Xu, W.; Xu, L.; Dong, B.; Bai, X.; Cui, H.; Song, H. High Brightness Blue Light-Emitting Diodes Based on CsPb(Cl/Br)₃ perovskite QDs with Phenethylammonium Chloride Passivation. *Nanoscale* **2020**, *12*, 11728–11734.
- (23) Dutta, A.; Behera, R. K.; Dutta, S. K.; Adhikari, S. Das; Pradhan, N.; Behera, R. K.; Dutta, S. K.; Adhikari, S. Das; Pradhan, N. Annealing CsPbX₃ (X = Cl and Br) Perovskite Nanocrystals at High Reaction Temperatures: Phase Change and Its Prevention. *J. Phys. Chem. Lett.* **2018**, *9*, 6599–6604.
- (24) Koscher, B. A.; Swabeck, J. K.; Bronstein, N. D.; Alivisatos, A. P. Essentially Trap-Free CsPbBr₃ Colloidal Nanocrystals by Postsynthetic Thiocyanate Surface Treatment. *J. Am. Chem. Soc.* **2017**, *139*, 6566–6569.
- (25) Wang, S.; Wang, Y.; Zhang, Y.; Zhang, X.; Shen, X.; Zhuang, X.; Lu, P.; Yu, W. W.; Kershaw, S. V.; Rogach, A. L. Cesium Lead Chloride/Bromide Perovskite Quantum Dots with Strong Blue Emission Realized via a Nitrate-Induced Selective Surface Defect Elimination Process. J. Phys. Chem. Lett. 2019, 10, 90–96.

- (26) Li, F.; Liu, Y.; Wang, H.; Zhan, Q.; Liu, Q.; Xia, Z. Postsynthetic Surface Trap Removal of CsPbX₃ (X = Cl, Br, or I) Quantum Dots via a ZnX₂/Hexane Solution toward an Enhanced Luminescence Quantum Yield. *Chem. Mater.* **2018**, *30*, 8546–8554.
- (27) Shen, X.; Wang, S.; Zhang, X.; Wang, H.; Zhang, X.; Wang, C.; Gao, Y.; Shi, Z.; Yu, W. W.; Zhang, Y. Enhancing the Efficiency of CsPbX₃ (X = Cl, Br, I) Nanocrystals via Simultaneous Surface Peeling and Surface Passivation. *Nanoscale* **2019**, *11*, 11464–11469.
- (28) Das, S.; De, A.; Samanta, A. Ambient Condition Mg²⁺ Doping Producing Highly Luminescent Green-and Violet-Emitting Perovskite Nanocrystals with Reduced Toxicity and Enhanced Stability. *J. Phys. Chem. Lett.* **2020**, *11*, 1178–1188.
- (29) Yong, Z.; Guo, S.; Ma, J.; Zhang, J.; Li, Z.; Chen, Y.; Zhang, B.; Zhou, Y.; Shu, J.; Gu, J.; Zheng, L.; Bakr, O. M.; Sun, H. Doping-Enhanced Short-Range Order of Perovskite Nanocrystals for Near-Unity Violet Luminescence Quantum Yield. *J. Am. Chem. Soc.* 2018, 140, 9942–9951.
- (30) Stam W. v. d., Geuchies J. J., Altantzis T., Bos K. H. W. v. d., Meeldijk J. D., Aert S. V., Bals S., Vanmaekelbergh D., D. C. d. M. Highly Emissive Divalent-Ion-Doped Colloidal CsPb_{1-x}MxBr₃ Perovskite Nanocrystals through Cation Exchange. *J. Am. Chem. Soc.* **2017**, 139, 4087–4097.
- (31) Bi, C.; Wang, S.; Li, Q.; Kershaw, S. V; Tian, J.; Rogach, A. L. Thermally Stable Copper(II)-Doped Cesium Lead Halide Perovskite Quantum Dots with Strong Blue Emission. *J. Phys. Chem. Lett.* **2019**, *10*, 943–952.
- (32) Pan, J.; Shang, Y.; Yin, J.; De Bastiani, M.; Peng, W.; Dursun, I.; Sinatra, L.; El-Zohry, A. M.; Hedhili, M. N.; Emwas, A. H.; Mohammed, O. F.; Ning, Z.; Bakr, O. M. Bidentate Ligand-Passivated CsPbI₃ Perovskite Nanocrystals for Stable Near-Unity Photoluminescence Quantum Yield and Efficient Red Light-Emitting Diodes. *J. Am. Chem. Soc.* **2018**, *140*, 562–565.

- (33) Krieg, F.; Ochsenbein, S. T.; Yakunin, S.; Ten Brinck, S.; Aellen, P.; Süess, A.; Clerc, B.; Guggisberg, D.; Nazarenko, O.; Shynkarenko, Y.; Kumar, S.; Shih, C. J.; Infante, I.; Kovalenko, M. V. Colloidal CsPbX₃ (X = Cl, Br, I) Nanocrystals 2.0: Zwitterionic Capping Ligands for Improved Durability and Stability. *ACS Energy Lett.* **2018**, *3*, 641–646.
- (34) Krieg, F.; Ong, Q. K.; Burian, M.; Rainò, G.; Naumenko, D.; Amenitsch, H.; Süess, A.; Grotevent, M. J.; Krumeich, F.; Bodnarchuk, M. I.; Shorubalko, I.; Stellacci, F.; Kovalenko, M. V. Stable Ultraconcentrated and Ultradilute Colloids of CsPbX₃ (X = Cl, Br) Nanocrystals Using Natural Lecithin as a Capping Ligand. *J. Am. Chem. Soc.* 2019, 141, 19839–19849.
- (35) Li, Y.; Cai, M.; Shen, M.; Cai, Y.; Xie, R. J. Bidentate Aliphatic Quaternary Ammonium Ligand-Stabilized CsPbBr₃ Perovskite Nanocrystals with High PLQY (92.3%) and Superior Stability. *J. Mater. Chem. C* **2022**, *10*, 8356–8363.
- (36) Chirvony, V. S.; Gonza, S.; Sua, I.; Galian, R. E.; Sessolo, M.; Bolink, H. J.; Mart, J. P.; Pe, J.; Materiales, I. D. C. D. L.; Valencia, U. De. Delayed Luminescence in Lead Halide Perovskite Nanocrystals. *J. Phys. Chem. C* 2017, *121*, 13381–13390.

CHAPTER 6

Concluding Remarks

CONCLUDING REMARKS CHAPTER 6

6.1. Overview

The thesis mainly focuses on the photophysical properties of a class of prominent emerging semiconductor materials, lead halide perovskites. These received great attention in current times due to their potential in photovoltaic and optoelectronic device applications such as in photodetector, TV display, laser, solar cell and LEDs due to their excellent optical properties. The purpose of this study is to explore methods of preparation of good quality $CsPbX_3$ (X = Cl, Br, I) perovskite NCs through post-synthetic treatment and direct synthesis and to understand their charge carrier recombination processes. The overall finding of this work is outlined below.

The CsPbX₃ perovskite NCs are not defect-free and have serious stability issues. Hence, the preparation of defect free lead halide perovskite NCs with high PL efficiency and stability is a challenging task. In this regard, we found that room-temperature post-synthetic treatment of the blue-emitting CsPb(Cl/Br)₃, green-emitting CsPbBr₃, and yellow-emitting CsPb(Br/I)₃ NCs with Na₂S₂O₃·5H₂O under ambient condition dramatically improves the PLQY (~90–100%) of these systems. The treated samples which cover a wide range of the visible spectrum also exhibit high stability under different external conditions. The results imply that the halide vacancy-related surface defects in these systems can be effectively passivated by small sulfur-containing systems through formation of strong Pb–S bonds with undercoordinated lead on the surface. The excellent photoluminescence properties and high stability of these NCs make them promising candidates for perovskite-based optoelectronic applications.

As of now, there are several reports available for green-, and red-emitting perovskite NCs to achieve near-unity PLQY but for the blue-emitting NCs, which are essential for blue and white LED, achieving this is a challenging task. To address this issue, we performed RT post-synthetic treatment of the blue-, cyan-, and green-emitting perovskite NCs with thioacetamide and achieved near-unity (~97-99%) PLQY. We have also improved moderately the PLQY of the violet-emitting CsPbCl₂Br and CsPbCl₃ NCs to ~62% and ~23% respectively. Further, a comparison of the stability of as-synthesized and treated NCs shows that the treated systems

CONCLUDING REMARKS CHAPTER 6

exhibit superior colloidal and photo stability. The investigation reveals that effective passivation of under-coordinated surface Pb²⁺ through formation of Pb-S and Pb-NH₂ bonds and removal of excess lead atoms suppress the nonradiative recombination channels and enhances the PLQY and stability of the NCs.

Our post-synthetic treatments are found to be not quite efficient for obtaining high quality violetemitting CsPbCl₃ and red-emitting CsPbI₃ NCs. We have identified a generic method of synthesis employing ethylenediammonium dihalide (EDAX₂) as a bidentate ligand for the preparation of high quality CsPbX₃ NCs. The as-synthesized NCs have uniform size distribution, and they show phase stability for several months in ambient conditions and PLQY of near-unity for the red-emitting CsPbI₃ and ~53% for violet emitting CsPbCl₃ NCs, respectively. The CsPbBr₃ NCs obtained by this method also exhibit near unity PLQY. The most important factor that contributes to this achievement is the strong binding of EDA²⁺ with surface Pb²⁺ which effectively eliminates the surface defects arising from undercoordinated Pb²⁺. The high phase purity, narrow size distribution, high PLQY and excellent stability of these NCs are attributed to the efficacy of this class of short chain ligands in passivating the defect states and providing necessary protection to the NCs.

6.2. Future Scope and Challenges

In working chapter 3 & 4, we focused that post-synthetic treatments of the CsPbX₃ (X = Cl, Br, I) NCs lead to the formation of the CsPbBr₃ NCs, which exhibit a PLQY of near-unity. But we could not achieve near-unity PLQY for violet-emitting CsPbCl₃ and red-emitting CsPbI₃ NCs. The treatments remove the halide-vacancy and excess lead atoms related surface defect and effectively passivate the under-coordinated Pb²⁺ of the surface by small sulfur-containing ligands. However, the CsPbCl₃ NCs show intrinsic defects in addition to the surface defects. The literature survey shows that metal doping (Cd, Ni etc.) can be a useful strategy for removing such intrinsic defects and enhancing the PLQY near-unity for CsPbCl₃ NCs. In the case of CsPbI₃ NCs, little or negligible change in PL efficiency using our ligands indicates that the defects in

CONCLUDING REMARKS CHAPTER 6

these NCs arise from the structural distortion. This issue was partially addressed in chapter 5 using bidentate ligand that resulted CsPbCl₃ and CsPbI₃ NCs with PLQY of ~53% and ~95%, respectively. In this regard, more studies are needed to improve the long term phase stability of the CsPbI₃ NCs and increase the PLQY to near-unity for the CsPbCl₃ NCs.

Appendices

Appendix-1

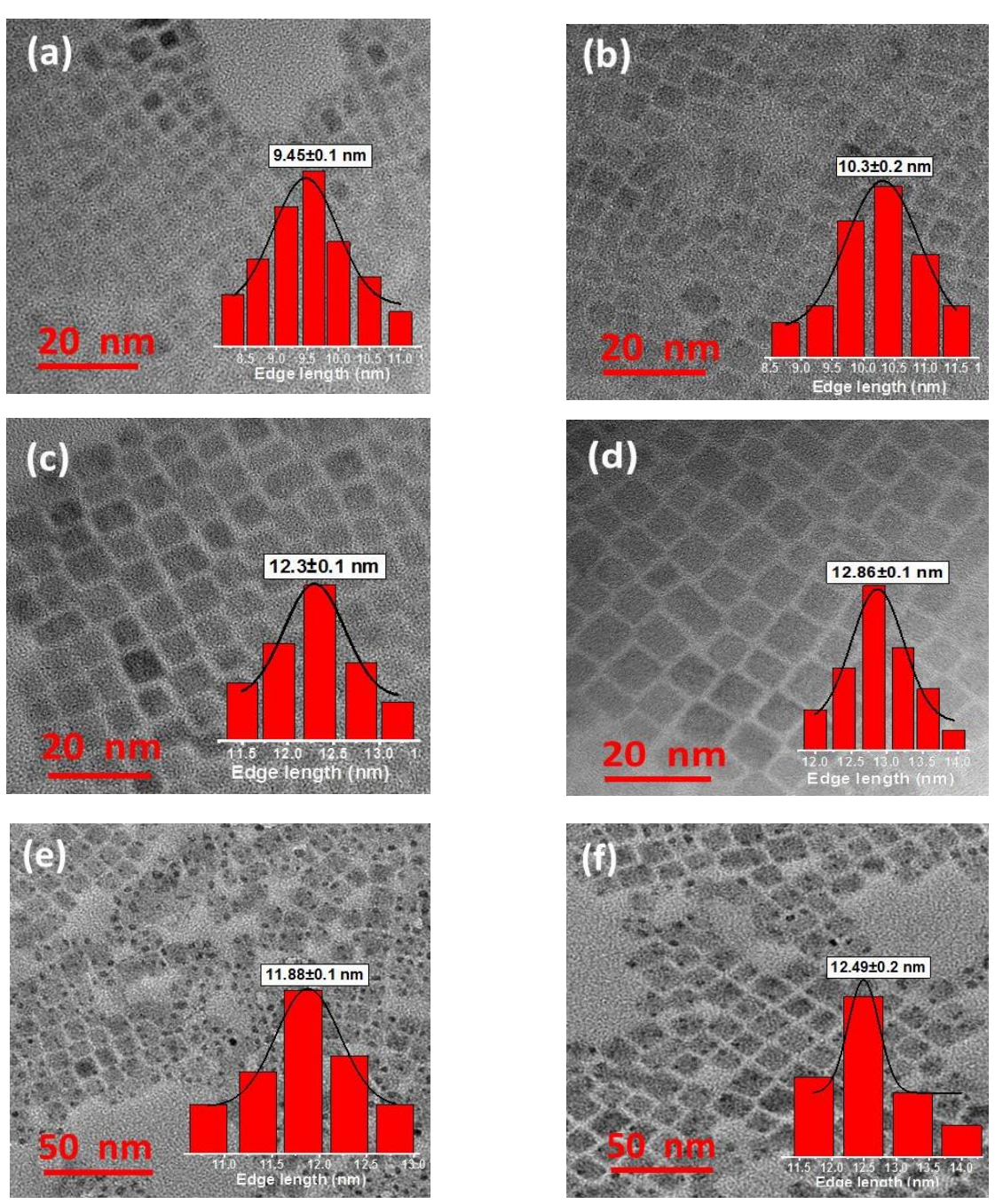


Figure A1.1. TEM images of the as-synthesized (a, c and e) and treated (b, d and f) CsPbCl_{1.5} Br_{1.5}, CsPbClBr₂ and CsPbBr_{1.5}I_{1.5} NCs, respectively. Scale bar for each of the images are indicated at bottom-left corner.

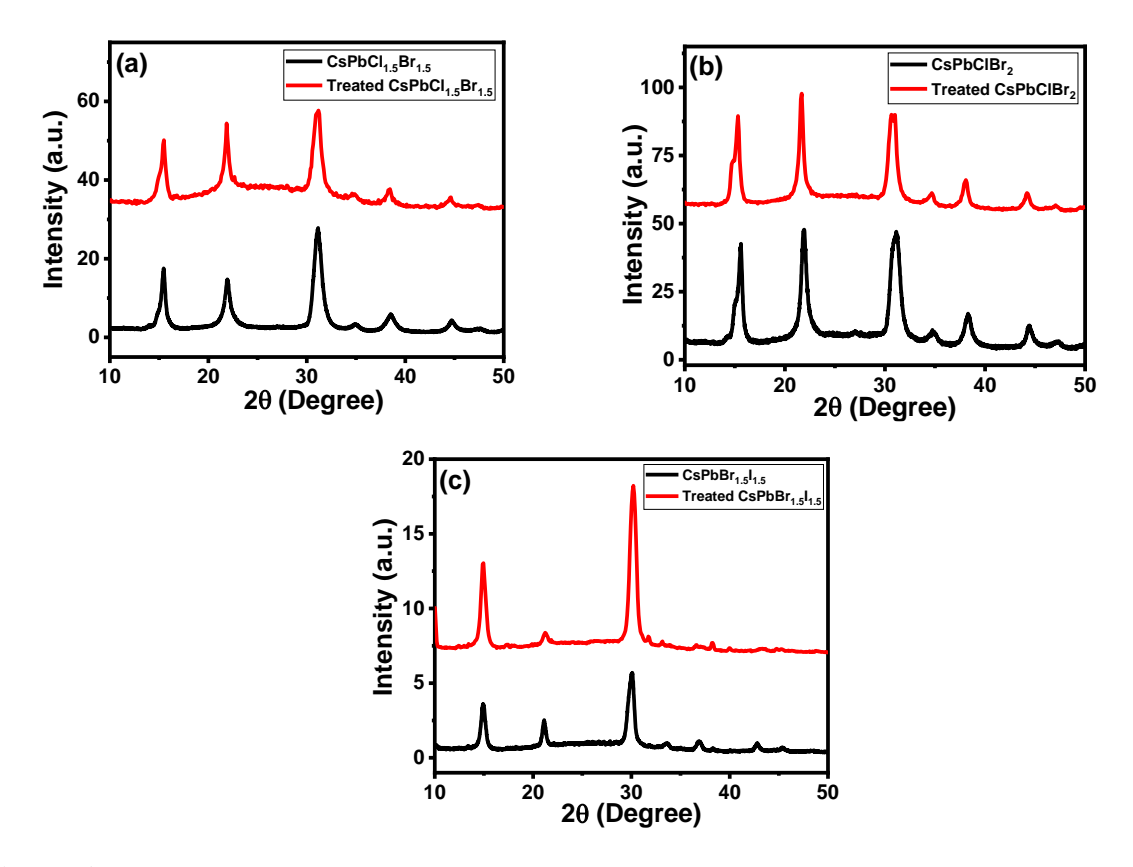


Figure A1.2. PXRD patterns of the as-synthesized and treated (a) $CsPbCl_{1.5}Br_{1.5}$, (b) $CsPbClBr_2$ and (c) $CsPbBr_{1.5}I_{1.5}$ NCs.

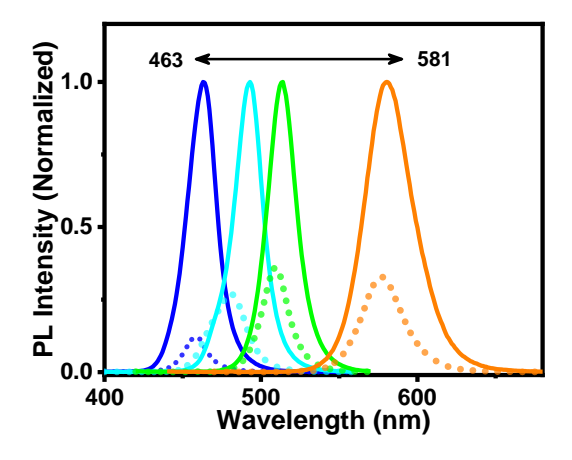


Figure A1.3. PL spectra of the NCs with different halogen composition emitting in the range of ~463 to 581 nm in the visible region before and after treatment with thiosulfate salt highlighting the effectiveness of the post-synthetic strategy over a wide range of wavelengths.

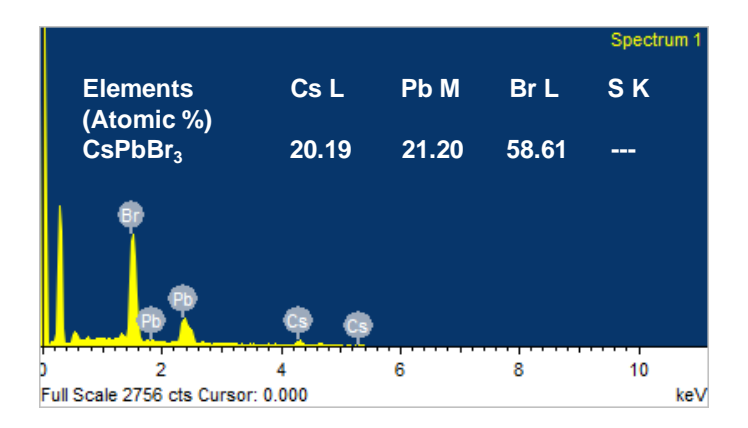


Figure A1.4. EDX spectra of the as-synthesized CsPbBr₃ NCs.

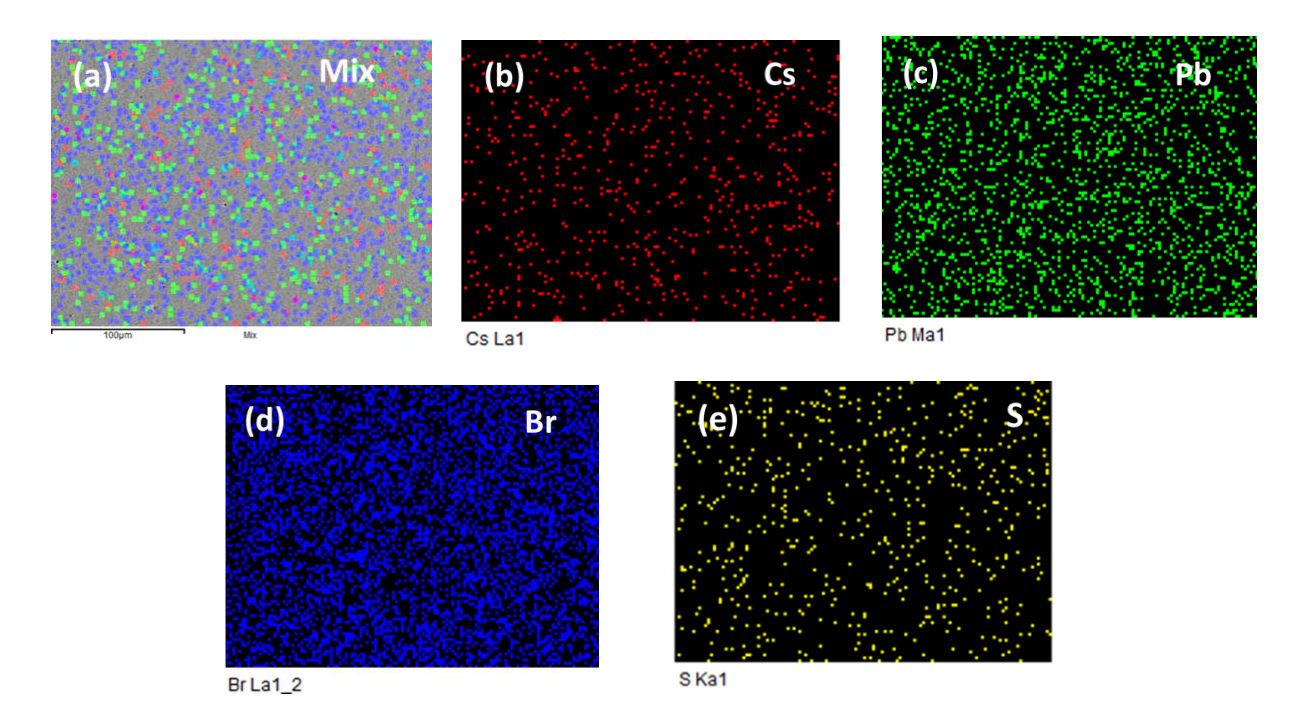


Figure A1.5. (a) FESEM image representing the scanned area with total distribution of all the elements. (b-e) EDX elemental mapping of Cs, Pb, Br and S in the scanned area indicating homogeneous distribution of individual elements in treated CsPbBr₃ NCs washed with methyl acetate.

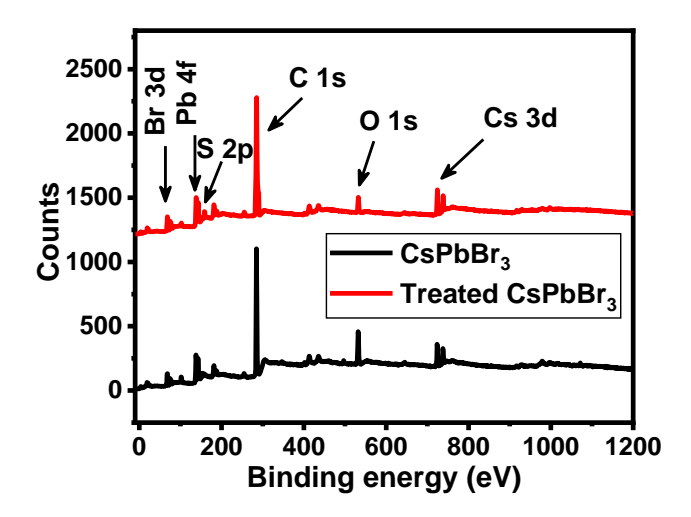


Figure A1.6. XPS survey spectra of the as-synthesized and treated CsPbBr₃ NCs. The presence of S is clearly visible in the survey spectra. The spectra were calibrated with respect to C1s peak at ~285.0 eV.

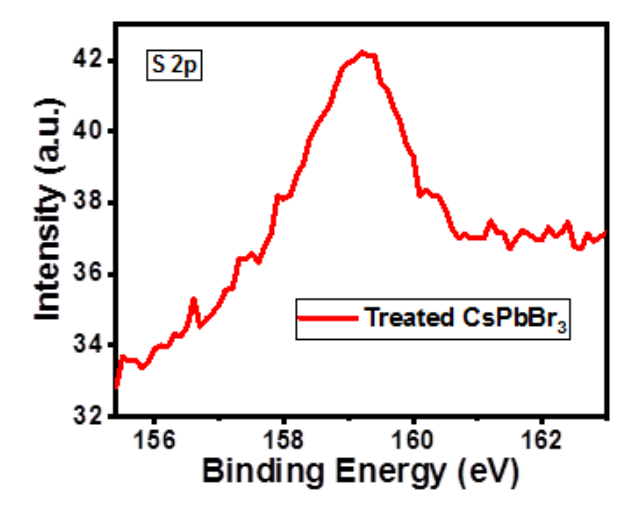


Figure A1.7. High resolution XPS spectra of S 2p of the treated CsPbBr₃ NCs washed with methyl acetate.

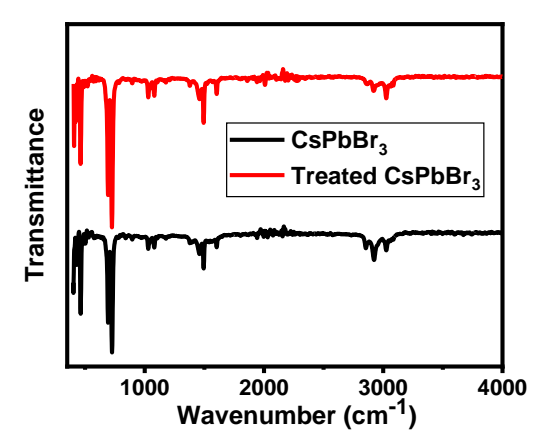


Figure A1.8. (a) FTIR spectra of the as-synthesized and treated CsPbBr₃ NCs.

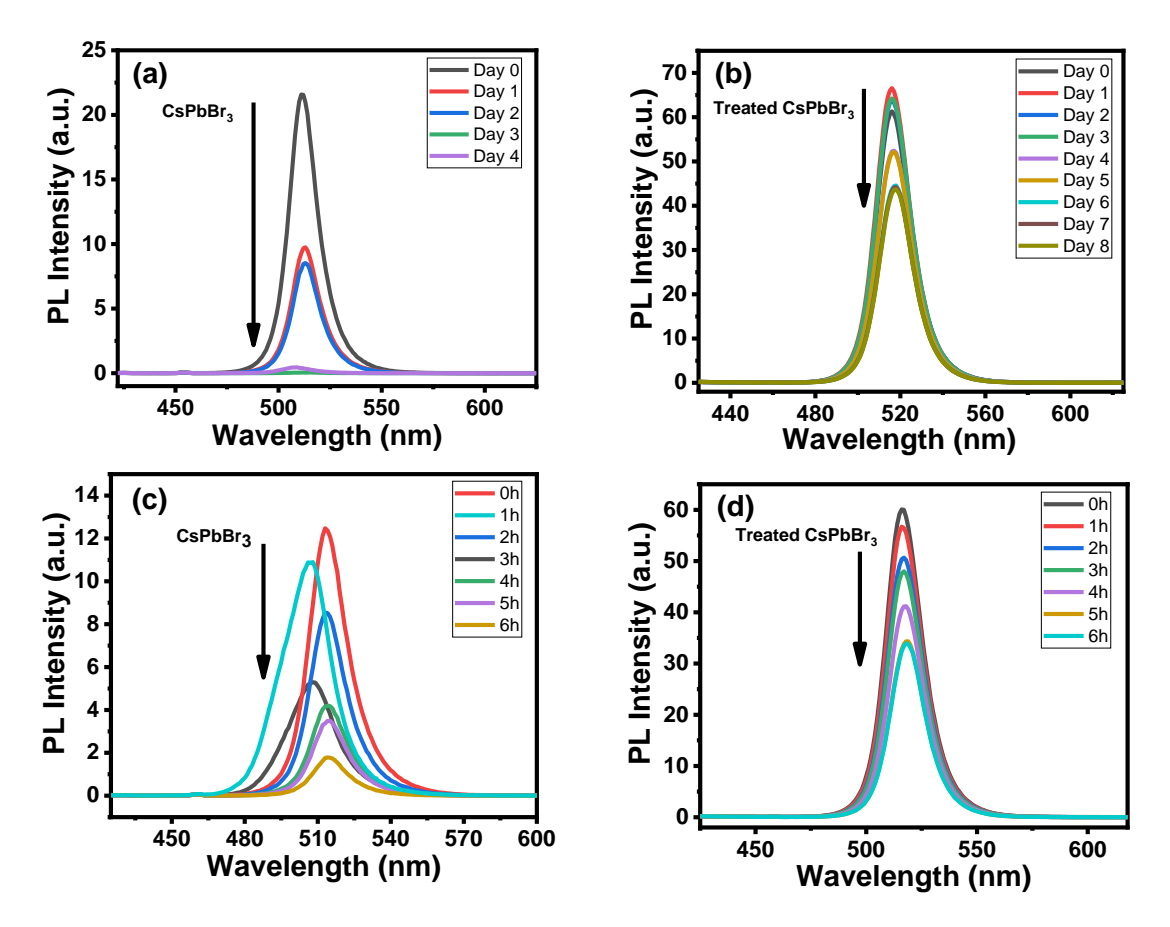
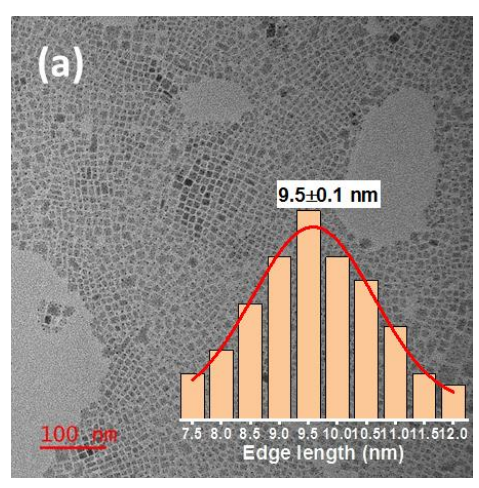
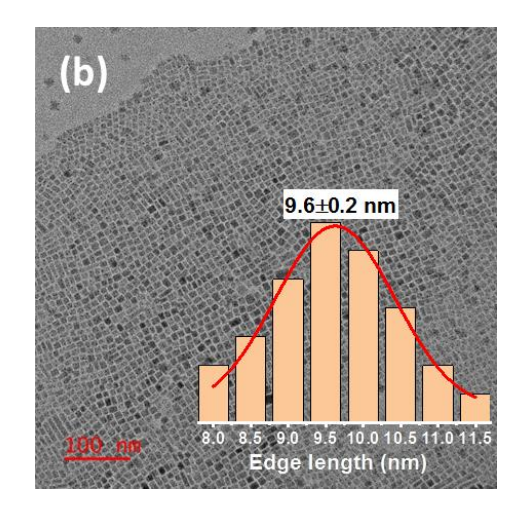
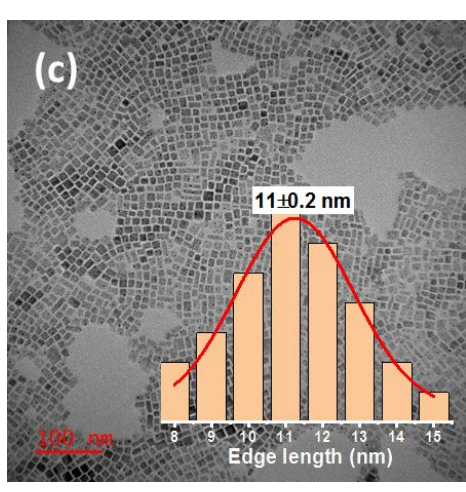


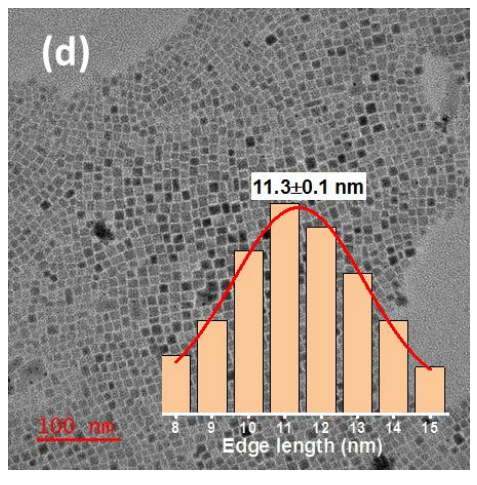
Figure A1.9. PL spectra of the as-synthesized and treated CsPbBr₃ NCs stored under (a, b) ambient condition and (c, d) UV illumination (365 nm, 8W).

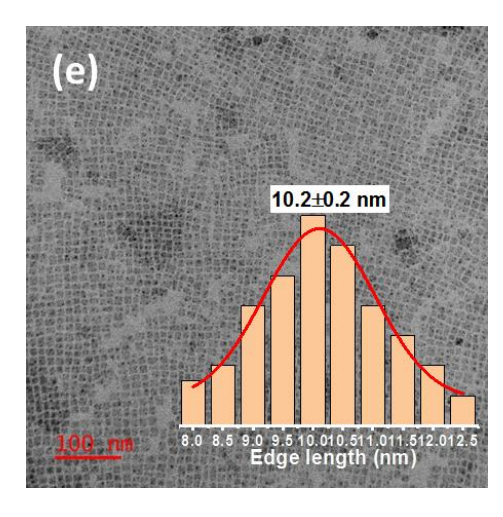
Appendix-2

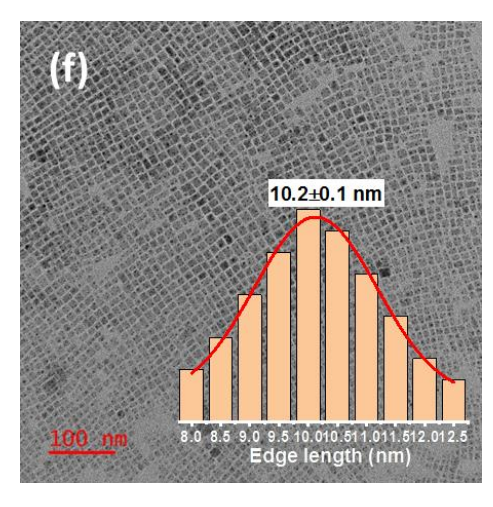


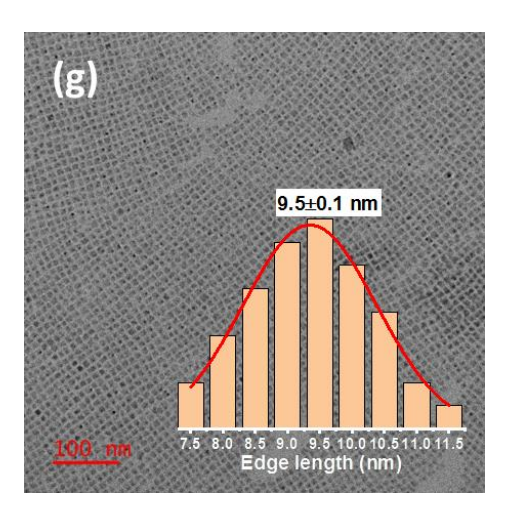












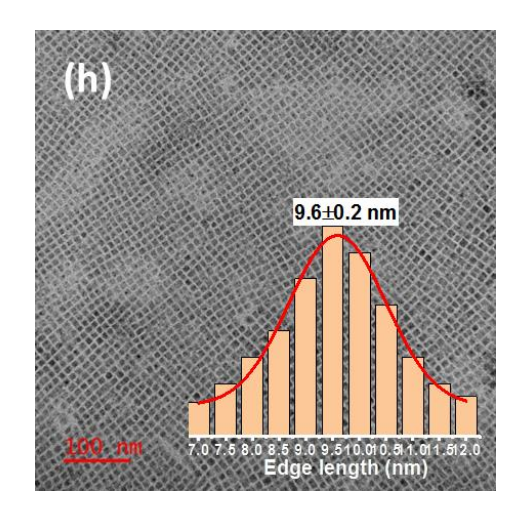


Figure A2.1. TEM images of (a, c, e, g) the as-synthesized and (b, d, f, h) treated CsPbCl_{1.5}Br_{1.5}, CsPbClBr₂, CsPbCl₂Br and CsPbCl₃ NCs with average edge-length of ~9.5, 11, 10.2 and 9.5 nm respectively.

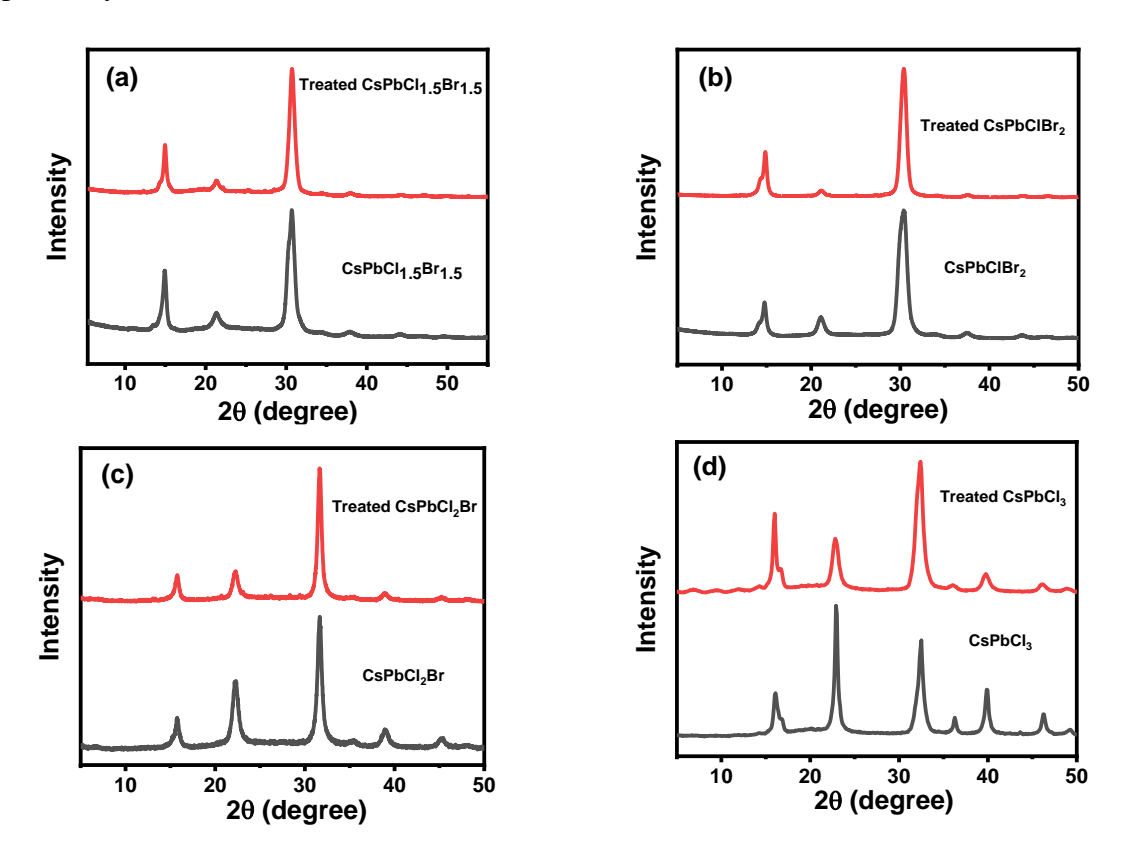


Figure A2.2. PXRD patterns of the as-synthesized and treated (a) CsPbCl_{1.5}Br_{1.5}, (b) CsPbClBr₂ (c) CsPbCl₂Br and (d) CsPbCl₃ NCs.

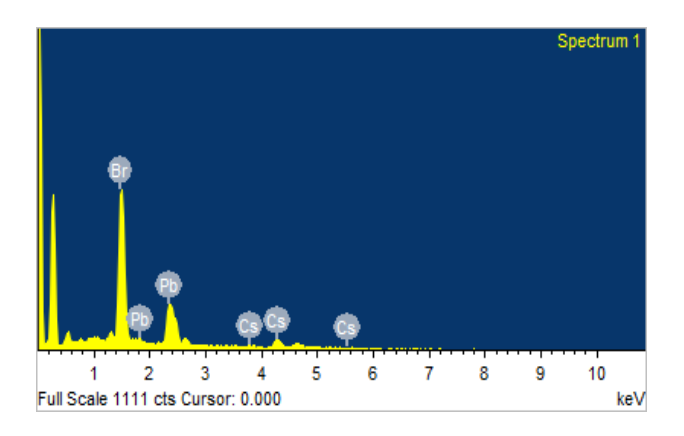


Figure A2.3. EDX spectra of as-synthesized CsPbBr₃ NCs indicating the individual peak of the elements.

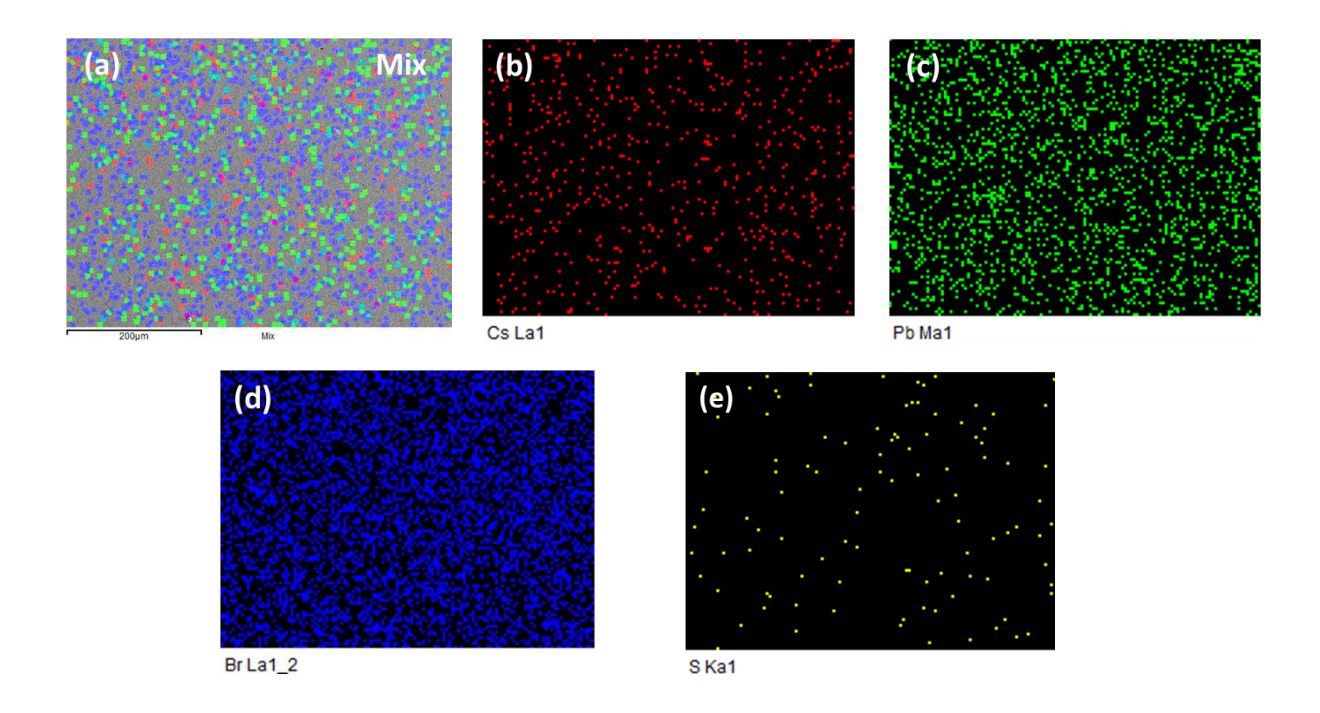


Figure A2.4. EDX elemental mapping of treated CsPbBr₃ NCs with homogeneous distribution of (a) All elements, (b) Cs, (c) Pb, (d) Br, and (e) S throughout the scanned area.

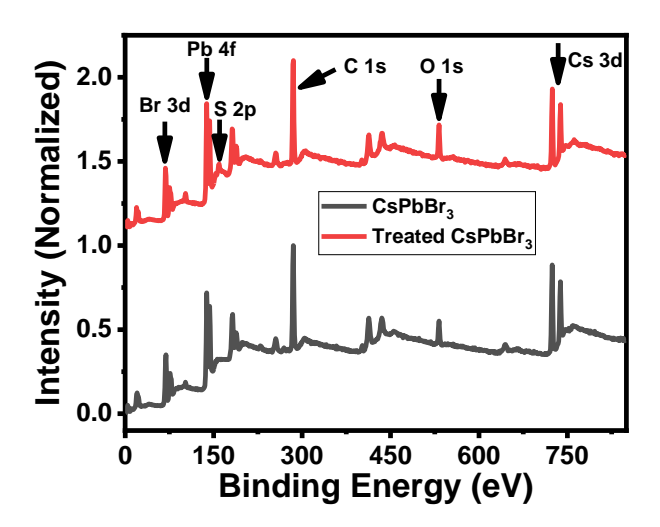


Figure A2.5. XPS survey spectra of the as-synthesized and treated CsPbBr₃ NCs. The presence of sulfur 'S 2p' peak is clearly visible in the treated sample. The spectra were calibrated with respect to C 1s peak at ~285 eV.

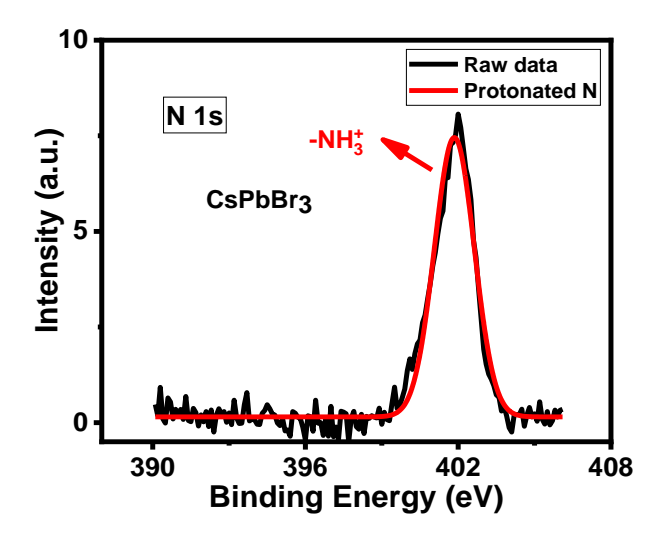


Figure A2.6. High-resolution N 1s XPS data of CsPbBr₃ NCs.

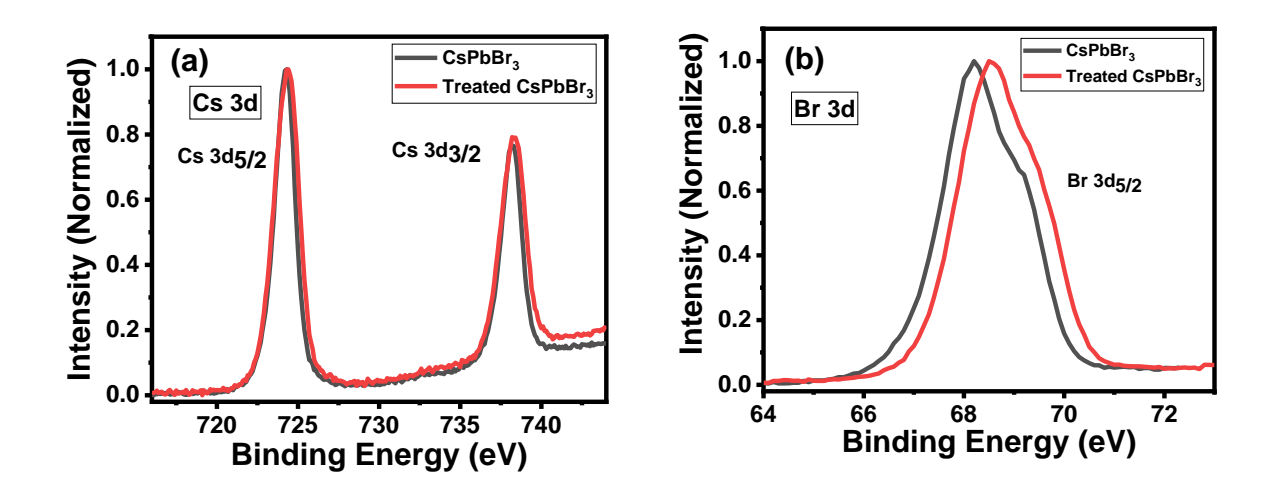


Figure A2.7. Core level XPS spectra of (a) Cs 3d and (b) Br 3d of as-synthesized and treated CsPbBr₃ NCs.

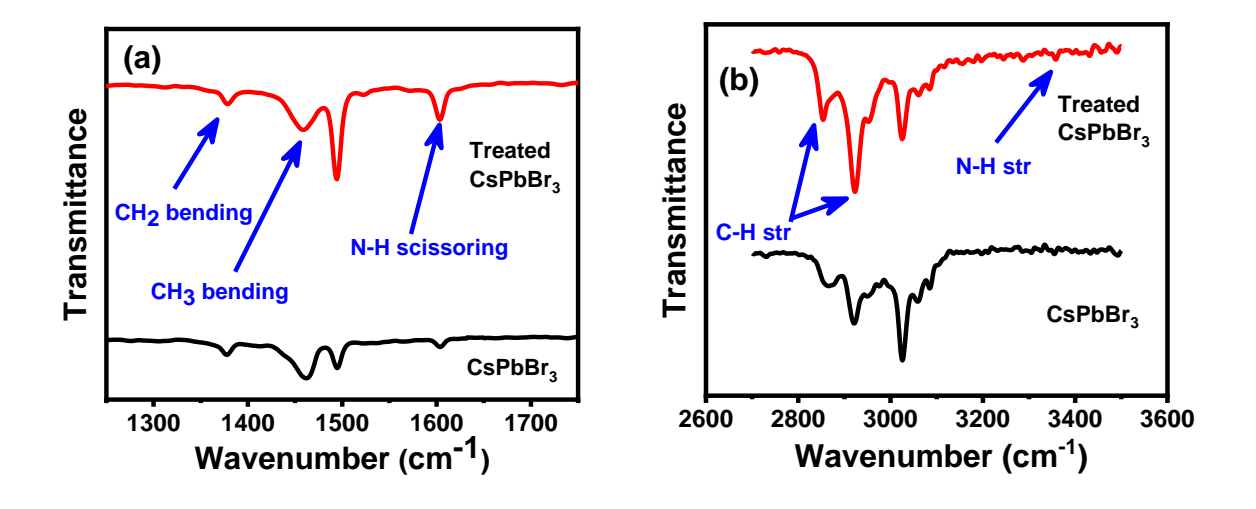


Figure A2.8. FTIR spectra of as-synthesized and treated CsPbBr₃ NCs showing enhanced intensity of the N-H and C-H stretching and bending modes for the treated NCs.

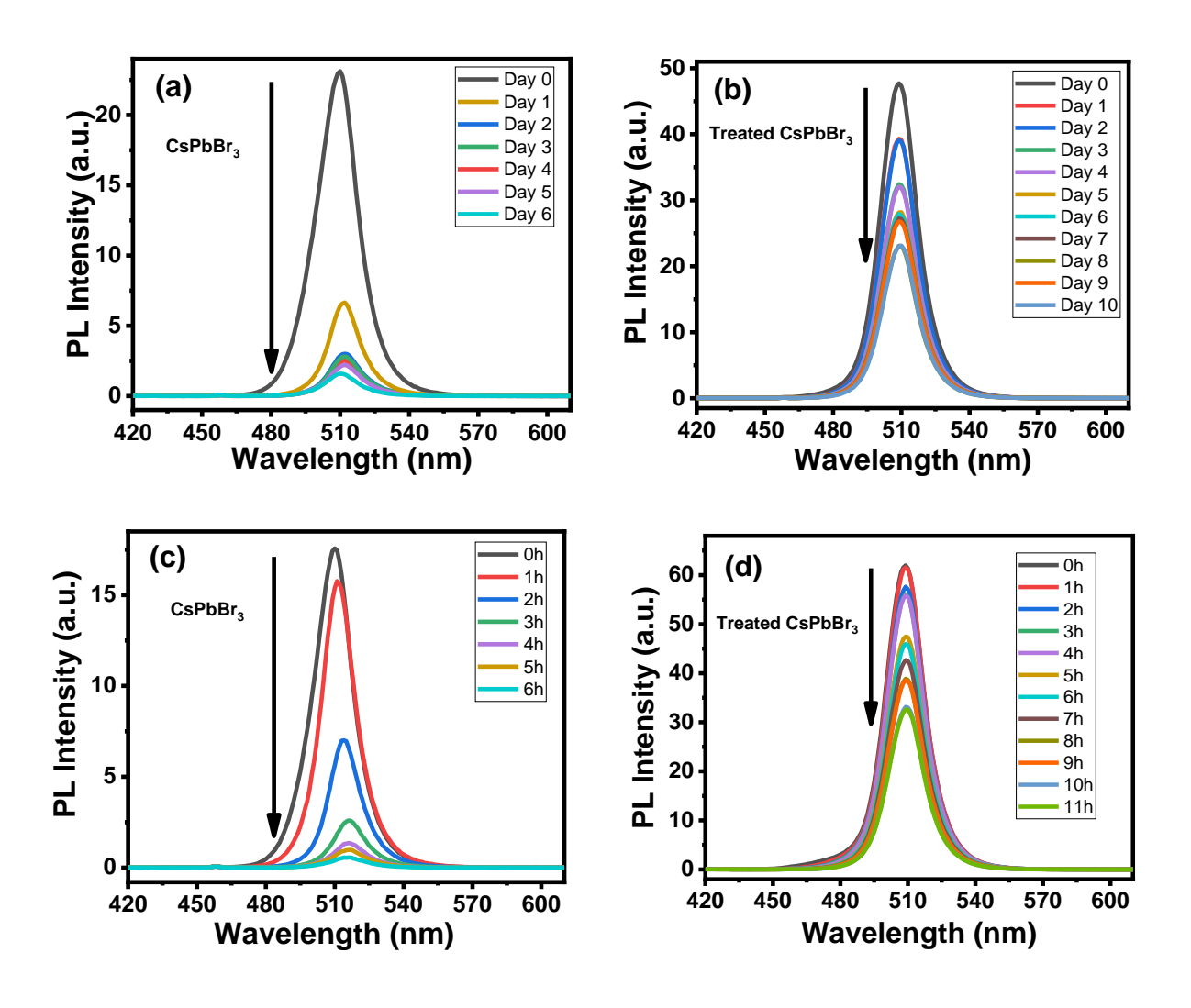


Figure A2.9. PL spectra of the as-synthesized and treated CsPbBr₃ NCs stored under (a, b) ambient condition and (c, d) continuous UV light illumination (365 nm, 8W).

Appendix-3

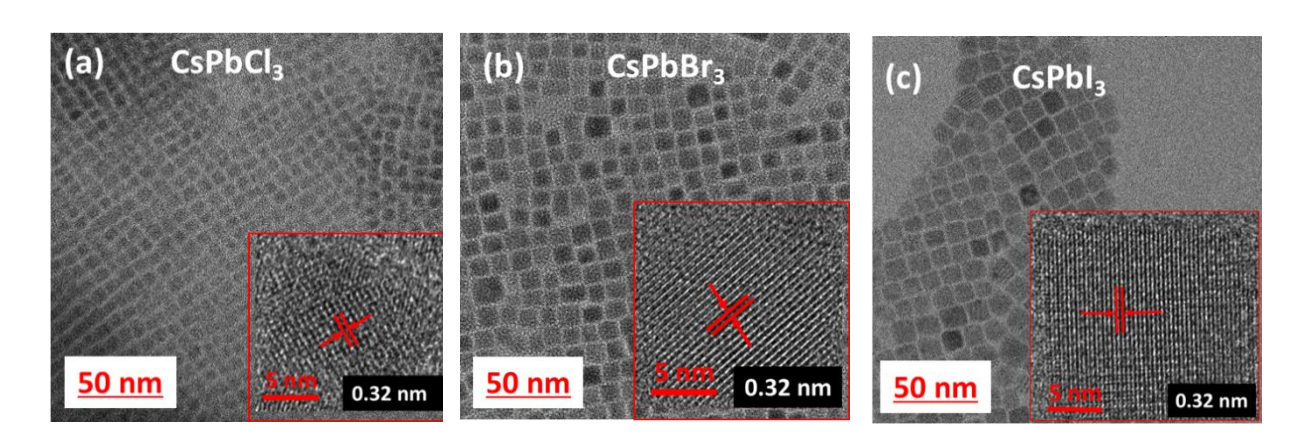


Figure A3.1.TEM image of (a) CsPbCl₃, (b) CsPbBr₃, (c) CsPbI₃ NCs. Insets high-resolution images show the lattice spacing.

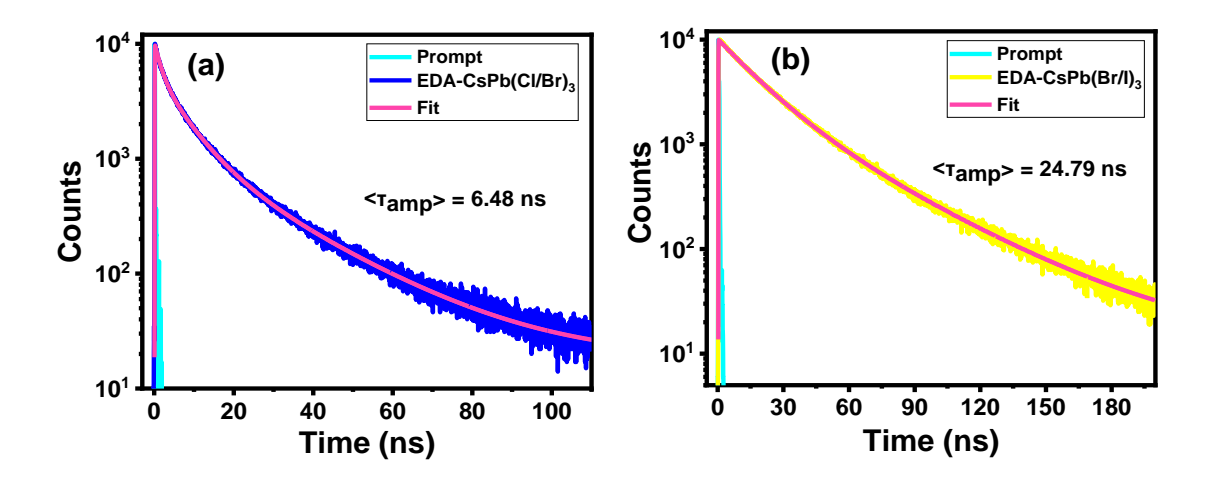


Figure A3.2. PL decay profile of (a) EDA-CsPb(Cl/Br)₃ NCs (b) EDA-CsPb(Br/I)₃ NCs. The excitation wavelengths were 375 nm and 481 nm for blue- and yellow-emitting NCs, respectively. PL decay were monitored at their respective emission maxima.

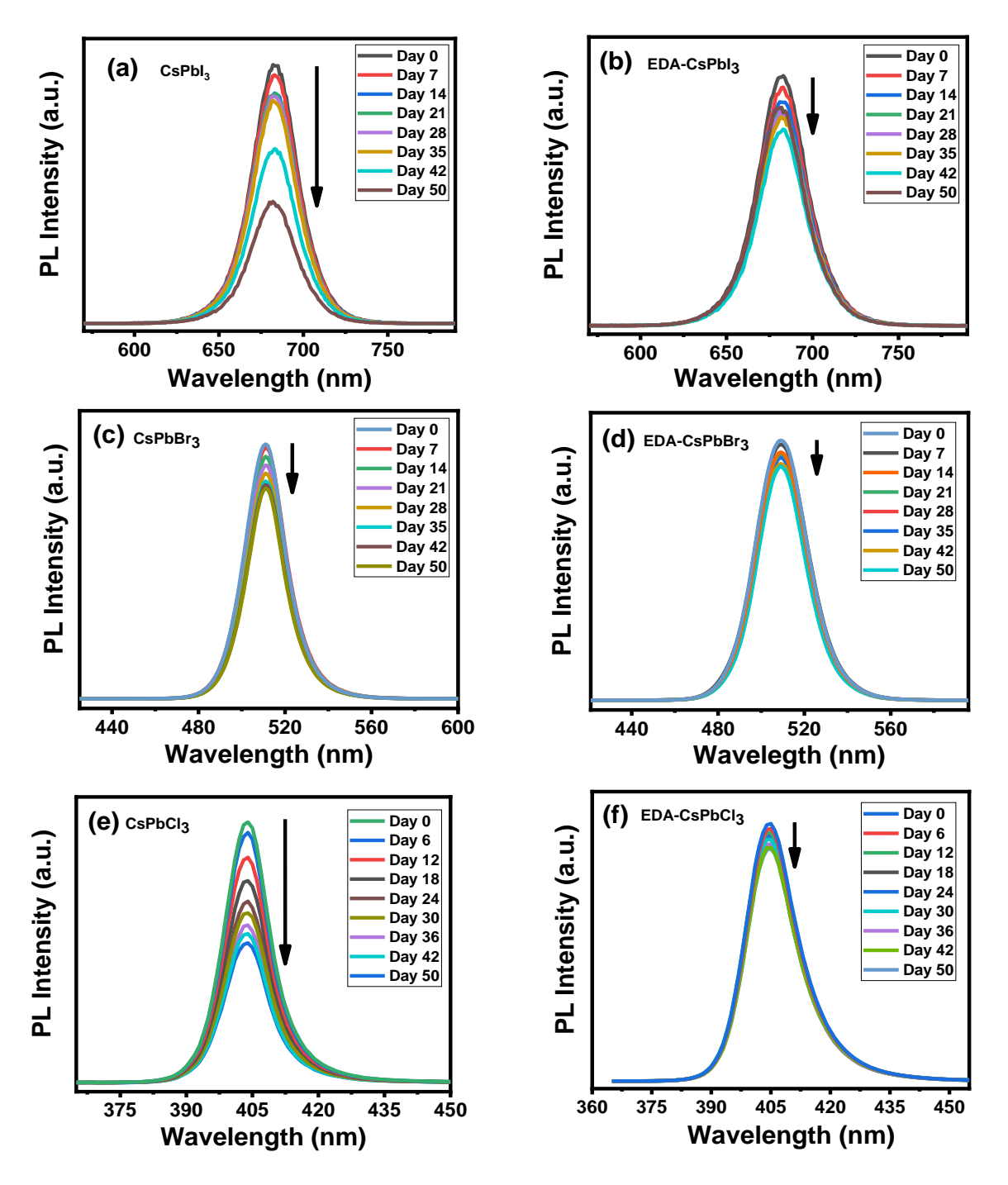


Figure A3.3. Comparison the relative PL intensity of colloidal dispersion of (a) CsPbI₃ (b) EDA-CsPbI₃ (c) CsPbBr₃ and (d) EDA-CsPbBr₃ (e) CsPbCl₃ and (f) EDA-CsPbCl₃ NCs stored under ambient condition.

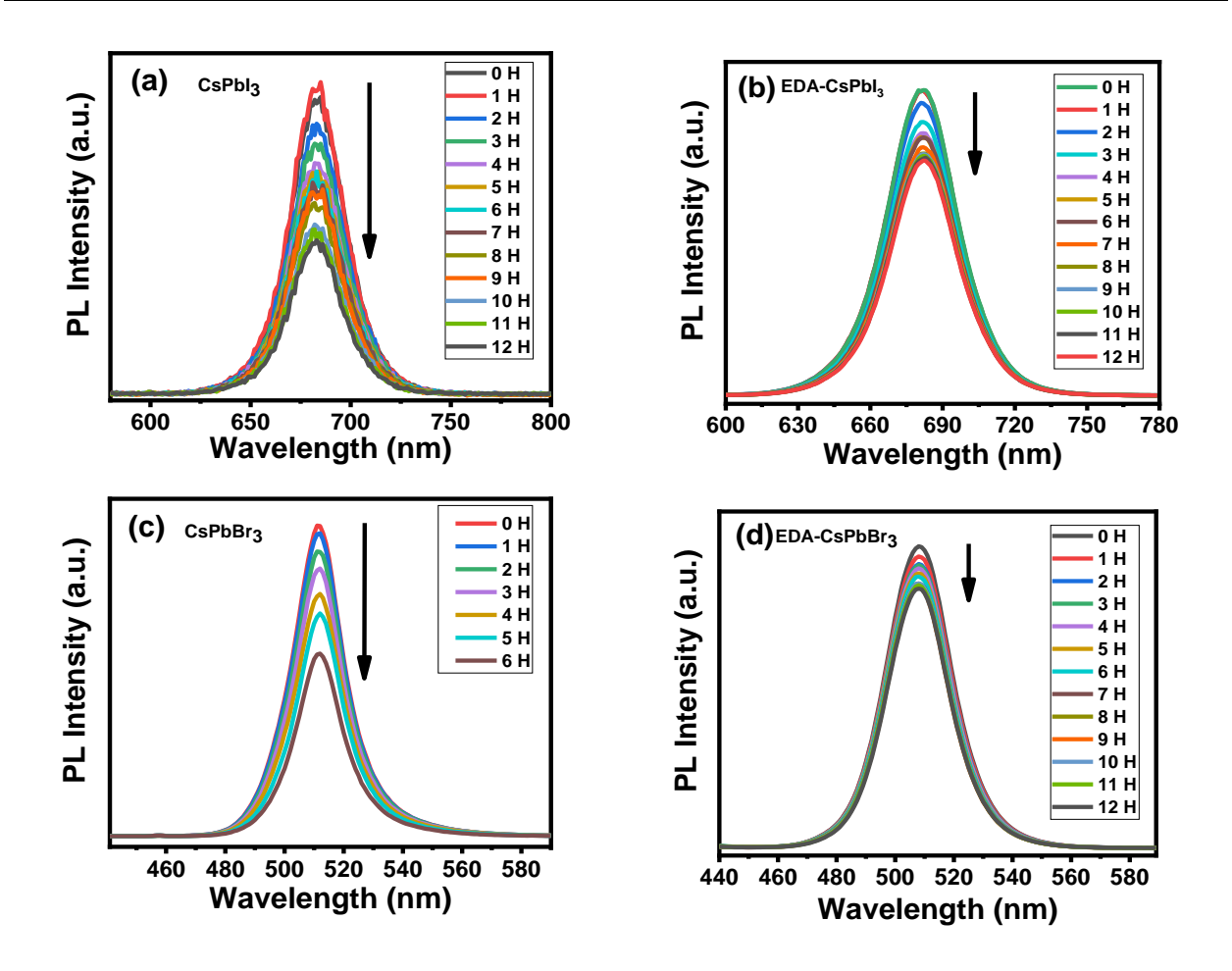
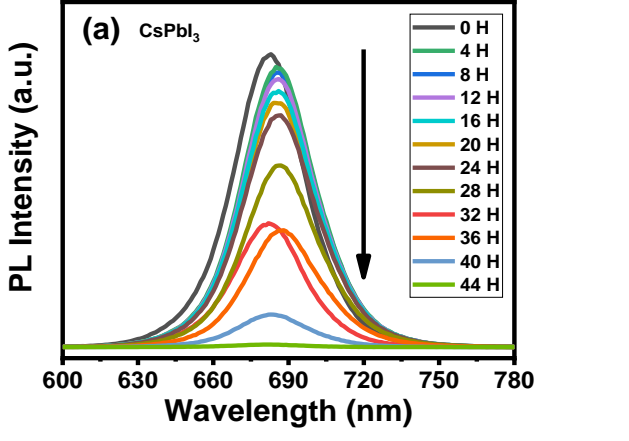
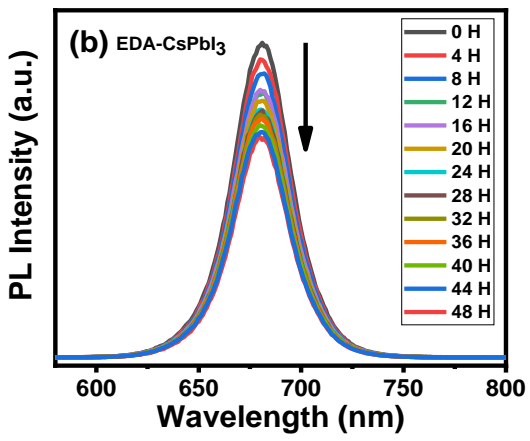


Figure A3.4. Comparison the relative PL intensity of colloidal dispersion of (a) CsPbI₃ (b) EDA-CsPbI₃ (c) CsPbBr₃ and (d) EDA-CsPbBr₃ NCs stored under continuous UV illumination (365 nm, 8 W).





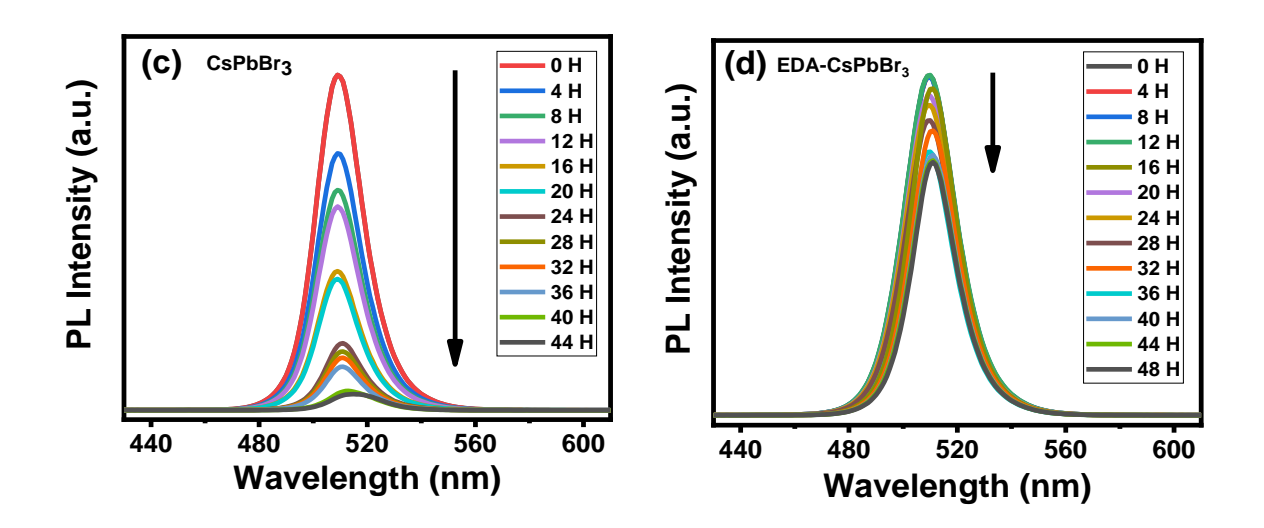


Figure A3.5. Comparison the relative PL intensity of colloidal dispersion of (a) CsPbI₃ (b) EDA-CsPbI₃ (c) CsPbBr₃ and (d) EDA-CsPbBr₃ NCs in presence of polar solvent water stored under ambient condition.

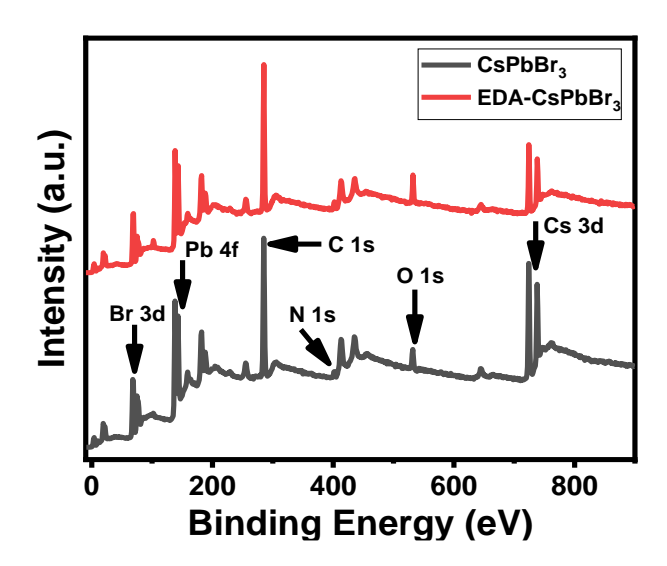


Figure A3.6. XPS survey spectra of the CsPbBr₃ and EDA-CsPbBr₃ NCs. The spectra were calibrated with respect to C 1s peak at ~285 eV.

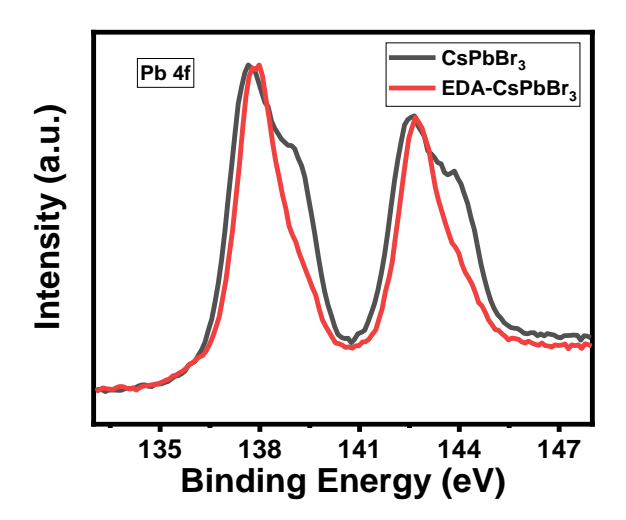


Figure A3.7. High-resolution XPS spectra of Pb 4f of CsPbBr₃ and EDA-CsPbBr₃ NCs.



pubs.acs.org/JPCC Article

Can Sulfur-Containing Small Systems Enhance the Photoluminescence and Stability of the Blue-, Green- and Yellow-Emitting Perovskite Nanocrystals? A Case Study with Sodium Thiosulfate

Rajesh Kumar Gautam, Somnath Das, and Anunay Samanta*

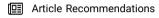


Cite This: J. Phys. Chem. C 2021, 125, 24170-24179



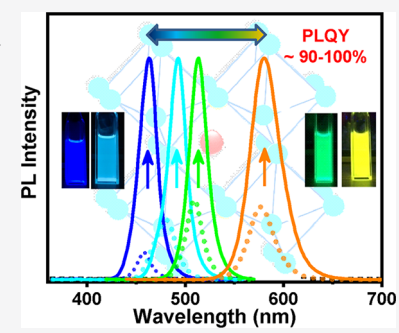
ACCESS I

Metrics & More



Supporting Information

ABSTRACT: Cesium lead halide perovskite nanocrystals (NCs) are the most promising materials for photovoltaic and optoelectronic applications in recent years. However, lack of long-term stability and consequent deterioration of optical properties with time have been major challenges for commercialization of the perovskite-based devices. In this context, we report that even room-temperature treatment of blue-emitting CsPbCl_{1.5}Br_{1.5} and CsPbClBr₂ NCs, green-emitting CsPbBr₃ NCs, and yellow-emitting CsPbBr_{1.5}I_{1.5} NCs with sodium thiosulfate (Na₂S₂O₃·5H₂O) can not only lead to huge enhancement of the photoluminescence quantum yield (PLQY, to ~100% for the blue/green-emitting NCs and ~90% for the yellow-emitting NCs) but also add superior stability to these NCs under different environmental stresses. While the time-resolved PL and ultrafast transient absorption studies show suppression of the nonradiative recombination channels, other measurements reveal that the improved optical characteristics and stability of these substances are by the formation



of Pb-S bonds between undercoordinated surface Pb and thiosulfate. The outstanding PLQY and much improved long-term stability of the treated NCs make them attractive components for perovskite-based optoelectronic applications.

1. INTRODUCTION

In recent years, cesium lead halide (CsPb X_3 , X = Cl, Br, and I) perovskite NCs have been receiving great attention because of their potential in photovoltaic and optoelectronic applications such as solar cells, 1,2 photodetectors, lasers, 4,5 and lightemitting diodes (LEDs)⁶ due to their excellent optical properties such as defect-tolerant nature, large absorption coefficient,8 tunable photoluminescence (PL) throughout the entire visible region, 8-10 high PLQY, 11-14 and narrow emission bandwidth (full width at half-maximum, FWHM).8 However, in their nanodimension, the PL properties are very sensitive to the surface of the NCs and the observed PLQY values are often far from satisfactory. 14-17 Stabilizing the fragile organic-inorganic interfaces of the CsPbX₃ NCs continues to remain as a challenging exercise even today. Even though oleic acid (OA) and oleylamine (OLA) are widely used as capping ligands for protecting and passivating the surface of the NCs, the environment of the capping ligands around the surface of the NCs is highly dynamic in nature. 18 Facile protonation and deprotonation of OLA and OA lead to a dynamic equilibrium, which facilitates desorption of surface-bound capping ligands, thus exposing the surface of the NCs (and creating uncoordinated lead ions on the surface), forming interbandgap trap (defect) states. 18-20 Due to low exciton binding energy in these systems, free carriers are readily formed at room temperature (RT), which undergo rapid nonradiative

recombination through the inter-bandgap surface trap states, thereby decreasing the PLQY. 8,18 This inefficient surface passivation also contributes to the deterioration of the colloidal stability of the NCs under ambient conditions. 18,21 While the trap states are energetically shallow for the green/red-emitting CsPbBr₃/CsPbI₃ NCs, but deep in nature for the blue-emitting CsPb(Cl/Br)₃ NCs, the latter exhibits poor optical properties with PLQY in a range of $\sim\!1-15\%$. 22 This impedes the utility of the blue-emitting NCs in optoelectronic applications as compared to the other perovskites. 23

Several *in situ* and post-synthetic strategies for suppression of the halide vacancy-related surface defects, ^{24–29} removal of the lead nanoparticles from the surface, ^{11,30–33} curing octahedral distortion by doping the B-site with smaller metal ions, ^{34–43} and capping the surface by ligands that bind stronger than the native ligands, OA and OLA, ^{4,12,44–48} have been reported to obtain stable and highly luminescent all-inorganic perovskite NCs. A judicious choice of the capping ligands is one of the most effective approaches for surface passivation of

Revised: August 18, 2021 Revised: October 15, 2021 Published: October 25, 2021





the NCs. Thiol-based systems are known to improve the optoelectronic and photovoltaic performance of lead-based metal chalcogenide quantum dots (QDs) because of the strong soft-soft interaction between Pb2+ (soft acid) and S2- (soft base) at the surface. 49 Pan et al. first applied this strategy to the perovskites and showed that post-synthetic treatment of CsPbBr₃ NCs with didodecyldimethylammonium sulfide increases their air-stability and enhances the PLQY from 49 to 70% through the formation of a sulfide-enriched protective surface layer. 4 Zheng and co-workers then fabricated a solar cell by using thiol-modified CH3NH3PbI3 as an energy harvester with improved stability and performance. 50 Relying on the strong affinity of sulfur with undercoordinated lead, the long-chain organic thiols have often been used for increasing the PLQY and stability of green-emitting CsPbBr3 NCs by suppressing the surface trap states. 44,51 Very recently, Bakr and co-workers succeeded in enhancing the PLQY of blue-emitting $CsPb(Br_xCl_{1-x})_3$ NCs close to near-unity by using long-chain organic thiocyanate. 45 The effect of small sulfur-containing inorganic salts on the optical properties of perovskite NCs has remained unexplored till date.

Herein, we explore how sulfur-containing small inorganic salt influences the stability and PL efficiency of the blue-emitting $CsPb(Cl/Br)_3$, green-emitting $CsPbBr_3$, and yellow-emitting $CsPbBr_{1.5}I_{1.5}$ perovskite NCs. We demonstrate that RT treatment of these systems with sodium thiosulfate results in an extraordinary improvement of PLQY to near-unity (~100%) for blue/green-emitting NCs and ~90% for the yellow-emitting NCs, thus covering a wide region of the visible spectrum. Effective elimination of the halide vacancy-related inter-bandgap defect states through the formation of strong Pb—S bonds at the surface is shown to be the key factor contributing toward the exceptional optical properties and improved stability of the NCs.

2. EXPERIMENTAL SECTION

- **2.1. Materials.** Cesium carbonate (Cs₂CO₃, 99.9%), octadecene (ODE, 90%), oleic acid (OA, 90%), oleylamine (OLA, technical grade 70%), tri-octylphosphine (TOP, 97%), PbCl₂ (99.99%), PbBr₂ (99.99%), PbI₂ (99%), and methyl acetate (MeOAc, anhydrous, 99.5%) were purchased from Sigma Aldrich. Sodium thiosulfate pentahydrate (>99%) was obtained from Merck. Toluene was purchased from Finar Chemicals and distilled by following the standard procedure. These chemicals were used without any further purification.
- **2.2. Synthesis of NCs.** All NCs were synthesized by following a reported procedure with slight modifications.⁸ The synthesis of the NCs involved two steps: the first step was the preparation of cesium-oleate (Cs-oleate) and the second one was the synthesis of the NCs.
- **2.3. Preparation of Cs-Oleate.** Cs_2CO_3 (0.102 g), OA (0.5 mL), and ODE (5 mL) were taken in a 50 mL double-neck round-bottom (RB) flask and heated at 120 °C under vacuum for 1 h. The temperature was then increased to 140 °C for complete solubilization of Cs_2CO_3 . To avoid precipitation at RT, the sample was preheated at 120 °C before every use.
- **2.4.** Synthesis of CsPbX₃ (X = Br, Cl/Br, and Br/l) NCs. ODE (5 mL), PbX₂ (0.188 mmol), OA (0.5 mL), and OLA (0.5 mL) were loaded in a 50 mL double-neck RB flask, and the mixture was heated at 120 °C under vacuum for 1 h. After complete solubilization of the PbX₂ salt, the temperature was increased to 160 °C under the N₂ environment, and once the reaction attained the set temperature, 0.5 mL of Cs-oleate

solution (preheated at 120 $^{\circ}$ C) was swiftly injected into the reaction medium. After 5 s, the reaction mixture was quenched by placing the RB flask in an ice-water bath. The synthesized NCs were separated from the crude reaction mixture through centrifugation at 7600 rpm for 8 min. The supernatant containing the solvent (ODE), unreacted salts, and excess ligands was discarded, and the precipitate was dispersed in 2 mL of toluene for further studies.

The post-synthetic treatment was performed under ambient conditions by taking $\sim\!\!2$ mL colloidal dispersion $(\sim\!nM)$ of the NCs in a 25 mL RB flask and magnetically stirring for 1 h, which was found to be the optimum time for completion of the treatment. As sodium thiosulfate $(Na_2S_2O_3\cdot 5H_2O)$ has very limited solubility in nonpolar toluene, it was separated from the NCs dispersion through centrifugation at 3000 rpm for 3 min. The supernatant containing the NCs in toluene was the treated NCs and used for future experiments.

- **2.5. Characterization.** *2.5.1. Steady-State UV–Vis Absorption and Fluorescence.* UV–Visible absorption and emission spectra were recorded by a Cary100 (Varian) spectrophotometer and FlouroLog-3 (Horiba Jobin Yvon) spectrofluorimeter, respectively.
- 2.5.2. Photoluminescence Quantum Yield (PLQY) Measurements. The PLQYs were calculated by following the equation below using an appropriate dye molecule as a reference.

$$QY_S = QY_R \times (I_S/I_R) \times (OD_R/OD_S) \times (n_S/n_R)^2$$

where *I* represents the integrated area under the PL spectrum and OD and *n* represent the optical density at the excitation wavelength and refractive index of the solvents, respectively. S and R correspond to the sample (i.e., NCs) and reference compound (i.e., dye), respectively. The reference compound used for PLQY measurements of CsPbCl_{1.5}Br_{1.5} and CsPbClBr₂ was 9,10-diphenylanthracene in toluene (QY = 0.93), for CsPbBr₃ NCs was coumarin 153 in ethanol (QY = 0.546), and for CsPbBr_{1.5}I_{1.5} NCs was rhodamine 6G in aqueous medium (QY = 0.95). $^{52-54}$

- 2.5.3. Powder X-ray Diffraction (PXRD). Powdered X-ray diffraction (PXRD) patterns were recorded on a Bruker D8 Advance diffractometer (Bruker-AXS, Karlsruhe, Germany) using Cu-K α X-radiation (λ = 1.5406 Å) at 40 kV and 30 mA power.
- 2.5.4. Transmission Electron Microscopy (TEM). The TEM images of the NCs were obtained using a transmission electron microscope (Tecnai G2 FE1 F12) at an accelerating voltage of 200 kV. The samples for TEM measurements were prepared by placing a drop of toluene solution of the NCs on a carbon-coated copper grid and keeping it in high vacuum for 24 h.
- 2.5.5. Photoluminescence Lifetime Measurements. A time-correlated single photon counting (TCSPC) spectrometer (Horiba Jobin Yvon IBH) was used for time-resolved luminescence measurements. Pico-Brite lasers with output at 404 and 375 nm and 1 MHz repetition rate were used as the excitation sources, and an MCP photomultiplier (Hammatsu R3809u-50) was used as a detector. The laser source information was recorded by using a dilute solution of Ludox in water (acting as a scatter) in the sample chamber. The fluorescence decay curves were analyzed using IBH DAS6 (version 2.2) software, which employs a nonlinear least-squares iteration procedure. The quality of the fits was determined by considering the χ^2 values and distribution of the residuals. Further details about the setup can be found elsewhere. S5

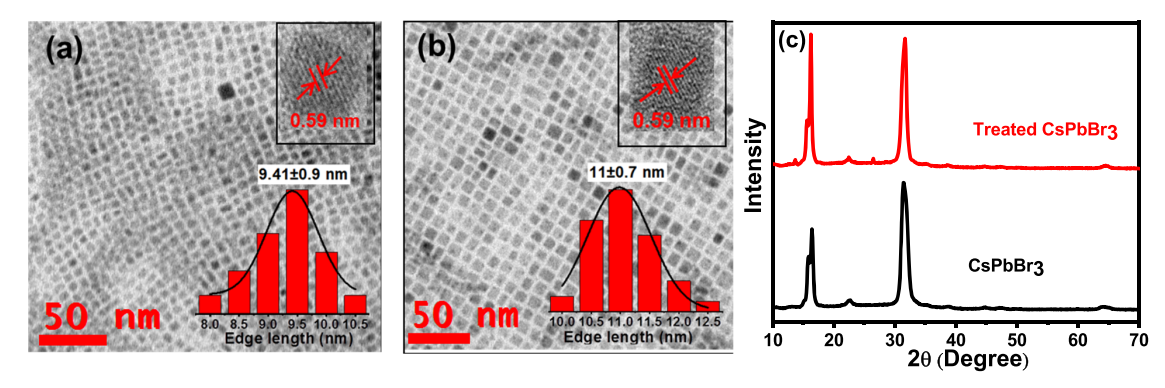


Figure 1. TEM images of the (a) as-synthesized CsPbBr₃ and (b) treated CsPbBr₃ NCs. The insets show high-resolution TEM images of the NCs with similar interplanar distance for (100) planes. (c) PXRD patterns of CsPbBr₃ NCs before and after the treatment.

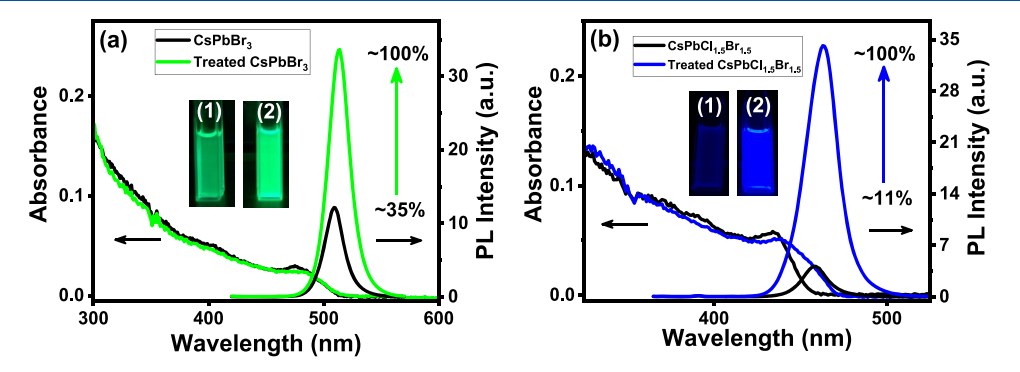


Figure 2. UV—Vis absorption and PL spectra of (a) $CsPbBr_3$ and (b) $CsPbCl_{1.5}Br_{1.5}$ NCs before and after the thiosulfate treatment. Insets show the digital images of both the NCs before (1) and after (2) the treatment under 365 nm UV light. A much brighter emission from the treated samples is clearly visible from the digital images.

2.5.6. Transient Absorption Measurements. The setup consisted of a mode-locked Ti:sapphire seed laser (Mai Tai, Spectra Physics) operating at 80 MHz repetition rate with an output centering at 800 nm, which was directed to a Ti:sapphire regenerative amplifier (Spitfire Ace, Spectra Physics). A high power Q-switched laser (Empower, Spectra Physics) was used for pumping the amplifier. The amplified output of 800 nm (4.2 W) operating at 1 KHz repetition rate was divided into two parts: The major part of the beam (3 W) was directed toward the optical parametric amplifier (Topasprime, Spectra Physics) to generate the excitation wavelength used here. The remaining part of the amplified beam was passed through an optical delay line of 4 ns followed by a CaF₂ crystal to generate white light continuum. The white light was passed through a beam splitter to generate a signal and reference beams and was directed to the detector (photodiode array) through a fiber coupling unit to record the pumpinduced changes at different delay times of the probe beam. All measurements were performed under very low excitation densities $(4-5 \mu J/cm^2)$ to avoid any nonlinear interaction. All spectra presented here were chirp-corrected, and the instrumental resolution was ~120 fs.

2.5.7. Fourier Transformed Infrared Spectroscopy (FTIR). FTIR measurements were made using a Bruker Tensor II spectrometer. For the FTIR studies, one drop of concentrated colloidal solutions of CsPbBr₃ NCs was used from the stock solution. The concentration of untreated and treated CsPbBr₃ NCs was kept similar for the measurement.

2.5.8. Field-Emission Scanning Electron Microscopy (FESEM). FESEM images were taken using a Carl Zeiss Ultra 55 microscope. Energy-dispersive X-ray (EDX) spectra and

elemental mappings measurements were obtained using an Oxford Instruments X-Max^N SDD (50 mm²) system and INCA analysis software. The samples for FESEM measurement were prepared by drop-casting colloidal solutions of the NCs on a clean thin quartz plate and drying the samples under vacuum for 12 h. For elemental mapping, purified CsPbBr₃ NCs were obtained by mixing toluene dispersion of the treated CsPbBr₃ NCs with MeOAc in 1:1 volume ratio, centrifuging the resulting solution at 12,000 rpm for 5 min, collecting the precipitate and redispersing it in toluene.

2.5.9. X-ray Photoelectron Spectroscopy (XPS). XPS measurements were performed using a Thermo Scientific K-Alpha+ spectrometer. A micro-focused monochromatic X-ray source was generated at 70 W with a spot size of 400 μ m. The energy resolution of the spectrometer was set at 0.5 eV at a pass energy of 50 eV. The base pressure of the chamber was maintained at 5×10^{-10} Torr during the analysis. Low energy electrons from the flood gun were used for charge compensation.

3. RESULTS AND DISCUSSION

The colloidal CsPbBr₃ and mixed-halide NCs were synthesized following a known procedure with some minor modifications (details in the Supporting Information). The colloidal dispersion of purified NCs in dry toluene was used for further investigations. The post-synthetic treatment was carried out at RT under ambient conditions, the details of which are provided in the Experimental Section.

The transmission electron microscope (TEM) images of the as-synthesized CsPbBr₃ NCs show cubic morphology with an average edge length of \sim 9.4 \pm 0.9 nm (Figure 1a).

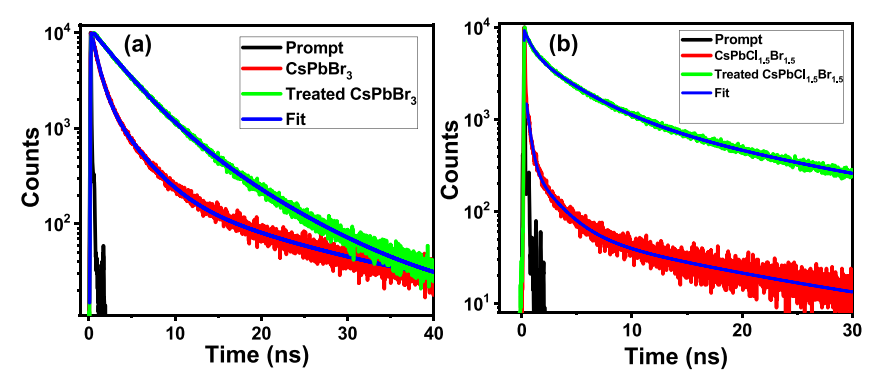


Figure 3. PL decay behavior of as-synthesized and treated (a) CsPbBr₃ and (b) CsPbCl_{1.5}Br_{1.5} NCs. Diode laser sources of λ_{ex} = 404 nm and λ_{ex} = 376 nm were used as the excitation source of CsPbBr₃ and CsPbCl_{1.5}Br_{1.5} NCs, respectively. The decay profiles were monitored at their respective PL maxima (512 and 463 nm, respectively).

Table 1. Fluorescence Decay Parameters of the As-synthesized and Treated CsPbBr₃ and CsPbCl_{1.5}Br_{1.5} NCs and Calculated Radiative (k_r) and Nonradiative (k_{nr}) Rate Constants

samples	$\tau_1(\alpha_1)^a$ (ns)	$\tau_2(\alpha_2)$ (ns)	$\tau_3(\alpha_3)$ (ns)	PLQY (%)	$\langle au_{\rm amp} \rangle^{b} \ ({\rm ns})$	$k_{\rm r}~({\rm ns}^{-1})$	$k_{\rm nr}~({\rm ns}^{-1})$
CsPbBr ₃	2.97(0.24)	14.5(0.02)	0.78(0.74)	35	1.58	0.22	0.41
treated CsPbBr ₃	3.43(0.8)	8.17(0.20)		~100	4.34	0.23	0.0023
$CsPbCl_{1.5}Br_{1.5}$	2.12(0.15)	15.8(0.03)	0.34(0.82)	11	1.07	0.10	0.83
treated CsPbCl _{1.5} Br _{1.5}	3.94(0.46)	15.5(0.14)	0.73(0.40)	~100	4.27	0.23	0.0023
a	. b,	S /S 1	DI OX//	11 /1	DI (37/) //		

 $^a\alpha_i$ is the fractional contribution associated with i-th life-time component. $^b\langle \tau_{\rm amp}\rangle = \Sigma \tau_i\alpha_i/\Sigma\alpha_i$, $k_{\rm r} = {\rm PLQY}/\langle \tau_{\rm amp}\rangle$, and $k_{\rm nr} = (1-{\rm PLQY})/\langle \tau_{\rm amp}\rangle$.

Interestingly, the treated CsPbBr₃ NCs, though they retain the cubic morphology, exhibit a slightly longer edge length of \sim 11.0 \pm 0.7 nm (Figure 1b). A small increase in particle size after post-synthetic treatment is not uncommon. This can happen due to self-repair or ripening of the NCs during ligand exchange and during the passivation of undercoordinated Pb²⁺ by thiosulfate ions at the surface (discussed later). 45,50,51 A similar trend is observed for the mixed-halide NCs as well upon thiosulfate treatment (Figure S1). Both pristine and treated CsPbBr3 NCs possess an identical interplanar spacing (d) of 0.59 nm corresponding to the (100) planes of the cubic NCs (insets of Figure 1a,b), indicating that the thiosulfate treatment does not affect the crystal structure of the NCs. The unchanged powder X-ray diffraction (PXRD) patterns (Figure 1c) also indicate that the pristine and treated CsPbBr₃ NCs possess a cubic phase and no additional peak for the treated samples implies that the post-synthetic treatment predominately takes place at the surface of the NCs. A similar unchanged PXRD pattern has also been observed for the pristine and treated mixed-halide systems (Figure S2).

The UV-Vis absorption and emission spectra of the pristine and treated NCs are similar in nature except that these are slightly red-shifted for the treated NCs (Figure 2 and Figure S3). The small red-shifts of the absorption and PL spectra are due to the small increase in the size of the NCs after treatment. 45,51 While the spectral features of the pristine and treated samples are not very different, the PL of the samples enhances dramatically after the treatment (Figure 2 and Figure S3) without any change in the FWHM of the PL spectra. The PLQY values of the treated samples of green-emitting CsPbBr₃ $(\lambda_{\rm em} = 512 \text{ nm})$ and blue-emitting CsPbCl_{1.5}Br_{1.5} NCs $(\lambda_{\rm em} =$ 463 nm) are found to be near-unity (~100%) from initial values of ~35 and ~11%, respectively, with ~3-5 nm red-shift of the PL maxima (Figure 2a,b). The other mixed-halide systems also exhibit an excellent PL enhancement after treatment. For example, the PLQY values of the as-synthesized

CsPbClBr₂ and CsPbBr_{1.5}I_{1.5} NCs increase from \sim 48 to \sim 100% in the cyan region and from \sim 30 to \sim 90% in the yellow region, respectively (Figure S3). Thus, we have been able to successfully enhance the PLQY of samples emitting in the range of \sim 463 to \sim 581 nm, demonstrating the effectiveness of our post-synthetic approach over a wide range of the visible spectrum covering from the blue-greenyellow-emitting region (Figure S4).

In order to understand the exceptional optical properties of the treated NCs, we have studied the time-resolved PL behavior of the systems using a time-correlated single photon counting (TCSPC) fluorescence technique. A substantially improved PL lifetime is observed for all the treated NCs (Figure 3 and Figure S5). The PL decay profiles of the assynthesized and treated CsPbBr3 and CsPbCl1.5Br1.5 NCs are shown in Figure 3, and the analyzed decay components are presented in Table 1. As can be seen, the as-synthesized CsPbBr3 NCs exhibit a tri-exponential decay behavior comprising a 2.97 ns component due to band-edge excitonic recombination,³⁰ whose amplitude is significantly higher for the treated CsPbBr₃ NCs (24% vs 80%). The longest component (14.5 ns) with a very small contribution (2%) is attributed to shallow trap-mediated excitonic recombination, 56 whose contribution also increases significantly for the treated NCs. Most interestingly, the shortest component (0.78 ns), which was the major radiative recombination process in pristine CsPbBr₃ NCs, completely vanishes after the treatment. Complete elimination of this shortest sub-nanosecond component, which arises due to the surface trap states, indicates that the treated CsPbBr3 NCs are largely free from surface defects. 30,42 In the case of CsPbCl_{1.5}Br_{1.5} NCs, the contribution of the band-edge radiative recombination increases from 15 to 46% and that of the trapping component decreases by nearly 50% (Figure 3b). A prominent influence of the post-synthetic treatment on the PL decay behavior of the other mixed-halide systems is also observed (Figure S5 and

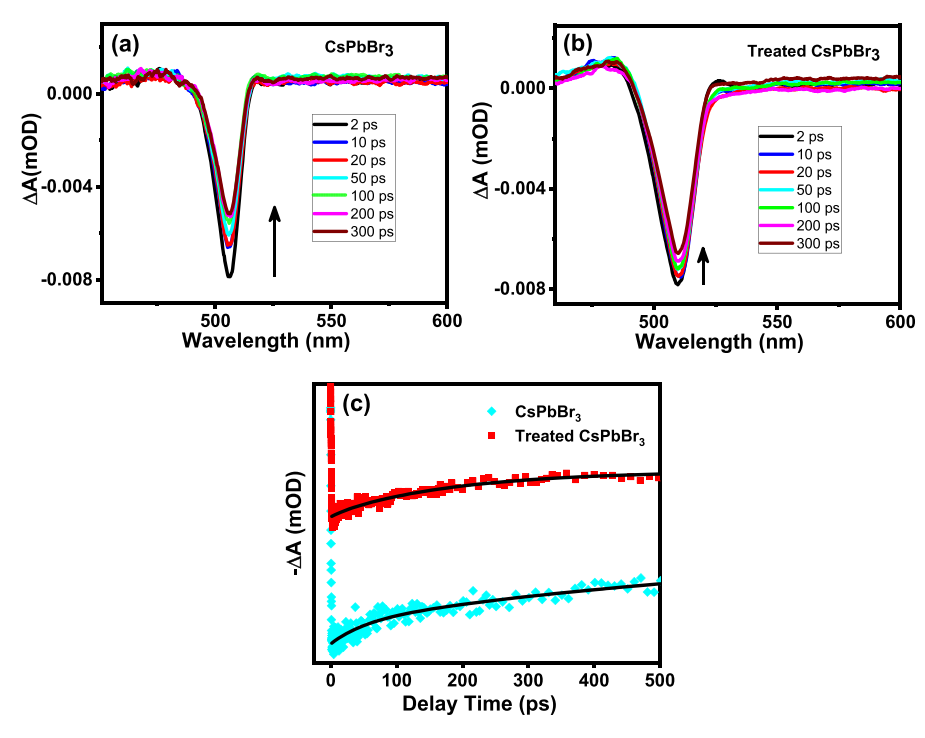


Figure 4. TA spectra (λ_{ex} = 350 nm) of the (a) as-synthesized and (b) treated CsPbBr₃ NCs. (c) Comparison of the bleach recovery dynamics of the two samples. The kinetic parameters obtained upon bi-exponential fitting to the data are 54.5 \pm 4.70 ps (0.23) and >850 ps (0.77) for the assynthesized CsPbBr₃ NCs, while in the case of the treated sample, the recovery dynamics is single exponential with a time constant of >850 ps.

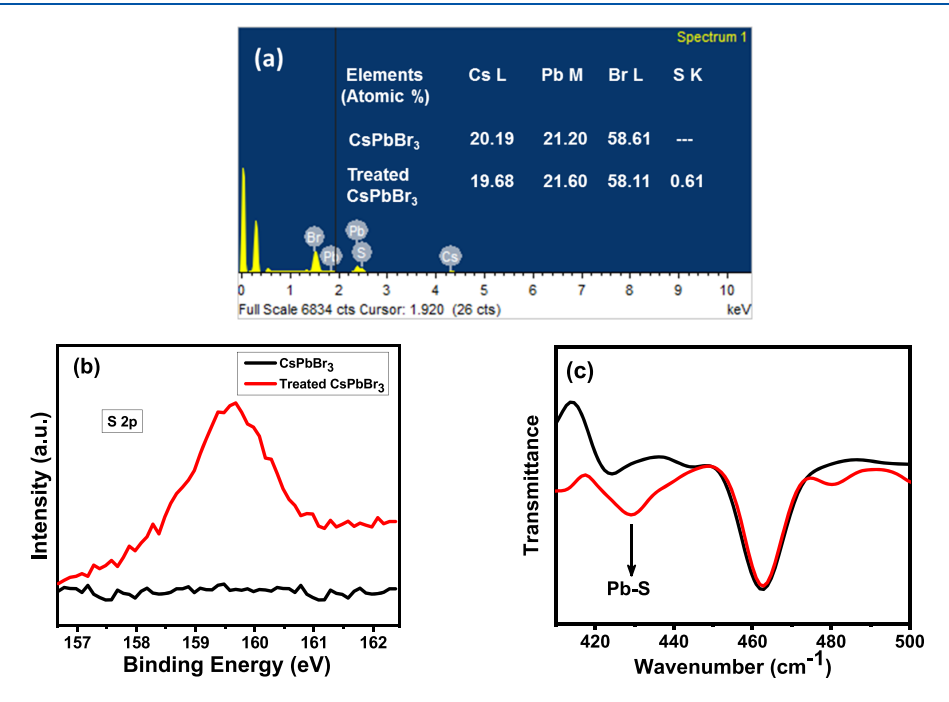


Figure 5. (a) EDX spectra, (b) high-resolution XPS spectra, and (c) FTIR spectra of as-synthesized and thiosulfate-treated CsPbBr₃ NCs in the $410-500 \text{ cm}^{-1}$ region. The XPS data was calibrated with respect to the C 1s peak at ~285.0 eV.

Table S1). The radiative and nonradiative rate constants ($k_{\rm r}$ and $k_{\rm nr}$, respectively), estimated from the measured PLQY and $\langle \tau_{\rm amp} \rangle$ values, show that the $k_{\rm nr}$ value decreases by factors of ~178 for CsPbBr₃ and ~360 for the CsPbCl_{1.5}Br_{1.5} NCs upon treatment (Table 1), indicating a significantly suppressed nonradiative recombination and high PLQY of the systems. The PL decay parameters of the other mixed-halide systems are listed in Table S1.

We also investigated the spectral and temporal characteristics of the transients produced upon the photoexcitation of the as-synthesized and treated CsPbBr₃ NCs by transient absorption (TA) measurements with femtosecond time resolution. As can be seen, the TA spectral features of both the as-synthesized and treated samples are characterized by a sharp negative excitonic bleach signal ($\Delta A = -\mathrm{Ve}$) and photoinduced absorption ($\Delta A = +\mathrm{Ve}$) at the higher energy side of it (Figure 4a,b). 42,57 A slight red-shift of the bleach

signal (from ~506 to 509 nm) on the surface treatment of the CsPbBr₃ NCs is consistent with the shift of the excitonic peak in the steady-state absorption spectra mentioned above. Although the TA spectral features of both the samples are very similar, bleach recovery is much faster for the assynthesized NCs (Figure 4a) compared to the treated sample (Figure 4b), which is clearly reflected in the bleach recovery dynamics of the samples. The bleach recovery dynamics (Figure 4c) of the as-synthesized CsPbBr3 NCs is biexponential with one ultrafast component of \sim 54.5 \pm 4.7 ps (23%) arising from carrier trapping and a long recombination component of >850 ps (77%). However, this dynamics is single exponential and much slower for the treated CsPbBr₃ NCs. The presence of only long (>850 ps) recombination component in the treated NCs indicates effective elimination of the pre-existing nonradiative trap centers in the treated CsPbBr₃ NCs, and therefore, electron-hole radiative recombination is the major process.

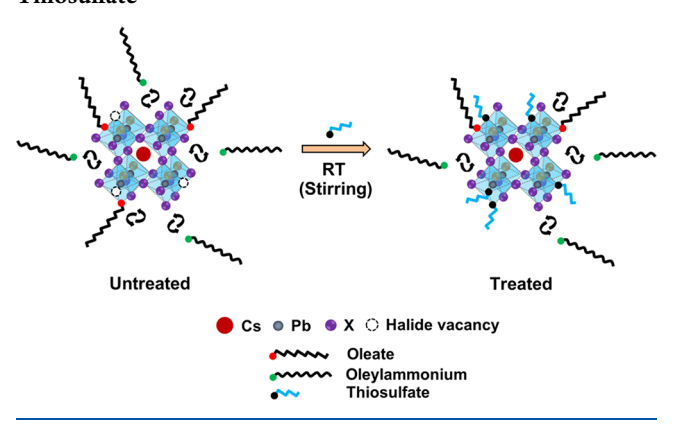
Let us now analyze various factors to determine what contribute(s) to the exceptional optical properties of the treated NCs. A similar lattice spacing and unchanged PXRD patterns of the NCs before and after the treatment suggest that the crystal structure of the NCs is not affected by the treatment, and the thiosulfate salt merely modifies the surface of the NCs. The elemental analysis of a large area of field emission scanning electron microscopy (FESEM) images of the as-synthesized and treated CsPbBr3 NCs by energydispersive X-ray (EDX) measurements (Figure 5a and Figure S6) shows that the Br:Pb ratio in as-synthesized CsPbBr₃ NCs is (~ 2.76) significantly lower than the expected ratio (3.0), indicating bromide deficiency (or undercoordinated Pb²⁺) in the sample. This is a common reason for the poor PLQY of the NCs as it enables rapid nonradiative recombination of the photogenerated charge carriers. 14,22 Very interestingly, in the treated CsPbBr₃ NCs, this ratio is even lower (Br:Pb ≈ 2.69). It is important to note that due to proximity of the S K and Pb M multiplets, the signal at ~2.4 keV appears as an overlapping signal of both the elements, and therefore, it is difficult to resolve the lines in our setup, which has a resolution of \sim 130 eV. 58,59 This is why the EDX signals of the as-synthesized (Figure S6) and treated (Figure 5a) CsPbBr₃ NCs are quite similar in the stated region. For this reason, even though the elemental analysis of the treated CsPbBr₃ NCs (Figure 5a) constantly exhibits a low (~0.61%) "S" content in the EDX spectra, it should not be used as convincing evidence of the presence of sulfur in the sample. However, elemental mapping of the treated CsPbBr₃ NCs washed with MeOAc, which shows a homogeneous distribution of "S" (in addition to the constituent elements Cs, Pb, and Br) throughout the scanned area of the sample, suggests the presence of S in the treated NCs (Figure S7). In order to obtain better insights into the chemical environment of the elements in the treated NCs, we have performed X-ray photoelectron spectroscopy (XPS) measurements of the as-synthesized and treated CsPbBr₃ NCs, which show characteristic peaks of the constituent elements Cs, Pb, and Br at their expected regions (Figure S8). The appearance of an additional peak at ~159 eV only for the treated CsPbBr3 NCs establishes the presence of thiosulfate at the surface of the treated NCs as this peak corresponds to the Pb-S bond (Figure 5b). 51 The presence of the "S 2p" peak even for the washed sample suggests the bound nature of thiosulfate to the NCs (Figure S9). As sulfide forms strong Pb-S bonds owing to a strong soft-acid and soft-base

interaction, both Pb 4f peaks $(4f_{5/2}$ and $4f_{7/2})$ of the treated CsPbBr₃ NCs are shifted to a higher binding energy by ~0.18 eV (Figure S10a).⁶⁰ Interestingly, the binding energy of the Br $3d_{5/2}$ core level spectra is also blue-shifted by ~ 0.7 eV in the treated NCs (Figure S10b). This indicates that the electron density around the central Pb2+ cation is impacted by the formation of the Pb-S bonds, leading to an adjustment in chemical bonding between Pb2+ and Br in the lead bromide octahedral units of the treated NCs, which in turn strengthens the Pb-Br bonds, causing a shift of the Br 3d XPS peak at higher energy. 60-62 Like in EDX measurements, here also the calculated Br/Pb ratio in treated CsPbBr₃ NCs is found to be slightly lower than that in as-synthesized CsPbBr₃ NCs (Table S2). The sulfur content obtained from XPS measurements is however found to be slightly higher to that obtained from EDX studies (Table S2). The surface ligand environment of the NCs is further assessed by FTIR measurements (Figure S11a). The emergence of a new peak at ~430 cm⁻¹ reconfirms the formation of Pb-S bonds at the surface in treated CsPbBr₃ NCs (Figure 5c).⁵⁰ It is interesting to note that the intensity of the peaks due to the asymmetric and symmetric stretching of the carboxylate (COO⁻) ion and N-H bending at 1541, 1400, and 1572 cm⁻¹, respectively,⁶³ is reduced for the treated CsPbBr₃ NCs, indicating that the thiosulfate ion replaces some of the oleate and oleylammonium ligands from the surface of the CsPbBr₃ NCs (Figure S11b,c). The partial replacement of the native surface ligands by sulfur-containing moieties, reported previously for CsPbBr3 NCs, is attributed to the strong binding affinity of sulfide toward uncoordinated lead, resulting in strong Pb–S bonds. 44,60 A distinct peak at $\sim\!1128$ cm⁻¹ in the FTIR spectra of treated CsPbBr₃ NCs, which is a characteristic absorption feature of the S=O bond, 64 suggests binding of thiosulfate with the surface Pb through its sulfur end (Figure S11d). The partial replacement of the native ligands with a concomitant decrease in their signals in FTIR spectra is a reflection of anchoring of thiosulfate at the surface of treated NCs. 44,55 Sodium thiosulfate is a stable compound; it decomposes when heated above 150 °C or in the presence of strong acids (like HCl and H₂SO₄).^{65,66} As our postsynthetic treatment was carried out at RT and in the absence of any strong acid, we believe that thiosulfate remains in its native form during and after the treatment. The possibility of the NCs catalyzing its decomposition, forming PbS, was also considered, but similar TEM images and PXRD patterns of the NCs before and after the treatment and the absence of any characteristic features of decomposition products including PbS rule out this possibility.

Bromide vacancy at the surface of as-synthesized CsPbBr₃ NCs results in the formation of undercoordinated Pb atoms with a net positive charge, which acts as potential electron-trapping centers.⁶⁷ The photogenerated electrons are readily trapped in these sites and subsequently recombine non-radiatively, resulting in poor PLQY.^{22,67} Thiosulfate fills the surface halide vacancies by interacting with the undercoordinated Pb atoms through the S atom, forming strong Pb–S bonds at the surface of the treated NCs. The passivation of halide vacancies through the formation of new Pb–S bonds effectively removes the pre-existing electron traps and enhances band-edge excitonic recombination, resulting in near-unity PLQY of the NCs.^{45,68} A small decrease in the Br/Pb ratio, as indicated by the EDX and XPS data, is presumably a reflection of the exchange of few oleylammonium cations with thiosulfate and their subsequent removal from the

surface as oleylammonium bromides of the treated CsPbBr₃ NCs. In addition, as indicated by the FTIR data, some of the oleate ions are also replaced by thiosulfate owing to the strong affinity of sulfur toward Pb. This agrees with literature information on the partial exchange of native ligands on the formation of Pb—S bonds with organic thiols and other sulfur-containing salts. Thus, effective passivation of under-coordinated Pb through the formation of strong Pb—S bonds with thiosulfate and concomitant suppression of the non-radiative recombination centers contribute to the exceptional optical properties of the treated NCs (Scheme 1). It is however

Scheme 1. Schematic Representation of Halide Vacancy Passivation and Partial Ligand Exchange at the Surface of $CsPbX_3$ NCs after Post-synthetic Treatment with Sodium Thiosulfate



important to note here that apart from the undercoordinated Pb sites, thiosulfate occupies very limited places on the NCs surface and hence do not remove all the native surface ligands as observed earlier in few instances. 11,30

The lack of long-term stability of the perovskite-based devices is probably one of the major issues for wide-scale applications of these substances. The treated NCs are found to be much more stable under different external conditions (Figure 6 and Figures S12 and S13). As can be seen from

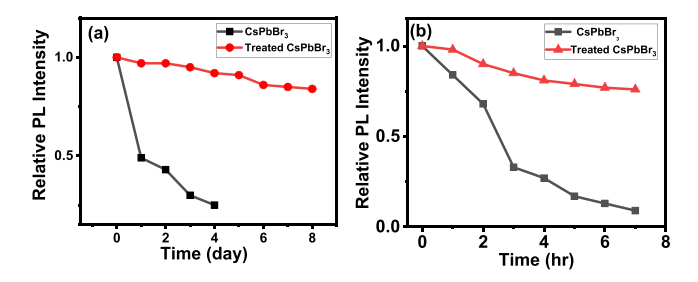


Figure 6. Comparison of the stability of as-synthesized and treated $CsPbBr_3$ NCs under (a) ambient conditions and (b) continuous UV light (365 nm, 8 W) illumination.

Figure 6a, the as-synthesized CsPbBr₃ NCs hold just ~24% of its initial PL intensity after 4 days under ambient conditions (with ~4 nm red-shift of the emission maxima, Figure S12); on the other hand, the treated NCs retain 84% of the same initial PL intensity for over a week under similar conditions (Figure 6a) without any shift of the PL maxima (Figure S12), demonstrating a much superior air-stability. The treated samples exhibit superior photostability as well. For example, under continuous illumination of UV light (365 nm, 8 W) for

7 h, the treated CsPbBr $_3$ NCs hold ~80% of its initial PL intensity, while the as-synthesized CsPbBr $_3$ NCs retains only <10% of the PL intensity under similar conditions (Figure 6b). A superior air- and photostability of treated CsPbBr $_{1.5}$ I $_{1.5}$ NCs is also observed (Figure S13). We attribute this much improved air- and photostability of the treated NCs to the formation of strong Pb–S bonds at the surface, which not only passivates the halide vacancies but also provides a robust and less fragile surface ligand environment than that present in assynthesized NCs. 44

4. CONCLUSIONS

A room-temperature post-synthetic treatment of the blue-emitting $CsPb(Cl/Br)_3$, green-emitting $CsPbBr_3$, and yellow-emitting $CsPb(Br/I)_3$ NCs with $Na_2S_2O_3\cdot 5H_2O$ under ambient conditions is shown to dramatically improve the PLQY (~90–100%) of these systems, which cover a wide range of the visible spectrum. The treated samples also exhibit high stability under different external conditions. The results imply that the halide vacancy-related surface defects in these systems can be effectively passivated by small sulfur-containing systems through formation of strong Pb–S bonds with undercoordinated lead on the surface. The excellent photoluminescence properties and high stability of these NCs make them promising candidates for perovskite-based optoelectronic applications.

ASSOCIATED CONTENT

Supporting Information

The Supporting Information is available free of charge at https://pubs.acs.org/doi/10.1021/acs.jpcc.1c07316.

TEM images and PXRD patterns of the as-synthesized and treated $CsPbCl_{1.5}Br_{1.5}$, $CsPbClBr_2$, and $CsPbBr_{1.5}I_{1.5}$ NCs; UV—Vis absorption, PL spectra, PL decay profiles, and decay parameters of the as-synthesized and treated $CsPbClBr_2$ and $CsPbBr_{1.5}I_{1.5}$ NCs; EDX spectra of assynthesized $CsPbBr_3$ NCs; XPS and FTIR spectra of assynthesized and treated $CsPbBr_3$ NCs; air-and photostability of as-synthesized and treated $CsPbCl_{1.5}Br_{1.5}$ NCs; and elemental % ratio for as-synthesized and treated $CsPbBr_3$ NCs obtained from XPS measurement (PDF)

AUTHOR INFORMATION

Corresponding Author

Anunay Samanta — School of Chemistry, University of Hyderabad, Hyderabad 500046, India; orcid.org/0000-0003-1551-0209; Email: anunay@uohyd.ac.in

Authors

9597

Rajesh Kumar Gautam — School of Chemistry, University of Hyderabad, Hyderabad 500046, India

Somnath Das — School of Chemistry, University of Hyderabad, Hyderabad 500046, India; orcid.org/0000-0002-3414-

Complete contact information is available at: https://pubs.acs.org/10.1021/acs.jpcc.1c07316

Notes

The authors declare no competing financial interest.

ACKNOWLEDGMENTS

This work is supported by the J. C. Bose Fellowship (to A.S.) of the Science and Engineering Research Board (SERB) and Institute of Eminence Grants (to University of Hyderabad) of the Ministry of Human Resource and Development (MHRD). The authors acknowledge the TEM facility of the Centre for Nanotechnology, University of Hyderabad, and the femtosecond laser, FESEM, and FTIR facilities of the school. Thanks are also due to National Chemical Laboratory, Pune for the XPS measurements. R.K.G. and S.D. thank the University of Hyderabad and University Grants Commission (UGC) for Fellowships, respectively.

REFERENCES

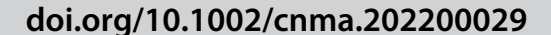
- (1) Kojima, A.; Teshima, K.; Shirai, Y.; Miyasaka, T. Organometal Halide Perovskites as Visible-Light Sensitizers for Photovoltaic Cells. *J. Am. Chem. Soc.* **2009**, *131*, 6050–6051.
- (2) Liang, J.; Wang, C.; Wang, Y.; Xu, Z.; Lu, Z.; Ma, Y.; Zhu, H.; Hu, Y.; Xiao, C.; Yi, X.; et al. All-Inorganic Perovskite Solar Cells. J. Am. Chem. Soc. **2016**, 138, 15829–15832.
- (3) Ramasamy, P.; Lim, D.-H.; Kim, B.; Lee, S.-H.; Lee, M.-S.; Lee, J.-S. All-inorganic cesium lead halide perovskite nanocrystals for photodetector applications. *Chem. Commun.* **2016**, 52, 2067–2070.
- (4) Pan, J.; Sarmah, S. P.; Murali, B.; Dursun, I.; Peng, W.; Parida, M. R.; Liu, J.; Sinatra, L.; Alyami, N.; Zhao, C.; et al. Air-Stable Surface-Passivated Perovskite Quantum Dots for Ultra-Robust, Single- and Two-Photon-Induced Amplified Spontaneous Emission. *J. Phys. Chem. Lett.* **2015**, *6*, 5027–5033.
- (5) Yakunin, S.; Protesescu, L.; Krieg, F.; Bodnarchuk, M. I.; Nedelcu, G.; Humer, M.; De Luca, G.; Fiebig, M.; Heiss, W.; Kovalenko, M. V. Low-threshold amplified spontaneous emission and lasing from colloidal nanocrystals of caesium lead halide perovskites. *Nat. Commun.* **2015**, *6*, 8056.
- (6) Zhang, X.; Lin, H.; Huang, H.; Reckmeier, C.; Zhang, Y.; Choy, W. C. H.; Rogach, A. L. Enhancing the Brightness of Cesium Lead Halide Perovskite Nanocrystal Based Green Light-Emitting Devices through the Interface Engineering with Perfluorinated Ionomer. *Nano Lett.* 2016, 16, 1415–1420.
- (7) Kovalenko, M. V.; Protesescu, L.; Bodnarchuk, M. I. Properties and potential optoelectronic applications of lead halide perovskite nanocrystals. *Science* **2017**, *358*, 745–750.
- (8) Protesescu, L.; Yakunin, S.; Bodnarchuk, M. I.; Krieg, F.; Caputo, R.; Hendon, C. H.; Yang, R. X.; Walsh, A.; Kovalenko, M. V. Nanocrystals of Cesium Lead Halide Perovskites (CsPbX₃, X = Cl, Br, and I): Novel Optoelectronic Materials Showing Bright Emission with Wide Color Gamut. *Nano Lett.* **2015**, *15*, 3692–3696.
- (9) Nedelcu, G.; Protesescu, L.; Yakunin, S.; Bodnarchuk, M. I.; Grotevent, M. J.; Kovalenko, M. V. Fast Anion-Exchange in Highly Luminescent Nanocrystals of Cesium Lead Halide Perovskites (CsPbX₃, X = Cl, Br, I). *Nano Lett.* **2015**, *15*, 5635–5640.
- (10) Dutt, V. G. V.; Akhil, S.; Mishra, N. Fast, tunable and reversible anion-exchange in CsPbBr₃ perovskite nanocrystals with hydrohalic acids. *CrystEngComm* **2020**, *22*, 5022–5030.
- (11) Koscher, B. A.; Swabeck, J. K.; Bronstein, N. D.; Alivisatos, A. P. Essentially Trap-Free CsPbBr₃ Colloidal Nanocrystals by Postsynthetic Thiocyanate Surface Treatment. *J. Am. Chem. Soc.* **2017**, *139*, 6566–6569.
- (12) Pan, J.; Shang, Y.; Yin, J.; De Bastiani, M.; Peng, W.; Dursun, I.; Sinatra, L.; El-Zohry, A. M.; Hedhili, M. N.; Emwas, A.-H.; et al. Bidentate Ligand-Passivated CsPbI₃ Perovskite Nanocrystals for Stable Near-Unity Photoluminescence Quantum Yield and Efficient Red Light-Emitting Diodes. *J. Am. Chem. Soc.* **2018**, *140*, 562–565.
- (13) Dutta, A.; Behera, R. K.; Pal, P.; Baitalik, S.; Pradhan, N. Near-Unity Photoluminescence Quantum Efficiency for All CsPbX₃ (X=Cl, Br, and I) Perovskite Nanocrystals: A Generic Synthesis Approach. *Angew. Chem., Int. Ed.* **2019**, *58*, 5552–5556.

- (14) Seth, S.; Ahmed, T.; De, A.; Samanta, A. Tackling the Defects, Stability, and Photoluminescence of CsPbX₃ Perovskite Nanocrystals. *ACS Energy Lett.* **2019**, *4*, 1610–1618.
- (15) Tachikawa, T.; Karimata, I.; Kobori, Y. Surface Charge Trapping in Organolead Halide Perovskites Explored by Single-Particle Photoluminescence Imaging. *J. Phys. Chem. Lett.* **2015**, *6*, 3195–3201.
- (16) Pradhan, N. Tips and Twists in Making High Photoluminescence Quantum Yield Perovskite Nanocrystals. *ACS Energy Lett.* **2019**, *4*, 1634–1638.
- (17) Dutt, V. G. V.; Akhil, S.; Mishra, N. Surface Passivation Strategies for Improving Photoluminescence and Stability of Cesium Lead Halide Perovskite Nanocrystals. *ChemNanoMat* **2020**, *6*, 1730–1742.
- (18) De Roo, J.; Ibáñez, M.; Geiregat, P.; Nedelcu, G.; Walravens, W.; Maes, J.; Martins, J. C.; Driessche, I. V.; Kovalenko, M. V.; Hens, Z. Highly Dynamic Ligand Binding and Light Absorption Coefficient of Cesium Lead Bromide Perovskite Nanocrystals. *ACS Nano* **2016**, 10, 2071–2081.
- (19) Yassitepe, E.; Yang, Z.; Voznyy, O.; Kim, Y.; Walters, G.; Castañeda, J. A.; Kanjanaboos, P.; Yuan, M.; Gong, X.; Fan, F.; et al. Amine-Free Synthesis of Cesium Lead Halide Perovskite Quantum Dots for Efficient Light-Emitting Diodes. *Adv. Funct. Mater.* **2016**, 26, 8757–8763.
- (20) Akhil, S.; Dutt, V. G. V.; Mishra, D. N. Completely Amine-Free Open-Atmospheric Synthesis of High-Quality Cesium Lead Bromide (CsPbBr₃) Perovskite Nanocrystals. *Chem. Eur. J.* **2020**, *26*, 1–9.
- (21) Dutta, A.; Dutta, S. K.; Adhikari, S. D.; Pradhan, N. Phase-Stable CsPbI₃ Nanocrystals: The Reaction Temperature Matters. *Angew. Chem. Int. Ed.* **2018**, *57*, 9083–9087.
- (22) Nenon, D. P.; Pressler, K.; Kang, J.; Koscher, B. A.; Olshansky, J. H.; Osowiecki, W. T.; Koc, M. A.; Wang, L.-W.; Alivisatos, A. P. Design Principles for Trap-Free CsPbX₃ Nanocrystals: Enumerating and Eliminating Surface Halide Vacancies with Softer Lewis Bases. J. Am. Chem. Soc. 2018, 140, 17760–17772.
- (23) Shamsi, J.; Urban, A. S.; Imran, M.; De Trizio, L.; Manna, L. Metal Halide Perovskite Nanocrystals: Synthesis, Post-Synthesis Modifications, and Their Optical Properties. *Chem. Rev.* **2019**, *119*, 3296–3348.
- (24) Woo, J. Y.; Kim, Y.; Bae, J.; Kim, T. G.; Kim, J. W.; Lee, D. C.; Jeong, S. Highly Stable Cesium Lead Halide Perovskite Nanocrystals through in Situ Lead Halide Inorganic Passivation. *Chem. Mater.* **2017**, 29, 7088–7092.
- (25) Wu, Y.; Wei, C.; Li, X.; Li, Y.; Qiu, S.; Shen, W.; Cai, B.; Sun, Z.; Yang, D.; Deng, Z.; et al. In Situ Passivation of PbBr₆⁴⁻ Octahedra toward Blue Luminescent CsPbBr₃ Nanoplatelets with Near 100% Absolute Quantum Yield. *ACS Energy Lett.* **2018**, *3*, 2030–2037.
- (26) Behera, R. K.; Adhikari, S. D.; Dutta, S. K.; Dutta, A.; Pradhan, N. Blue-Emitting CsPbCl₃ Nanocrystals: Impact of Surface Passivation for Unprecedented Enhancement and Loss of Optical Emission. *J. Phys. Chem. Lett.* **2018**, *9*, 6884–6891.
- (27) Shao, H.; Zhai, Y.; Wu, X.; Xu, W.; Xu, L.; Dong, B.; Bai, X.; Cui, H.; Song, H. High brightness blue light-emitting diodes based on CsPb(Cl/Br)₃ perovskite QDs with phenethylammonium chloride passivation. *Nanoscale* **2020**, *12*, 11728–11734.
- (28) Dutta, A.; Behera, R. K.; Dutta, S. K.; Adhikari, S. D.; Pradhan, N. Annealing $CsPbX_3$ (X = Cl and Br) Perovskite Nanocrystals at High Reaction Temperatures: Phase Change and Its Prevention. *J. Phys. Chem. Lett.* **2018**, *9*, 6599–6604.
- (29) Chen, Y.-C.; Chou, H.-L.; Lin, J.-C.; Lee, Y.-C.; Pao, C.-W.; Chen, J.-L.; Chang, C.-C.; Chi, R.-Y.; Kuo, T.-R.; Lu, C.-W.; et al. Enhanced Luminescence and Stability of Cesium Lead Halide Perovskite CsPbX₃ Nanocrystals by Cu²⁺-Assisted Anion Exchange Reactions. *J. Phys. Chem. C* **2019**, *123*, 2353–2360.
- (30) Ahmed, T.; Seth, S.; Samanta, A. Boosting the Photoluminescence of $CsPbX_3$ (X = Cl, Br, I) Perovskite Nanocrystals Covering a Wide Wavelength Range by Postsynthetic Treatment with Tetrafluoroborate Salts. *Chem. Mater.* **2018**, *30*, 3633–3637.

- (31) Wang, S.; Wang, Y.; Zhang, Y.; Zhang, X.; Shen, X.; Zhuang, X.; Lu, P.; Yu, W. W.; Kershaw, S. V.; Rogach, A. L. Cesium Lead Chloride/Bromide Perovskite Quantum Dots with Strong Blue Emission Realized via a Nitrate-Induced Selective Surface Defect Elimination Process. J. Phys. Chem. Lett. 2019, 10, 90–96.
- (32) Li, F.; Liu, Y.; Wang, H.; Zhan, Q.; Liu, Q.; Xia, Z. Postsynthetic Surface Trap Removal of CsPbX₃ (X = Cl, Br, or I) Quantum Dots via a ZnX₂/Hexane Solution toward an Enhanced Luminescence Quantum Yield. *Chem. Mater.* **2018**, *30*, 8546–8554.
- (33) Shen, X.; Wang, S.; Zhang, X.; Wang, H.; Zhang, X.; Wang, C.; Gao, Y.; Shi, Z.; Yu, W. W.; Zhang, Y. Enhancing the efficiency of CsPbX₃ (X = Cl, Br, I) nanocrystals via simultaneous surface peeling and surface passivation. *Nanoscale* **2019**, *11*, 11464–11469.
- (34) Yong, Z.-J.; Guo, S.-Q.; Ma, J.-P.; Zhang, J.-Y.; Li, Z.-Y.; Chen, Y.-M.; Zhang, B.-B.; Zhou, Y.; Shu, J.; Gu, J.-L.; et al. Doping-Enhanced Short-Range Order of Perovskite Nanocrystals for Near-Unity Violet Luminescence Quantum Yield. J. Am. Chem. Soc. 2018, 140, 9942—9951.
- (35) Yao, J.-S.; Ge, J.; Han, B.-N.; Wang, K.-H.; Yao, H.-B.; Yu, H.-L.; Li, J.-H.; Zhu, B.-S.; Song, J.-Z.; Chen, C.; et al. Ce3+-Doping to Modulate Photoluminescence Kinetics for Efficient CsPbBr₃ Nanocrystals Based Light-Emitting Diodes. *J. Am. Chem. Soc.* **2018**, *140*, 3626–3634
- (36) De, A.; Das, S.; Mondal, N.; Samanta, A. Highly Luminescent Violet- and Blue-Emitting Stable Perovskite Nanocrystals. *ACS Materials Lett.* **2019**, *1*, 116–122.
- (37) Vitoreti, A. B. F.; Agouram, S.; Solis de la Fuente, M.; Muñoz-Sanjosé, V.; Schiavon, M. A.; Mora-Seró, I.; Fuente, M. S. d. l.; Muñoz-Sanjosé, V.; Schiavon, M. A.; Mora-Seró, l. Study of the Partial Substitution of Pb by Sn in Cs-Pb-Sn-Br Nanocrystals Owing to Obtaining Stable Nanoparticles with Excellent Optical Properties. *J. Phys. Chem. C* 2018, 122, 14222–14231.
- (38) Li, S.; Shi, Z.; Zhang, F.; Wang, L.; Ma, Z.; Yang, D.; Yao, Z.; Wu, D.; Xu, T.-T.; Tian, Y.; et al. Sodium Doping-Enhanced Emission Efficiency and Stability of CsPbBr₃ Nanocrystals for White Light-Emitting Devices. *Chem. Mater.* **2019**, *31*, 3917–3928.
- (39) Van Der Stam, W.; Geuchies, J. J.; Altantzis, T.; Van Den Bos, K. H. W.; Meeldijk, J. D.; Van Aert, S.; Bals, S.; Vanmaekelbergh, D.; De Mello Donega, C. Highly Emissive Divalent-Ion-Doped Colloidal CsPb1–xMxBr₃ Perovskite Nanocrystals through Cation Exchange. *J. Am. Chem. Soc.* **2017**, *139*, 4087–4097.
- (40) Bi, C.; Wang, S.; Li, Q.; Kershaw, S. V.; Tian, J.; Rogach, A. L. Thermally Stable Copper(II)-Doped Cesium Lead Halide Perovskite Quantum Dots with Strong Blue Emission. *J. Phys. Chem. Lett.* **2019**, 10, 943–952.
- (41) Mondal, N.; De, A.; Samanta, A. Achieving Near-Unity Photoluminescence Efficiency for Blue-Violet-Emitting Perovskite Nanocrystals. *ACS Energy Lett.* **2019**, *4*, 32–39.
- (42) Das, S.; De, A.; Samanta, A. Ambient Condition Mg²⁺ Doping Producing Highly Luminescent Green- and Violet-Emitting Perovskite Nanocrystals with Reduced Toxicity and Enhanced Stability. *J. Phys. Chem. Lett.* **2020**, *11*, 1178–1188.
- (43) Zhang, X.; Wang, H.; Hu, Y.; Pei, Y.; Wang, S.; Shi, Z.; Colvin, V. L.; Wang, S.; Zhang, Y.; Yu, W. W. Strong Blue Emission from Sb³⁺-Doped Super Small CsPbBr₃ Nanocrystals. *J. Phys. Chem. Lett.* **2019**, *10*, 1750–1756.
- (44) Uddin, M. A.; Mobley, J. K.; Masud, A. A.; Liu, T.; Calabro, R. L.; Kim, D.-Y.; Richards, C. I.; Graham, K. R. Mechanistic Exploration of Dodecanethiol-Treated Colloidal CsPbBr₃ Nanocrystals with Photoluminescence Quantum Yields Reaching Near 100%. *J. Phys. Chem. C* 2019, *123*, 18103–18112.
- (45) Zheng, X.; Yuan, S.; Liu, J.; Yin, J.; Yuan, F.; Shen, W.-S.; Yao, K.; Wei, M.; Zhou, C.; Song, K.; et al. Chlorine Vacancy Passivation in Mixed Halide Perovskite Quantum Dots by Organic Pseudohalides Enables Efficient Rec. 2020 Blue Light-Emitting Diodes. ACS Energy Lett. 2020, 5, 793–798.
- (46) Almeida, G.; Ashton, O. J.; Goldoni, L.; Maggioni, D.; Petralanda, U.; Mishra, N.; Akkerman, Q. A.; Infante, I.; Snaith, H. J.;

- Manna, L. The Phosphine Oxide Route toward Lead Halide Perovskite Nanocrystals. J. Am. Chem. Soc. 2018, 140, 14878–14886. (47) Pan, J.; Quan, L. N.; Zhao, Y.; Peng, W.; Murali, B.; Sarmah, S.
- (4/) Pan, J.; Quan, L. N.; Zhao, Y.; Peng, W.; Murali, B.; Sarmah, S. P.; Yuan, M.; Sinatra, L.; Alyami, N. M.; Liu, J.; et al. Highly Efficient Perovskite-Quantum-Dot Light-Emitting Diodes by Surface Engineering. *Adv. Mater.* **2016**, *28*, 8718–8725.
- (48) Akhil, S.; Dutt, V. G. V.; Mishra, N. Surface Modification for Improving Photoredox Activity of CsPbBr₃ Nanocrystals. *Nanoscale Adv.* **2021**, *3*, 2547–2553.
- (49) Barkhouse, D. A. R.; Pattantyus-Abraham, A. G.; Levina, L.; Sargent, E. H. Thiols Passivate Recombination Centers in Colloidal Quantum Dots Leading to Enhanced Photovoltaic Device Efficiency. *ACS Nano* **2008**, 2, 2356–2362.
- (50) Cao, J.; Yin, J.; Yuan, S.; Zhao, Y.; Li, J.; Zheng, N. Thiols as interfacial modifiers to enhance the performance and stability of perovskite solar cells. *Nanoscale* **2015**, *7*, 9443–9447.
- (51) Ruan, L.; Shen, W.; Wang, A.; Zhou, Q.; Zhang, H.; Deng, Z. Stable and conductive lead halide perovskites facilitated by X-type ligands. *Nanoscale* **2017**, *9*, 7252–7259.
- (52) Rurack, K.; Spieles, M. Fluorescence Quantum Yields of a Series of Red and Near-Infrared Dyes Emitting at 600–1000 nm. *Anal. Chem.* **2011**, 83, 1232–1242.
- (53) Morris, J. V.; Mahaney, M. A.; Huber, J. R. Fluorescence quantum yield determinations. 9,10-Diphenylanthracene as a reference standard in different solvents. *J. Phys. Chem.* **1976**, 80, 969–974
- (54) Kubin, R. F.; Fletcher, A. N. Fluorescence quantum yields of some rhodamine dyes. *J. Lumin.* **1982**, *27*, 455–462.
- (55) De, A.; Das, S.; Samanta, A. Hot Hole Transfer Dynamics from CsPbBr₃ Perovskite Nanocrystals. *ACS Energy Lett.* **2020**, *5*, 2246–2252.
- (56) Chirvony, V. S.; González-Carrero, S.; Suárez, I.; Galian, R. E.; Sessolo, M.; Bolink, H. J.; Martínez-Pastor, J. P.; Pérez-Prieto, J. Delayed Luminescence in Lead Halide Perovskite Nanocrystals. *J. Phys. Chem. C* **2017**, *121*, 13381–13390.
- (57) Mondal, N.; Samanta, A. Complete ultrafast charge carrier dynamics in photo-excited all-inorganic perovskite nanocrystals (CsPbX₃). *Nanoscale* **2017**, *9*, 1878.
- (58) Newbury, D. E. Mistakes Encountered During Automatic Peak Identification of Minorand Trace Constituents in Electron-Excited Energy Dispersive X-RayMicroanalysis. *Scanning* **2009**, *31*, 91–101.
- (59) Thompson, K. The Role of Energy Resolution in Collecting World-Class Data for EDS. *Thermo Fisher Scientific Technical Notes* 52537 **2013**.
- (60) Baek, S.; Kim, Y.; Kim, S.-W. Highly photo-stable $CsPbI_3$ perovskite quantum dots via thiol ligand exchange and their polymer film application. *J. Ind. Eng. Chem.* **2019**, 83, 279–284.
- (61) Chen, J.-K.; Ma, J.-P.; Guo, S.-Q.; Chen, Y.-M.; Zhao, Q.; Zhang, B.-B.; Li, Z.-Y.; Zhou, Y.; Hou, J.; Kuroiwa, Y.; et al. High-Efficiency Violet-Emitting All-Inorganic Perovskite Nanocrystals Enabled by Alkaline-Earth Metal Passivation. *Chem. Mater.* **2019**, 31, 3974—3983.
- (62) Huynh, K. A.; Bae, S.-R.; Nguyen, T. V.; Do, H. H.; Heo, D. Y.; Park, J.; Lee, T.-W.; Le, Q. V.; Ahn, S. H.; Kim, S. Y. Ligand-Assisted Sulfide Surface Treatment of CsPbI₃ Perovskite Quantum Dots to Increase Photoluminescence and Recovery. *ACS Photonics* **2021**, 8, 1979–1987.
- (63) Berti, I. O. P. D.; Cagnoli, M. V.; Pecchi, G.; Alessandrini, J. L.; Stewart, S. J.; Bengoa, J. F.; Marchetti, S. G. Alternative low-cost approach to the synthesis of magnetic iron oxide nanoparticles by thermal decomposition of organic precursors. *Nanotechnology* **2013**, 24, 175601–175612.
- (64) Yang, D.; Li, X.; Zhou, W.; Zhang, S.; Meng, C.; Wu, Y.; Wang, Y.; Zeng, H. CsPbBr₃ Quantum Dots 2.0: Benzenesulfonic Acid Equivalent Ligand Awakens Complete Purification. *Adv. Mater.* **2019**, 31, 1900767–1900774.
- (65) Dinegar, R. H.; Smellie, R. H.; Mer, V. K. L. Kinetics of the Acid Decomposition of Sodium Thiosulfate in Dilute Solutions. *J. Am. Chem. Soc.* **1951**, 73, 2050–2054.

- (66) Mizoguchi, T.; Takei, Y.; Okabe, T. The Chemical Behaviour of Low Valence Sulfur Compounds. X. Disproportionation of Thiosulfate, Trithionate, Tetrathionate and Sulfite under Acidic Conditions. Bull. Chem. Soc. Jpn. 1976, 49, 70–75.
- (67) Noel, N. K.; Abate, A.; Stranks, S. D.; Parrott, E. S.; Burlakov, V. M.; Goriely, A.; Snaith, H. J. Enhanced Photoluminescence and Solar Cell Performance via Lewis Base Passivation of Organic—Inorganic Lead Halide Perovskites. *ACS Nano* **2014**, *8*, 9815–9821.
- (68) Cai, T.; Li, F.; Jiang, Y.; Liu, X.; Xia, X.; Wang, X.; Peng, J.; Wang, L.; Daoud, W. A. In situ inclusion of thiocyanate for highly luminescent and stable CH₃NH₃PbBr₃ perovskite nanocrystals. *Nanoscale* **2019**, *11*, 1319–1325.







Check for updates

www.chemnanomat.org

Room-Temperature Treatment with Thioacetamide Yielding Blueand Green-Emitting CsPbX₃ Perovskite Nanocrystals with Enhanced Photoluminescence Efficiency and Stability

Rajesh Kumar Gautam, Somnath Das, and Anunay Samanta*[a]

Abstract: While multiple protocols are currently available for obtaining green- and red-emitting lead halide perovskite nanocrystals (NCs) with near-unity photoluminescence quantum yield (PLQY), achieving this target for the blue-emitting NCs is still quite challenging. This is an impediment to the development of perovskite-based highly efficient white LEDs of which blue is an essential component. Herein, we show that room-temperature treatment of the blue-emitting CsPbCl_{1.5}Br_{1.5}, cyan-emitting CsPbClBr₂ and green-emitting CsPbBr₃ NCs with thioacetamide not only enhances the PLQY

to near-unity (\sim 97–99%) without affecting the PL maximum and bandwidth, but also improves the stability of the systems significantly. The investigation reveals that effective passivation of under-coordinated surface Pb²+ through formation of Pb–S and Pb–NH₂ bonds and removal of excess lead atoms suppress the nonradiative recombination channels and enhances the PLQY and stability of the NCs. Outstanding PL efficiency and superior long-term stability make these systems potential ingredients for various lighting and display applications.

Introduction

Cesium lead halide (CsPbX₃ X=Cl, Br or I) perovskite NCs have attracted considerable attention in recent years as promising materials for optoelectronic applications as photodetectors, [1] light-emitting diodes (LEDs), [2] TV displays and laser [3,4] due to their excellent optical properties, such as high PLQY [5–8] with narrow emission bandwidth, [9] composition- and size-dependent tunability of the band gap over the entire visible region of the electromagnetic spectrum. [9–12]

However, the PL properties of these NCs are very sensitive to the surface due to high surface-to-volume ratio. [7,13,14] Indeed, sub-unity PLQY and instability of the colloidal solution are reflection of the surface defects in these systems that need to be eliminated for obtaining NCs with high PLQY and greater colloidal stability.^[7] The literature suggests that excess lead from lead-rich (or halide-deficient) surface creates deep or shallow inter-bandgap energy levels, which trap the charge carriers and decrease the PLQY of the perovskite NCs. [5] An important point to note here is that as these trap states are shallow in nature in green- emitting CsPbBr₃ NCs, these systems possess fairly high PLQY (typically, ~50-80%). In contrast, the trap states are deep in nature in violet-emitting CsPbCl₃ and blue-emitting CsPb(Cl/ Br)₃ NCs and the PLQY of these systems are typically <5% and < 40%, respectively.[15-17] It is quite challenging to produce brightly luminescent blue-emitting NCs with near-unity PLQY. The literature suggests that post-synthetic surface modification is an effective way of eliminating excess lead from the surface^[5,18-20] and suppressing halide deficiency related defects.[21-25] However, a common post-synthetic method for enhancing the PLQY of both green and blue-emitting NCs to near-unity is rather limited.[18,26] Taking advantage of strong interaction between sulfur and lead sulfur-containing systems are often used for the suppression of defects arising from under-coordinated Pb2+ of the halide deficient surface. [27,28] It should be noted in this context that most of the surface passivation studies on green-emitting CsPbBr₃ NCs have been carried out using long chain thiols except in two cases. [26,29] Bakr and co-workers recently used a thiocyanate salt to enhance the PLQY of the CsPb(Br_vCl_{1,v})₃ NCs in a post-synthetic treatment. [29] Relying on the formation of strong Pb-S bonds with undercoordinated lead atoms, we recently showed that PLQY of the green-emitting CsPbBr₃, blue-emitting CsPb(Cl/Br)₃ and yellowemitting CsPb(Br/l)₃ NCs can be boosted to near-unity upon treatment with sodium thiosulfate. [26] Zhang and co-workers showed that an aqueous solution of thiourea post-synthetically changes CsPbBr₃ NCs to stable nanowires with enhanced PLQY of ~60%. [30] However, this is again limited only to the greenemitting CsPbBr₃ NCs.

In this work, we examine how a small sulfur-containing system, thioacetamide (TAA), which is structurally similar to thiourea, can influence the optical properties and stability of the perovskite NCs. The results show that room temperature (RT) post-synthetic treatment of blue-emitting CsPbCl_{1.5}Br_{1.5}, cyan-emitting CsPbClBr₂ and green-emitting CsPbBr₃ NCs with TAA enhances the PLQY from an initial value of ~12–25% to near-unity (~97–99%). The experimental data suggests that effective passivation of under-coordinated Pb²⁺ of the surface and removal of excess Pb by TAA impart exceptional PLQY to the NCs through suppression of nonradiative recombination channels. Furthermore, formation of strong Pb–S bonds provides robust ligand environment around the NCs that

[[]a] R. K. Gautam, S. Das, Prof. A. Samanta School of Chemistry University of Hyderabad, Hyderabad 500046 (India) E-mail: anunay@uohyd.ac.in

Supporting information for this article is available on the WWW under https://doi.org/10.1002/cnma.202200029





improves their colloidal stability under various external conditions.

Results and Discussion

The colloidal CsPbBr $_3$ and mixed halide CsPb(Cl/Br) $_3$ NCs were synthesized by minor modification of a known method (details in experimental section). The purified NCs were dispersed in toluene for further studies. A diluted version (μ M concentration) of the above colloidal solution was used for the post-synthetic treatment with TAA under ambient condition.

The transmission electron microscope (TEM) images show cubic morphology of the as-synthesized and treated CsPbBr₃ NCs with average edge length of ~9.7 nm, which remains unchanged after the post-synthesis treatment (Figure 1a, b). A similar observation is made for the CsPbCl₃, CsPbCl_{1.5}Br_{1.5}, CsPbClBr₂ and CsPbCl₂Br NCs with average edge lengths between ~9.5 to 11.3 nm (Figure S1). The high resolution TEM images of the as-synthesized and treated CsPbBr₃ NCs show identical inter-planar distance (d) of ~0.58 nm corresponding to the (100) lattice plane (insets figure 1a, b). [9] The unchanged powder X-ray diffraction (PXRD) patterns of the CsPbBr₃ NCs and absence of any additional peak after the post-synthetic treatment indicate no change in crystal structure of the NCs (Figure 1c) implying that it is only the surface that gets modified after the TAA treatment. The splitting of the (100) diffraction peak is perhaps an indication of the presence of orthorhombic phase, whose proportion increases slightly after treatment, as evident from switching of the peak intensities around ~14 degrees.[31] The blue-emitting CsPbCl_{1.5}Br_{1.5}, cyan-emitting CsPbClBr₂, and violet-emitting CsPbCl₂Br and CsPbCl₃ NCs also preserve their cubic crystal structure after the treatment (Figure S2).

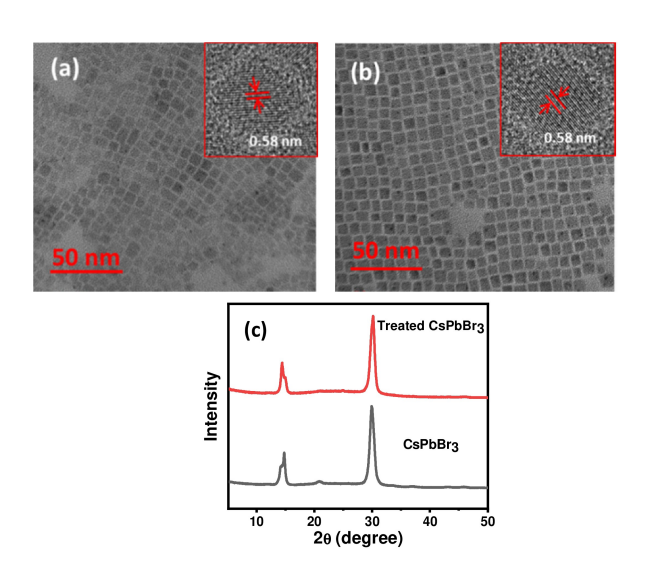


Figure 1. TEM images of the (a) as-synthesized and (b) treated CsPbBr₃ NCs. The insets show corresponding HR-TEM images indicating same interplanar distance. (c) XRD patterns of as- synthesized and treated CsPbBr₃ NCs.

Although the absorption and emission spectral features of the systems before and after the treatment are very similar, a substantial enhancement of the PL intensity for all the systems is observed following the treatment. For example, the PLQY of green-emitting CsPbBr₃, blue-emitting CsPbCl_{1.5}Br_{1.5} and cyanemitting CsPbClBr₂ NCs is increased to near-unity (~97-99%) from the initial values of 25%, 12%, and 15%, respectively (Figure 2 and S3a). Even for the violet-emitting CsPbCl₃ and CsPbCl₂Br NCs, a substantial improvement of the PLQY to ~23% and ~62% from the initial values of <1% and 14%, respectively is noticed (Figure S3b, c). Thus, our post-synthetic method is quite effective for a variety of systems emitting in the 400-510 nm region of the visible spectrum. The bright digital images of the treated NCs highlight the enhanced PL of the NCs (inset of Figure 2). A point to note here is that a small (~2 nm) blueshift of the PL maxima is observed after the treatment only in the case of CsPbBr₃ NCs, though no such shift of the absorption spectrum observed. This blue-shift is presumably due to the removal of shallow trap states of the as-synthesized CsPbBr₃ NCs. The observation of near-unity PLQY of the treated mixedhalide NCs is quite remarkable considering that these are blueemitting NCs and very few post-synthetic strategies can achieve this feat.

In order to understand the associated photophysical processes in the NCs before and after the treatment, PL decay behavior of the systems is studied using a time-correlated single photon counting (TCSPC) fluorescence setup. The PL decay profile of the as-synthesized CsPbBr₃ NCs changes from tri-exponential to a bi-exponential one after the treatment (Figure 3a). The contribution of the 3.02 ns component (Table 1), which arises from band-edge excitonic recombination, [18] increases from 25% to 85% on treatment indicating more efficient radiative recombination process in the treated system. Similarly, the long-component (16.60 ns), which arises from shallow trap-mediated band-edge radiative recombination^[32] increases from just 2% to 15%. Interestingly, the shortest subnanosecond component (0.56 ns), which was the major radiative recombination process in as-synthesized CsPbBr₃ NCs, vanishes after the treatment. This component, which can be attributed to surface defect related nonradiative recombination process in as-synthesized CsPbBr₃ NCs, is completely eliminated in the treated system. [18,31] In the case of CsPbCl_{1.5}Br_{1.5} NCs (Figure 3b), though the PL decay profile remains tri-exponential even after the treatment, a much higher contribution of the

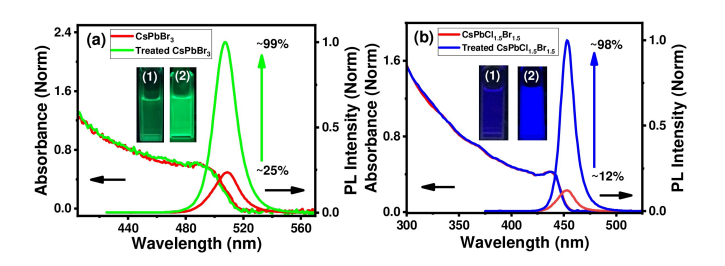


Figure 2. Absorption and PL spectra of as-synthesized and treated (a) $CsPbBr_3$ and (b) $CsPbCl_{1.5}Br_{1.5}$ NCs. Insets show the photographs of assynthesized (1) and treated (2) NCs under 365 nm UV light.



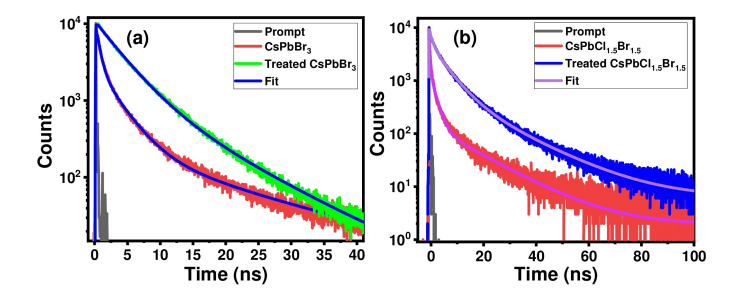


Figure 3. PL decay profiles of the as-synthesized and treated (a) $CsPbBr_3$ and (b) $CsPbCl_{1.5}Br_{1.5}$ NCs. The decay profiles were obtained by exciting the spectrum at 405 nm using a diode laser and by monitoring the PL at their respective PL maxima.

band-edge excitonic recombination (16% vs 50%), with substantial decrease of the trapping component (82% vs 43%) corroborates significant suppression of nonradiative recombination and much improved PLQY of the treated NCs (Table 1). In all cases, the shortest component is attributed to surface trap related nonradiative recombination, the intermediate one to direct band-edge radiative recombination and the long component to shallow trap related band-edge radiative recombination process.[18,31-33] A quantitative estimate of the radiative and nonradiative rate constants (k_r and k_{nr}, respectively) in assynthesized and treated NCs is made from the measured PLQY and lifetime data. A decrease in the k_{nr} value by a factor of ~215-230 in treated CsPbBr₃ and CsPbCl_{1.5}Br_{1.5} NCs, demonstrates significant suppression of the nonradiative recombination processes. The much improved decay profile, associated decay parameters, and the k_r, k_{nr} values of the cyan-emitting CsPbClBr₂ and violet-emitting CsPbCl₂Br and CsPbCl₃ NCs are provided in the SI (Figure S4 and Table S1).

As mentioned already, TAA-treatment modifies the surface of the NCs without affecting the crystal structure of the system. We now attempt to determine the nature of change of the surface environment. Elemental analysis of the as-synthesized and treated NCs, made by scanning a large area of field emission scanning electron microscopy (FESEM) images (EDX measurement), shows a Br:Pb ratio of ~2.72 in CsPbBr₃, indicating a bromide deficient or lead-rich surface of the assynthesized NCs (Figure S5). The increase of this ratio to ~2.96 after treatment indicates removal of excess lead from the surface of NCs (Figure 4a). [5,18, 19] It is important to note that

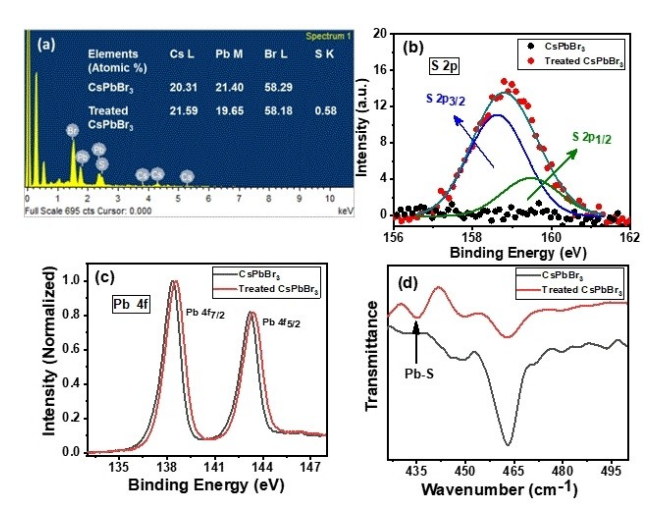


Figure 4. (a) EDX spectra of treated CsPbBr₃ NCs. The inset shows atomic % of the constituting elements. High resolution XPS spectra of (b) S 2p (c) Pb 4f of as-synthesized and treated CsPbBr₃ NCs. The S 2p peak is deconvoluted into $2p_{1/2}$ and $2p_{3/2}$ peaks. (d) FTIR spectra of as-synthesized and treated NCs, respectively. The XPS data was calibrated with respect to C 1s peak at ~285 eV.

although the EDX spectra and elemental analysis of the treated CsPbBr₃ NCs show a small but reproducible value of S, close proximity and multiplet nature of Pb M and S L lines make it difficult to comment on the presence of 'S' in treated NCs from this data.[34,35] However, evenly distributed S in the elemental mapping of the treated CsPbBr₃ NCs confirms the presence of sulfur containing species at the surface of the treated NCs (Figure S6). Further insight on the environment of the surface elements is accessed through XPS measurements. The XPS survey spectra of the as-synthesized and treated CsPbBr₃ NCs show very similar energy bands of Cs, Pb and Br, indicating similar elemental composition for both the NCs (Figure S7 and S8). Interestingly, a clear peak at ~159.11 eV corresponding to 'S 2p' is observed in the high-resolution XPS spectra of only the treated CsPbBr₃ NCs (Figure 4b), reconfirming the presence of TAA at the surface of the NCs. The 'S 2p' peak can be easily deconvoluted into two peaks at 159.5 and 158.5 eV corresponding to $2p_{1/2}$ and $2p_{3/2}$, respectively (Figure 4b). [27] The S $2p_{3/2}$ signal in treated sample suggests that TAA binds to undercoordinated Pb²⁺ of the surface through S.^[28,30] Interestingly,

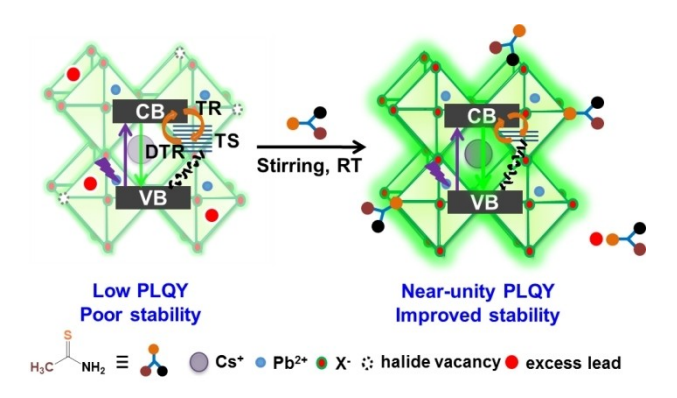
CsPbBr ₃ and CsPbCl _{1.5} Br _{1.5} NCs.							
Samples	$\tau_{\scriptscriptstyle 1}[\alpha_{\scriptscriptstyle 1}]/ns$	$\tau_2[\alpha 2]/ns$	$\tau_{\scriptscriptstyle 3}[\alpha 3]/ns$	PLQY [%]	$<\!\tau_{\text{amp}}\!>^{\S}\!/\!ns$	$k_{\rm r}/ns^{-1}$	k_{nr}/ns^{-1}
CsPbBr ₃	3.02 (0.25)	16.6 (0.02)	0.56 (0.72)	~25	1.55	0.16	0.48
Treated	3.63	9.66	(0.72)	~ 99	4.33	0.22	2.2×10^{-3}
CsPbBr ₃	(0.85)	(0.15)					
CsPbCl _{1.5} Br _{1.5}	2.04	15.61	0.34	~12	0.83	0.14	1
	(0.16)	(0.01)	(0.82)				
Treated	5.55	17.14	1.29	~98	4.53	0.21	4.4×10^{-3}
CsPbCl _{1.5} ,Br _{1.5}	(0.50)	(0.07)	(0.43)				

 $^{\sharp}\alpha_{i}$ represents the amplitude of the i-th lifetime component. $^{5}<\tau_{amp}>=\Sigma\tau_{i}\alpha_{i}/\Sigma\alpha_{\nu}$ $k_{r}=PLQY/<\tau_{amp}>$ and $k_{nr}=(1-PLQY)/<\tau_{amp}>$.



the high-resolution 'N 1s' XPS spectra of the CsPbBr₃ NCs also show a noticeable change after the treatment (Figure S9). In case of treated CsPbBr₃ NCs, this signal can easily be deconvoluted into two signals with peaks at 400.1 and 401.8 eV, corresponding to unprotonated amine (-NH₂) and protonated amine (-NH₃⁺), respectively (Figure S9b). ^[36] The lowenergy peak suggests formation of Pb-NH2 bond as well in treated NCs through coordination of the -NH2 moiety of TAA with under-coordinated Pb²⁺. [36,37] In the high resolution spectra, both the Pb 4f peaks $(4f_{7/2}$ and $4f_{5/2})$ are shifted to higher binding energy by ~0.27 eV for the treated NCs (Figure 4c), which can be explained by the formation of strong Pb-S and Pb-NH₂ bonds at the surface. [26,28,38] The calculated Br/Pb ratio of 2.7 and 2.94 in as-synthesized and treated CsPbBr₃ NCs, respectively (Table S2) indicates removal of excess lead atoms from the surface of the NCs. This observation is in agreement with the EDX data discussed above. It is important to note that in this particular case, the amount of surface lead atoms is probably very less (typically < 15%), and is beyond the detection limit of XPS. [5] This is why no spectral feature for the Pb⁰ species could be observed at the lower energy side of 4f_{7/2} and $4f_{5/2}$ peaks in the high resolution Pb 4f XPS spectra. A similar observation was made in the case of post-synthesis surface treatment of CsPbBr₂ NCs with thiocvanate salts.^[5] The attachment of TAA through formation of Pb-S bond is also confirmed by observation of distinct Pb-S stretching band at ~435 cm⁻¹ in the FTIR spectra of the treated CsPbBr₃ NCs (Figure 4d).[39] The adsorption of TAA also contributes to higher intensity of the C-H stretching and N-H bending (scissoring) bands of the treated NCs (Figure S10).[40] Thus it is evident that TAA passivates the surface of the NCs by attaching it with the under-coordinated surface Pb2+ through both 'S' and 'N' ends of the amino moiety. Thiophene and pyridine having donor sites similar to that in TAA are also known to form coordinate or dative covalent bond with under-coordinated Pb2+ leading to effective suppression of surface defects.[41]

Lead rich surface of the perovskite NCs is known to have deleterious effect on the optical properties of the NCs providing inter band-gap (shallow or deep) trap states at the surface of the NCs, which facilitate nonradiative recombination of the photo-generated charge carriers and decrease the PLQY of the systems. [5,18] It is evident from the above discussion that removal of excess lead atoms from the lead-rich surface of the assynthesized NCs by post-synthetic treatment with TAA effectively suppresses the shallow-electron trap states in treated NCs and enhances the PLQY of the system. Our post-synthetic treatment not only removes excess lead atom from surface, but also passivates the surface trap-states arising from halide vacancies, which form under-coordinated Pb²⁺, a positive charge center.[41] The photogenerated electrons are dragged into these trap sites and later recombine with holes nonradiatively. TAA can interact with these centers and neutralize the excess positive charge forming strong Pb-S and Pb-NH₂ bonds that suppresses the nonradiative recombination process. [29,41] Therefore, as pictorially shown in Scheme 1, effective suppression of the surface defects through elimination of excess lead atoms and passivation of under-coordinated Pb²⁺



Scheme 1. Schematic representation of the associated photophysical processes in the untreated and treated CsPbX $_3$ NCs. The VB, CB, TR, DTR and TS denote valence band, conduction band, trapping recombination, detrapping recombination and trap states, respectively.

enhances the radiative recombination greatly leading to dramatically improved PLQY of the NCs.

Long chain commonly used surface capping agent like oleylammonium cation (OAm⁺), which is for protecting the surface of the perovskite NCs, acts as insulating layer that obstructs the charge transport process and deteriorates the device performance.^[42] Additionally, the binding of OAm⁺ with the surface is dynamic in nature due to its deprotonation by oleate or halides. This exposes the surface of the NCs to the external environment and destabilizes the particles.[43,44] Postsynthetic surface treatment with quaternary ammonium salt like didodecyldimethylammonium bromide (DDAB) though improves the optical properties and stability of the perovskite NCs, [45,46] in some cases, it produces morphological species with reduced PLQY.[47] Surface passivation by small ligands is an attractive approach of protecting a surface without obstructing the charge transport process in real applications. Relying on the strong binding affinity of sulfur towards lead, small sulfurcontaining species are expected to be effective alternatives to the long chain insulating ligands (including thiols). However, Bakr and co-workers although succeeded in enhancing the PLQY of the CsPb(Br_vCl_{1-v})₃ NCs to near-unity using thiocyanate, the method works only for one blue-emitting ($\lambda_{em} = 468 \text{ nm}$) NCs. [29] Li et al. found that post-synthetic treatment of the CsPbBr₃ NCs with thiourea leads to morphological transformation of these NCs into 1D nanowires.[30] Though these two reports on post-synthetic surface treatment with small sulfurcontaining ligands are not very encouraging, our recent study involving thiosulfate shows effective passivation of the undercoordinated Pb2+ through formation of strong Pb-S bond and near-unity PLQY of a range of systems emitting in the 460-580 nm region without affecting the morphology and crystal structure of the NCs.[26] In the present work, however, we demonstrate that RT-treatment not only passivates the trapstates related to the under-coordinated Pb²⁺ ions by forming strong bonds with TAA, but unlike other sulfur-containing systems, it also effectively removes excess lead atom from the surface enabling near-unity PLQY and much improved stability of the NCs emitting in a wide blue - green region. Table S3



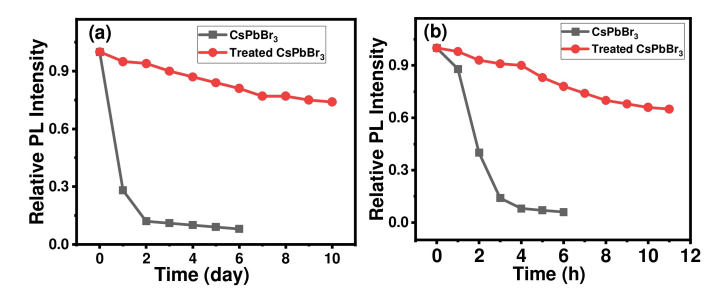


Figure 5. A comparison of the PL stability of as-synthesized and treated CsPbBr₃ NCs under (a) ambient condition and (b) continuous UV light (365 nm, 8 W) illumination.

collects the data on post-synthetic treatment of the perovskite NCs with small sulfur-containing ligands.

Lack of long-term stability of the perovskite NCs is a major limiting factor for their wide scale applications. Interestingly, we found that the treated perovskite NCs exhibit significantly improved stability compared to the as-synthesized NCs under various conditions (Figure 5). For example, while the assynthesized NCs hold just ~8% of its initial PL after 6 days under ambient condition with ~3 nm red-shift of emission maximum, the treated CsPbBr₃ NCs maintains ~76% of its initial PL intensity even after 10 days under similar condition without any shift of the PL spectrum (Figure 5a, S11a, b). The treated CsPbBr₃ NCs also exhibit much improved photo-stability. Almost ~65% of its initial PL intensity is retained after 11 h continuous illumination of UV light (365 nm, 8 W), whereas the assynthesized NCs can hold just ~6% of the same under similar condition for the 6 h (Figure 5b, S11c, d). The treated blueemitting CsPbCl_{1.5}Br_{1.5} NCs are also found to be much more stable compared to the untreated sample. For example, the treated CsPbCl_{1.5}Br_{1.5} NCs maintain ~80% of initial PL intensity after ~11 days under ambient conditions (Figure S12), whereas untreated sample retains just ~5% of the initial PL intensity after 8 days of storage under similar condition. The treated CsPbCl_{1.5}Br_{1.5} NCs are more resistant to UV light as well (Figure S12b). Similarly the treated CsPbCl₃ NCs are found to be more stable retaining ~90% and ~75% of initial PL (as against \sim 10% and \sim 25% of the untreated sample) after 6 days and 7 h under ambient condition and continuous irradiation of UV light, respectively (Figure S13). It is thus evident that the treated NCs not only exhibit exceptional optical properties, but also show much improved air- and photo-stability in colloidal dispersion. Formation of strong Pb-S bond with higher bond dissociation energy compared to the Pb-Br or Pb-Cl bonds^[48] provides a robust and less fragile ligand environment at the surface of the NCs and superior colloidal air stability of the treated NCs.

Conclusion

In conclusion, we have shown that a facile RT post-synthetic surface modification of the blue-emitting CsPbCl_{1.5}Br_{1.5}, cyan-emitting CsPbClBr₂ and green-emitting CsPbBr₃ NCs with TAA

dramatically enhances their PLQY up to near-unity (~97–99%) with moderate improvement up to ~62% and ~23% even for the violet-emitting CsPbCl₂Br and CsPbCl₃ NCs, covering a wide 400–510 nm region of the visible spectrum. Removal of excess lead atoms and passivation of under-coordinated Pb²⁺ effectively suppress the surface trap states, leading to enhanced radiative recombination, enabling dramatically improved PLQY of the NCs. Formation of strong Pb–S bonds at the surface contributes toward the superior stability of the treated NCs under various external stresses making them potentially attractive systems for optoelectronic applications.

Experimental Section

Materials: Cesium carbonate (Cs₂CO₃, 99.9%), 1-octadecene (ODE, 90%), oleic acid (OA, 90%), oleylamine (OLA, technical grade 70%), PbCl₂ (99.99%), PbBr₂ (99.99%) methyl acetate (MeOAc, anhydrous, 99.5%), tri-octylphosphine (TOP, 97%) and thioacetamide (TAA, ACS reagent, > 99.0%) were purchased from Sigma Aldrich. Hexane and toluene were purchased from Finar Chemicals and used without any further purification or distillation.

Synthetic Methods

Preparation of Cs-oleate: The stock solution of cesium oleate was prepared by following a reported procedure with slight modifications. [9] Initially, Cs₂CO₃ (0.102 g), OA (0.5 mL) and ODE (5 mL) were loaded into a 50 mL double-necked flask. The solution was dried for 1 h at 120 °C under vacuum condition and then heated to 140 °C until completion of reaction of the entire Cs₂CO₃ with OA. After complete solubilization of Cs₂CO₃, the solution was kept in stock and preheated at 120 °C before use.

Synthesis of CsPbX₃ (X=CI, Br and Cl/Br) NCs: Subsequently, ODE (5 mL), PbX₂ (0.188 mmol), OA (0.5 mL) and OLA (0.5 mL) were loaded into a 50 mL double-necked flask and heated at 120 °C under vacuum for 1 h until the complete solubilization of the PbX₂ salt. The temperature of the solution was subsequently increased to 160 °C under N₂ environment and thereafter, 0.5 mL of preheated Cs-oleate solution was rapidly injected into the solution. The reaction mixture was cooled in an ice bath after 5 sec of injection. For CsPbCl₃ NCs, 1 mL TOP at 150 °C was added for complete solubilization of PbCl₂. For purification, MeOAc was added to the reaction mixture (1:1 volume ratio), centrifuged at 7600 rpm for 10 min to separate unreacted species from the NCs and discarded it. Then, the precipitate was collected and dispersed in 3 mL toluene for further studies.

Surface Treatment: We performed the post-synthetic treatment at room-temperature under ambient conditions. For this purpose, $\sim 1~\rm mL$ diluted solution of the NCs (of μM concentration) in toluene was taken and stirred with solid TAA for 1 h, which was found to be the optimum time for the treatment of the NCs after which no change in the optical properties was noted. Due to limited solubility of TAA in toluene, it was removed easily from the solution through centrifugation at 7600 rpm for 10 min. The supernatant containing NCs was then mixed with methyl acetate (1:1 volume ratio) and then again centrifuged at 7000 rpm for 5 min to further confirm the elimination of excess unreacted salt. The supernatant was discarded and the precipitate of the treated NCs was dispersed in toluene for further studies.





Characterization

Steady state UV-Vis absorption and fluorescence: UV-Visible absorption and emission spectra were obtained using Cary100 (Varian) spectrophotometer and FluoroLog-3 (Horiba Jobin Yvon) spectrofluorimeter, respectively.

Photoluminescence quantum yield (PLQY) measurements: The PLQYs were calculated using appropriate dye compound as reference and using the following equation

$$QY_S = QY_R \times (I_S/I_R) \times (OD_R/OD_S) \times (n_S/n_R)^2$$

Where, I is the integrated area under the PL spectrum, OD and n denote the optical density at the excitation wavelength and refractive index of the solvents, respectively of the sample (S) and reference compound (R). For blue-emitting CsPbCl₃ and CsPb(Cl/Br)₃ NCs 9,10-diphenylanthracene in toluene (QY = 0.93) and for green-emitting CsPbBr₃ NCs coumarin 153 in ethanol (QY = 0.546) were used as reference compound. [49,50]

Powder X-ray diffraction (PXRD): Powdered X-ray diffraction (PXRD) patterns were measured on a Bruker D8 Advance Diffractometer (Bruker-AXS, Karlsruhe, Germany) using Cu–K α X-radiation (λ = 1.5406 Å) at 40 kV and 30 mA power.

Transmission electron microscopy (TEM): The TEM images of the NCs were recorded using JEM-F200 transmission electron microscope (JEOL) at an accelerating voltage of 200 kV. The samples for TEM measurements were prepared by placing a drop of hexane solution of the NCs on a carbon-coated copper grid and keeping it in high vacuum for 24 h.

Photoluminescence lifetime measurements: Fluorescence intensity decay measurements were performed by using a time-correlated single photon counting (TCSPC) spectrometer (Horiba Jobin Yvon IBH). Pico-Brite lasers with output at 375 or 405 nm and 1 MHz repetition rate were used as the excitation sources and an MCP photomultiplier (Hammatsu R3809u-50) was used as a detector. The laser source information was recorded by using a dilute solution of Ludox in water (acting as a scatter) in the sample chamber. The fluorescence decay curves were analyzed using IBH DAS6 (version 2.2) software, which employs a nonlinear least-squares iteration procedure. The quality of the fits was assessed by considering the χ^2 values and distribution of the residuals. Further details about the setup can be found elsewhere. $^{[51]}$

Fourier transformed infrared spectroscopy (FTIR): FTIR measurements were performed using Bruker Tensor II spectrometer. Single drop of colloidal solution of as-synthesized and treated CsPbBr₃ NCs was used from the stock solution (in hexane). The concentration of as-synthesized and treated CsPbBr₃ NCs was kept similar for the measurement.

Field-Emission Scanning Electron Microscopy (FESEM): FESEM images were recorded using a Carl Zeiss Ultra 55 microscope. Energy dispersive X-ray (EDX) spectra and elemental mappings measurements were recorded using Oxford Instruments X-Max^N SDD (50 mm²) system and INCA analysis software. The as-synthesized and treated sample for the FESEM measurement was made by drop-casting the colloidal solutions on thin quartz glass plate, followed by drying under vacuum for 12 h.

X-ray photoelectron spectroscopy (XPS): XPS measurements were performed using Thermo Scientific K-Alpha + spectrometer. Microfocused monochromatic X-ray source was generated at 70 W with a spot size of 400 μ m. The energy resolution of the spectrometer was set at 0.5 eV at a pass energy of 50 eV. The base pressure of the chamber was maintained at 5×10^{-10} Torr during the analysis. Low

energy electrons from the flood gun were used for charge compensation.

Acknowledgements

This work is supported by the J. C. Bose National Fellowship (to A.S.) of the Science and Engineering Research Board (SERB) and Institute of Eminence Grants (to University of Hyderabad) of the Ministry of Human Resource and Development (MHRD). The authors acknowledge the TEM, FESEM and FTIR facility of the School. Thanks are also due to National Chemical Laboratory, Pune for the XPS measurements. R.K.G. and S.D. thank the University of Hyderabad and University Grants Commission (UGC), respectively for Fellowships.

Conflict of Interest

The authors declare no conflict of interest.

Data Availability Statement

The data that support the findings of this study are available from the corresponding author upon reasonable request.

Keywords: perovskite nanocrystals \cdot photoluminescence quantum yield \cdot post-synthetic treatment \cdot surface passivation \cdot thioacetamide

- [1] P. Ramasamy, D.-H. Lim, B. Kim, S.-H. Lee, M.-S. Lee, J.-S. Lee, Chem. Commun. 2016, 52, 2067.
- [2] X. Zhang, H. Lin, H. Huang, C. Reckmeier, Y. Zhang, W. C. H. Choy, A. L. Rogach, *Nano Lett.* **2016**, *16*, 1415.
- [3] J. Pan, S. P. Sarmah, B. Murali, I. Dursun, W. Peng, M. R. Parida, J. Liu, L. Sinatra, N. Alyami, C. Zhao, E. Alarousu, T. K. Ng, B. S. Ooi, O. M. Bakr, O. F. Mohammed, J. Phys. Chem. Lett. 2015, 6, 5027–5033.
- [4] S. Yakunin, L. Protesescu, F. Krieg, M. I. Bodnarchuk, G. Nedelcu, M. Humer, G. D. Luca, M. Fiebig, W. Heiss, M. V. Kovalenko, *Nat. Commun.* 2015, 6, 8056.
- [5] B. A. Koscher, J. K. Swabeck, N. D. Bronstein, A. P. Alivisatos, J. Am. Chem. Soc. 2017, 139, 6566–6569.
- [6] J. Pan, Y. Shang, J. Yin, M. D. Bastiani, W. Peng, I. Dursun, L. Sinatra, A. M. El-Zohry, M. N. Hedhili, A.-H. Emwas, O. F. Mohammed, Z. Ning, O. M. Bakr, J. Am. Chem. Soc. 2018, 140, 562–565.
- [7] S. Seth, T. Ahmed, A. De, A. Samanta, ACS Energy Lett. 2019, 4, 1610– 1618.
- [8] S. Das, A. Samanta, ACS Energy Lett. 2021, 6, 3780.
- [9] L. Protesescu, S. Yakunin, M. I. Bodnarchuk, F. Krieg, R. Caputo, C. H. Hendon, R. X. Yang, A. Walsh, M. V. Kovalenko, *Nano Lett.* 2015, 15, 3692–3696.
- [10] G. Nedelcu, L. Protesescu, S. Yakunin, M. I. Bodnarchuk, M. J. Grotevent, M. V. Kovalenko, Nano Lett. 2015, 15, 5635–5640.
- [11] V. G. V. Dutt, S. Akhil, N. Mishra, CrystEngComm. 2020, 22, 5022.
- [12] A. Dey, J. Ye, A. De, E. Debroye, S. K. Ha, E. Bladt, A. S. Kshirsagar, Z. Wang, J. Yin, Y. Wang, L. N. Quan, F. Yan, M. Gao, X. Li, J. Shamsi, T. Debnath, M. Cao, M. A. Scheel, S. Kumar, J. A. Steele, M. Gerhard, L. Chouhan, K. Xu, X.-g. Wu, Y. Li, Y. Zhang, A. Dutta, C. Han, I. Vincon, A. L. Rogach, A. Nag, A. Samanta, B. A. Korgel, C.-J. Shih, D. R. Gamelin, D. H. Son, H. Zeng, H. Zhong, H. Sun, H. V. Demir, I. G. Scheblykin, I. Mora-Seró, J. K. Stolarczyk, J. Z. Zhang, J. Feldmann, J. Hofkens, J. M. Luther, J. Pérez-Prieto, L. Li, L. Manna, M. I. Bodnarchuk, M. V. Kovalenko, M. B. J.





- Roeffaers, N. Pradhan, O. F. Mohammed, O. M. Bakr, P. Yang, P. Müller-Buschbaum, P. V. Kamat, Q. Bao, Q. Zhang, R. Krahne, R. E. Galian, S. D. Stranks, S. Bals, V. Biju, W. A. Tisdale, Y. Yan, R. L. Z. Hoye, L. Polavarapu, *ACS Nano* **2021**, *15*, 10775–10981.
- [13] N. Pradhan, ACS Energy Lett. 2019, 4, 1634-1638.
- [14] V. G. V. Dutt, S. Akhil, D. N. Mishra, ChemNanoMat. 2020, 6, 1730.
- [15] D. P. Nenon, K. Pressler, J. Kang, B. A. Koscher, J. H. Olshansky, W. T. Osowiecki, M. A. Koc, L.-W. Wang, A. P. Alivisatos, J. Am. Chem. Soc. 2018, 140, 17760–17772.
- [16] S. Paul, T. Ahmed, S. Das, A. Samanta, J. Phys. Chem. C 2021, 125, 23539–23547.
- [17] A. De, S. Das, N. Mondal, A. Samanta, ACS Materials Lett. 2019, 1, 116.
- [18] T. Ahmed, S. Seth, A. Samanta, Chem. Mater. 2018, 30, 3633–3637.
- [19] S. Wang, Y. Wang, Y. Zhang, X. Zhang, X. Shen, X. Zhuang, P. Lu, W. W. Yu, S. V. Kershaw, A. L. Rogach, J. Phys. Chem. Lett. 2019, 10, 90–96.
- [20] F. Li, Y. Liu, H. Wang, Q. Zhan, Q. Liu, Z. Xia, Chem. Mater. 2018, 30, 8546–8554.
- [21] X. Shen, S. Wang, X. Zhang, H. Wang, X. Zhang, C. Wang, Y. Gao, Z. Shi, W. W. Yu, Y. Zhang, *Nanoscale* 2019, 11, 11464.
- [22] J. Y. Woo, Y. Kim, J. Bae, T. G. Kim, J. W. Kim, D. C. Lee, S. Jeong, Chem. Mater. 2017, 29, 7088–7092.
- [23] Y. Wu, C. Wei, X. Li, Y. Li, S. Qiu, W. Shen, B. Cai, Z. Sun, D. Yang, Z. Deng, H. Zeng, ACS Energy Lett. 2018, 3, 2030–2037.
- [24] R. K. Behera, S. D. Adhikari, S. K. Dutta, A. Dutta, N. Pradhan, J. Phys. Chem. Lett. 2018, 9, 6884–6891.
- [25] H. Shao, Y. Zhai, X. Wu, W. Xu, L. Xu, B. Dong, X. Bai, H. Cui, H. Song, Nanoscale 2020, 12, 11728.
- [26] R. K. Gautam, S. Das, A. Samanta, J. Phys. Chem. C 2021, 125, 24170– 24179.
- [27] M. A. Uddin, J. K. Mobley, A. A. Masud, T. Liu, R. L. Calabro, D.-Y. Kim, C. I. Richards, K. R. Graham, J. Phys. Chem. C 2019, 123, 18103–18112.
- [28] L. Ruan, W. Shen, A. Wang, Q. Zhou, H. Zhang, Z. Deng, *Nanoscale* 2017, 9, 7252.
- [29] X. Zheng, S. Yuan, J. Liu, J. Yin, F. Yuan, W.-S. Shen, K. Yao, M. Wei, C. Zhou, K. Song, B.-B. Zhang, Y. Lin, M. N. Hedhili, N. Wehbe, Y. Han, H.-T. Sun, Z.-H. Lu, T. D. Anthopoulos, O. F. Mohammed, E. H. Sargent, L.-S. Liao, O. M. Bakr, ACS Energy Lett. 2020, 5, 793–798.
- [30] P. Li, D. Yang, Y. Tan, M. Cao, Q. Zhong, M. Chen, H. Hu, B. Sun, Y. Xu, Q. Zhang, ACS Appl. Mater. Interfaces 2019, 11, 3351–3359.
- [31] S. Das, A. De, A. Samanta, J. Phys. Chem. Lett. 2020, 11, 1178–1188.
- [32] V. S. Chirvony, S. Gonzalez-Carrero, I. Suarez, R. E. Galian, M. Sessolo, H. J. Bolink, J. P. Martínez-Pastor, J. Perez-Prieto, J. Phys. Chem. C 2017, 121, 13381–13390.

- [33] V. G. V. Dutt, S. Akhil, N. Mishra, Nanoscale 2021, 13, 14442.
- [34] D. E. Newbury, Scanning 2009, 31, 91.
- [35] K. Thompson, Thermo Fisher Scientific Technical Note 52537, 2013.
- [36] C. Zhang, Q. Wan, L. K. Ono, Y. Liu, W. Zheng, Q. Zhang, M. Liu, L. Kong, L. Li, Y. Qi, ACS Energy Lett. 2021, 6, 3545–3554.
- [37] Q. Zhong, M. Cao, Y. Xu, P. Li, Y. Zhang, H. Hu, D. Yang, Y. Xu, L. Wang, Y. Li, X. Zhang, Q. Zhang, Nano Lett. 2019, 19, 4151.
- [38] S. Baek, Y. Kim, S.-W. Kim, J. Ind. Eng. Chem. 2020, 83, 279.
- [39] J. Cao, J. Yin, S. Yuan, Y. Zhao, J. Lib, N. Zheng, Nanoscale 2015, 7, 9443.
- [40] C. Lu, H. Li, K. Kolodziejski, C. Dun, W. Huang, D. Carroll, S. M. Geyer, Nano Res. 2018, 11, 762.
- [41] N. K. Noel, A. Abate, S. D. Stranks, E. S. Parrott, V. M. Burlakov, A. Goriely, H. J. Snaith. ACS Nano 2014, 8, 9815.
- [42] J. Tang, K. W. Kemp, S. Hoogland, K. S. Jeong, H. Liu, L. Levina, M. Furukawa, X. Wang, R. Debnath, D. Cha, K. W. Chou, A. Fischer, A. Amassian, J. B. Asbury, E. H. Sargent, *Nat. Mater.* 2011, 10, 765.
- [43] F. Krieg, S. T. Ochsenbein, S. Yakunin, S. t. Brinck, P. Aellen, A. Süess, B. Clerc, D. Guggisberg, O. Nazarenko, Y. Shynkarenko, S. Kumar, C.-J. Shih, I. Infante, M. V. Kovalenko, ACS Energy Lett. 2018, 3, 641.
- [44] S. Akhil, V. G. V. Dutt, N. Mishra, Chem. Eur. J. 2020, 26, 17195.
- [45] C. Lee, Y. Shin, A. Villanueva-Antolí, S. D. Adhikari, J. Rodriguez-Pereira, J. M. Macak, C. A. Mesa, S. Giménez, S. J. Yoon, A. F. Gualdrón-Reyes, I. Mora-Seró, Chem. Mater. 2021, 33, 8745–8757.
- [46] J. Pan, L. N. Quan, Y. Zhao, W. Peng, B. Murali, S. P. Sarmah, M. Yuan, L. Sinatra, N. M. Alyami, J. Liu, E. Yassitepe, Z. Yang, O. Voznyy, R. Comin, M. N. Hedhili, O. F. Mohammed, Z. H. Lu, D. H. Kim, E. H. Sargent, O. M. Bakr, Adv. Mater. 2016, 28, 8718.
- [47] S. K. Balakrishnan, P. V. Kamat, Chem. Mater. 2018, 30, 74.
- [48] D. R. Lide, CRC Handbook of Chemistry and Physics, 87 ed., CRC Press: Boca Raton, FL. 2007.
- [49] J. V. Morris, M. A. Mahaney, J. R. Huber, J. Phys. Chem. 1976, 80, 969.
- [50] K. Rurack, M. Spieles, Anal. Chem. 2011, 83, 1232.
- [51] A. De, S. Das, A. Samanta, ACS Energy Lett. 2020, 5, 2246–2252.

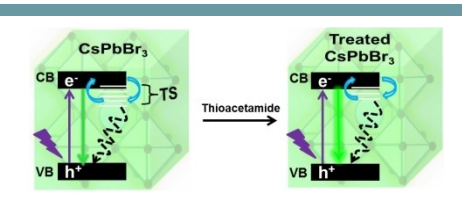
Manuscript received: January 18, 2022 Revised manuscript received: February 18, 2022 Accepted manuscript online: February 18, 2022 Version of record online:





RESEARCH ARTICLE

A simple room-temperature postsynthetic treatment with thioacetamide enhances the PLQY to nearunity and improves the stability of blue- and green-emitting CsPbX₃ (X=Cl/Br and Br) perovskite NCs. Removal of excess lead and suppression of halide vacancy related surface defects by forming strong Pb—S and Pb—NH₂ bonds impart such exceptional qualities to the treated NCs.



R. K. Gautam, S. Das, Prof. A. Samanta*

1 – 8

Room-Temperature Treatment with Thioacetamide Yielding Blue- and Green-Emitting CsPbX₃ Perovskite Nanocrystals with Enhanced Photoluminescence Efficiency and Stability



Exploring Strategies for Obtaining Cesium Lead Halide Perovskite Nanocrystals with High Photoluminescence Efficiency and Stability

by Rajesh Kumar Gautam

Librarian

Indira Gandhi Memorial Library
UNIVERSITY OF HYDERABAD
Central University P.O.

HYDERABAD-500 046.

Submission date: 23-Jun-2023 02:58PM (UTC+0530)

Submission ID: 2121338351

File name: Thesis_Plagiarism_check_Rajesh_SoC_UoH.pdf (665.38K)

Word count: 13336 Character count: 69665

Exploring Strategies for Obtaining Cesium Lead Halide Perovskite Nanocrystals with High Photoluminescence Efficiency and Stability

ORIGINALITY REPORT

59% SIMILARITY INDEX

14%

59%

4%

SIMILARITY INDEX

INTERNET SOURCES

PUBLICATIONS

STUDENT PAPERS

PRIMARY SOURCES

Rajesh Kumar Gautam, Somnath Das, Anunay Samanta. "Can Sulfur-Containing Small Systems Enhance the Photoluminescence and Stability of the Blue-, Green- and Yellow-Emitting Perovskite Nanocrystals? A Case Study with Sodium Thiosulfate", The Journal of Physical Chemistry C, 2021

27%

PROF. ANUNAY SAMANTA
O SCHOOL OF CHEMISTRY
UNIVERSITY OF HYDERABAD
HYDERABAD - 500 046

Publication

Rajesh Kumar Gautam, Somnath Das, Anunay Samanta. "Room Temperature Treatment with Thioacetamide Yielding Blue - and Green - Emitting CsPbX3 Perovskite Nanocrystals with Enhanced Photoluminescence Efficiency and Stability", ChemNanoMat. 2022

(19%) Our publication

Publication

Rajesh Kumar Gautam, Somnath Das, Anunay Samanta. "Room - Temperature Treatment with Thioacetamide Yielding Blue - and Green - Emitting CsPbX Perovskite 6%

Ohn publication

Nanocrystals with Enhanced Photoluminescence Efficiency and Stability ", ChemNanoMat, 2022

Publication

4	Submitted to University of Hyderabad, Hyderabad Student Paper	1%
5	pubs.acs.org Internet Source	1%
6	Somnath Das, Anunay Samanta. "On direct synthesis of high quality APbX (A = Cs, MA and FA; X = Cl, Br and I) nanocrystals following a generic approach ", Nanoscale, 2022	1%
7	Sumanta Paul, Anunay Samanta. "Phase- Stable and Highly Luminescent CsPbl Perovskite Nanocrystals with Suppressed Photoluminescence Blinking ", The Journal of Physical Chemistry Letters, 2022	1%
8	Nadesh Fiuza-Maneiro, Kun Sun, lago López- Fernández, Sergio Gómez-Graña et al. "Ligand Chemistry of Inorganic Lead Halide Perovskite Nanocrystals", ACS Energy Letters, 2023	1%

9	Somnath Das, Modasser Hossain, Anunay Samanta. "Stable and Intense Violet-Emitting CsPbCl Nanocrystals for Light-Emitting Diodes: Directly Obtained by L-Type Surface Passivation ", ACS Applied Nano Materials, 2023 Publication	1 %
10	www.researchgate.net Internet Source	<1%
11	Franziska Krieg, Stefan T. Ochsenbein, Sergii Yakunin, Stephanie ten Brinck et al. "Colloidal CsPbX (X = Cl, Br, I) Nanocrystals 2.0: Zwitterionic Capping Ligands for Improved Durability and Stability ", ACS Energy Letters, 2018 Publication	<1%
12	Javad Shamsi, Alexander S. Urban, Muhammad Imran, Luca De Trizio, Liberato Manna. "Metal Halide Perovskite Nanocrystals: Synthesis, Post-Synthesis Modifications, and Their Optical Properties", Chemical Reviews, 2019	<1%
13	V. Naresh, Nohyun Lee. "Zn(II)-Doped Cesium Lead Halide Perovskite Nanocrystals with	<1%

High Quantum Yield and Wide Color Tunability

for Color-Conversion Light-Emitting Displays",

ACS Applied Nano Materials, 2020

14	dx.doi.org Internet Source	<1%
15	Anirban Dutta, Rakesh Kumar Behera, Poulami Pal, Sujoy Baitalik, Narayan Pradhan. "Near - Unity Photoluminescence Quantum Efficiency for All CsPbX (X=Cl, Br, and I) Perovskite Nanocrystals: A Generic Synthesis Approach ", Angewandte Chemie, 2019 Publication	<1%
16	Sumanta Paul, Tasnim Ahmed, Somnath Das, Anunay Samanta. "Effect of Lead:Halide Precursor Ratio on the Photoluminescence and Carrier Dynamics of Violet- and Blue- Emitting Lead Halide Perovskite Nanocrystals", The Journal of Physical Chemistry C, 2021	<1%
17	digital.lib.washington.edu Internet Source	<1%
18	hdl.handle.net Internet Source	<1%
19	onlinelibrary.wiley.com Internet Source	<1%
20	Jiaqing Qiu, Weinan Xue, Wei Wang, Yan Li. "Effective surface passivation on CsPbBr3	<1%

nanocrystals via post-treatment with aromatic carboxylic acid", Dyes and Pigments, 2021

Publication

Publication

21

Navendu Mondal, Apurba De, Anunay Samanta. "Achieving Near-Unity Photoluminescence Efficiency for Blue-Violet-Emitting Perovskite Nanocrystals", ACS Energy Letters, 2018

<1%

Exclude quotes

On

Exclude matches

< 14 words

Exclude bibliography

On